
9 Liquid–Multiple Solid Phase Equilibria in Fats *Theory and Experiments*

*Leendert H. Wessdorp, J.A. van Meeteren,
S. de Jong, R. van der Giessen,
P. Overbosch, P.A.M. Grootscholten,
M. Struik, E. Royers, A. Don, Th. de Loos,
C. Peters, and I. Gandasasmita*

9.1 INTRODUCTION AND PROBLEM DEFINITION

It is important to control the melting and solidification behavior of edible oils and fats for the production of fat-containing food products. The objective of this work is to develop a method to predict the melting range and solid phase composition of fats from their overall composition. Fats consist of triacylglycerols (TAGs), which show polymorphism in the solid phase. The polymorphic behavior is reviewed. The nomenclature for TAGs and groups of TAGs used in this work is explained. Existing methods for solid phase prediction are discussed.

9.1.1 SOLID–LIQUID PHASE EQUILIBRIA AND FATS

The fact that many languages have different words for the solid and liquid state of mixtures of triacylglycerols (triglycerides) indicates that the solid–liquid phase behavior of TAGs is something everyone encounters in daily life. Coconut “oil” can be conveniently used as table oil in many tropical countries, while in Northwest Europe it is considered a stone hard “fat.”

Edible oils and fats usually consist of more than 95% of a complex mixture of TAGs. Typically an edible oil or fat can contain more than 500 different TAGs. Edible oils and fats therefore do not possess a distinct melting point, but exhibit a long melting range.

This melting range is one of the main factors determining the properties of fat-containing food products, like fat spreads, dressings, chocolate, cakes, ice cream, and cookies. A fat spread, for example, must contain enough liquid fat at refrigerator temperature in order to make it a spreadable, soft solid. At ambient temperature, it still must contain enough solid fat to prevent the spread from becoming pourable

and oiling out. To give the spread a nice taste, the fat should be liquid at mouth temperature (Poot and Biernorth, 1986; Figures 9.1 and 9.2).

A fat with an optimal melting range for a particular application is obtained by carefully blending natural and modified oils and fats. Of course, the edible fats industry boasts of an ability to blend fats to a constant melting range regardless of the raw materials used. In other applications, like chocolate, cocoa butter is sometimes mixed with other fats, that require a very specific TAG composition to get a good chocolate. These are often obtained by fractional crystallization of natural fats like palm oil. Simulation of this fractionation process requires calculation of the dependence of the crystal composition on process conditions. Both melting range

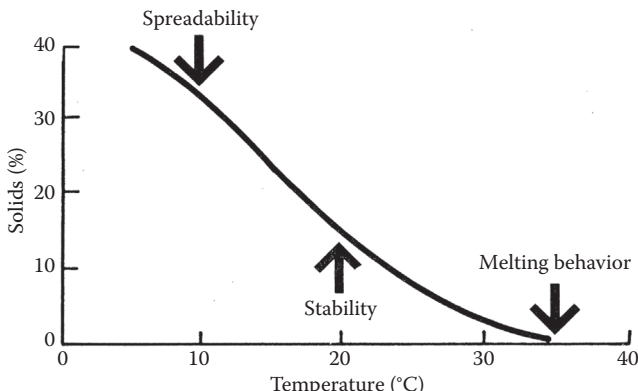


FIGURE 9.1 Requirements for the melting range of a fat spread.

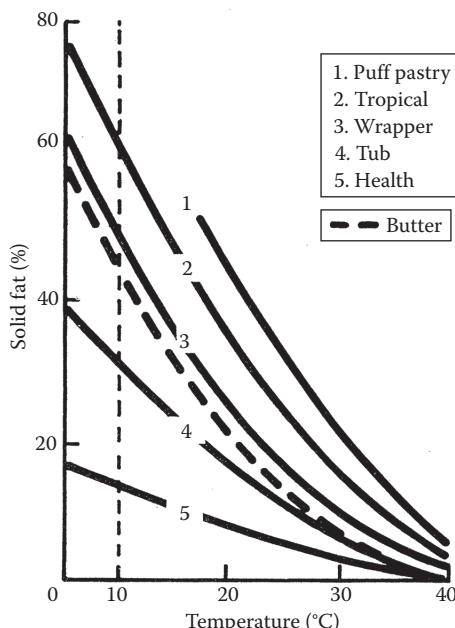


FIGURE 9.2 Melting ranges of some types of fat spreads.

and phase composition of a fat are primarily determined by the solid–liquid phase equilibrium in the fat. Describing the phase behavior of edible oils and fats is therefore a necessity for the edible fats industry.

The objective of this work is to develop a method that enables prediction of the melting range and the solid phase composition of edible oils and fats.

9.1.2 TRIACYLGLYCEROLS: NOMENCLATURE

Edible oils and fats consist mainly of triacylglycerols (TAGs). For convenience, TAGs will be identified by a three-letter code in this work. Each of the three characters in the code represents one of the fatty acids that is esterified with the glycerol. So glycerol-1-palmitate-2, 3-disterate will be represented by PSS. The middle character always indicates the fatty acid that is esterified on the 2-position of the glycerol. The characters used to represent the fatty acids are given in Table 9.1.

It is sometimes convenient to be able to refer to groups of TAGs. Table 9.2 defines a set of letter codes that represent a number of fatty acids.

Hence the TAG-group h₃ contains all TAGs that can be made from the four long chain fatty acids, like SSS, PPP, SPP, PPS, PSP, AAA, BBB, ASA, ASB, etc., while hOh stands for all TAGs having oleic acid on the 2-position and one of the four long chain fatty acids on the 1- and the 3-position of the glyceryl group like SOS, POP, POS, AOS, etc.

TABLE 9.1
Characters Used for Representing Individual Fatty Acids

Code	Fatty Acid	Code	Fatty Acid
2	Acetic acid	P	Palmitic acid (hexadecanoic acid)
4	Butyric acid	S	Stearic acid (octadecanoic acid)
6	Hexanoic acid	O	Oleic acid (<i>cis</i> -9-octadecenoic acid)
8	Octanoic acid	E	Elaidic acid (<i>trans</i> -9-octadecenoic acid)
C	Capric acid (Decanoic acid)	I	Linoleic acid (<i>cis-cis</i> -9, 12-octadecadienoic acid)
L	Lauric acid (Dodecanoic acid)	A	Arachidic acid (eicosanoic acid)
M	Myristic acid (Tetradecanoic acid)	B	Behenic acid (docosanoic acid)

TABLE 9.2
**Letter Codes Used for Representing Groups
of Fatty Acids**

Code	Fatty Acids
m	Medium chain fatty acids (8 + C + L + M)
h	Long chain saturated fatty acids (P + S + A + B) (“hydrogenated”)
u	<i>cis</i> -C18 unsaturated fatty acids (O + I + linolenic acid)

9.1.3 TRIACYLGLYCEROLS: POLYMORPHISM

The existence of a number of alternative crystal structures is a characteristic property of all lipids (alkanes, fatty acids, soaps, methyl esters of fatty acids, and TAGs) (Larsson, 1986). This is due to the fact that there are a number of different possibilities of packing the long hydrocarbon chains into a crystal lattice. This phenomenon is called polymorphism and each different crystal structure is called a polymorphic form or modification of the lipid. Two types of polymorphism occur in lipids. When each form is thermodynamically stable in a definite range of temperature and pressure, it is called enantiotropic polymorphism. Each enantiotropic polymorph transforms into another polymorph at the transition temperature. The opposite case, when only one polymorphic form is thermodynamically stable, is called monotropic polymorphism. TAGs show monotropic polymorphism, while long chain odd alkanes show enantiotropic polymorphism (see Section 9.9.4.1–9.9.4.3).

The polymorphism of TAGs was first observed by Duffy (1853), but only in the early 1960s, some agreement was reached about the number, structure, and nomenclature of the different polymorphic forms of TAGs (Chapman, 1962; Larsson, 1964). They occur in three different basic polymorphic forms, α , β' , and β , which are characterized by a particular carbon chain packing and stability. Recent accurate experimental techniques, combined with better purity of the samples, have brought about a new controversy about the existence, number, and nomenclature of submodifications of each polymorphic form (Hernqvist and Larsson, 1982; Simpson and Hagemann, 1982; Hagemann and Rothfuss, 1983; Gibon, 1984; Sato, 1987; Sato et al., 1989; Kellens et al., 1990).

It is not the objective of this work to enter into a discussion on submodifications. However the subject of this work, phase equilibria in TAGs, requires an opinion on TAG polymorphism.

9.1.3.1 Basic Polymorphic Forms of TAGs

This work will use the nomenclature proposed by Larsson (1964, 1986) in the form applied by de Jong (1980). Basically the fatty acid chains of TAGs can be packed into three main polymorphic forms, characterized by the short spacings in the x-ray diffraction pattern:

1. The α -modification, characterized by only one strong short-spacing line in the x-ray diffraction pattern near 0.415 nm. In the α -modification the chains are arranged in a hexagonal chain packing, without an order to the zig-zag chain planes. The chains do not have an angle of tilt (Figure 9.3a).
2. The β -modification, characterized by two strong short-spacing lines in the x-ray diffraction pattern near 0.38 and 0.42 nm. It also has a doublet in the 720 cm^{-1} region of the infrared absorption spectrum. The chain packing in the modification is orthorhombic, with a perpendicular arrangement of the zig-zag chain planes. The chains have an angle of tilt between 50° and 70° (Figure 9.3b).
3. The β' -modification, characterized by a strong short-spacing line in the x-ray diffraction pattern near 0.455 nm and a number of other strong lines around 0.36–0.39 nm. The β' -modification is the most densely packed polymorph. The chains are arranged in a triclinic chain packing, with a parallel arrangement of the zig-zag chain planes. The chains have an angle of tilt between 50° and 70° (Figure 9.3c).

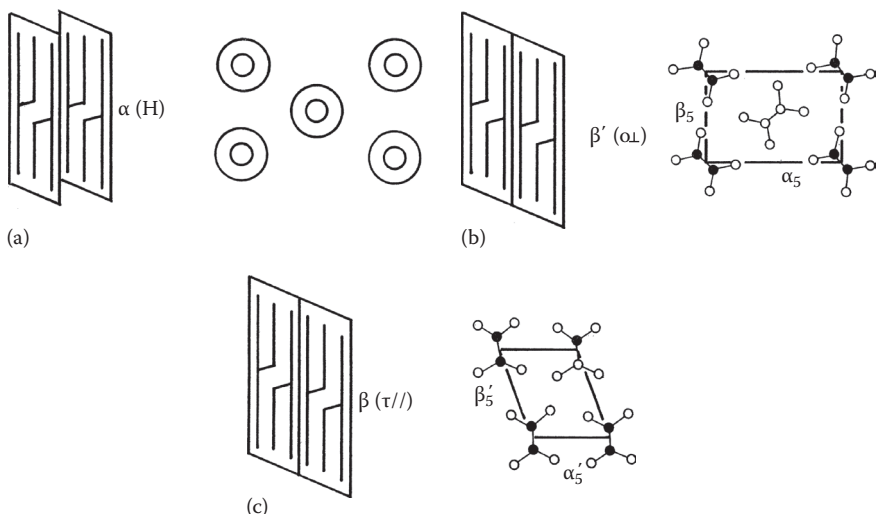


FIGURE 9.3 Schematic representation of orientation of the TAGs in their three basic polymorphic forms, together with the respective chain packing subcell. One zig-zag is seen in the direction of the hydrocarbon chains, open circles are hydrogen, filled circles carbon. (a) α : Unstable, lifetime <60 s present during process, (b) β' : Metastable (>60 s \rightarrow years) present in products, and (c) β : Stable. (From Hernquist, L., Thesis, University of Lund, Sweden, 1984.)

Based on the arrangement of the TAGs themselves in the crystal, two forms can be distinguished for each modification: a form with layers made up of two fatty acid chains and one with layers of three fatty acid chains (Figure 9.4). These forms are characterized by their long spacing in the x-ray diffraction pattern. To distinguish between the two forms, a suffix is added to the symbol that indicates the modification, for example, β -2 and β -3.

The -2 forms are the most stable and the -3 forms are therefore only found for TAGs of which the chain packing in the -2 form would be very unfavorable: in TAGs with *cis*-unsaturated fatty acids and in TAGs in which the fatty acid chains differ by 6 or more.

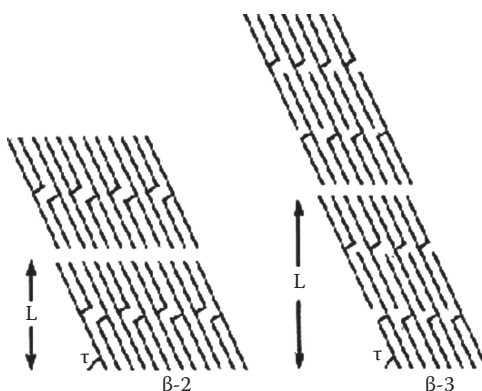


FIGURE 9.4 β -2 and β -3 arrangements of TAGs. (From de Jong, S., Thesis, Rijksuniversiteit Utrecht, the Netherlands, 1980.)

9.1.3.2 Submodifications

If submodifications exist, they will be indicated by a subscript in order of decreasing melting point, for example, $\beta_1\text{-}2$ and $\beta_2\text{-}2$.

9.1.3.2.1 Saturated TAGs

De Jong (1980) has done an excellent, extensive study of molecular packing possibilities in the β -modification. He shows that in theory a β -2-forming TAG can crystallize in at least two but often three different β -2 submodifications. For the β -3 modification, two submodifications are possible. He found that in practice, each TAG only occurs in one of these submodifications, although different TAGs crystallized in different submodifications.

Simpson and Hernqvist (Hernqvist and Larsson, 1982; Simpson and Hagemann, 1982) reported simultaneously the existence of two β' -submodifications for saturated TAGs, and somewhat later Hagemann and Rothfuss (1983) managed to distinguish even three β' submodifications, two α -submodifications, and two β -submodifications in his differential scanning calorimetry (DSC) thermograms. The submodifications were never obtained as pure solid phases on their own, but they rapidly transformed to the most stable submodification. Consequently, reliable melting points or heats of fusion could not be determined. The x-ray diffraction patterns of the submodifications show only very subtle differences. The pattern of a less stable submodification has much broader peaks and shows less details than that of the most stable submodification.

Rapid polymorphic transitions used to be hard to study by x-ray. The polymorphic transition takes 5 min, while one x-ray scan takes 15 min. This makes the unambiguous identification of very unstable submodifications difficult. Very recent experimental techniques allow so-called time resolved x-ray diffraction and neutron scattering studies (Cebula et al., 1990; Kellens et al., 1990). These new techniques need only 5 s for a scan, which means that the actual order of events during a polymorphic transition can be followed.

Kellens et al. (1990) find that the polymorphic transitions take place in a very specific order. Reordering along the three different crystallographic axes is not achieved simultaneously but takes place sequentially. This is in agreement with computer simulation results of Hagemann and Rothfus (1988), who showed that, due to sterical hindrance, the minimal energy path for the rearrangement in the crystal packing follows a very specific order of events. Also Sato et al. (1989) has observed this phenomenon. Kellens states that melting the crystal in a transitional state, where it has not yet reached full crystallinity, can very well result in DSC thermograms similar to those from which Hagemann concluded the existence of unstable submodifications.

Kellens et al. also show that the melting entropies of Hagemann's and Hernqvist's submodifications are far too low to identify these submodifications as one of the differently packed β' and β forms of de Jong (1980). Moreover, they found that the height of the shoulder or small prepeak in the DSC thermogram did not increase upon increasing scan rate, which is contradictory to the existence of an unstable submodification that rapidly transforms into a more stable one.

Hagemann could not show during all his experiments that the recrystallization from α to one of the β forms was actually complete. The observed less stable

β_2 -form can therefore also be explained as the melting peak of the β -form in the presence of a little bit of liquid.

Kellens final conclusion is that these submodifications may very well not be separate polymorphic forms in a thermodynamic sense, but transitional variants with lower crystal perfection and crystallinity.

Due to the serious doubts that one may have on the actual occurrence of a large number of submodifications of saturated TAGs and the plausible alternative explanations available, this work assumes that only the three basic modifications occur.

9.1.3.2.2 *Unsaturated TAGs*

Only the polymorphism of hOh-type TAGs has been studied in more detail, because of their importance for explaining the phase behavior of cocoa butter. As before, there is no agreement at all on the existence, properties, and number of submodifications.

Perhaps the best results come from Sato et al. (1989). His x-ray diffraction results show very convincingly a fourth polymorph, the γ -modification, characterized by two strong short spacings, at 0.470 and 0.390 nm, and a weaker one at 0.45 nm, characteristic of orthorhombic chain packing with parallel orientation of the chain zig-zag planes. The thermodynamic properties are almost that of the perpendicular orthorhombic β' -modification. This γ -modification is of little practical importance; it is less stable than α -modification and converts readily into the β' -modification. It is not observed in mixtures. This γ -modification is also known under the names β'' , sub- β -3, L₂, and form 4. This chapter will use Sato's nomenclature.

Sato, and other authors, also found 2 β' and 2 β -submodifications, which hardly differ in x-ray pattern and stability. The existence and properties of β' -submodifications, which only occurred in POP and not in SOS and BOB, strongly depend on the level of impurities.

Therefore similar doubts arise for the existence of these submodifications as for Hagemann's submodifications of saturated TAGs. This work will only consider one β' -modification, having properties of the most stable of the β' -submodifications that are reported.

The existence of two β -submodifications is quite certain (Sato et al., 1989), as they can actually be obtained in pure form. The transition to the most stable form is extremely slow and takes several weeks. X-ray diffraction shows that the differences in structure must be minor. De Jong (1980) suggests that the forms only differ in layer stacking. The most stable β_1 -3 form has in this view a slightly higher symmetry and a heat of fusion that is only 1 kJ/mol more. This explains why the most stable form takes so long to form and why the 2 β -forms are only observed in pure components and mixtures of hOh-TAGs that are nearly isomorphous, like cocoa butter. In more complex mixtures that contain high amounts of hOh-type TAGs, like palm oil (Timms, 1984) and the mixtures that Hernqvist (1984) used, only one β -form is observed. Therefore, for most practical purposes, the possible existence of β -submodifications can be neglected. However, for systems with very high concentrations (>80%) of one hOh-type TAG, we need to be aware of the possible occurrence of β -submodifications.

9.1.3.2.3 Conclusion

The discussion on submodifications is still very confusing and clear evidence has not been put forward for their existence, nor is there any agreement about their properties. In most cases, alternative explanations, like those of Kellens et al. (1990), are possible for the observed changes in x-ray patterns and the shoulders and shifts in the DSC thermograms. This work it will therefore assume that each TAG crystallizes in three different polymorphic forms only.

9.1.3.3 Stability

The α -modification is the least stable and it converts within several minutes into the β' -modification. The α -form is found in edible fat products during their preparation.

The β' -modification is the stable modification for odd-chain TAGs and a number of even chain TAGs (like PSP). In other TAGs, it converts into the β -modification within several minutes to hours. In mixtures, this transition is often delayed to several months or years. It is therefore the modification that is encountered most frequently in normal edible fat products.

The β' -modification is the stable modification. It only occurs in edible fat products during their lifetime, if the fat is composed of TAGs that are nearly isomorphous, like hardened rape-seed oils (Nyvlt, 1967) and cocoa butter (Timms, 1984).

All three modifications can be obtained directly from the liquid, by varying the degree of supercooling. The transformation of α to β , however, always takes place via the β' -modification (Hernqvist, 1984; Hagemann and Rothfus, 1988; Kellens et al., 1990; Figure 9.5).

9.1.4 METHODS FOR PREDICTING SOLID PHASE COMPOSITION AND QUANTITY

The objective of this work is to develop a method to predict the melting range and composition of the solid phase of edible oils and fats from the overall composition of the fats. If the exact molecular composition of a fat is known, prediction of its properties is in principle possible. The vegetable oils and fats became only analytically accessible by the progress in high-performance liquid chromatography (HPLC) techniques made since the 1980s, while the analysis of animal oils and fats is still troublesome. Besides, the theoretical understanding of solid–liquid phase equilibria in multicomponent systems was not at all adequate to deal with even very simple oils. Nevertheless, some (semi) empirical methods for prediction of solid phase content were developed. They will be briefly discussed in this section.

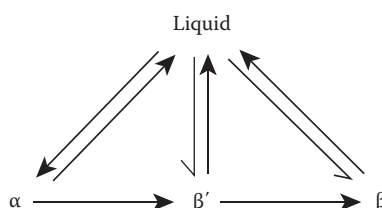


FIGURE 9.5 Simple picture of the possible polymorphic transitions in TAGs.

9.1.4.1 Linear Programming/Multiple Regression

This method is frequently used in the industry (Timms, 1984). The composition of the fat blend is defined in terms of the natural and modified oils of which it is made (e.g., 50% palm oil, 50% bean oil). The solid phase content of the mixture is expressed as a linear function of the concentration of these components:

$$\%S = k_1x_{\text{oil}1} + k_2x_{\text{oil}2} + \dots \quad (9.1)$$

The coefficients k are obtained by multiple linear regression on the data of a number of mixtures. For limited ranges of compositions and solid phase contents, this method is very useful. It does have disadvantages:

1. The predictive equation has no theoretical basis at all. Extrapolation outside the range of experimental data is not possible and gives dangerously erroneous results.
2. The equations cannot be easily extended to incorporate new component fats. The complete regression analysis and experimental work must be repeated and all coefficients will change.
3. Understanding is not obtained about the actual phase behavior, which implies that a solution cannot be found for undesired recrystallization phenomena and other crystallization phenomena that may be observed in practice. Polymorphism is neglected.

9.1.4.2 Excess Contribution Method

Timms (1984) shows the application of an empirical method developed by Nyvlt (1967) to fats. The method is an extension of the multiple linear regression method of Section 9.1.4.1. The solid phase content is expressed as

$$\%S = \sum_{i=1}^n \%S_i \cdot x_i + \sum_{j=1}^n \sum_{i=1}^{j-1} I_{ij} \cdot \frac{x_i x_j}{x_i + x_j} \quad (9.2)$$

The concentrations x are weight fractions of the constituting oils, and the binary interactions must be determined from measurements of a number of mixtures of the two oils concerned. The advantages over the linear method are twofold:

1. The equation is in principle valid over larger concentration ranges.
2. If a new component fat is to be added, only the binary mixtures with all other component fats have to be measured in order to determine the interaction parameters. All other interactions remain unaffected.

Timms (1984) shows that the predictions are considerably worse than with the linear method, with deviations of 30% around the measured values. Again the model is totally empirical, the meaning of the parameters is unclear and it offers no real insight in the underlying crystallization phenomena.

9.1.4.3 TAGs Inductors de Crystallization Method

The first method that attempts to predict solid phase content from TAG composition is the TAGs Inductors de Crystallization Method (TGIC method) of Perron (1986). He assumes the following:

- A crystallized fat consists of a number of solid phases in equilibrium with each other and with the liquid phase present.
- Each solid phase consists mainly of one TAG, called the TGIC. All solid phases contain impurities, which modify its melting point and heat of fusion.
- Upon heating, each solid phase melts independently. The fraction of the solid phase that has disappeared at a certain temperature is given by a point on a Kessis curve. A Kessis curve is a general mathematical representation of a DSC or differential thermal analysis (DTA) melting peak of a single component in a liquid solvent. By adjustment of the parameters, it can be used to describe a measured DSC curve, including the thermal lag.
- The solid phase content at a certain temperature can be obtained from an addition of all contributions from the Kessis curves of each TGIC at that temperature.

Although Perron's notion of a number of coexisting solid phases is correct, the method he has developed is not sound at all:

1. His selection of the number and composition of the coexisting solid phases has no physical ground.
2. There is no reason why the solid phases should melt according to a Kessis curve. Moreover, the width of the Kessis curve is normally determined by the DSC apparatus and the scan rate selected. It is therefore not a property of the fat and any assumption about the width of such a curve is arbitrary.

The criticism Timms (1984) applied to an earlier version of Perron's TGIC method is still valid. Contrary to the two empirical methods mentioned, the method is not even useful for practical purposes.

9.1.4.4 Classification of TAGs Method

Wieske (1970) proposed a method in which he groups the TAGs into all possible TAG-groups that can be formed from elaidic acid (E) and the three fatty acid groups of [Table 9.2](#): h, m, and u. These TAG classes are supposed to form separate solid phases in a crystallized fat. The fraction of each class that has not crystallized is given by the Hildebrand equation, assuming an average melting point and heat of fusion for each TAG-class. The Hildebrand equation reads as follows:

$$\ln x_i^L = \frac{\Delta H_{f,i}}{R} \left(\frac{1}{T_{f,i}} - \frac{1}{T} \right) \quad (9.3)$$

This method has a physical background. It assumes that oil can be considered as a mixture of a limited number of pseudocomponents that do not form mixed crystals. However, the predictions from this method are of a similar poor quality as those of the excess contribution method. Wieske's choice of the pseudocomponents, as well as the assumption of solid immiscibility, and the selection of melting points and heats of fusion can be criticized. This method does not offer any understanding of the actual, underlying solid–liquid phase behavior of TAGs.

9.1.4.5 Other TAG-Based Methods

Several attempts have been made to find an empirical correlation between the TAG composition of a fat and its solid phase content (Wieske, 1970; Wieske and Brown, 1986). None of these attempts was very successful. Moreover, the methods have the same disadvantages as the linear method of Section 9.1.4.1.

9.1.5 CONCLUSION

The objective of this work is to develop a method that predicts the melting range and solid phase composition in an edible oil from the overall fat composition.

Existing predictive methods have no sound physical basis, are not generally applicable, and offer no understanding at all of the actual solid–liquid phase behavior of TAGs.

TAGs show polymorphism in the solid phase. This work will assume that each TAG crystallizes in three different polymorphs only: the unstable α -modification, the β' -modification, and the stable β -modification.

Due to their poor analytical accessibility, animal fats will not be considered in this work.

9.2 APPROACH TO THE PROBLEM

The ultimate amount and composition of the solid phase in a fat are determined by the position of the thermodynamic equilibrium solely, but the crystallization process may lead to significant deviations from the equilibrium composition in practical situations. Yet it appears that the starting point for any general predictive method of solid phase content in fats is a description of the solid–liquid phase equilibrium for all three polymorphic forms in which fats can crystallize. The thermodynamic equations that describe these equilibria are worked out. A number of steps are identified that need to be taken before a complete thermodynamic description can be obtained.

9.2.1 SOLID–LIQUID EQUILIBRIUM THERMODYNAMICS

In the end, the amount and the composition of the solid phase in a crystallized fat will be determined by the position of the solid–liquid phase equilibrium in that fat. Therefore, a general method for prediction of the solid fat content and the fat crystal composition from the fat composition must be based on a description of the solid–liquid phase equilibrium thermodynamics in TAGs.

Fats are mixtures of many different TAGs. It is known that many pairs of TAGs only show limited miscibility in the solid phase (Timms, 1984). Therefore it is very likely that

“solid fat” often will consist of a number of different coexisting solid phases. These solid phases do not necessarily have the same polymorphic form. A thermodynamic description of this complicated liquid–multiple solid equilibrium can be developed as follows.

Suppose a crystallized fat in equilibrium consists of N components and contains P phases (a liquid phase and $P - 1$ solid phases). The phase equilibrium must satisfy the following equations (Prausnitz, 1986):

1. The condition of thermodynamic equilibrium: the chemical potential of each component i in each phase must be equal to that in any other phase:

$$\mu_i^{\text{solid}} = \mu_i^{\text{liquid}} \quad (9.4)$$

for each solid phase. This equation can be worked out for solid–liquid equilibria as follows:

$$\mu_i^{0,S} + RT \ln \gamma_i^S x_i^S = \mu_i^{0,L} + RT \ln \gamma_i^L x_i^L \quad (9.5)$$

γ is the activity coefficient, and x the mol fraction.

$$\ln \left(\frac{\gamma_i^S x_i^S}{\gamma_i^L x_i^L} \right) = \frac{1}{RT} (\mu_i^{0,L} - \mu_i^{0,S}) \quad (9.6)$$

$$\ln \left(\frac{\gamma_i^S x_i^S}{\gamma_i^L x_i^L} \right) = \frac{\Delta H_{f,i}}{R} \left(\frac{1}{T} - \frac{1}{T_f} \right) - \frac{\Delta c_{p,i}}{R} \left(\frac{T_{f,i} - T}{T} \right) + \frac{\Delta c_{p,i}}{R} \ln \frac{T_{f,i}}{T} \quad (9.7)$$

With $\Delta c_p = 0.2 \text{ kJ/mol}$ and $T_f - T$ never greater than 70 and usually between 0 and 20 the terms with Δc_p are comparatively small and tend to cancel due to their opposite sign. As an approximation, they can therefore be neglected and there remains

$$\ln \left(\frac{\gamma_i^S x_i^S}{\gamma_i^L x_i^L} \right) = \frac{\Delta H_{f,i}}{R} \left(\frac{1}{T} - \frac{1}{T_f} \right) \quad (9.8)$$

2. The mole balance: the sum of the amount of each compound i in each phase f , present in fraction Φ^f must be equal to the overall amount of i , z_i (P is the total number of phases):

$$\sum_{f=1}^P x_i^f \Phi^f = z_i \quad (9.9)$$

3. The stoichiometric condition: the sum of the concentrations of the components in each phase must be equal to 100%:

$$\sum_{i=1}^n x_i^f = 1 \quad (9.10)$$

For P phases, this results in $PN + P$ equations with $PN + P$ unknowns. (P^*N mol fractions x and the quantity of P phases). This set of equations can in principle be solved to obtain the number of phases, the phase quantities and the composition of each phase from the overall composition and the temperature.

However, in order to solve these equations, four things are needed:

1. Values for the pure component properties: the heat of fusion and the melting point
2. Knowledge of the activity coefficients in the liquid phase
3. Knowledge of the activity coefficients in the solid phase
4. A method to solve this complex set of nonlinear equations.

Each of these points will be handled in separate sections of this chapter, so that in the end a full description of the liquid–multiple solid equilibrium in fats will evolve.

9.2.2 KINETICS OF CRYSTALLIZATION

Although the ultimate amount of solid phase and the solid phase composition are determined by thermodynamics solely, it is well known that due to the extremely slow diffusion rate in solids the equilibrium state is not always reached in practical situations (Zief and Wilcox, 1967). Hence both crystal composition and amount of solid phase that are observed may deviate considerably from what is predicted by thermodynamics. To avoid possible pitfalls, the effect of kinetic factors on the amount and composition of the solid phase of fats should be considered.

9.2.2.1 Polymorphism and Kinetics of Crystallization

When fats crystallize, they usually first crystallize in the most unstable polymorph, the α -modification, followed by slow recrystallization to more stable polymorphs. Direct crystallization into the β' - or β -modifications only takes place under conditions where little or no supercooling of the less stable modification is present. Palm oil crystallizes into the α -modification when supercooled to 10°C, into the β' -modification when cooled to 25°C, and into the β -modification when crystallized at 32°C (van Putte and Bakker, 1987). In all three cases, the thermodynamically most stable state is the β -modification.

Obviously solid fat content and crystal composition calculated for the β -modification using thermodynamics are poor predictions if the fat has crystallized in another polymorphic form. For a lot of practical situations, the most stable thermodynamic state is irrelevant: the residence time in the process line after the

onset of fat crystallization is only a few minutes for many edible fat products, so the unstable α -modification is the phase that should be considered. During the life of most edible fat products, the recrystallization to the β -modification does not take place: the product is already consumed while it is still in the β' -modification.

In spite of their limited lifetime, the β' -modification and even the α -modification may coexist very well during their existence in thermodynamic equilibrium with the liquid oil. Hence thermodynamics can be applied to predict the amount and composition of these intermediate solid phases. Application of equilibrium thermodynamics to unstable states is quite common: a mixture of benzene and air is not thermodynamically stable but should disintegrate into carbon dioxide and water, yet a vast amount of the literature exists about vapor–liquid phase equilibria with benzene.

9.2.2.2 Shell Formation

If a fat is slowly cooled while it is crystallizing, shell formation may occur. At each instant during the crystallization process, the surface of the growing crystals has the equilibrium composition. As temperature decreases, the equilibrium composition changes, but the composition of the inner part of the crystal does not change due to the low solid state diffusion rate. An inhomogeneous solid phase results, having a concentration gradient from the center of the crystals outward. The solid phase composition deviates from the equilibrium composition. It is reported that the solid fat content can decrease to only 80% of the equilibrium value (Timms, 1984) due to shell formation.

If diffusion limitations do not occur during crystallization, shell formation can be prevented by crystallizing isothermally. The rate-determining step in normal fat crystallization is the surface incorporation (Knoester et al., 1968; van Putte and Bakker, 1987). Indeed, when the crystal composition of an isothermally crystallizing fat is plotted against the reaction coordinate, shell formation seems absent ([Figure 9.6](#)).

Phase equilibrium thermodynamics will only give a reliable prediction of the solid phase composition and content if shell formation is absent. However, the effect of shell formation on solid phase content can be calculated from the equilibrium composition as a function of temperature, as will be shown in [Section 9.9.3.1](#).

9.2.2.3 Poor Crystallinity

If fat is crystallizing rapidly, it may result in poorly packed crystals. The clear point of such poorly packed solid phases may be considerably lower than the clear point predicted by thermodynamics. Through recrystallization, these badly packed crystals can rearrange into well-packed crystals. The results of Gibon (1984) show that without the presence of a liquid phase, badly packed crystal forms may persist for years. However, recrystallization via the liquid phase can occur relatively easily (Zief and Wilcox, 1967). Norton (Norton et al., 1985b) shows that partially hydrogenated palm oil initially crystallizes in a very badly packed β' -form, but that in the presence of about 50% of liquid oil, it only takes a few hours to rearrange into well-packed crystals. Also the rate of polymorphic transitions was observed to be much larger in the presence of liquid (Norton et al., 1985a).

Most fats used in edible fat products only contain 0%–40% of solid fat that is purposely crystallized into very small (1 μm and less) crystals. Deviations from thermodynamic predictions due to bad crystal packing will therefore be of minor influence.

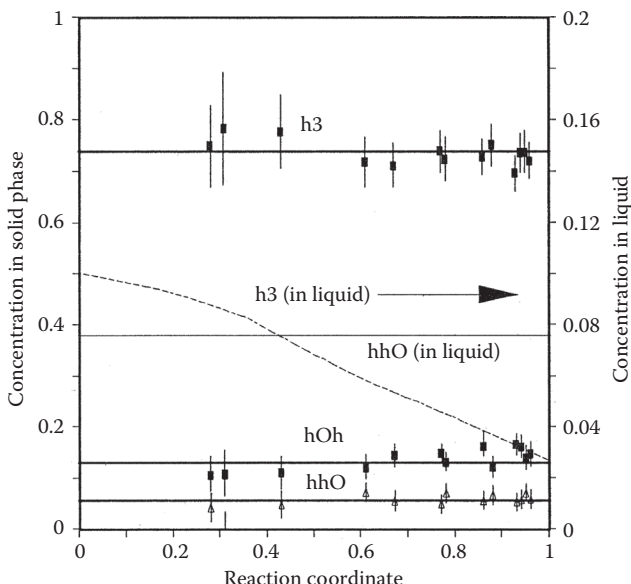


FIGURE 9.6 Composition of fat crystals from palm oil against the reaction coordinate of crystallization at 30°C. (Overall palm oil composition: h3, 0.1; hOh, 0.295; hhO, 0.075; hh, 0.104; hOO, 0.246; liquid, 0.176.) The palm oil was heated to 80°C, rapidly cooled to 30°C, and stored in a stirred tank. At regular time intervals over totally 21 h samples were taken. The solid fat content of the sample was measured and a small amount of liquid phase was rapidly filtered off and analyzed by AgNO_3 -HPLC. Crystal composition is calculated from overall composition, solid fat content, and the TAG analyses of the liquid phase of the samples. The error margin is indicated.

9.2.3 CONCLUSION AND APPROACH TO THE PROBLEM

The ultimate amount and composition of the solid phase in a fat are determined by the position of the thermodynamic equilibrium solely. The set of equations that describe a solid–liquid phase equilibrium can be solved, if a number of requirements are fulfilled.

For prediction of the amount and the composition of the solid phase that can crystallize from an oil in practical situations, calculation of the most stable state by solid–liquid phase equilibrium thermodynamics is insufficient. The solid–liquid phase equilibria of unstable polymorphic forms must be considered as well.

The crystallization route that is followed may lead to inhomogeneous solid phases, of which amount and composition can deviate significantly from the equilibrium composition. Yet in order to calculate the effect of the crystallization process on the solid phase composition, the equilibrium solid phase composition as a function of temperature must be known.

From this, it is clear that for a prediction of the amount and composition of the solid phase in fats as a function of temperature, the first requirement is a good description of the solid–liquid phase equilibrium for all three modifications in which fats crystallize. This work will therefore concentrate upon the development of this

description for liquid–multiple solid phase equilibria in fats. The end of this chapter will briefly come back to the influence of the crystallization process.

In Section 9.2.1, it was shown that for the description of the solid–liquid phase equilibrium four steps must be taken:

1. Find a method to solve the complex set of nonlinear equations that describe the liquid–multiple solid phase equilibrium.
2. Find values for the pure component properties: the heat of fusion and the melting point for all of the hundreds of TAGs involved.
3. Predict the activity coefficients of TAGs in the liquid phase.
4. Predict the activity coefficients in all possible solid phases.

These steps, in the order in which they are listed, are the subjects of the next chapters of this book.

9.3 FLASH CALCULATIONS

Solving the set of nonlinear equations that describe both the phase equilibrium between a liquid phase and a number of solid solutions in order to obtain the number and amount of coexisting phases and the composition of each phase present from a given overall composition and temperature is called a “solid flash” calculation. There is not any literature on such solid flash calculations. This section will try to alter the best existing algorithms for vapor–liquid flash calculations so that they can deal with polymorphism and a number of solid solutions.

9.3.1 INTRODUCTION

A flash calculation requires the simultaneous solution of the set of nonlinear equations (Equations 9.8 through 9.10). As this set cannot be solved analytically, an iterating procedure has to be used, that involves the following steps:

1. First make an estimate of the number of phases that will be present, the amount of phases and their composition.
2. Calculate the activity coefficients.
3. Make a new estimate, applying Equations 9.4 through 9.9, using the activity coefficients of 2.
4. Repeat steps 2 and 3 until a convergence criterion is met.
5. Perform a stability test to check whether the initial estimate of the number of phases is correct. If not, an extra phase is added with an estimate of its composition.
6. Repeat steps 2 through 4 until convergence is obtained and a stability criterion is met.

Whether quick convergence is obtained in steps 2 and 3 depends on the quality of the initial estimate and on the reliability of the stability test. If the initial estimate is poor, convergence may be slow, to a local, rather than a global minimum or to a

trivial solution with two phases having the same composition. A poor stability test will lead to an incorrect number of phases. A robust convergence procedure leads to the solution, even with a poor initial estimate. It follows that for composing a flash algorithm for fats, one needs the following:

1. A procedure to test the phase stability and provide an initial estimate for the phase compositions
2. An iterating procedure to solve the phase equilibrium and mass balance equations

9.3.2 INITIAL ESTIMATES AND STABILITY TESTS

There are no algorithms that directly give an estimate of the total number of phases that coexist. All methods start with assuming a single phase, either liquid or vapor. A simple calculation of the overall Gibbs energy learns which of the two is the most stable. For fats, the equivalent procedure is a comparison between the molar Gibbs energy of the fat in the liquid state and those in the α , β' , and β polymorphic forms:

$$g^f = \sum_{i=1}^n z_i (\mu_i^{0,f} + RT \ln \gamma_i^f z_i) \quad (9.11)$$

For convenience the authors set in the remainder of this chapter the chemical potential in the pure liquid reference state arbitrary to 0, so that Equation 9.11 reduces for the liquid state to

$$\frac{g^L}{RT} = \sum_{i=1}^n z_i (\ln z_i) \quad (9.12)$$

and for the 3 solid states to

$$\frac{g^m}{RT} = \sum_{i=1}^n z_i \left(\frac{\Delta H_f^m}{R} \left(\frac{1}{T} - \frac{1}{T_f^m} \right) + \ln \gamma_i^m z_i \right) \quad (9.13)$$

(with $m = \alpha$, β' , or β and neglecting all terms with Δc_p).

The phase that has the lowest molar Gibbs energy is the starting point for the stability test. The stability test checks whether addition of a new phase giving a decrease in the overall Gibbs energy is possible. Two types of stability tests for multicomponent, multiphase systems can be found in the literature: methods using a “splitting component” and methods based upon the tangent plane criterion of Gibbs.

9.3.2.1 Splitting Component Method

An example of this method is that of Gautam and Seider (1979). Shah (1980) uses a nearly similar procedure. Asselineau and Jacq (1989) proposes a simpler procedure where the “splitting component” has to be known beforehand. That is not the case for fats. Gautam and Seider first search all phases to locate the component with the highest activity. That component is named the “splitting component.” Secondly, the phase in which the splitting component is found is searched for the component that has the highest activity in a binary mixture with the splitting component, taking concentrations proportional to those in the splitting phase. Next, these two components are distributed over two trial phases by solving Equations 9.8 through 9.10 for this binary system using the well-known two phase flash Equation (Prausnitz, 1986) (Box 9.1), starting with two pure phases.

BOX 9.1 METHOD TO SOLVE A TWO-PHASE FLASH EQUATION

If an initial amount S is assumed for the first trial phase, then Equations 9.8 through 9.10 (the material balance combined with the phase equilibrium equation) give

$$x_i^B = \frac{z_i}{1 + S(K_i^{AB} - 1)} \quad (9.14)$$

and

$$x_i^A = \frac{z_i K_i^{AB}}{1 + S(K_i^{AB} - 1)} \quad (9.15)$$

where K is the distribution constant x^A/x^B that follows directly from Equation 9.8.

Subsequently a function $f(S)$ is defined:

$$f(S) = x_1^B + x_2^B - x_1^A - x_2^A = \sum_{i=1}^2 \frac{z_i (1 - K_i^{AB})}{1 + S(K_i^{AB} - 1)} \quad (9.16)$$

The equilibrium value for the phase split S is determined by calculating the zero of this function by a Newton–Raphson iteration:

$$S_n = S_{n-1} - \frac{f(S)_{n-1}}{\left(\frac{df(S)}{dS}\right)_{n-1}} \quad (9.17)$$

When S is found, the mole fractions are calculated and next the values of the distribution constants K are recalculated, using the new values for x . If the new K -values differ too much from the old ones, the function $f(S)$ is solved again, using the new values of K . If the value of S is not between 0 and 1, the split is considered unsuccessful.

Source: From Prausnitz, J.M., *Molecular Thermodynamics of Fluid Phase Equilibria*, Prentice Hall, New York, 1986.

If this calculation results in a split, then the remaining components are distributed over the two trial phases in order of decreasing binary activity with the splitting component. The distribution coefficients that are needed are obtained using the composition of the trial phases calculated so far for getting the activity coefficients.

$$K_i^{A,B} = \frac{x_i^A}{x_i^B} = \frac{\gamma_i^B}{\gamma_i^A} \quad (9.18)$$

This procedure is repeated, taking the component with the second highest activity as splitting component, etc. The Gibbs energy of all these trial splits is compared and that one with the lowest Gibbs energy is taken as initial estimate for a subsequent iterating procedure. If none of the binary flashes is successful, no trial phases can be formed and the solution is considered stable.

This procedure can be easily extended to deal with polymorphism in the solid phase. The number of trial splits needs to be extended: instead of one binary flash at each trial split, four flashes need to be considered; for example, if a component in a β phase is selected as “splitting” not only a β – β split but also β – β' split, a β – α split, and a β –liquid split must be considered. For a P -phase, N -component system maximally $4P(N - 1)$ trial splits must be evaluated.

9.3.2.2 Michelsen's Tangent Plane Criterion Method

The second approach is based on an extension of the well-known tangent plane criterion of Gibbs (Prausnitz, 1986) for phase stability to the multicomponent, multiphase situation. The tangent plane criterion says that if the tangent to the Gibbs free energy curve at the solution at no point lies above the Gibbs free energy curve then the Gibbs free energy is at a global minimum. The mixture is stable and will not show further demixing. In Figure 9.7, the tangent to the Gibbs free energy curve at F lies partially above the curve: F is an unstable mixture and will demix in A and B . The tangent to the curve at G lies at no point above the curve and G represents a stable mixture.

The general formulation of the tangent plane criterion is presented by Michelsen (1982) and the parts of interest for this work will be given next.

The total Gibbs energy of an original P -phase system ($P \geq 1$) apparently in equilibrium ($\mu_i^B = \mu_i^A$) and to be tested for stability is

$$G^{(I)} = \sum_{j=1}^P \sum_{i=1}^n n_i^j \mu_i^j = \sum_{i=1}^n n_i \mu_i^{(I)} \quad (9.19)$$

A different phase split into $L = P + 1$ phases with mole fractions y_i^j and totally N_1 mole in phase has a Gibbs energy of

$$G^{(II)} = \sum_{j=1}^L \sum_{i=1}^n N_j y_i^j \mu_i^j \quad (9.20)$$

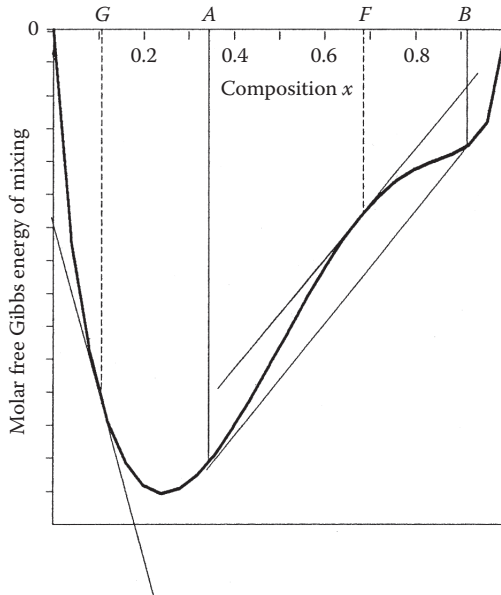


FIGURE 9.7 Gibbs free energy of mixing as a function of composition.

The energy difference between the two situations is

$$\begin{aligned}
 G^{(II)} - G^{(I)} &= \sum_{j=1}^L \sum_{i=1}^n N_j y_i^j \mu_i^j - \sum_{i=1}^n n_i \mu_i^{(I)} \\
 &= \sum_{j=1}^L \left(\sum_{i=1}^n y_i^j (\mu_i^j - \mu_i^{(I)}) \right) = \sum_{j=1}^L N_j F_j
 \end{aligned} \tag{9.21}$$

A phase split into L phases will occur if the Gibbs energy change is negative. That can only be so if at least one of the F_j is negative. Hence the stability criterion becomes: a system is stable if for any extra trial phase L with trial composition y :

$$F_L = \sum_{i=1}^n y_i^L (\mu_i^L - \mu_i^{(I)}) \geq 0 \tag{9.22}$$

This is the general form of the tangent plane criterion.

F_L is positive for any composition y if the minimum of F_L is positive. The composition of the extra phase L at that minimum of F_L is found by simple

differentiation of F_L to the $n - 1$ independent mole fractions y_i and setting all derivatives to O :

$$\frac{\partial F_L}{\partial y_i} = \frac{\partial \left((\mu_n^L - \mu_n^{(I)}) + \sum_{i=1}^{n-1} y_i [(\mu_i^L - \mu_i^{(I)}) - (\mu_n^L - \mu_n^{(I)})] \right)}{\partial y_i} \\ = (\mu_i^L - \mu_i^{(I)}) - (\mu_n^L - \mu_n^{(I)}) = 0 \quad (9.23)$$

which gives $\mu_i - \mu_i^{(I)} = \mu_j - \mu_j^{(I)} = K$, a constant. The minimum of F should be greater than zero for stability:

$$F(\min) = \sum y_i K = K \geq 0 \quad (9.24)$$

It is often simpler to deal with activity coefficients rather than chemical potentials. The activity coefficients of the trial phase L are introduced with the help of Equation 9.5:

$$k = \frac{K}{RT} = \frac{\mu_i^{0,L} - \mu_i^{(I)}}{RT} + \ln \gamma_i^L + \ln y_i^L \quad (9.25)$$

If addition to a trial phase L gives a negative value of k , then the addition of an infinitesimal amount of phase L (infinitesimal, in order not to change composition of the other phases and so $\mu^{(I)}$ will lower the Gibbs energy. The original situation was unstable. The composition of the trial phase L with minimum value for k can be found from an initial estimate of L by iterating

$$\ln(y_i^L e^{-k}) = \frac{\mu_i^{(I)} - \mu_i^{0,L}}{RT} - \ln \gamma_i^L \quad (9.26)$$

From the calculated values of $y_i^L e^{-k}$, the composition of the new trial phase is obtained from

$$y_i = \frac{y_i^L e^{-k}}{\sum_i y_i^L e^{-k}}$$

If the denominator in this equation is smaller than 1, it corresponds to $k > 0$ and so to stability.

If there is no minimum of K located on the plane between the initial estimate of the trial phase and one of the existing phases, the iteration procedure converges to a trivial solution, in which the trial phase has the same composition as one of the existing phases. Therefore a number of initial estimates are necessary, to ensure that the minimum of K is found if it exists.

Michelsen recommends taking a pure phase of each component as initial estimate plus a trial phase with a composition that is the average of the composition of all phases present. He has shown that the iterations need not be continued to convergence: for each initial estimate four iterations suffice. The trial phase with the most negative value of K is used as the initial estimate for the new phase, which will form after the split. If no negative values of K are found for all initial estimates, then only the one with the least positive value of K is converged. If this trial phase still yields positive values of K , then the original situation is considered stable.

Sometimes the authors found in highly nonideal systems after four iterations a phase with a negative K , indicating instability. But upon continuing iterations to convergence, it occurred that K turned greater than 0, indicating stability. Stopping after four iterations would have led to a false conclusion. Therefore always converge the trial phase that has the smallest K after four iterations.

Michelsen's stability test can be applied to solid–liquid equilibria in TAGs simply by increasing the number of initial estimates for the trial phases: pure β , β' , and α phases of each component plus a β , a β' , an α , and a liquid phase (if not already present) with a composition being the average of all phases already present. In an N -component, P -phase system maximally $3N + 4$ trial phases must be considered, about a factor P less than with the splitting component approach.

Michelsen's stability test has the advantage of being derived from the proven thermodynamic tangent plane criterion and requiring only a small number of trial phases, while the method of Gautam and Seider and like methods have no fundamental guarantee that phase instability is always detected. However, in Michelsen's procedure the true minimum of K may be overlooked because of the selection of starting values for the trial phases. The algorithm of Michelsen and a number of algorithms similar to that of Gautam and Seider have been tested on several different vapor liquid and vapor liquid–liquid–liquid equilibria (Swank and Mullins, 1986). Generally Michelsen's algorithm proved to be the most reliable. In this chapter, the performance of both methods with solid–liquid equilibria in fats will be tested.

9.3.3 ITERATING PROCEDURES

Once a good initial estimate of the number of phases, their polymorphic form, and their composition is obtained, the equilibrium composition and phase quantities can be calculated by solving Equations 9.8 through 9.10. The iterating procedures to solve these phase equilibria and mass balance equations fall into two categories:

1. The direct substitution methods
2. Methods involving the minimization of the Gibbs free energy

9.3.3.1 Direct Substitution

This is the multiphase multicomponent analogue of the two- phase two-component flash equation, described in Box 9.1 (Equations 9.15 and 9.16).

The function $f(S)$ is redefined for the P -phase analogue as a set of $P - 1$ equations:

$$\sum_{i=1}^n \frac{z_i (K_i^{mP} - 1)}{1 + \sum_{f=1}^{P-1} \Phi_f (K_i^{fP} - 1)} = 0 \quad (m = 1, 2, \dots, P - 1) \quad (9.27)$$

where

m ranges from 1 to $P - 1$

K^{mP} is the distribution coefficient of a component over the phases m and P

The solution of these sets of equations to obtain the $P - 1$ phase fractions is carried out by Newton–Raphson iteration. Then using these phase fractions, new compositions are obtained. Next, new values for the distribution constants are calculated with the appropriate thermodynamic models. If these new values do not agree with the previous ones within a certain tolerance, the set equations is solved again for the $P - 1$ phase fractions, using the new values of K .

Direct substitution is a very fast and reliable method for phase equilibria where the values of the activity coefficients do not depend strongly on the phase composition. It therefore seems most suited for calculating a phase equilibria, where all activity coefficients are 1 (see Section 15.5) and the values of K only depend on temperature, so that only one iteration will be sufficient.

When the activity coefficients strongly depend on the phase composition and/or when phase envelopes are very narrow, like it is often the case in the β - and β' -modifications, the direct substitution method converges very slowly. Examples of the need for several hundreds of iterations are known (Crowe and Nishio, 1975; Michelsen, 1982). Various acceleration procedures exist, the general dominant eigenvalue method (GDEM) of Crowe and Nishio (1975) being recommended by Michelsen (1982) and by Swank and Mullins (1986). Even with these methods, convergence is not always obtained in the case of vapor–liquid equilibria, and other methods had to be used (Michelsen, 1982).

The authors found for the systems in this work that three GDEM acceleration steps are sufficient, each after five iterations and using more than two eigenvalues, even when more than three phases were present, offered no significant improvement in acceleration. This is in agreement with the findings of Michelsen (1982) and Swank and Mullins (1986).

9.3.3.2 Gibbs Free Energy Minimization

The other method to solve the phase equilibrium and material balance equations is to minimize the Gibbs free energy. When the Gibbs energy is at its minimum the requirement for equilibrium, Equation 9.4 is satisfied. The problem can hence be reformulated for a N -component, P -phase system as

Find the minimum of

$$G_{\vec{n}} = \sum_{j=1}^P \sum_{i=1}^N n_i^j \mu_i^j = \vec{n} \cdot \vec{\mu} \quad (9.28)$$

subject to the constraints of the mass balance and the requirement of all $n_i^j \geq 0$.

The two vectors are defined as

$$\vec{n} = \begin{pmatrix} n_1^1 \\ n_2^1 \\ \cdot \\ \cdot \\ n_N^P \end{pmatrix}, \quad \vec{\mu} = \begin{pmatrix} \mu_1^1 \\ \mu_2^1 \\ \cdot \\ \cdot \\ \mu_N^P \end{pmatrix} \quad (9.29)$$

The Gibbs free energy can be minimized by several variations on Newton's method (Box 9.2).

BOX 9.2 NEWTON'S METHOD FOR FINDING A MINIMUM IN THE GIBBS ENERGY FUNCTION

The Gibbs free energy close to an initial estimate of the solution is given by a Taylor expansion:

$$\begin{aligned} G_{\vec{n} + \vec{\Delta n}} &= G_{\vec{n}} + \overrightarrow{\nabla G_{\vec{n}}} \cdot \overrightarrow{\Delta n} + \frac{1}{2} \overrightarrow{\Delta n}^T \cdot \nabla^2 G_{\vec{n}} \cdot \overrightarrow{\Delta n} \\ &= G_{\vec{n}} + \sum_{j=1}^P \sum_{i=1}^N \frac{\partial G_{\vec{n}}}{\partial n_i^j} \Delta n_i^j + \frac{1}{2} \sum_{j=1}^P \sum_{i=1}^N \sum_{k=1}^P \sum_{h=1}^N \frac{\partial^2 G_{\vec{n}}}{\partial n_i^j \partial n_h^k} \Delta n_i^j \Delta n_h^k \end{aligned} \quad (9.31)$$

Since the first term of this equation is constant, the minimum Gibbs energy is obtained when the two right-hand side terms

$$\Phi_{\vec{\Delta n}} = \overrightarrow{\nabla G_{\vec{n}}} \cdot \overrightarrow{\Delta n} + \frac{1}{2} \overrightarrow{\Delta n}^T \cdot \nabla^2 G_{\vec{n}} \cdot \overrightarrow{\Delta n}$$

have a minimum.

The minimum of this quadratic function Φ is easily calculated by setting its derivative to zero:

$$\nabla^2 G_{\vec{n}} \cdot \overrightarrow{\Delta n} = -\overrightarrow{\nabla G_{\vec{n}}} \quad (9.32)$$

This set of linear equations in Δn_i^j is readily solved and the resulting vector $\overrightarrow{\Delta n}$ is called the Newton direction. $\vec{n} + \overrightarrow{\Delta n}$ is an improved estimate of the composition at the minimum.

The next step would be to calculate new values for $\overrightarrow{\nabla G}$ and $\nabla^2 G$ at this improved estimate, determine the Newton direction from this point, and repeat this until convergence is obtained.

Two criteria are added to the standard Newton method:

1. The solution should be within the constraints imposed by the mass balance and not result in negative concentrations.
2. It should be verified that the extreme obtained is actually a minimum and not a maximum or a saddle point.

The mass balance Equation 9.9 can be equivalently formulated for each component i as follows:

The elements i of the vector $\vec{\Delta n}$ should obey

$$\sum_{j=1}^P \Delta n_i^j = 0 \quad (9.30)$$

This set of N linear constraints can be used to eliminate N variables from Equation 9.32, so that indeed the mass balance is satisfied. Box 9.3 describes a general way of doing this.

BOX 9.3 MODIFICATION OF NEWTON'S METHOD OF BOX 9.2 TO SATISFY MASS BALANCE CONSTRAINTS

The set of linear mass balance constraints can be alternatively formulated as follows:

$$A \cdot \vec{\Delta n} = \vec{0}, \quad A = (I_1, I_2, \dots, I_P) \quad (9.33)$$

The $(P*N) \times N$ matrix A consists of P identity matrices with dimension N .

If a second matrix Z of which its columns form a basis for the set of all vectors orthogonal to the rows of A is defined, then any vector $\vec{\Delta n} = Z \cdot \vec{\Delta n}^z$ will satisfy the mass balance constraints: $A \cdot \vec{\Delta n} = A \cdot Z \cdot \vec{\Delta n}^z = 0 \cdot \vec{\Delta n}^z = 0$.

Such a matrix Z of which the columns are orthogonal to the rows of A is

$$Z = \begin{pmatrix} I_1, I_2, \dots, I_{p-1} \\ -I_\mu \end{pmatrix} \quad (9.34)$$

in which I is an identity matrix of dimension N and I_μ is an identity matrix of dimension N and I_μ is an identity matrix of dimension $(N-1)*P$.

If $\vec{\Delta n}$ in Equation 9.31 is substituted by $\vec{\Delta n}^z$, then the solution to the constrained problem of Equation 9.32 is given by

$$\begin{aligned} \nabla^2 G_{\vec{n}}^Z \cdot \vec{\Delta n}^Z &= -\nabla G_{\vec{n}}^Z, \quad \nabla^2 G^Z = Z^T \cdot \nabla^2 G \cdot Z \\ \nabla G^Z &= Z^T \cdot \nabla G \end{aligned} \quad (9.35)$$

The solution $\vec{\Delta n}^z$ is transformed to the original $\vec{\Delta n}$ by multiplication with Z .

Non-negative values for the mole numbers can be assured by introduction of a so-called step size λ . The new estimate for the composition is set to: $\vec{n} + \lambda \vec{\Delta n}$. The step size λ is taken as the largest possible value not exceeding 1 that

- Still results in a new estimate of the solution in which all mole numbers n_i^j are greater than a small positive number δ
- Gives a decrease in Gibbs free energy

The value that is chosen for δ depends on the precision of the computer used. In this way, Δn^z is guaranteed that no negative mole numbers will occur and that the calculations remain numerically stable. λ should differ from unity only in the first few Newton iterations.

A Newton direction that points to a minimum in the Gibbs energy is only obtained when the matrix of the second derivative of the Gibbs energy to all mole numbers, $\nabla^2 G_{\vec{n}}$, the so-called Hessian, is positive definite, that is, has only positive eigenvalues. In the case of activity coefficients only slightly different from 1 this is so. However, in case of solid β and β' phases, it is not necessarily true. If the Hessian is not positive definite, the iterations may converge to a maximum in the Gibbs energy or even not converge at all.

Gautam and Seider (1979) solve this problem by ignoring the second derivative of the excess Gibbs energy (ignoring the compositional derivatives of the activity coefficients). This is called the “Rand method.” The Hessian is in that case always positive definite. Because of the inaccurate Hessian used, the Rand method will converge slower than when the full-second derivative is used.

Michelsen (1982) recommends the method of Murray et al. (1981). In cases where the Hessian is not definite, an approximate Hessian is calculated that is positive definite and looks as much as possible like the original Hessian (Box 9.4).

BOX 9.4 MURRAY'S METHOD TO FORCE A POSITIVE DEFINITE SECOND DERIVATIVE OF THE GIBBS ENERGY TO ALL MOLE NUMBERS

The Hessian is decomposed by a so-called Cholesky decomposition into a lower triangular matrix L and a diagonal matrix D :

$$\nabla^2 G = L \cdot D \cdot L^T \quad (9.36)$$

The j th column of the L matrix is defined from the previous columns by the following equations:

$$d_j = \nabla^2 G_{jj} - \sum_{s=1}^{j-1} d_s l_{js}^2 \quad (9.37)$$

BOX 9.4 (continued)

$$l_{ij} = \frac{1}{d_j} \left(\nabla^2 G_{ij} - \sum_{s=1}^{j-1} d_s l_{js} l_{is} \right) \quad (9.38)$$

If the Hessian is positive definite, all the elements of the diagonal of D are positive. In the other case, the decomposition results in a matrix D with some negative elements and a matrix L with sometimes extremely large values. Murray's method modifies the elements of the L and D matrices during decomposition, and if during decomposition an element d_j becomes smaller than a small positive number Δ , d_j is replaced by Δ . The value of delta is determined by computer precision. If, by using this value of d_j for the calculation of the next column of L , one of the values of the elements of L next exceeds a certain maximum, the value of d_j is increased such that the elements of L will be below that maximum. The maximum of the elements of the column of L to be calculated is given by

$$l_{ij}^2 \leq \frac{1}{d_j} \cdot \max \left(\gamma, \frac{\xi}{\sqrt{N^2 - 1}}, \epsilon_M \right) \quad (9.39)$$

where

- γ is the largest diagonal element of the Hessian
- ϵ is the largest off-diagonal element of the Hessian
- ϵ_M is the precision of the computer used

Using the modified forms of the L and D matrices, a modified Hessian is calculated. This modified Hessian is positive definite. The decomposition and recombination of the original Hessian is numerically stable. The resulting modified Hessian is a very close positive definite approximation of the original Hessian.

Instead of using the original Hessian, the modified Hessian is subsequently used when solving Equation 9.32; then the resulting Newton direction always points to smaller values of the Gibbs energy.

9.3.3.3 Removal of Phases

Occasionally, it is necessary to remove one of the phases while solving the flash equations. This can occur in cases where initially a liquid phase is most stable, next a phase split occurs into liquid and β , thereafter a second split into liquid, β and β' , and during subsequent iterations, the amount of liquid starts to approach zero. Calculations become increasingly inaccurate in that case. Therefore, if the amount of

any of the phases present drops below 5% during iterations, it is examined whether two phases can “coalesce” such that a reduction in Gibbs energy is obtained. In that case, iterations are continued with a reduced number of phases.

9.3.4 COMPARING METHODS

9.3.4.1 Criteria

The procedures that were outlined and modified in the previous section have to be compared on their performance with multicomponent multiphase solid–liquid flashes. Unfortunately, experimental data do not exist in which the number of coexisting solid phases and their composition are known. It is probably impossible to obtain such data for TAG systems. As an alternative the following procedure is adopted.

Both stability tests are applied and the initial estimates are converged using all three convergence methods. Criteria for performance of the stability tests are as follows:

1. Indication of instability where this is not the case: the test indicates instability and results in a phase split while during subsequent convergence this phase is removed again.
2. Failure to predict instability: one test indicates instability, and the other does not, while the resulting converged phase split indeed has a reduced Gibbs free energy.
3. Number of iterations needed to converge the initial estimate.

Performance criteria for the convergence methods are as follows:

1. Convergence
2. The total computing time to reach convergence

As test cases the following systems were considered:

1. Fully hardened palm oil (PO58), a six-component system containing all TAGS that can be formed from palmitic and stearic acids, at temperatures between 40°C and 70°C.
2. A ternary system of SSS, PPP, and SES, where two components that are completely immiscible in the solid phase are combined with a component that is partially miscible with both. Temperature is varied between 50°C and 75°C.

As description of the excess Gibbs energy both the 2-suffix and the 3-suffix Margules equation were used (see Section 9.7.7.1). The necessary binary interaction coefficients were obtained by fitting the data of de Brujne (Knoester et al., 1972; Section 9.7.2.4). Calculations were performed three times, first only allowing the formation of the α -modification, secondly only allowing the β' -modification, and finally allowing all modifications.

Swank and Mullins (1986) performed a similar exercise with a number of vapor–liquid phase equilibria. They judged Michelsen's stability test as the most reliable and direct substitution as the quickest convergence method. However, not all problems could be solved by direct substitution.

A combination of Michelsen's stability test plus a Murray minimization always lead to the correct solution.

9.3.4.2 Test Results

A computer program was written in Turbo Pascal 5.0 for MS-DOS PCs that implements the two initial estimate and stability test procedures and the three methods to solve the flash equations.

The stability test of Michelsen clearly performs better than the algorithm of Gautam and Seider. It is faster and more reliable; especially in the ternary test system the splitting component approach indicates instability, where this is not the case.

Both tests were perfectly able to deal with polymorphism in the solid phase. The coexistence of a number of stable β and β' phases in PO58 was obtained without problems.

The three convergence algorithms are compared in Table 9.3.

“No conv.” in the table means that convergence to a gradient norm of 10^{-12} was not obtained within 50 iterations. Except for the α phase and cases where no convergence was obtained, direct substitution converged within 6–25 iterations, while the Murray method needed 2–6 iterations.

For α phase calculations (in Section 15.5 it is shown that miscibility in the α -modification is ideal, so only one solid phase plus a liquid phase are present), direct substitution is especially for larger systems ($N = 6–50$) the quickest method that will converge safely.

The Rand method has, as expected, problems with converging in highly nonideal systems and in systems where the initial estimate contains concentrations close to zero. Performance is inferior to both other methods.

TABLE 9.3
Average Time per Flash (of 60 Flashes) for the Test Systems
(on a Compaq 386/25 PC under MS DOS)

System	Number of Phases	Direct Substitution	Rand	Murray (s)
PO58 (α form)	2	0.1 s	0.3 s	0.3
PO58 (β' , 2 suffix)	3	0.5 s	no conv.	0.8
PO58 (β' , 3 suffix)	3	no conv.	no conv.	1.4
PO58 ($\beta' + \beta$, 2 suffix)	4	no conv.	no conv.	2.0
PO58 ($\beta' + \beta$, 3 suffix)	5	no conv.	no conv.	2.7
(SSS/PPP/SES) α	2	0.08 s	0.12 s	0.12
(SSS/PPP/SES) β'	2	0.16 s	0.3 s	0.12
(SSS/PPP/SES) β	3	0.16 s	0.2 s	0.24

The Murray method always resulted in a reasonably fast and safe convergence and is therefore the best method to be used for the β' - and β -modifications, where demixing in the solid phase can occur. It is slower than the direct substitution method but is more reliable.

These conclusions are in line with those of Michelsen: for vapor–liquid flashes with one liquid phase, he suggests the use of direct substitution method, while for VLL and VLLL flashes a Murray minimization works out better.

For flash calculations in fats, it is therefore recommended to use Michelsen's stability test for initial estimates and Murray minimization of the Gibbs free energy for obtaining the final solution. For the α -modification, the direct substitution method should be used.

9.3.5 CALCULATION OF DIFFERENTIAL SCANNING CALORIMETRY CURVES

DSC is one of the most frequently used techniques to study the solid phase behavior of TAGs.

With DSC, the apparent heat capacity of a sample is measured as a function of the temperature. It is often used as a tool to characterize a crystallized fat (Juriaanse, 1985; Christoffersen, 1986; Busfield et al., 1990; Wesdorp and Struik, 1990) and slowly replaces the more traditional methods for quality control of cocoa butter equivalents and replacers (Smith, 1988). Comparison of experimental and calculated DSC curves enables a better interpretation of those curves.

Make the simplifying approximation that the heat capacity of solid and liquid fat is equal, then the equilibrium DSC curve at infinitive slow scanning rate of any fat mixture can be calculated from

$$c_p^{\text{apparent}} = c_p + \left(\frac{\partial H}{\partial T} \right)_n \quad (9.40)$$

$$H = H^E + \sum_{j=1}^P \sum_{i=1}^N n_i^j H_i^{0,j}$$

For convenience, set H (liquid) to zero for each component, which implies that H^0 becomes equal to the heat of fusion of the pure component in that modification. Another assumption is to neglect the excess entropy, which will be most likely comparatively small. The DSC curve can then be calculated from

$$c_p^{\text{apparent}} = c_p + \frac{\partial G^E}{\partial T} + \sum_{j=1}^P \sum_{i=1}^N H_i^j \frac{\partial n_j^i}{\partial T} \quad (9.41)$$

The two partial derivatives in this formula are easily obtained by numerical differentiation, which requires two flash calculations for each point on a DSC curve. Calculations are speeded up considerably when the outcome of the flash calculation for one point is used as initial estimate for calculation of the next point.

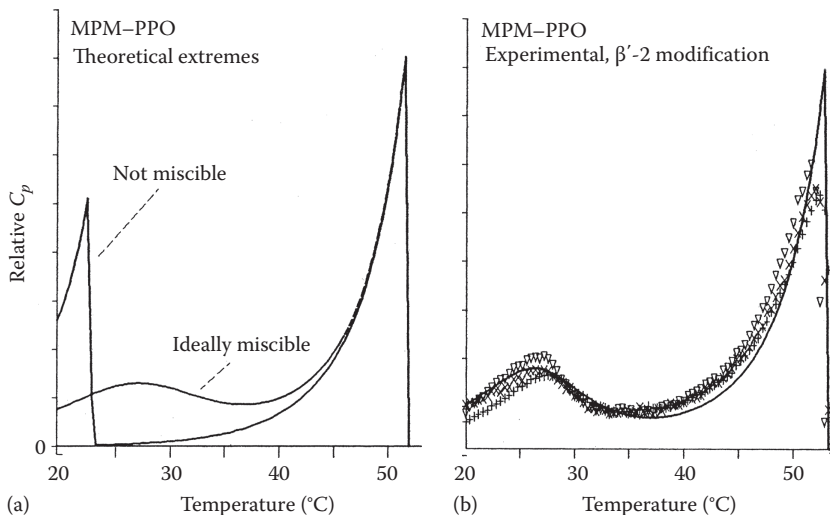


FIGURE 9.8 DSC melting curves of a mixture of 25% MPM, 25% PPO, and 50% OOO: (a) theoretical extremes: ideal and no solid state miscibility; (b) experimental (points) and calculated (line) curves.

Norton et al. (1985) constructs a DSC curve by using the Hildebrand equation for calculating the partial derivatives. The applicability of this approach is rather limited, because the Hildebrand equation describes only the phase behavior of pure (=completely demixed) solid phases. Solid phase miscibility has a large influence on the shape of a DSC curve as is shown in Figure 9.8 for the ternary system 25 MPM/25 PPO/50 000 in the β' form. This system cannot be described by the Hildebrand equation.

As will be shown in Section 9.7.5.4, the ternary of Figure 9.8 can be described by the 2-suffix Margules equation in which the binary interaction coefficient $A_{\text{MPM-PPO}}$ is 1.8 + 0.3. Although no demixing of the solid phase takes place, still two peaks occur in the DSC curve. In the literature, the appearance of two peaks in DSC thermograms of a fat is often used as indication for the presence of two solid phases (Murray et al., 1981; Timms, 1984; Yap et al., 1989; Wesdorp and Struik, 1990). In fact, it only indicates the presence of two groups of TAGs in the fat that have a clear difference in melting point, but may have cocrystallized.

Figure 9.8 also shows that DSC, together with the calculation procedures of this report, forms an elegant method for determination of binary interaction parameters and verification of excess Gibbs energy models.

9.3.6 CONCLUSION

A flash calculation consists of two parts: a stability test that gives an initial estimate of the phase compositions when it detects that a phase split can occur, and a convergence method that determines the phase compositions and phase quantities at equilibrium starting from the initial estimate. As no procedures for solid–liquid flashes were available, several existing methods for vapor–liquid flashes were adapted and tested for their performance with solid–liquid flashes in fats.

1. The best stability test is the so-called stability test of Michelsen, that, with some small changes, can perfectly handle solid fats and polymorphism.
2. Only in the case of the α -modification (ideal solid miscibility) the normal direct substitution method for solving the flash equation gives a quick, reliable result.
3. For the β' - and β -modifications (highly nonideal solid phases), direct substitution is unreliable. The flash problem can better be solved with a Gibbs free energy minimization using Murray's method (a modified Newton method). This method is somewhat slower but very reliable.
4. Flash calculations can be applied for simulation of DSC curves of fat blends.

9.4 PURE COMPONENT PROPERTIES

For a thermodynamic description of the solid–liquid phase equilibrium in a fat, the enthalpy of fusion and melting point of each modification of each TAG in the mixture are needed. These pure component properties can impossibly be measured for all TAGs. Therefore correlations between structural characteristics and the properties must be developed. Existing correlations for heat of fusion and melting point are only reliable for mono-acid TAGs. Therefore, after having appended literature data with a set of experimental data, correlations for the heats of fusion and the melting points of TAGs in the α -, β' -, and β -modifications are developed.

9.4.1 LITERATURE DATA AND CORRELATIONS

9.4.1.1 Correlating Enthalpy of Fusion and Melting Points of Lipids

It is often assumed (Bailey, 1950; Broadhurst, 1962; Flory and Vrij, 1963; Wurflinger, 1972; Billmeyer, 1975; Zacharis, 1977; Timms, 1978; Dollhopf et al., 1981; de Brujne and Eedenburg, 1983; Perron, 1984; Bommel, 1986; Larsson, 1986) that the enthalpy and entropy of fusion of lipids (alkanes, fatty acids, methyl esters, TAGs) can be seen as the sum of a contribution of the hydrocarbon chains that depends linearly on the chain length and a contribution of the end and head groups that is independent of chain length (Equations 9.42 and 9.43, and Figure 9.9).

$$\Delta H_f = hn + h_0 \quad (9.42)$$

$$\Delta S_f = sn + s_0 \quad (9.43)$$

where n is the carbon number of the component.

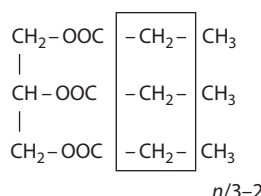


FIGURE 9.9 Schematic representation of the head group, the hydrocarbon chain and the end group of a TAG.

TABLE 9.4
Values for the Incremental Hydrocarbon Chain Contribution to the Enthalpy of Fusion (*h*) and the Entropy of Fusion (*s*)

Compound	Polymorph	<i>h</i> (kJ/mol CH ₂)	<i>s</i> (J/K, mol CH ₂)
<i>n</i> -Alkanes	α	2.64 ⁴³ , 2.5 ⁴⁴	6.4 ⁴³ , 6.0 ⁴⁴
TAGs	α	2.5 ⁴⁵ , 3.4 ⁵² , 3.6 ⁵³	6.1 ⁴⁵
<i>n</i> -Alkanes	β'	3.2 ⁴³ , 3.8 ⁴⁴ , 3.98 ⁴⁶ , 3.86 ⁴⁷	7.7 ⁴³ , 9.7 ⁴⁴ , 9.52 ⁴⁶
Methylesters	β'	3.78 ⁴⁸	9.2 ⁴⁸
TAGs	β'	3.87 ⁴⁵ , 3.25 ⁴⁹	9.8 ⁴⁵
<i>n</i> -Alkanes	β	4.11 ⁴³ , 4.12 ⁵⁰	9.9 ⁴³ , 9.89 ⁵⁰
Methylesters	β	4.28 ⁴⁸	10.3 ⁴⁸
Fatty acids	β	4.2 ² , 4.3 ⁴⁹	11.1 ⁴⁹
Diglycerides	β	4.28 ⁴⁹	10.5 ⁴⁹
Monoglycerides	β	4.28 ⁴⁹	10.5 ⁴⁹
TAGs	β	4.28 ⁴⁹ , 4.20 ⁴⁵	10.5 ⁴⁵ , 10.6 ⁴⁹

Note: Numbers in superscript are references.

In this view, the incremental hydrocarbon chain contributions *h* and *s* do not depend on the nature of the compound but only on the way the hydrocarbon chains are packed: *h* and *s* are universal lipid constants that only depend on the polymorphic form in which the lipid has crystallized. This is experimentally confirmed (Table 9.4). Only the values for *h* of Bailey (1950) and de Brujne and Eedenburg (1983) for the α-modification of TAGs deviate. Perron (1984) showed that these numbers were derived from very unreliable data.

The end group contributions *h*₀ and *s*₀ are specific to each class of lipids. Correlating the properties of alkanes and methylesters results in different values for *h*₀ and *s*₀ for these two groups of components.

The melting point *T* is simply given by the ratio of the enthalpy and entropy of fusion:

$$T_f = \frac{\Delta H_f}{\Delta S_f} = \frac{hn + h_0}{sn + s_0} \quad (9.44)$$

Expanding the denominator in this equation into a power series of 1/*n* gives

$$T_f = \frac{h}{s} \left(1 + \left(\frac{h_0}{h} - \frac{s_0}{s} \right) \frac{1}{n} - \frac{s_0}{s} \left(\frac{h_0}{h} - \frac{s_0}{s} \right) \frac{1}{n^2} + \dots \right) \quad (9.45)$$

This equation can be cut off after the second or the third term:

$$T_f = T_\infty \left(1 + \frac{A}{n} - \frac{AB}{n^2} \right) \quad (9.46)$$

$$T_f = T_\infty \left(1 + \frac{A}{n} \right) \quad (9.47)$$

The constants T_∞ , A , and B are given by

$$T_\infty = \frac{h}{s}, \quad A = \frac{h_0}{h} - \frac{s_0}{s}, \quad B = \frac{s_0}{s} \quad (9.48)$$

This implies that if the melting points of a class of lipids have been correlated, only one data point for the enthalpy of fusion is in principle sufficient to obtain a correlation for the enthalpy of fusion of the complete class of lipids.

Equation 9.44 has successfully been used by Zacharis (1977) to correlate the melting points of a large number of lipids: *n*-alkanes, methylesters, ethylesters, fatty acids, mono-acids, mono-, di-, and tria-cylglycerols, phosphoglycerides, and dicarboxylic acids. He has found values for T_∞ that vary between 390 and 410 K.

9.4.1.2 Data and Correlations for TAGs

The main difficulty in the development of correlations for the thermal properties of TAGs is that TAGs do not belong to one class of lipids in the sense of Section 15.4.1.1. Not all TAGs share the same end group. This becomes clear when a saturated TAG is formally denoted by the lengths p , q , and r of its three fatty acid chains, that is, p , q , and r . P is always the shortest of the fatty acid chains on the 1- and 3-position of the glycerol group. For example, myristoyl-stearoyl-palmitoyl-glycerol (MSP) is denoted as 14.18.16. The chain length differences x and y are defined as follows:

$$x = q - p$$

$$y = r - p$$

Only TAGs having the same value of x and y belong to a family of TAGs that share the same end group. For TAGs that differ in x and y , the value of the head and end group contributions h_0 and s_0 from Equations 9.39 and 9.40 are different.

The dependency of the “head and end group” contributions h_0 , s_0 , A , and B from x and y and from the presence of unsaturation in the hydrocarbon chains must be accounted for in the development of general correlations for all TAGs. In this work, this will be accomplished by the addition of two extra terms to Equations 9.39 and 9.40:

$$\Delta H_f = hn + h_0 + h_{xy}f_{xy} + h_{unsat}f_{unsat} \quad (9.49)$$

$$\Delta S_f = sn + s_0 + s_{xy}f_{xy} + s_{unsat}f_{unsat} \quad (9.50)$$

The functions f_{xy} and f_{unsat} should account for the effects on the thermodynamic properties of differences in chain length and degree of unsaturation. Their functional form cannot a priori be established.

9.4.1.2.1 Literature

The literature on the enthalpy of fusion of TAGs was reviewed up to 1975 by Timms (1978). Timms provided the enthalpy of fusion of 42 triglycerides, 19 saturated (16 beta and 3 beta'), and 23 unsaturated TAGs. The data were correlated using Equation 9.39:

$$\Delta H_f^\beta = 4.28n - 32.6 \text{ kJ/mol} \quad (9.51)$$

$$\Delta H_f^{\beta'} = 0.76\Delta H_f^\beta \quad (9.52)$$

For mixed acid saturated TAGs the enthalpy of fusion should be reduced by 18.3 kJ/mol. The enthalpy of fusion of unsaturated TAGs was described by setting an effective carbon number for each unsaturated fatty acid (O [oleic acid] = 10.4, E [elaidic acid] = 13.9, I [linoleic acid] = 8.9). The root mean square error between experimental and predicted data is 4.3 kJ/mol. The values for h agree with those reported for other compounds (**Table 9.4**).

Since 1975, various data on the enthalpy of fusion of the stable beta modification of saturated fatty acids have been reported (Hagemann, 1975, 1988; Zacharis, 1975; Lovegren, 1976; Gray and Lovegren, 1978; Ollivon and Perron, 1979, 1982; Hagemann and Rothfuss, 1983; Norton, 1984; Perron, 1984; Gibon, 1986; Garti et al., 1988; Sato et al., 1989). The majority of these data concern mono-acid TAGs. There is only one observation for the α -enthalpy of fusion of a mixed acid saturated TAG (PSP, Gray and Lovegren, 1978). The data for the β' -modification of saturated TAGs mainly concern PSP and LML. Some data on the mono-acid saturated TAGs are available, but they show large deviations (Ollivon and Perron, 1982; Hagemann and Rothfuss, 1983; Perron, 1984), which are ascribed to the existence of a second, less stable β' -form. Only the data for the most stable β' -form were taken. The number of data for the lesser stable forms was too small and the data showed no consistency.

The data of Hagemann (1975) for AAA to 30.30.30 for the β' form and for BBB to 26.26.26 for the β' -form look very unreliable: the enthalpy of fusion levels off and starts to decrease with increasing carbon number, which is in contradiction to the generally observed trend in lipids. The same holds for the data of Perron (Ollivon and Perron, 1982) for the β' -form of AAA and BBB, which is also admitted by Perron in a later article (Perron, 1984).

The data reported by Garti, Schlichter, and Sarig (Gray and Lovegren, 1978) for all modifications differ completely from all other values reported. Therefore they are disregarded in this report.

Perron (Bommel, 1986) has carried out the most extensive work on development of correlations for the enthalpy of fusion and melting points of TAGs since Timms. His correlations for the enthalpy of fusion of mono-acid TAGs are as follows:

$$\Delta H_f^\alpha = 2.5n - 27.5 \text{ kJ/mol} \quad (9.53)$$

$$\Delta H_f^{\beta'} = 3.87n - 19.2 \text{ kJ/mol} \quad (9.54)$$

$$\Delta H_f^\beta = 4.20n - 29.9 \text{ kJ/mol} \quad (9.55)$$

TABLE 9.5
**Number of TAGs for Which Melting
 Points and Enthalpies of Fusion Are
 Available in the Literature**

	ΔH_f			T_f		
	α	β'	β	α	β'	β
Saturated	10	10	30	65	54	87
Unsaturated	8	11	16	50	47	49

Perron modeled the enthalpy of fusion of an unsaturated TAG as that of the corresponding saturated TAG minus a contribution of the double bonds:

$$\Delta H_f(\text{unsat}) = \Delta H_f(\text{sat}) - 115(1 - e^{-0.706\Delta}) \quad (9.56)$$

where Δ = number of double bonds in the TAG.

Perron's values for h agree very well with those for other compounds given in Table 9.4.

Perron did not give relations for the enthalpy of fusion of mixed acid TAGs. However, he correlated the α - and β -melting points of 19 different TAG families using Equation 9.44. It resulted, as expected, in large fluctuations of the constant A .

The total collection of data from the literature and from the database of Unilever Research Vlaardingen resulted in 152 values for the enthalpy of fusion and 944 melting points. Many of these data are multiple measurements for the same TAG. The polymorphic form of the solid phase is not always given.

The number of different TAGs for which data are available is much less (Table 9.5).

9.4.1.2.2 Conclusion

There is a disappointing lack of data for the heat of fusion of TAGs. The heat of fusion data that are available for the unstable modifications are mainly for mono-acid TAGs. Consequently, the correlations that have been developed are only valid for mono-acid TAGs. An experimental program is required before these correlations can be extended to mixed acid TAGs.

A considerable amount of melting points that is reasonably well spread over the modifications and TAG families is available. Correlations have been developed for a number of individual TAG families, but a general correlation is not available. This correlation will be developed in Section 9.4.3.

9.4.2 EXPERIMENTAL WORK

The enthalpy of fusion and melting points of 42 saturated mixed acid TAGs and 9 unsaturated TAGs were determined for all three polymorphic forms. The pure TAGs were taken from the stock of reference materials of Unilever Research Vlaardingen. Their purity exceeds 95%.

The experimental program was carried out on a Perkin-Elmer differential scanning calorimeter (DSC-7). This DSC-7 is equipped with a TAG 7/3 datalogger and a liquid nitrogen cooling accessory. Control of the apparatus is achieved by means of a PE computer. A more extensive description of DSC is given in Section 15.7.

The thermal data for each modification were obtained by the following procedures:

The data for the β -modification were obtained from the melting curve of the samples as they were delivered after several months to years of storage at room temperature.

The α -modification was obtained by rapidly quenching the TAGs from 10°C above the β -melting point to at least 20°C below the α -melting point. The enthalpy of fusion was obtained from the cooling curves. The melting curves were normally not suited for determination of α -thermal data, as the α -melting peak interfered with the β' - and β -crystallization peaks.

The β' -modification was most difficult to prepare as a pure substance; interference of the β' -melting peak with the α - β' or the β' - β recrystallization peaks was often obtained. Although the authors did not always succeed in preparing pure β' , in general one of the two following methods gave good results:

1. The TAG was crystallized into the α -modification by quenching. Next it was heated till α -melting set in and stabilized at that temperature for, depending on the TAG used, 1 min to 1 h. The melting curve was taken.
2. If a β' - β transition interfered in procedure A, the TAG was melted to 10°C above the β -melting point, rapidly cooled to 1°C or 2°C above the α -melting point and stabilized for 30 min to 1 h. The melting curve was taken.

The results are reported in Appendix 9.A, marked by an asterisk (*).

9.4.3 DEVELOPMENT OF THE CORRELATION

In the development of the correlations, data for TAGs containing acetic acid, butyric acid, and hexanoic acid are not used. The chain length of these fatty acids is so short, that they cannot be looked upon as long chain hydrocarbons.

9.4.3.1 Saturated TAGs

9.4.3.1.1 Melting Enthalpy

If the data for mono-acid TAGs are regressed against the carbon number n (Equation 9.39), leaving out data that have a residual more than two times the root mean square error (RMSE) of the regression through all mono-acid data, we obtain

$$\Delta H_f^\alpha = 2.4n - 17.6 \text{ kJ/mol}, \quad \text{RMSE} = 4.6, \quad r^2 = 0.98 \quad (9.57)$$

$$\Delta H_f^{\beta'} = 3.95n - 59.2 \text{ kJ/mol}, \quad \text{RMSE} = 4.7, \quad r^2 = 0.97 \quad (9.58)$$

$$\Delta H_f^\beta = 4.13n - 27.6 \text{ kJ/mol}, \quad \text{RMSE} = 6.1, \quad r^2 = 0.97 \quad (9.59)$$

The RMSE is in the order of magnitude of the experimental error (5–8 kJ/mol) and the values of the constants h agree with those of Perron (1984) and those for other lipids, given in Table 9.4.

If all data are used for a regression of ΔH_f against the carbon number, the values of the incremental chain contribution h do not change significantly, but the RMSE goes up to 20 and the correlation coefficient decreases to 0.7. A RMSE of 20 is too large for a reliable correlation and a correction term for chain length differences must be introduced.

It cannot be assumed that the end group contribution and the variables x and y that define a TAG family are neatly correlated.

Neither is there any function f_{xy} that is self-evident for use. When the residual error of data predicted by the mono-acid relation with the experimental data is plotted against x and y , it becomes clear that the end group contribution and (x, y) are correlated. The enthalpy of fusion drops more or less quadratically when the difference in chain lengths, represented by x and y , increases. x and y behave similarly and their effect seems additive. From the data for the β -modification, it can be seen that the effect of x and y levels off at values of x or y of 6 and more. This is probably associated with the transition from the β -2 form to the β -3 form. At large x or y , the β -3 forms become more stable than the corresponding β -2 forms.

A function that can describe the influence of chain length differences on the melting enthalpy that is observed is a general quadratic function:

$$\Delta H_f = hn + h_0 + h_x x + h_{x^2} x^2 + h_{xy} xy + h_y y + h_{y^2} y^2 \quad (9.60)$$

In order to introduce the leveling-off at high x or y , a cut-off value of 6 is used in the calculations instead of the real value of x or y when x or y exceeded 6. The resulting fit to the experimental data was very good: a RMSE nearly equal to that of a fit to the mono-acid data only was obtained. Melting enthalpies deviating more than 20 kJ/mol from the model predictions were rejected. The resulting values for h are in agreement with those of other lipids given in Table 9.4.

9.4.3.1.2 Melting Points

If Equation 9.43 is used to fit the mono-acid data, it results in a RMSE of 1.5°C for the α - and β -modifications and 3°C for the β' -modification. This compares very well with the experimental error in the melting points of 1°C–2°C. The RMSE increases to 7°C–10°C when Equation 9.43 is fitted to all data of saturated TAGs. A closer look to the differences between experimental melting points and those predicted by the fit to the mono-acid data suggests a quadratic relationship between x and y and the model parameters A and B :

$$\begin{aligned} A &= A_0 + A_x x + A_{x^2} x^2 + A_{xy} xy + A_y y + A_{y^2} y^2 \\ B &= B_0 + B_x x + B_{x^2} x^2 + B_{xy} xy + B_y y + B_{y^2} y^2 \end{aligned} \quad (9.61)$$

If the model of Equation 9.57 is fitted to the data, the RMSEs that result are most satisfying. A subdivision of the modifications into their -2 and -3 forms (β -2 and β -3, etc.) does not give an improved fit.

The values for T_∞ are in agreement with the values that were found by Zacharis (1977).

9.4.3.1.3 Simultaneous Fit of Melting Points and Melting Enthalpies

Although the empirical relations that were derived are perfectly useful as such, a few unsatisfying aspects must be mentioned:

1. According to Equation 9.45, the values for the parameters of relationship (Timms, 1978) for the melting enthalpy can be derived from the parameters values of relation 43 plus 58 for the melting point. If this is actually done so, the resulting parameters for the melting enthalpy are completely different from those given in Table 9.6. The melting enthalpies that are calculated in this way do not at all agree with the experimental data. Apparently, the parameters of Table 9.7 are not consistent with those in Table 9.6.
2. The melting enthalpy data for the β -modification showed clearly that the influence of x and y levels off when the values of x or y are greater than 6. The melting points did not seem to show such effect. However, if the correlation for the melting points extrapolated to extreme values of x or y , absurd results are obtained, indicating that leveling off of the influence of x and y should be introduced.

Therefore, this section will attempt to derive a unified model for both the enthalpies of melting, the entropies of melting and the melting points of saturated TAGs, by fitting the ΔH_f and T_f data simultaneously.

TABLE 9.6
Parameters That Result When Equation 9.57 Is Fitted
to the Experimental

Parameter	α -Modification		β' -Modification		β -Modification	
	Estimate	SE	Estimate	SE	Estimate	SE
h	2.39	0.1	4.17	0.2	4.03	0.1
h_0	-16.3	5	-68.4	8	-24.4	4
h_x	1.98	0.3	17.3	1.6	2.16	0.4
h_{x_2}	-0.54	0.07	-3.25	0.3	-0.63	0.07
h_{xy}	—		-1.07	0.3	—	
h_y	—		-9.03	1.2	-7.28	0.5
h_{y_2}	-0.64	0.08	—		—	
RMSE	5.2		6.0		7.1	

TABLE 9.7
Parameters That Result When Equations 9.44
and 9.58 Are Fitted to the Experimental
Melting Points of Even Saturated TAGs

Parameter	α	β'	β
A_0	-9.0581	-8.4543	-8.0481
A_x	0.00290	-0.10360	0.074130
A_{x_2}	-0.0619116	-0.018881	-0.0348596
A_{xy}	0.115128	0.0739411	0.00771420
A_y	-0.453461	-0.49721	-0.404136
A_{y_2}	-0.005827	0.0115995	0.0111938
B_0	-4.4841	-0.26501	2.66923
B_x	-0.00111	0.54997	-0.31675
B_{x_2}	0.148938	0.074136	0.085967
B_{xy}	-0.365917	-0.340928	0.040642
B_y	1.41154	2.34238	0.55040
B_{y_2}	-0.001766	-0.135735	-0.000945
T_∞	401.15	401.15	401.15
RMSE	2.3°C	2.9°C	3.0°C

The function f_{xy} , as defined in Equations 9.46 and 9.47, should account for the observed decrease in melting enthalpies and melting points as differences between the three chain lengths increase. It should be chosen in such a way that this effect does not grow indefinitely with increasing x and/or y but levels off. The general quadratic relations with cut-off value, which were previously used, did not perform well. The function finally arrived at is

$$f_{xy} = 2 - \exp\left\{-\left(\frac{x - x_o}{k_x}\right)^2\right\} - \exp\left\{\left(\frac{y}{k_y}\right)^2\right\} \quad (9.62)$$

which increases from 0 (for small values of both x and y) via 1 (for a large absolute value of either x or y) to 2 (for large values of both x and y). We have investigated a more complex variation of this function:

$$f'_{xy} = 2 - \left(1 + \frac{1}{2}\delta\right) \exp\left\{-\left(\frac{x' - x_0}{k_x}\right)^2\right\} - \left(1 - \frac{1}{2}\delta\right) \exp\left\{-\left(\frac{y' - y_o}{k_y}\right)^2\right\} \quad (9.63)$$

with

$$\begin{aligned} x' &= \cos\theta x + \sin\theta y \\ y' &= \cos\theta y - \sin\theta x \end{aligned}$$

The more general Equation 9.60 allows for a rotation over an angle of θ of the (x, y) axes to (x', y') -axes a difference in scaling along these directions (k_x and k_y) instead of a common k , a non-zero offset y_0 , and a relative difference in the maximal effects along the two directions expressed by the parameter δ . It appeared, however, that Equation 9.59, which is a special case of the more general Equation 9.60 (viz. $\theta = 0$, $k_x = k_y = k$, $y_0 = 0$, $\delta = 0$) gave a satisfactory fit to the data. Therefore, the results reported further on refer to this simpler model.

One must also take into account the possible effect of asymmetry on melting points. This is done by including an additional $R \ln 2$ term in the expression for the melting entropy to distinguish symmetric ($y = 0$) from asymmetric ($y \neq 0$) TAGs. The work of de Jong and van Soest has shown that for the β -phase the inclusion of such a term is appropriate (de Jong and van Soest, 1978; Birker et al., 1991). In the β -modification, random mixing of the two mirror images is not possible. For the loosely packed α phase, we do not expect that this term is needed. The β' phase takes an intermediate position and it is not clear beforehand whether the inclusion of the $R \ln 2$ term will improve or worsen the fit.

Finally, consider the phenomenon of melting point alternation: odd mono-acid TAGs tend to melt systematically lower than expected on the basis of interpolation from even mono-acid TAGs. Again, anticipate that allowance for this effect will improve the fit for melting points of β -phase TAGs. For the α -phase TAGs, do not expect any benefit and it is not known for the β' -phase TAGs.

The full expressions for the enthalpy and entropy of melting then read as follows:

$$\Delta H_f = hn + h_0 + h_{xy}f_{xy} + h_{\text{odd}} \cdot \text{odd} \quad (9.64)$$

$$\Delta S_f = sn + s_0 + s_{xy}f_{xy} + s_{\text{odd}} \cdot \text{odd} + R \ln 2 \cdot \text{asym} \quad (9.65)$$

Here “asym” and “odd” are indicator variables taking the value 1 (“true”) when an asymmetric TAG or an odd TAG is involved and the value 0 (“false”) otherwise. A TAG is considered “odd” when at least one of the fatty acid chains has an odd number of carbon atoms chains in the TAG. ΔH_f^{sat} is the melting enthalpy of the corresponding saturated TAG that can be obtained from the data in [Tables 9.6](#) or 9.7.

The eight parameters h_0 , h_n , s_0 , s_n , h_{xy} , s_{xy} , k , and x_0 were estimated by simultaneously fitting the ΔH_f model, Equations 9.59 and 9.61, to observed melting enthalpy data and the T_f model based on Equations 9.41, 9.59, 9.61, and 9.62 to observed melting points. The models were fit using weighted nonlinear least-squares regression taking a factor 6 for the ratio of the variances of melting enthalpies and melting points.

Enthalpies of fusion deviating more than 20 kJ/mol from the model fit have been rejected. Exclude all melting points which could not be fit well, that is, that deviated more than 10°. In all, the enthalpies of some 40 TAGs and the melting points of about 70 TAGs were fitted for the α , β' , and β phases separately.

TABLE 9.8
Estimates and Standard Errors of the Parameters
from Equations 9.61 and 9.62 When Simultaneously
Fitted to Melting Points and Melting Enthalpies of All
Saturated TAGs

Parameter	α -Modification		β' -Modification		β -Modification	
	Estimate	SE	Estimate	SE	Estimate	SE
h_0	-31.95	3.00	-35.86	5.88	-17.16	4.83
h	2.70	0.07	3.86	0.13	3.89	0.10
s_0	-19.09	10.56	-39.59	19.28	31.04	15.81
s	6.79	0.25	10.13	0.42	9.83	0.34
h_{xy}	-13.28	2.42	-19.35	2.81	-22.29	2.08
s_{xy}	-36.70	7.79	-52.51	8.76	-64.58	6.45
k	4.39	0.50	1.99	0.24	2.88	0.35
x_0	1.25	0.27	2.46	0.19	0.77	0.27
t_∞	397	4.1	381	3.6	395	3.3
h_{odd}	—	—	—	—	2.29	0.44
RMSE (ΔH)	8.6		9.2		10.3	
RMSE (T)	2.5		3.7		3.7	

The main results are collected in Appendix 9.A. Measured values are averaged over several observations with the number of independent observations given in the column labeled FREQ. Zero FREQ values refer to cases excluded from the estimation procedure. The heats of fusion that were measured in this work are separately listed. The estimated parameter values along with their standard errors are given in Table 9.8.

It turned out that the inclusion of the symmetry/asymmetry term ($R \ln 2$) improved the fit for the β phase in contrast to the α phase and the β' phase where the fit became worse. A similar result was obtained for the even/odd term: no significant improvement for the α and β' phase and a much better fit for the β -phase odd TAGs.

The resulting RMSEs for the melting points are only slightly more than those obtained by fitting the melting points solely. The RMSEs for the melting enthalpy have increased by 50%, but are still acceptable when compared to the experimental error of 5–7 kJ/mol. The values for h and s agree very well with those of other lipids, given in Table 9.4. The values for h_{xy} , which represent the maximum decrease in ΔH_f that is caused by chain length differences and which are likely to be related to the enthalpy difference between the β -2 and β -3 form of a mono-acid TAG, compare well with the stability difference between the two forms that was calculated by de Jong (1980) (10–20 kJ/mol). The values of h_{xy} and s_{xy} increase from α to β , in accordance with the expectation that the influence of chain length differences is more pronounced in a more densely packed polymorph. In the β -modification, the influence of x and y levels off at x or $y = 6$ (2 k), as was found previously.

A much more consistent correlation has been obtained at the expense of only a relatively small increase of the RMSEs.

9.4.3.2 Unsaturated TAGs

9.4.3.2.1 Melting Enthalpy

The authors have chosen to model the effect of unsaturation on the melting enthalpy of a TAG as a correction to the melting enthalpy of the corresponding saturated TAG (Equation 9.46). The model proposed by Perron (Bommel, 1986) did not perform very well; it resulted in a RMSE of more than 24 kJ/mol. After having investigated several other functions, the following model evolved:

$$\Delta H_f^{\text{unsat}} = \Delta H_f^{\text{sat}} + h_0 n_0 + h_E n_E + h_l n_l \quad (9.66)$$

Here n_0 stands for the number of oleic chains, n_E stands for the number of elaidic chains and n_l for the number of linoleic chains in the TAG.

The authors have fitted this model for the α -, β -, and β' -modifications. The complete data set contained over 80 melting enthalpies of only 16 different TAGs: 20 observations for 12 TAGs in the α -modification, 21 observations for 13 TAGs in the β' -modification, and 44 observations for 16 TAGs in the β -modification. The authors rejected data that deviated more than 30 kJ/mol from the predicted values. The data and the predictions are given in Appendix 9.A (see also [Figure 9.10](#)). The resulting parameters are given in [Table 9.9](#).

The values of the parameters that were obtained for the β -modification agree very well with the effective carbon numbers that Timms derived for the unsaturated fatty acids. The large RMSE for the β' -modification is solely due to the β' -melting enthalpy of POP (104 kJ/mol vs. a predicted value of 128 kJ/mol). If POP is left out, the RMSE decreases to 9.7, while the parameter values do not change. POP is the only *cis*-unsaturated TAG in the data set that crystallizes in the β' -2 form (Sato et al., 1989), which may explain its deviating behavior.

There is a lack of data for the unstable modifications of TAGs with linoleic acid, so that the model parameter h_l for these modifications could not be calculated. The parameter that describes the effect of the fatty acid that is most similar to linoleic acid (h_0) is nearly independent from the modification. Assume that this also holds for h_l .

A good fit to the available data was altogether obtained; the RMSEs are nearly equal to those of the saturated TAGs. A better general model can only be developed if more experimental data are made available, over a wider range of carbon numbers, including linoleic acid and including mixed unsaturated fatty acid TAGs.

9.4.3.2.2 Melting Point

An approach to model the melting points of unsaturated TAGs is start from a model for the saturated TAGs and add a correction term that accounts for the presence of O, E, 1, and linolenic acid (le) (Equations 9.15 and 9.46). After exploring various simpler models, it was learned that it was necessary to model interactions between

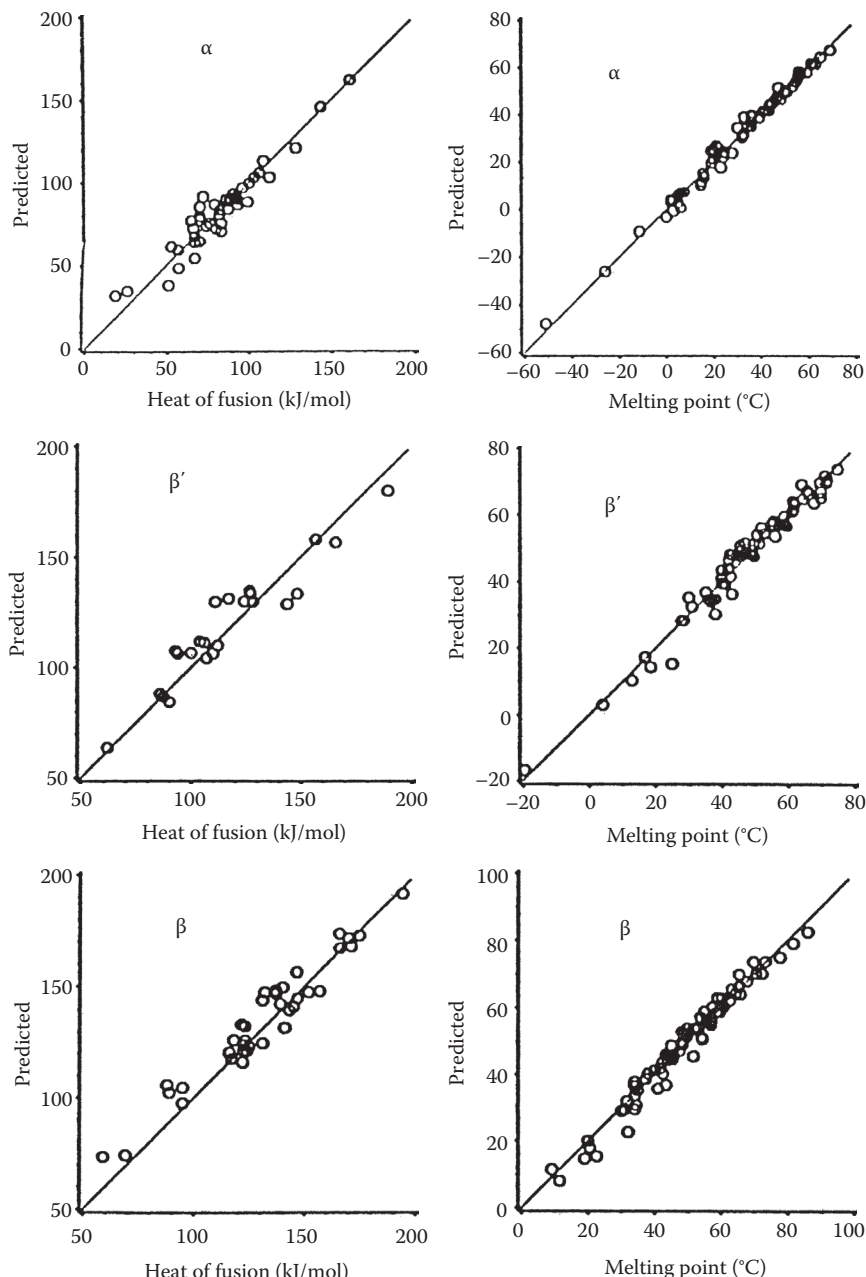


FIGURE 9.10 Values of the melting enthalpy and the melting points of saturated TAGs, calculated using the relations (9.62) and (9.63) plotted against the experimental data.

TABLE 9.9
**Estimates and Standard Errors of the Parameters
 of Equation 9.63 Fitted to the Melting Enthalpies
 of Unsaturated TAGs**

Parameter	α -Modification		β' -Modification		β -Modification	
	Estimate	SE	Estimate	SE	Estimate	SE
h_0	−31.7	1.8	−28.3	1.8	−30.2	1.4
h_E	−11.7	1.3	(−15.9)		−15.9	0.9
h_I	(−37.7)		(−37.7)		−37.7	2.5
RMSE	8.3		22		11.1	

Note: SE standard error. Values in brackets were guessed, due to lack of data.

unsaturated chains. The final model giving the best results is Equation 9.44 for which A is given by

$$\begin{aligned}
 A = & A_{\text{sat}} + A_O n_O + A_E n_E + A_I n_I + A_{\text{le}} n_{\text{le}} \\
 & + A_{OO} n_{OO} + A_{EE} n_{EE} + A_{II} n_{II} + A_{\text{lele}} n_{\text{lele}} \\
 & + A_{OI} n_{OI} + A_{Ole} n_{Ole} + A_{Ile} n_{Ile}
 \end{aligned} \tag{9.67}$$

and for which B is given by the much simpler expression:

$$B = B_{\text{sat}} + B_O n_O + B_I n_I + B_{\text{le}} n_{\text{le}} \tag{9.68}$$

Here, for example, n_O stands for the number of oleic chains in the TAG and n_{OI} for the number of O–I pairs. A_{sat} and B_{sat} can be obtained from Table 9.7 and Equation 9.58 or from Table 9.8, using Equations 9.45 and 9.60 through 9.62.

The authors have fit this model for the α -, β' -, and β -modifications. The complete data set contained over 120 melting points of *cis*-unsaturated TAGs, of which 18 were left out, because they involved unsaturated fatty acids other than o, I, and le. Of the remaining 102 melting point data, 13 were associated with the α -modification, 16 with the β' -modification, 13 with the β -modification, and for 60 data points the modification was not specified. The modification was not known for 13 of the 47 melting points of the *trans*-containing TAGs.

In these cases, the authors chose to assign the melting point to that modification, which gave the best fit. This assignment had to be done in an iterative manner using the results of the previous regression to determine the best modification input for the next regression analysis and carrying this process through till internal consistency was achieved. This laborious procedure can be viewed as a maximum likelihood estimation of both the melting point–structure relationship

TABLE 9.10
Estimates and Standard Errors of the Parameters in Equations 9.64 and 9.65 Fitted to the Melting Points of Unsaturated TAGs

Parameter	α -Modification		β' -Modification		β -Modification	
	Estimate	SE	Estimate	SE	Estimate	SE
A_0	3.46	0.39	2.20	0.36	2.93	0.24
A_E	1.38	0.16	1.34	0.22	1.68	0.11
A_l	3.35	0.66	2.5	1.1	4.69	0.50
A_{le}	4.2	2.1	2.2	2.1	5.2	1.9
A_{OO}	0.11	0.16	-0.27	0.14	-0.89	0.10
A_{EE}	0.01	0.19	-0.04	0.34	-0.40	0.13
A_{ll}	3.68	0.87	-0.55	0.26	-1.21	0.17
A_{lele}	1	1.9	-1.51	0.92	-1.38	0.60
A_{Ol}	-0.53	0.24	1.0	0.32	-0.71	0.15
A_{Ole}	-0.83	0.34	-0.76	0.22	-0.69	0.18
A_{lle}	3.0	1.3	-1.12	0.36	-0.73	0.52
B_O	0	1.6	-4.3	1.5	-3.7	0.8
B_l	5.4	2.3	-7.8	5.3	-1.5	1.6
B_{le}	2.6	8	-13.7	11.8	-1.8	7.0
RMSE	3.2°C		4.1°C		2.6°C	

and the unknown modifications. The data and the resulting assignments are given in Appendix 9.A. Data deviating more than 10°C from the predicted value were disregarded. The parameters are given in Table 9.10.

The standard deviations are only slightly larger than those for the saturated TAGs. We do not expect that these values can be substantially improved by another model. It should be realized that the reliability of the input data probably varies considerably. The data have been collected from the literature spanning nearly a century. The authors have screened the data to some extent and discarded a number of *a priori* very unlikely cases. In general, however, it is very difficult to assess the quality of the data reported. Thus, some of the input data may have a substantial error and this will cause some lack of fit.

In future work, we will extend the number of available melting enthalpy data and attempt to correlate the melting enthalpy and melting points of unsaturated TAGs simultaneously.

9.4.4 CONCLUSION

A compilation of literature data of melting points and melting enthalpies of TAGs was made. This data set was extended by measurements of melting enthalpies of 51 mixed acid saturated and unsaturated TAGs in all three modifications.

Reliable relations were developed that give the melting point and melting enthalpy as a function of the carbon number, chain length differences, and degree of unsaturation for the α -, β' -, and β -modifications.

9.5 MIXING BEHAVIOR IN LIQUID STATE

Before a study on solid TAG phases that are in equilibrium with a liquid TAG phase can be started, knowledge of the mixing behavior of TAGs in the liquid state is required. Although it is generally assumed that TAGs mix ideally in the liquid state, experimental evidence is lacking. Therefore the activity coefficients in mixtures of TAGs in the liquid state are measured using gas-liquid chromatography with a liquid stationary TAG phase. The results are compared with activity coefficients calculated with the UNIFAC group contribution method.

9.5.1 LITERATURE

It is generally stated in the literature on the phase behavior of TAGs that the miscibility of TAGs in the liquid state is ideal (Hannewijk et al., 1964; de Brujne et al., 1972; Timms, 1984). Yet the experimental evidence on which this conclusion is based is only very minor:

1. In dilatation experiments on pure TAGs and binary mixtures of TAGs no volume effect was observed (Hannewijk et al., 1964; Hendriske). However, although ideal miscibility implies a zero excess volume of mixing, the opposite is not necessarily true.
2. For liquid alkanes, it was found that the heat of mixing is less than 0.1 kJ/mol (Wurflinger, 1972; de Brujne et al., 1972), even for hydrocarbons considerably differing in chain length. Compared to the heat of fusion this heat of mixing is negligible. It was reasoned that if alkanes have almost no heat of mixing, then TAGs, which are chemically very similar to alkanes, will also have no heat of mixing. Again, ideal miscibility implies the absence of a heat of mixing, while the reverse is not necessarily true.
3. Mixtures of high-melting saturated TAGs and liquid unsaturated TAGs were often found to obey the Hildebrand solubility equation (Equation 9.69):

$$\ln x_i^L = \frac{\Delta H_f}{R} \left(\frac{1}{T_f} - \frac{1}{T} \right) \quad (9.69)$$

It is stated that therefore liquid mixtures of TAGs are ideal and if the Hildebrand equation is not obeyed, it is often ascribed to liquid phase nonideality (de Brujne et al., 1972; Norton et al., 1985). The Hildebrand equation assumes no solid phase miscibility and ideal liquid phase miscibility. In Sections 9.6 and 9.7, it will be shown that TAGs do show solid phase miscibility. Whether the Hildebrand equation is obeyed or not is therefore no indication for ideality of the liquid state, as the solid state behavior may not be disregarded.

Summarizing, it is clear that the evidence for ideal miscibility of liquid TAGs is not very convincing. Yet, before any description of solid–liquid phase behavior and nonideality in the solid phase can be given, the mixing behavior of TAGs in the liquid state needs to be known. In the next sections, measurements of activity coefficients of TAGs in the liquid state are reported and compared with activity coefficients that are estimated using the UNIFAC group contribution method.

9.5.2 MODEL CALCULATIONS

In order to enable the estimation of activity coefficients in mixtures for which no experimental data are available, Fredenslund, Rasmussen, and coworkers developed the UNIFAC method (Fredenslund et al., 1977). The UNIFAC method was shown to perform quite well in phase equilibrium calculations for many hydrocarbon systems (Fifth International Conference on Phase Equilibria for Chemical Process Design, 1989).

The basic idea of the UNIFAC method is that although there are thousands of different chemical components of interest for the chemical technology, the number of functional groups that constitute these compounds is much smaller. A natural oil contains thousands of different TAGs, but it only consists of CH_3- , $-\text{CH}_2-$, $-\text{CH}-$, $-\text{CH}=\text{CH}-$, $-\text{OH}$, and $\text{CH}_2\text{COO}-$ functional groups. UNIFAC assumes that the activity coefficient of each component in the mixture is a function of the individual contributions of the components' functional groups. Therefore, activity coefficients can be calculated from a limited number of parameters for the functional groups. An excellent and clear description of the method is given by Fredenslund et al. (1977).

The activity coefficients of TAGs in a set of TAG mixtures were calculated: in three binary mixtures of SSS and MMM (Table 9.11), three binary mixtures of MMM and 8C8 (Table 9.12), three binary mixtures of SSS and 8C8, and in a mixture of the six main TAGs and the two main partial glycerides occurring in palm oil (Table 9.13). The authors used a computer program and a database that were obtained from the department of Prof. J.M. Prausnitz (University of California, Berkeley) for the calculations.

The results confirm the assumption made in the literature and show that the activity coefficients of all TAGs are unity, so ideal mixing of TAGs is predicted. In view of the chemical similarity between all components, this is not too surprising. The two partial glycerides are predicted to have activity coefficients considerably larger than unity, as may be expected for polar compounds in an apolar solvent (Table 9.13).

TABLE 9.11
Activity Coefficients in the Liquid
Phase for Binary Mixture of SSS
with MMM and 8C8, Calculated
with UNIFAC

SSS [1] and MMM [2]			SSS [1] and 8C8 [2]		
T (°C)	x ₁	y ₁	T (°C)	x ₁	y ₁
100	0.25	1.007	100	0.25	1.091
100	0.50	1.003	100	0.50	1.020
100	0.75	1.000	100	0.75	1.004
120	0.25	1.006	120	0.25	1.079
120	0.50	1.002	120	0.50	1.022
120	0.75	1.000	120	0.75	1.003

TABLE 9.12
Activity Coefficients in the Liquid Phase for Binary Mixtures of MMM with 8C8, Calculated with UNIFAC

MMM [1] and 8C8 [2]		
T (°C)	x ₁	y ₁
100	0.25	1.046
100	0.50	1.015
100	0.75	1.003
120	0.25	1.041
120	0.50	1.014
120	0.75	1.002

TABLE 9.13
Activity Coefficients in the Liquid Phase for the Six Main TAGs and the Two Main Partial Glycerides of Palm Oil at 50°C, Calculated with UNIFAC

Palm Oil without Partial Glycerides			Palm Oil with Partial Glycerides		
Component	x	y	Component	x	y
PPP	0.08	0.9974	PPP	0.08	1.0005
POP	0.26	0.9997	POP	0.26	1.0018
PPO	0.14	0.9997	PPO	0.12	1.0018
PLP	0.10	1.0004	PLP	0.08	1.0008
POO	0.25	0.9998	POO	0.23	1.0009
OOO	0.17	0.9982	OOO	0.17	0.9982
Mono-P	—	—	Mono-P	0.01	4.2000
Di-P	—	—	Di-P	0.05	1.3518

9.5.3 EXPERIMENTS

9.5.3.1 Method for Determination of Activity Coefficients of Mixtures of Nonvolatile Liquids

Activity coefficients in the liquid phase are often determined by measuring to what extent the vapor pressure of a liquid mixture deviates from Raoult's law.

$$p_i = p_i^* x_i^L \quad (9.70)$$

However, the vapor pressure of TAGs is less than 1 Pa at temperatures between 0°C and 80°C, the temperature region in which solid fat crystallizes. This is unmeasurably

small and therefore another method for determination of activity coefficients must be developed.

A well-known method for determination of activity coefficients at infinite dilution of volatile compounds in nonvolatile liquids is the use of gas-liquid chromatography (GLC). The nonvolatile liquid is used as stationary phase and the volatile component is injected into the carrier gas stream. The activity coefficient is calculated from the retention time. The GLC method is discussed in many textbooks on gas chromatography (Box 9.5; Desty et al., 1962; Grob, 1985).

BOX 9.5 GLC METHOD TO DETERMINE ACTIVITY COEFFICIENTS OF NONVOLATILE LIQUIDS

The net retention volume of an injected sample is defined as the product of the net retention time and the flow rate of carrier gas, corrected for the pressure drop over the chromatographic column:

$$V_n = t_n \Phi_v \cdot \frac{3(p_{in}/p_{out})^2}{2(p_{in}/p_{out})^3} \quad (9.71)$$

The specific retention volume is defined as the net retention volume per unit mass of liquid stationary phase at 273.15°C. It is given by

$$V_g = \frac{273.15 V_n}{m_L T} \quad (9.72)$$

It is assumed that

- The sample concentration in mobile and stationary phase always have the equilibrium values
- That the sample volume is very small in comparison with mobile and stationary phase volume (infinite dilution)

In that case the mole fraction of the sample that is in the mobile phase must be equal to the ratio of the volume of the mobile phase and the retention volume (=net retention volume + mobile phase volume). The equilibrium distribution coefficient of the sample over mobile (L) and stationary phase (G) is therefore given by

$$K_{LG} = \frac{x^L}{x^G} = \frac{V_n}{n_L} \cdot \frac{n_G}{V_G} \quad (9.73)$$

The condition for equilibrium between stationary and mobile phase for infinite sample dilution is (if the mixture of carrier gas and sample behaves ideally)

$$px^G = p^* \gamma^\infty x^L \quad (9.74)$$

BOX 9.5 (continued)

By rearranging the latter two equations, one obtains an expression for the activity coefficient at infinite dilution of the sample in the stationary phase as a function of net retention volume:

$$\gamma^\infty = \frac{n_L}{p^* V_n} \cdot \frac{pV_G}{n_G} \quad (9.75)$$

The last term in this equation reduces to RT if the ideal gas law may be applied to a mixture of a carrier gas and a sample.

When the influence of the pressure drop over the column and the nonideality of the mobile gas phase are taken into account, a correction term must be added to Equation 9.72. Replacing the net retention volume by the specific retention volume and the vapor pressure by the corrected vapor pressure according to Prausnitz (1986), Desty et al. (1962) obtains the following corrected expression for the activity coefficient at infinite dilution:

$$\ln \gamma^\infty = \ln \left(\frac{273.15R}{p^* V_g M_L} \right) - p^* \left(\frac{B_{11} - v}{RT} \right) \quad (9.76)$$

The second virial coefficient B_{11} and the molar volume v of the liquid probe at the measuring temperature can be obtained from one of the correlations based on the principle of corresponding states given in Prausnitz (1986) and Smith and ness (1987).

Although the correction term is significant for the activity coefficients at infinite dilution of the samples that are used in this work, it is of no influence on the calculated interaction between the nonvolatile components in the stationary phase, as will be clear from Equations 9.77 and 9.82 in the next section. In that case, the correction term can therefore be neglected.

Desphande et al. (1974) have extended the use of this GLC method, using so-called “probes” to measure the interaction between two nonvolatile liquids:

First, two GLC columns are prepared, each containing a pure nonvolatile liquid as stationary phase and the activity coefficient of a volatile “probe” in these two pure stationary phases is determined by the method outlined earlier.

Next a number of GLC columns are prepared, containing mixtures of the two nonvolatile components as stationary phase. The activity coefficients of the probe in these mixed stationary phases are determined.

The interaction between the two nonvolatile components will affect their affinity for the probe, which will be expressed in the retention time of the probe. The interaction between the two liquid components can therefore be obtained by comparing the activity coefficients of the probe in the pure liquids with those in mixtures of the liquid components.

For simple regular solutions, this can be worked out as follows: A system of two non-volatile components [1] and [2] and a probe [pr] are considered. The activity coefficient of the probe in a mixture of the two other components is given by (Prausnitz, 1986)

$$RT \ln \gamma_{\text{pr},12} = A_{\text{pr},1}x_1^2 + A_{\text{pr},2}x_2^2 + (A_{\text{pr},1} + A_{\text{pr},2} - A_{1,2})x_1x_2 \quad (9.77)$$

At infinite dilution, we obtain for a binary system of the probe and one of the non-volatile components

$$RT \ln \gamma_{\text{pr},1}^\infty = A_{\text{pr},1} \quad (9.78)$$

and for the complete ternary mixture

$$RT \ln \gamma_{\text{pr},12}^\infty = A_{\text{pr},1}x_1 + A_{\text{pr},2}x_2 - A_{1,2}x_1x_2 \quad (9.79)$$

The interaction between the two nonvolatile components can now be determined from the experimental activity coefficients at infinite dilution of the probe by

$$\frac{A_{1,2}}{RT} = \frac{x_1 \ln \gamma_{\text{pr},1}^\infty + x_2 \ln \gamma_{\text{pr},2}^\infty - \ln \gamma_{\text{pr},12}^\infty}{x_1x_2} \quad (9.80)$$

It is clear that this elegant method can be applied straightforwardly to TAGs. The result should be independent of the probe used. If indeed TAGs mix ideally, the interaction coefficient $A_{1,2}$ must turn out to be zero.

9.5.3.2 Experimental Work

The mixing behavior of the binary SSS–MMM and of the binary SSS–8C8 was studied. The TAGs were obtained from Dr. A. Fröhling of Unilever Research Vlaardingen and were GC-pure.

9.5.3.2.1 Experimental Procedure

The stationary phases were prepared by mixing a predetermined amount of the carrier material Chromosorb W (80–100 mesh, acid washed, DCMS treated) that was suspended in chloroform, with a predetermined amount of the TAG or TAG mixture, dissolved in chloroform. The chloroform was slowly evaporated at 60°C under occasional stirring. The last remnants of chloroform were removed by heating 3 h at 80°C. It was checked by weighing whether no loss of carrier material or TAGs had occurred. The stationary phase was brought into a glass column of 1 m length and 2 mm diameter and the column was conditioned for 10 h at 150°C. Measurements were carried out at the Technical University of Delft (Gandasasmita, 1987) in a modified VARIAN 3700 gas chromatograph with a thermal conductivity detector. The retention times were determined with a VARIAN CDS-11 integrator. Helium was used as carrier gas.

In order to confirm that the probe that is used has no influence indeed on the calculated TAG–TAG interaction, measurements were repeated using eight different probes:

1. *n*-pentane
2. *n*-hexane
3. *n*-heptane
4. 2-methyl-pentane
5. 3-methyl-pentane
6. benzene
7. toluene
8. cyclohexane

All measurements were repeated at two carrier gas flow rates (17 and 38 mL/min) and with two columns, containing 10% and 20% of the stationary phase on carrier. About 0.1 μ L of the probe was injected.

9.5.3.2.2 Measurements

The specific retention volumes of the eight probes were determined at 82°C, 92°C, 102°C, 112°C, 123°C, and 133°C for the following stationary phases (concentrations in mole fractions):

SSS	0.4487	SSS, 0.5513	MMM	0.1557	SSS, 0.8443	8C8
MMM	0.7116	SSS, 0.2884	MMM	0.3593	SSS, 0.6407	8C8
8C8				0.6023	SSS, 0.3977	8C8

The results are given in Appendix 9.B. The average experimental error in the retention volumes is 3%.

9.5.3.3 Results and Discussion

The activity coefficients at infinite dilution of the probes can be calculated from the specific retention volumes with Equation 9.73. It turns out that they do not depend on temperature, as is illustrated for some of the probes and some stationary phases in Figure 9.11. The variation as a function of temperature is less than the experimental error of 3% in the activity coefficients. This indicates that the probe–TAG mixtures behave athermal, that is, that the excess Gibbs energy is nearly equal to the excess entropy of mixing.

Because a dependency on temperature was not found, the averages over all temperatures of the activity coefficients are used in further discussions. They are given in Table 9.14.

The interaction coefficients between the TAGs for the regular solution theory can now be calculated using Equation 9.77. The results are given in Table 9.15.

The results for the binary SSS–MMM clearly indicate that within experimental error these two TAGs mix ideally. The results are very consistent for both binary mixtures and all probes used.

The results for the binary SSS–8C8 clearly indicate that this binary does not mix ideally in the liquid phase. The interaction parameters significantly differ from zero.

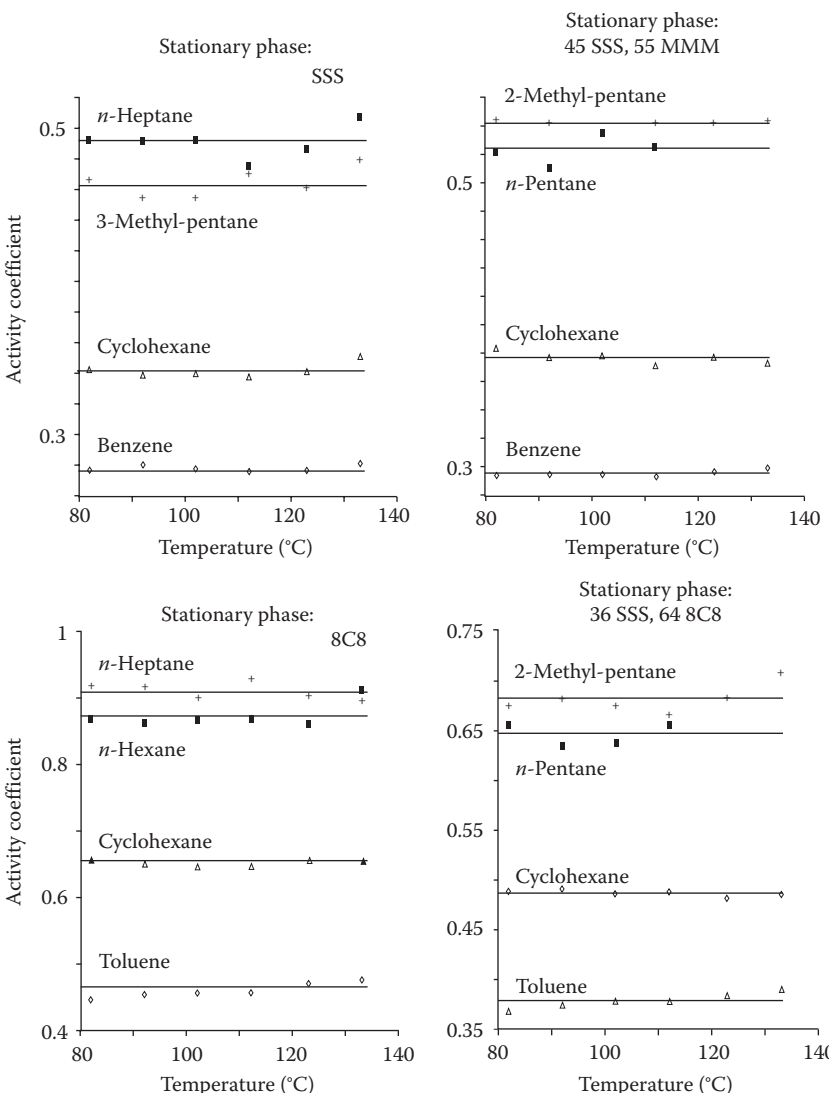


FIGURE 9.11 Activity coefficients at infinite dilution of a number of different probes in stationary TAG phases as a function of temperature.

And even worse, they also depend on the concentration of the TAGs. The simple regular solution model is therefore not a correct description for the nonideal behavior of this binary pair.

9.5.3.3.1 Interpretation with the Flory–Huggins Theory

The main difference between MMM and 8C8 is their difference in molecular size. This must be the cause of the large differences found in mixing behavior with SSS. An excess Gibbs energy model that accounts for such size differences

TABLE 9.14
Average Activity Coefficients at Infinite Dilution of Several Probes
in a Number of Liquid TAG Mixtures Determined by GLC

x_{SSS}	1	0.449	0.712	0.156	0.359	0.602
x_{MMM}	1	0.551	0.288			
x_{8C8}	1			0.844	0.641	0.398
Probe						
<i>n</i> -Pentane	0.45	0.55	0.85	0.52	0.49	0.75
<i>n</i> -Hexane	0.47	0.57	0.87	0.52	0.50	0.75
<i>n</i> -Heptane	0.49	0.59	0.91	0.54	0.52	0.78
2-Methyl-pentane	0.49	0.59	0.90	0.54	0.52	0.77
3-Methyl-pentane	0.46	0.56	0.87	0.52	0.49	0.73
Benzene	0.28	0.32	0.43	0.30	0.29	0.39
Toluene	0.29	0.33	0.46	0.31	0.31	0.41
Cyclohexane	0.34	0.41	0.65	0.38	0.37	0.55
					0.49	0.42

Note: The experimental error in the activity coefficients is 3%. Concentrations in mole fractions.

TABLE 9.15
Regular Solution Interaction Parameters A_{12}/RT
for the Interaction between the TAGs Determined
from GLC Results, Using Different Probes

x_{SSS}	0.449	0.712	0.156	0.359	0.602
x_{MMM}	0.551	0.288			
x_{8C8}			0.844	0.641	0.398
Probe					
<i>n</i> -Pentane	-0.15	-0.11	-2.61	-0.99	-0.58
<i>n</i> -Hexane	0.03	-0.03	-2.23	-0.93	-0.47
<i>n</i> -Heptane	0.01	-0.04	-2.29	-0.98	-0.50
2-Methyl-pentane	-0.01	-0.02	-2.25	-0.94	-0.48
3-Methyl-pentane	-0.02	-0.03	-2.29	-1.01	-0.47
Benzene	0.05	-0.02	-1.69	-0.73	-0.36
Toluene	0.02	-0.06	-1.77	-0.79	-0.41
Cyclohexane	0.03	-0.05	-2.41	-0.99	-0.50
Average	-0.01	-0.05	-2.19	-0.92	-0.47
Stand. dev.	0.06	0.03	0.29	0.10	0.06

Note: Experimental error in the parameters is 0.1. Concentrations in mole fractions.

is the Flory–Huggins theory for polymer solutions 89. According to this theory, the activity coefficient in the ternary system of probe [pr] and the two TAGs [1] and [2] is

$$\begin{aligned}\ln \gamma_{\text{pr},12} = & \ln \left(\frac{v_{\text{pr}}}{x_{\text{pr}}v_{\text{pr}} + x_1v_1 + x_2v_2} \right) + \left(1 - \frac{v_{\text{pr}}}{v_1} \right) \phi_1 + \left(1 - \frac{v_{\text{pr}}}{v_2} \right) \phi_2 \\ & + x_{\text{pr},1}\phi_1^2 + x_{\text{pr},2}\phi_2^2 + (x_{\text{pr},1} + x_{\text{pr},2} - x_{1,2})\phi_1\phi_2\end{aligned}\quad (9.81)$$

The volume fraction ϕ_i is defined as

$$\phi_i = \frac{x_i v_i}{\sum_{j=1}^N x_j v_j} \quad (9.82)$$

in which v_i represents the molar volume.

At infinite dilution, we obtain for a binary system of the probe and one of the TAGs

$$\ln \gamma_{\text{pr},1}^\infty = \ln \left(\frac{v_{\text{pr}}}{v_1} \right) + \left(1 - \frac{v_{\text{pr}}}{v_1} \right) + x_{\text{pr},1} \quad (9.83)$$

and for the complete ternary mixture

$$\ln \gamma_{\text{pr},12}^\infty = \ln \left(\frac{v_{\text{pr}}}{x_1 v_1 + x_2 v_2} \right) + \left(1 - \frac{v_{\text{pr}}}{v_1} \right) \phi_1 + \left(1 - \frac{v_{\text{pr}}}{v_2} \right) \phi_2 + x_{\text{pr},1}\phi_1 + x_{\text{pr},2}\phi_2 - x_{1,2}\phi_1\phi_2 \quad (9.84)$$

The Flory–Huggins interaction parameter x_{12} for the two TAGs can be determined from the experimental activity coefficients at infinite dilution by

$$x_{12} = \frac{\phi_1 \left(\ln \gamma_{\text{pr},1}^\infty - \ln \left(\frac{v_1}{x_1 v_1 + x_2 v_2} \right) \right) + \phi_2 \left(\ln \gamma_{\text{pr},2}^\infty - \ln \left(\frac{v_2}{x_1 v_1 + x_2 v_2} \right) \right) - \ln \gamma_{\text{pr},12}^\infty}{\phi_1 \phi_2} \quad (9.85)$$

When the molecular volumes of the two TAGs are equal, the Flory–Huggins interaction parameter x becomes equal to the regular solution interaction parameter A_{12}/RT and Equation 9.82 reduces to Equation 9.77 for the regular solution theory. The Flory–Huggins interaction parameters are given in [Table 9.16](#).

The interaction parameters of both binaries do not depend on the probe used and not on the concentration of the two TAGs in the binary mixture. The values of interaction parameters, -0.04 ± 0.1 for SSS–MMM and 0.07 ± 0.1 for SSS–8C8,

TABLE 9.16
Flory–Huggins Interaction Parameters X_{12} for the Interaction between the TAGs Determined from GLC Results, Using Different Probes

x_{SSS}	0.449	0.712	0.156	0.359	0.602
x_{MMM}	0.551	0.288			
x_{8C8}			0.844	0.641	0.398
Probe					
<i>n</i> -Pentane	−0.17	−0.15	−0.07	−0.02	−0.08
<i>n</i> -Hexane	0.01	−0.05	0.17	0.04	0.05
<i>n</i> -Heptane	−0.01	−0.06	0.17	0.02	0.04
2-Methyl-pentane	−0.02	−0.04	0.21	0.06	0.08
3-Methyl-pentane	−0.04	−0.05	0.24	0.02	0.11
Benzene	0.05	−0.03	0.14	0.04	0.09
Toluene	0.01	−0.07	0.14	0.01	0.04
Cyclohexane	0.01	−0.07	0.17	0.04	0.07
Average	−0.02	−0.07	0.15	0.03	0.05
Stand. dev.	0.06	0.03	0.09	0.02	0.06
Total av.		−0.04		0.07	
Stand. dev.		0.05		0.08	

Note: Experimental error in the parameters is 0.1. Concentrations in mole fractions.

do not differ significantly from zero, which implies that the TAGs have no specific interaction in the mixtures. The deviation from ideality that was found for SSS–8C8 is entirely explained by the extra entropy of mixing that arises from the large difference in molecular size of the two TAGs. The activity coefficients at infinite dilution of the three possible binary TAG mixtures, calculated with Equation 9.80, and in agreement with measurements, are given in Table 9.17.

TABLE 9.17
Activity Coefficients at Infinite Dilution of the Three TAGs Studied, Calculated Using the Flory–Huggins Theory for the Excess Entropy of Mixing (Equation 9.80)

	$1ny_{I,\text{SSS}}^{\infty}$	$1ny_{I,\text{MMM}}^{\infty}$	$1ny_{I,\text{SCS}}^{\infty}$	$y_{I,\text{SSS}}^{\infty}$	$y_{I,\text{MMM}}^{\infty}$	$y_{I,\text{SCS}}^{\infty}$
SSS	—	−0.02	−0.16	1	0.98	0.85
MMM	−0.03	—	−0.07	0.97	1	0.93
8C8	−0.24	−0.09	—	0.79	0.91	1

9.5.3.3.2 Implications for Natural Edible Oils

The results imply that deviations from ideal miscibility only become noticeable when an oil contains reasonable amounts of TAGs that have a carbon number that differs more than about 10 with the average carbon number of the mixture.

In normal vegetable oils and fats, the differences in molecular size of the TAGs are of the order of the differences between MMM and SSS. For practical purposes, liquid vegetable oils can therefore be treated as ideal mixtures of TAGs.

In animal oils and fats, like fish oil, butter fat, and edible tallow, the spread in molecular size of the TAGs is much larger, although the concentrations of very small and very large TAGs are limited. Treating these oils as ideal mixtures may, depending on the situation, lead to errors of about 10%–15% in calculation results.

This chapter considers the TAGs that occur in normal vegetable oils and fats. The liquid TAG phase may therefore safely be treated as an ideal mixture.

9.5.4 CONCLUSION

TAGs that differ not too much in molecular size mix ideally in the liquid state. The deviation from ideality that becomes noticeable at differences in carbon number greater than about 15–20 can entirely be ascribed to the extra entropy of mixing that occurs in mixtures of molecules that differ considerably in size. No specific TAG–TAG interactions were found.

In the liquid state, the vegetable oils that are normally used in the edible fats industry may be treated as ideal mixtures of TAGs.

9.6 MIXING BEHAVIOR IN THE α -MODIFICATION

Contrary to the β - and β' -modifications, in the α -modification the fatty acid chains still appear to oscillate and rotate with considerable molecular freedom. The formation of mixed crystals will therefore hardly disturb the α -crystal packing. As a consequence, mixing in the α phase may be nearly ideal. With this assumption α -melting ranges of a number of common fat blends are calculated and compared with experimental data.

9.6.1 EVIDENCE FOR PARTIAL RETAINED CHAIN MOBILITY IN THE α -MODIFICATION

Not only TAGs, but many lipids, like alkanes, *n*-alcohols, and simple esters solidify upon quick cooling from the melt in a crystal form with hexagonal chain packing, which for TAGs is called the α -modification. In 1932, it was suggested by Müller (1932) that the hexagonal polymorph of *n*-alkanes has complete rotational disorder of the chains in the crystal. Therefore the hexagonal polymorph of *n*-alkanes has been called the “rotator phase.” At present, the rotational disorder in the rotator phase of *n*-alkanes has been extensively studied and is well established (Broadhurst, 1962; Flory and Vrij, 1963; Wurflinger, 1972; Larsson, 1986). A curious property of lipid crystals in the rotator phase is their plasticity. Due to this property, esters occurring in this form have been called waxes.

Contrary to *n*-alkanes, the chains in the α -modification of TAGs cannot have complete freedom of rotation. For sterical reasons, chain mobility near the glyceryl group must be restricted. Yet the heat of fusion and the entropy of fusion of the

TABLE 9.18
Enthalpy and Entropy of Fusion of Some TAGs and Some *n*-Alkanes

TAG Name	ΔH_f (kJ/mol)			ΔS_f (J/mol K)		
	α	β'	β	α	β'	β
MMM	84	107	145	275	334	440
PPP	98	132	169	309	399	501
SSS	113	156	193	343	464	561
<i>n</i> -C19	45	60	—	147	197	—
<i>n</i> -C21	48	63	—	153	203	—

α -modification of TAGs correspond closely to that of the rotator phase of alkanes. Moreover, the entropy of fusion is only 60% of that of the very crystalline β and 75% of that of the β' -modification, indicating that in the remaining part of the molecule still a considerable disorder must exist (Table 9.18).

The melting dilatation (the volume increase upon melting) of the α -modification is only 60%–70% of that of the β' -modification (Small et al., 1984). This clearly demonstrates a less dense packing of the TAG molecules in the α -modification.

In pulse NMR for the determination of solid fat content (Human et al., 1989) the so-called *f*-factor, which is inversely proportional to the relaxation time, is only 1.2–1.3 for the α -modification, compared to 1.4–1.5 for the β' -modification and about 1.6 for the β -modification. This indicates a more disordered and liquid-like packing of the fatty acid chains in the α -modification.

Hernqvist and Larsson (1982) observed that the long spacing of the α -modification of SSS depends on temperature. A temperature dependence of the same order of magnitude was one of the main arguments for Luzatti et al. in their classical work on liquid crystallinity (Luzatti et al., 1960) to suggest a liquid state of hydrocarbon chains in liquid crystals. Hernqvist and Larsson also measured Raman spectra of TAGs. The β' - and β -modifications showed sharp peaks at 1065 and 1130 cm^{−1} (C–C stretching vibrations), while liquid TAGs have a broad band near 1090 cm^{−1}. The Raman spectra of the α -modification had a significant liquid-like character.

The most convincing evidence for chain mobility comes from Norton et al. (1985a). He concludes from high-resolution CP/MAS¹³C-NMR spectra of the liquid state and the three polymorphs of SSS and PPP that in the α -modification, like in the liquid phase and contrary to the β' - and β -modifications, the 1- and 3-position of the glycerol are equivalent. He was able to study molecular motion by application of interrupted decoupling (switching of the ¹³C–¹H decoupling for a short time, which suppresses the signal of immobile protonated carbons). The results clearly show that the mobility of the fatty acid chains near the glycerol group is very limited in all three polymorphs. In the α -modification, the main hydrocarbon chain still possesses some mobility, while the carbons near the methyl end plane are very mobile. Main chain mobility is still present to some extent in the β' -modification, while the β -modification shows no main chain mobility. Even in the β -modification, the methyl end group has retained some mobility.

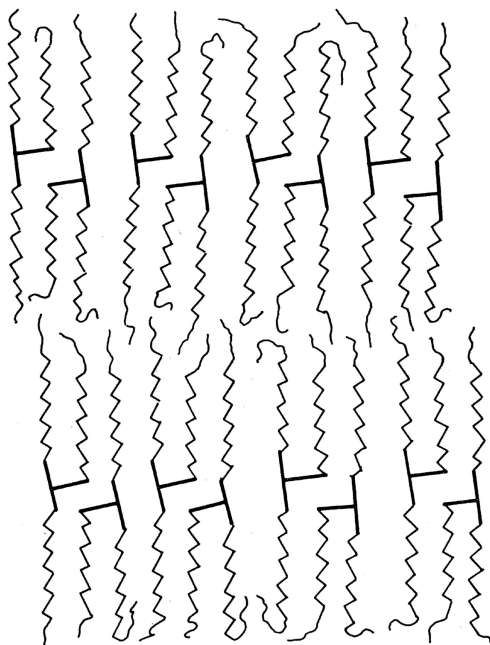


FIGURE 9.12 Chain disorder in the α -modification.

The good correspondence with the rotator phase of alkanes and all facts that are mentioned earlier clearly support the view of Hernqvist (1984) on the α -modification. In the α -modification, close to the methyl end plane, the fatty acid chains are disordered like a lamellar liquid crystalline phase. Close to the glycerol group, chain mobility is absent (Figure 9.12).

9.6.1.1 Supercooling of the α -Modification

One of the other arguments that is often mentioned in favor of chain mobility in the α -modification is the observation of van den Tempel (1979) that the α -modification, like lamellar liquid crystalline phase, cannot be supercooled (Muller, 1932).

This is not entirely correct. The authors have observed that in oil-in-water emulsions with a relatively small droplet size, supercooling of the α -modification could be obtained. Moreover the author has found a whole class of very slowly crystallizing fat blends, where the main crystallizing TAGs are of the unsymmetric hhu type, in which even in a bulk phase under shear supercooling of the α -modification could be obtained (Wesdorp and van Meeteren, 1989). Crystallization to equilibrium was extremely quick and took place in about 1 min. A noticeable transition to the β' -modification only occurred after about 1 h.

In all other fat blends investigated, the authors could not obtain supercooling of the α -modification in sheared bulk phases.

This effect in the experiments is described in Section 9.6.2.

9.6.1.2 Excess Gibbs Energy in the α -Modification

In normal crystalline phases, ideal mixing is only found when the components that are mixed and are nearly isomorphous (Zief and Wilcox, 1967). In all other cases, incorporation of a second component causes disturbances in the extremely regular crystal lattice, leading to nonideal mixing. However, the α -modification may be an exception. The large degree of liquid-like disorder that exists, especially in the methyl end-plane region, may very well enable the incorporation of TAGs with considerably longer or shorter fatty acid chains into the crystal “lattice,” without causing much extra disorder or misfittings. In other words, the excess Gibbs energy of mixing is likely to be very small, or even zero in the α -modification.

There exists some evidence in the literature that in the α -modification of TAGs, considerable solid solubility occurs (Murray et al., 1981; Norton et al., 1985a), but the data are too inaccurate and too scarce to allow any quantification. However, the phase diagrams of the rotational phase–liquid equilibrium of *n*-alkanes (Wurflinger, 1972) indicate clearly that mixing in the rotational phase must be nearly ideal at atmospheric pressure. The topic will come back to the solid–liquid phase behavior of *n*-alkanes in Section 15.9.

Assume that TAGs mix ideally in the α -modification and with this assumption the α -melting range of a fat can be predicted. In the next section, it will be investigated whether such predicted α -melting ranges agree with the experimental melting ranges.

9.6.2 COMPARISON OF EXPERIMENTAL AND CALCULATED α -MELTING RANGES

9.6.2.1 Experimental Procedure

The α -modification is extremely unstable. In normal fats it transforms to the β' -modification within 3–20 min. This instability poses some problems in the determination of α -phase equilibria. The normal thermal techniques for studying solid–liquid equilibria, like DSC and DTA, are too slow. A faster method must be defined.

The fact that it is very hard to supercool the α -modification in a bulk fat phase that is subjected to shear, while it is very easy to supercool the β' - and β -modifications under those conditions, can be used to determine the α -melting range of a fat blend. The following procedure takes advantage of this phenomenon:

1. About 2 kg of the fat blend is heated in a stirred tank to a temperature at least 10°C above the slip melting point of the fat. Next the fat is circulated through a gear pump, two lab-scale scraped surface heat exchangers (SSHE) for cooling and a tubular heat exchanger for remelting, in the setup depicted in [Figure 9.13](#). The volume of the SSHEs is 18 mL, the total cooling surface 7×10^{-3} m². As coolant ethanol is used at temperatures between 5°C and –20°C, samples can be taken directly after the SSHEs. The solid fat content of these samples can be measured in a Bruker Minispec p120i pulse NMR device. The NMR is operated with a 90_x -T-90_y pulse sequence, which not only gives the solid fat content, but also the *f*-factor, a number that is characteristic for the modification in which the fat has crystallized (van den Tempel, 1979).
2. The fat is cooled in the SSHEs to 1°C below its α -cloud point. Next the throughput is increased, while keeping the SSHE exit temperature constant,

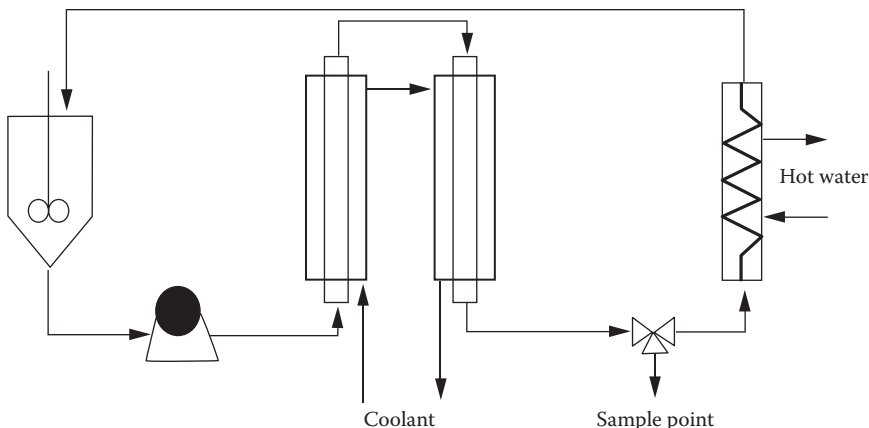


FIGURE 9.13 Experimental setup with two SSHEs and a remelter for measurements of α -melting ranges.

until no decrease in solid content is observed upon further increase of throughput. Usually this is obtained at about 16 kg/h (4.4 g/s). Thus it is made sure that the transition to the β' -modification has not yet started in the SSHEs and that the solid phase is still completely in the α -modification. Sample temperature and solid phase content are recorded.

3. Next the fat temperature is decreased in steps of about 2°C . When the solid phase content and temperature have stabilized, a sample is taken and the solid phase content and temperature are recorded. Eight data points are usually taken in duplicate for each fat blend.
4. The plot of solids content against temperature is called an α -line and represents the α -melting range of the fat blend.

During experiments, the pulse NMR always returned f -factors of about 1.25. An f -factor of 1.25 is indicative for the α -modification.

It may be argued that the α -line obtained in this way is not a line representing the α -liquid-phase equilibrium, but a line representing the maximum possible supercooling of the fat under the conditions used. Such lines of maximal supercooling usually depend strongly on the specific conditions, like impeller speed, that are applied (Pamplin, 1980; Grootscholten, 1986) (Figure 9.14a). However the α -lines, which were measured, were found to be totally independent of the rotational shaft speed of the SSHEs, coolant temperature, and throughout, once the throughput was high enough to prevent the formation a β' phase in the SSHE (Figure 9.14b).

Nine fat blends were selected that cover the area of compositions and melting ranges normally occurring in household and industrial fat spreads. The TAG compositions of the fat blends were obtained by calculation from average TAG compositions of the fat blend components. The average TAG compositions of the fat blend components, like sunflower oil or hardened palm oils, were taken from the Edible Fats Database of Unilever Research Vlaardingen ([Table 9.19](#)).

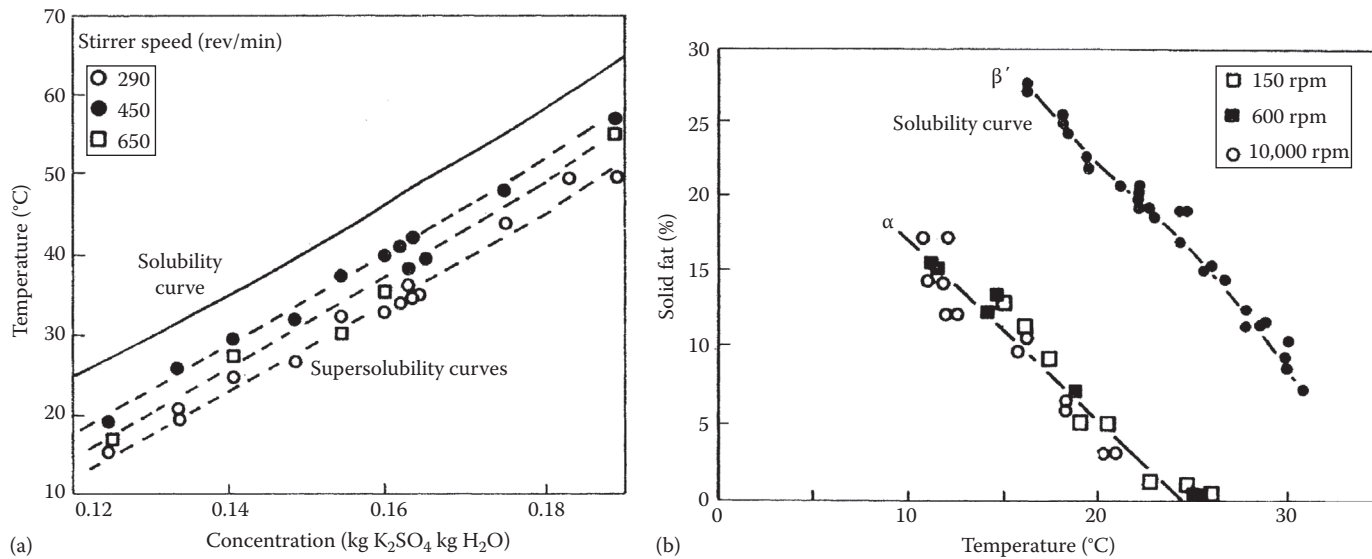


FIGURE 9.14 Effect of crystallizer impeller speed on the position of the supersolubility curve: (a) Potassium sulfate and (b) a mixture of soybean oil and hardened soybean oils. (From Pamplin, B.R., *Crystal Growth*, Pergamon Press, New York, 1980, pp. 526–530.)

TABLE 9.19
Summarized TAG Compositions of Nine Fat Blends of Commercial Fat Spreads

TAG	1	2	3	4	5	6	7	8	9
SSS				0.005	0.002			0.002	0.010
S ₂ P				0.009	0.005	0.001		0.004	0.020
SP ₂	0.006	0.002	0.006	0.006	0.005	0.011	0.002	0.003	0.014
PPP	0.011	0.004	0.019	0.001	0.002	0.032	0.004		0.003
SES			0.001		0.007		0.002	0.004	0.025
PES	0.006	0.009			0.012	0.002	0.006	0.006	0.034
PEP	0.018	0.020			0.007	0.001	0.009	0.002	0.011
SSE			0.002		0.007		0.003	0.008	0.025
PSE	0.002	0.006			0.011	0.002	0.009	0.012	0.034
PPE	0.006	0.009			0.006	0.002	0.010	0.005	0.011
P ₂ m	0.004		0.001	0.006	0.002	0.004			0.004
PSm	0.002			0.020	0.004				0.013
S ₂ m				0.010	0.002				0.009
SOS	0.001	0.001	0.003	0.001	0.003	0.001	0.001	0.002	0.007
POS	0.020	0.015	0.052	0.002	0.007	0.021	0.004	0.004	0.010
POP	0.078	0.057	0.230	0.001	0.004	0.090	0.005	0.002	0.004
SIS				0.001	0.002	0.002			0.001
PIS	0.008	0.005	0.009	0.004	0.004	0.008	0.003	0.003	0.002
PIP	0.027	0.014	0.035	0.003	0.003	0.029	0.004	0.002	0.002
SSO				0.002	0.003	0.001	0.002	0.005	0.007
PSO	0.010	0.007	0.008	0.004	0.008	0.013	0.006	0.009	0.010
PPO	0.033	0.016	0.031	0.003	0.005	0.052	0.007	0.004	0.004
SSI	0.001		0.001	0.003	0.002			0.002	0.001
PSI	0.011	0.005	0.005	0.008	0.005	0.007	0.005	0.006	0.003
PPI	0.030	0.009	0.009	0.006	0.004	0.020	0.007	0.005	0.004
SE ₂	0.002	0.018			0.041	0.010	0.031	0.027	0.084
PE ₂	0.009	0.034			0.036	0.014	0.050	0.021	0.056
Pm ₂	0.013			0.011	0.001				0.002
Sm ₂	0.003			0.018	0.001				0.004
EEE	0.003	0.037			0.059	0.020	0.063	0.021	0.047
mmm	0.014			0.007					
SmE					0.010				0.034
PmE					0.012				0.022
E ₂ m					0.017			0.001	0.034
SEO	0.002	0.018			0.029	0.010	0.031	0.031	0.054
PEO	0.010	0.034			0.035	0.014	0.049	0.025	0.036
SEl		0.002			0.023	0.001	0.004	0.003	0.005
PEl	0.001	0.004			0.021	0.002	0.006	0.003	0.004
SmO	0.002			0.005					
PmO	0.012			0.003					
mOm	0.006								

TABLE 9.19 (continued)
Summarized TAG Compositions of Nine Fat Blends of Commercial Fat Spreads

TAG	1	2	3	4	5	6	7	8	9
mlm	0.001								
mmO	0.013			0.002					
mml	0.003				0.001				
E ₂ O	0.004	0.055				0.049	0.030	0.094	0.037
E ₂ I		0.007				0.058	0.004	0.012	0.004
SO ₂	0.20	0.007	0.009	0.008	0.021	0.013	0.004	0.012	0.009
PO ₂	0.120	0.039	0.049	0.012	0.028	0.101	0.011	0.014	0.010
Liquid	0.485	0.560	0.530	0.836	0.437	0.481	0.557	0.706	0.272

9.6.2.2 Calculations

The α -melting ranges were calculated using the standard multicomponent two-phase flash algorithm and Michelsen's stability test for the initial estimate, both described in Section 15.3. Ideal mixing in the solid and liquid phases was assumed; therefore, all activity coefficients were unity. The TAG compositions from Table 9.8 were used, while all pure component properties were estimated using the correlations developed in Section 15.4.

9.6.2.3 Results

The results of the calculations and the measurements are given in Figures 9.15 through 9.17.

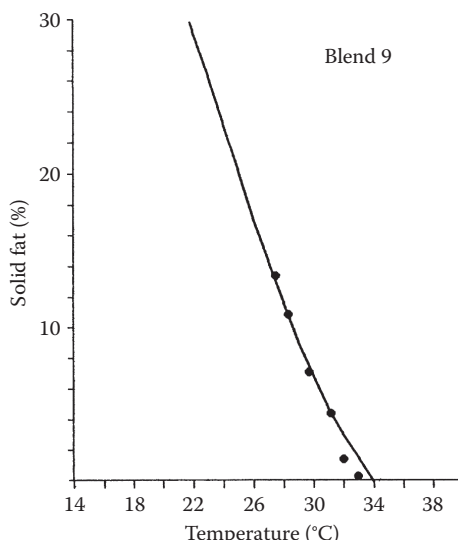


FIGURE 9.15 Measured (points) and calculated (lines) α -melting ranges of the commercial fat-blends of Table 9.19. The blend number indicated above the graphs corresponds to the compositions of Table 9.19.

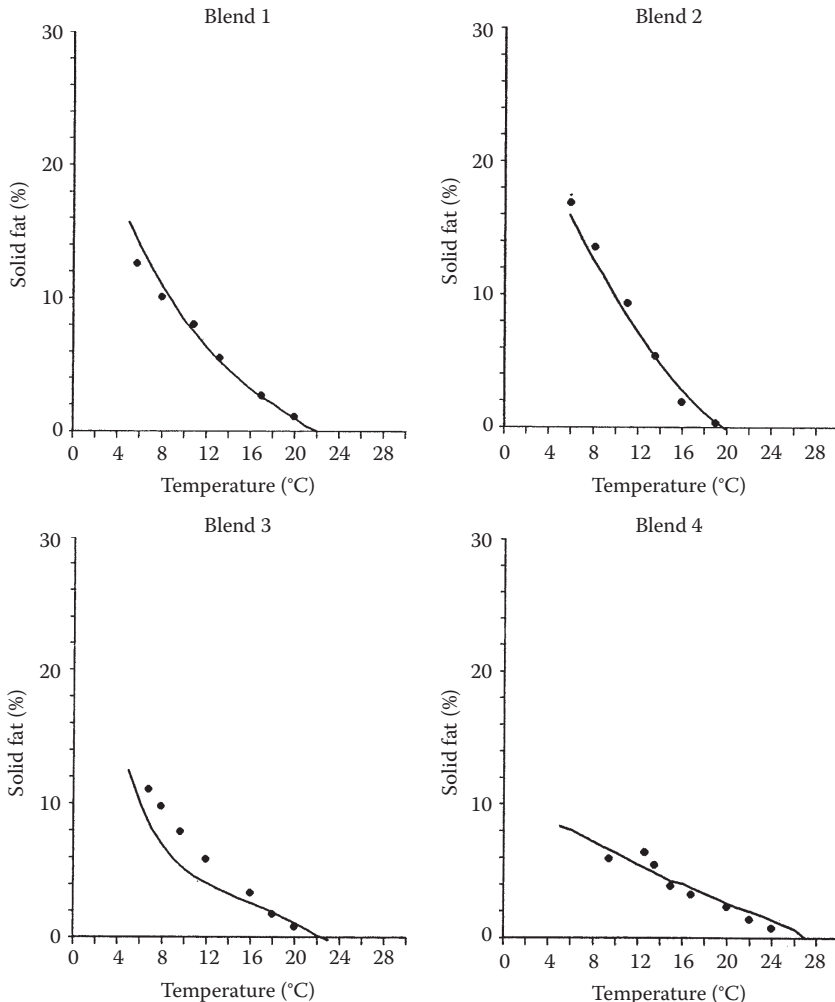


FIGURE 9.16 Measured (points) and calculated (lines) α -melting ranges of the commercial fat-blends of Table 9.19. The blend number indicated above the graphs corresponds to the compositions of Table 9.19.

The outcome is very surprising: it appears possible to predict the behavior of the extremely unstable α -modification by phase equilibrium thermodynamics. The agreement between predictions and measurements is striking.

9.6.3 CONCLUSION

A good description of the phase behavior of TAGs in the very unstable α -modification is obtained when it is assumed that TAGs form ideal solid solutions in the α -modification.

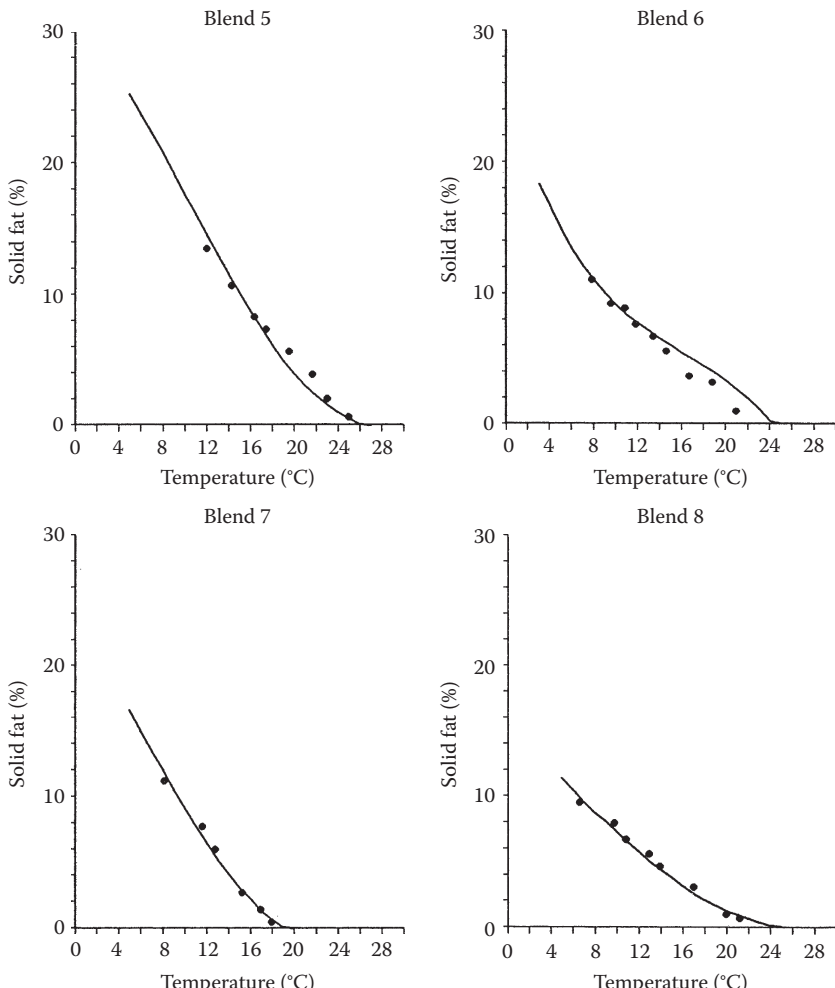


FIGURE 9.17 Measured (points) and calculated (lines) α -melting ranges of the commercial fat-blends of Table 9.19. The blend number indicated above the graphs corresponds to the compositions of Table 9.19.

9.7 MIXING BEHAVIOR IN THE β' - AND β -MODIFICATIONS

The miscibility of TAGs in the β' - and β -modifications is highly nonideal. It is attempted to describe this nonideal mixing with the simplest possible excess Gibbs energy models. A compilation of existing binary T, x, y solid–liquid phase diagrams is used to determine the binary interaction parameters that occur in these models. A new method is developed to determine binary interaction parameters from a single, complete DSC melting curve of ternary mixtures. Some ternary phase diagrams are considered.

9.7.1 EXCESS GIBBS ENERGY

It is well known (Murray et al., 1981; Timms, 1984) that the mixing behavior of TAGs in the β' - and β -modifications is highly nonideal. Therefore, in order to be able to solve the “solid-flash” problem of Chapter 3, we need to know the activity coefficient of each TAG in the β' - or β -solid phase as a function of the phase composition. Usually this is obtained from an excess Gibbs energy model:

The Gibbs energy of a phase is given by (Prausnitz, 1986)

$$G = \sum_{i=1}^N n_i \mu_i = G^{\text{ideal}} + RT \sum_{i=1}^N n_i \ln \gamma_i \quad (9.86)$$

when Equation 9.5 is used for the chemical potential. The excess Gibbs energy of this phase is subsequently defined as

$$G^E = G - G^{\text{ideal}} = RT \sum_{i=1}^N n_i \ln \gamma_i \quad (9.87)$$

As the chemical potential is by definition the partial molar Gibbs energy, it follows that an activity coefficient is a partial molar excess Gibbs energy:

$$\mu_i = \left(\frac{\partial G}{\partial n_i} \right)_{P,T,n_j} \Rightarrow RT \ln \gamma_i = \left(\frac{\partial G^E}{\partial n_i} \right)_{P,T,n_j} \quad (9.88)$$

This implies that once a model for the excess Gibbs energy has been formulated, the activity coefficients, needed for solving the set of equilibrium Equations 9.4 through 9.8 to obtain the number of phases and the amount and composition of each phase present, are readily obtained.

9.7.1.1 Excess Gibbs Energy Models

Hardly any literature on excess Gibbs energy models for solid mixtures is available. In thermodynamic calculations, it is nearly always assumed that solid phases are pure phases. Deviations between experiments and calculations are explained with “mixed crystal formation”, but without any quantification.

Kitaigorodskii (1973) and Haget et al. (1985) propose a parameter, the “degré d’isomorphisme cristallin” that expresses how well a molecule will fit into the crystal of another compound. The parameter was successfully used for qualitatively predicting complete, partial, or no miscibility in the solid phase of mixtures of several substituted naphthalenes, but could not be used for quantitative predictions.

In a few cases, existing liquid phase excess Gibbs energy models were applied to solid mixtures: a regular solution model for petroleum waxes (Won 1986, 1989; Hansen et al., 1987) and van Laar and Wilson equations (Prausnitz, 1986) for sodium carbonate and sodium sulfate (Null, 1980). General guidelines cannot be distilled from the literature.

The excess Gibbs energy of a pure phase is zero: $G^E = 0$ (if $x_i \rightarrow 1$). The simplest relation meeting this requirement is the regular solution or two suffix Margules model. For a binary system, it is given by (Prausnitz, 1986)

$$g^E = A_{12}x_1x_2 \rightarrow RT \ln \gamma_1 = A_{12}x_2^2 \quad (9.89)$$

and for multicomponent system by

$$\begin{aligned} g^E &= \sum_{i=1}^N \sum_{j=i+1}^N A_{ij}x_i x_j \\ RT \ln \gamma_i &= -g^E + \sum_{j=1, j \neq i}^N A_{ij}x_j \end{aligned} \quad (9.90)$$

It contains one interaction parameter per binary.

Usually the very regular crystal lattice of a pure component will be disturbed when a molecule of another size is incorporated. This results in a positive excess Gibbs energy. Therefore, normally the interaction parameters A_{12} in the solid phase will be positive and the activity coefficients will be greater than unity.

The two suffix Margules equation is symmetric: a mixture of 10% PPP and 90% SSS would have the same excess Gibbs energy as a mixture of 10% SSS with 90% PPP. However, symmetric behavior in the solid phase is unlikely; the effect of incorporating a large molecule in a crystal lattice of smaller molecules probably differs from the effect of the reverse case. The two suffix Margules equation is therefore not the most obvious excess Gibbs energy model to be used for solid fats.

The simplest models, able to describe demixing, that can account for the expected asymmetric behavior are the van Laar and the three suffix Margules equations. Both contain two interaction parameters per binary pair. More complex models are not justified (Prausnitz, 1986): they require very accurate and extensive data, which are not available for TAGs and in view of the experimental difficulties probably impossible to obtain. Because of its somewhat wider versatility (Prausnitz, 1986) the 3-suffix Margules equation is used in this work. For a binary system it is given by

$$\begin{aligned} g^E &= (A_{21}x_1 + A_{12}x_2)x_1x_2 \\ RT \ln \gamma_1 &= x_2^2 [A_{12} + 2(A_{21} - A_{12})x_1] \\ \ln \gamma_1^\infty &= \frac{A_{12}}{RT}, \quad \ln \gamma_2^\infty = \frac{A_{21}}{RT} \end{aligned} \quad (9.91)$$

The main disadvantage of 3-suffix Margules equation (and also of the van Laar equation) is its lack of a rational base for extension to multicomponent systems. An extra assumption has to be made. Assuming that an i, j pair in the multicomponent system gives the same contribution to g^E as in the binary mixture at the

same relative concentrations (Fischer and Moeller, 1985), then the multicomponent 3-suffix Margules equation becomes

$$g^E = \sum_{i=1}^N \sum_{j=i+1}^N \left(A_{ij} \frac{x_j}{x_i + x_j} + A_{ji} \frac{x_i}{x_i + x_j} \right) x_i x_j \quad (9.92)$$

$$RT \ln \gamma_i = -g^E + \sum_{j=1, j \neq i}^N x_j \left(\frac{A_{ji}(x_i^2 + 2x_i x_j) + A_{ij}x_j^2}{(x_i + x_j)^2} \right)$$

When both interaction parameters are equal, the equations reduce to the 2-suffix Margules equations.

9.7.1.2 Regular or Athermal?

The parameters in the Margules equations are usually taken to be independent of temperature. This is equivalent to assuming that the excess entropy equals zero. Mixtures with this behavior are called regular. The opposite case is assuming that the excess enthalpy is zero. Mixtures with this property are called athermal. The interaction parameters are inversely proportional to temperature. In reality, the situation usually lies in between: both excess enthalpy and entropy deviate from zero.

The data of Haget and Chanh (Haget et al., 1985) for substituted naphthalenes in the solid state as well as the data of Maroncelli et al. (1985) and Snyder for *n*-alkanes in the solid state suggest that these mixed solid phases of chemically very similar compounds show nearly regular behavior. The temperature differences that are considered in this chapter are probably too small to be able to discriminate between both extreme situations. The authors could not obtain any improvement of fit to binary phase diagrams of TAGs by replacing the assumption of regular behavior with athermal mixing. Therefore, it is arbitrarily assumed in this work that TAGs form regular mixtures.

9.7.1.3 Phase Diagram

The solid–liquid phase behavior of two components is usually represented by a *T, x, y* phase diagram. Figure 9.18a and b illustrates the types of binary *T, x, y* phase diagrams that can be obtained assuming an ideal liquid phase (Section 15.4) and a nonideal solid phase that is described by the 2- or the 3-suffix Margules equation.

The following aspects feature:

1. The eutectic composition is determined almost completely by the difference in melting point of the two components when the 2-suffix Margules equation is used. Using the 3-suffix Margules equation, the eutectic composition can still be shifted about 0.05 mol fraction in both directions.
2. Peritectic diagrams cannot be obtained using the 2-suffix Margules equation.
3. The position of the liquidus is hardly influenced by the magnitude of the interaction coefficients:
 - If the value of the interaction coefficients A/RT exceeds 4
 - If the difference between the melting points of the components is more than about 15°C

In the first case, that of a eutectic diagram, the magnitude of the interaction coefficients only influences the position of the solidus at mole fractions less than 0.1 or greater than 0.9. In the second case, the position of the solidus hardly depends on the value of the interaction parameters at mole fractions of the lowest melting component less than or equal to 0.5. Only at very low concentrations of the highest melting component there is influence of the interaction parameters on the liquidus. However, in this region, the experimental errors are normally most pronounced.

According to Timms (1984), four types of phase diagrams are observed for TAGs: monotectic with continuous solid solubility, eutectic, monotectic with partial solid solubility, and peritectic diagrams. Only the 3-suffix Margules equation is able to describe all these diagrams.

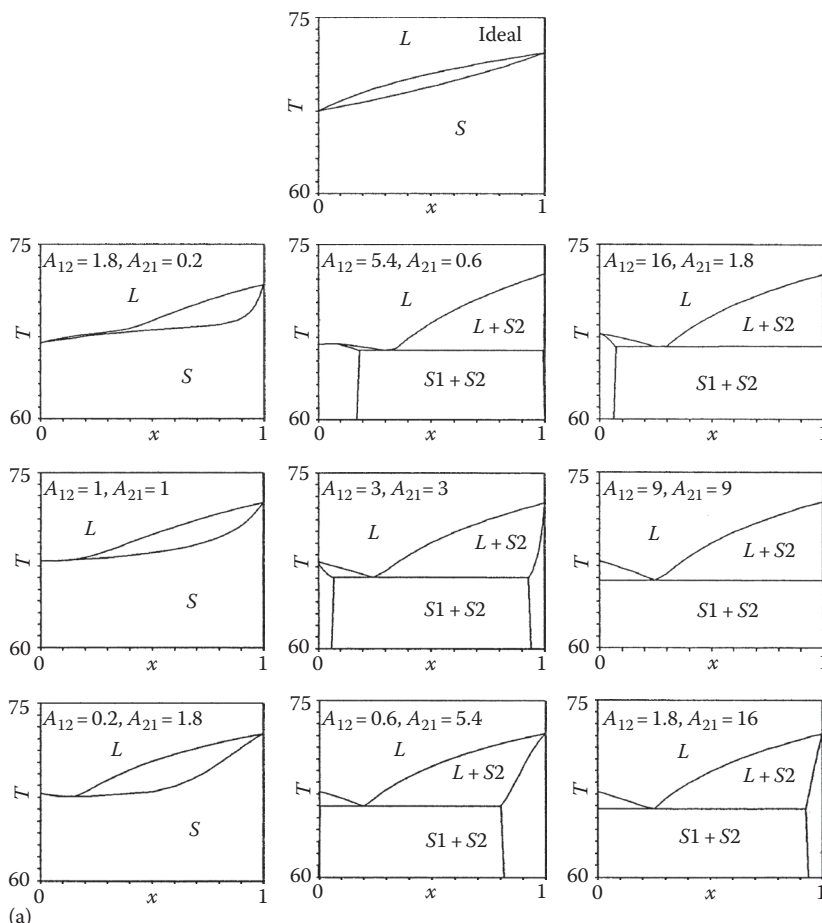


FIGURE 9.18 (a) Theoretically possible T , x , y solid–liquid phase diagrams of PSS–SSS calculated using the 3-suffix Margules equation. The values of the binary interaction parameters are indicated.

(continued)

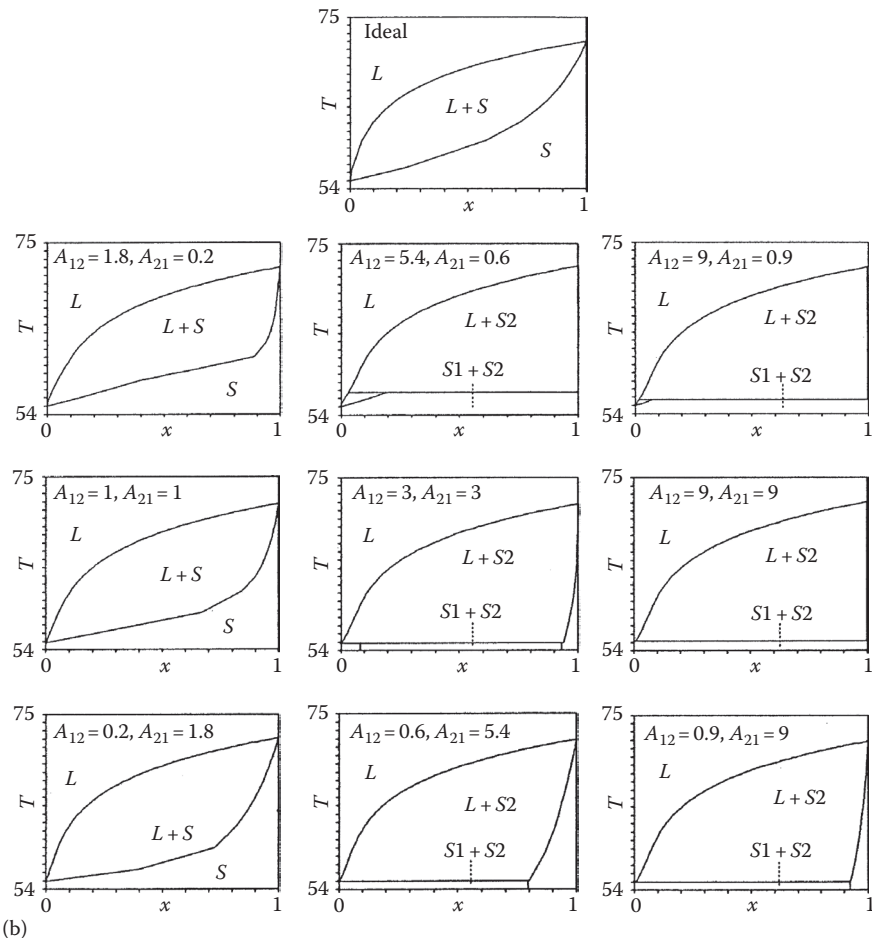


FIGURE 9.18 (continued) (b) Theoretically possible T,x,y solid-liquid phase diagrams of MMM-SSS calculated using the 3-suffix Margules Equation 9.91. The values of the binary interaction parameters are indicated in the figure.

9.7.1.3.1 Nomenclature

Henceforth the liquidus and solidus that are obtained when ideal mixing in the solid phase is assumed will be called ideal liquidus and ideal solidus. The interaction parameters of the excess Gibbs energy models are zero. The liquidus and the solidus that are obtained in the opposite case, when no mixing in the solid phase occurs, will be called eutectic liquidus and eutectic solidus. Then the interaction parameters of the G^E models are infinite, which is in practice equivalent to values of A/RT greater than or equal to 9.

The eutectic liquidus is also obtained from the well-known Hildebrand equation (Equation 9.39), which assumes the absence of mixed solid phases. In the literature, this liquidus is often referred to as the ideal solubility line, in spite of the highly nonideal solid phase behavior that is implicitly assumed.

A point on the liquidus is called the clear point and a point on the solidus will be referred to as the softening point of a mixture.

9.7.1.3.2 Use of Phase Diagrams to Determine Interaction Parameters

Experimental binary phase diagrams of TAGs can be used to determine the interaction parameters that occur in an excess Gibbs energy model. Using a fitting procedure, the interaction parameters are adjusted until the calculated and measured phase behavior agree.

There is one important limitation: in the aforesaid cases where the position of the liquidus hardly depends on the magnitude of the interaction parameters, it will be very hard to obtain reliable values of those interaction parameters from a phase diagram. That would require a number of solidus points at mole fractions less than 0.1 and greater than 0.9. Such data points are seldom available.

Therefore, the use of phase diagrams to determine interaction parameters is in practice limited to binaries of components that still show considerable solid miscibility and that differ less than about 15°C in melting point. It is possible to fit the phase diagram of other binaries; however, without learning much of the performance of the G^E model that is applied.

9.7.2 EXPERIMENTAL PHASE DIAGRAMS OF TAGS

9.7.2.1 Measuring Phase Diagrams

Rossell (1967) reviews all phase diagrams of TAGs that were published before 1967. Although he gives no quantitative interpretation of the phase diagrams, he recognizes the main problems that occur when determining a binary solid–liquid T, x, y phase diagram:

1. Impurities
2. Incomplete and incorrect stabilization
3. Other experimental errors

9.7.2.1.1 Impurities

Impurities generally lead to an increase of the observed melting range and may cause an erroneous picture of mutual solid solubility. The position of both liquidus and solidus are affected by the presence of impurities. Good determination of TAG purity by GLC, TLC, or HPLC is only possible since about 1965. Therefore older data may be suspect.

9.7.2.1.2 Stabilization

Due to the extremely low diffusion rates in the solid phase, lengthy stabilization procedures are required to ensure that the solid phase composition has its equilibrium value. The polymorphic behavior of TAGs complicates the stabilization even more. Part of the solid phase may persist in an unstable polymorphic form with a deviating equilibrium composition. Except for the combination of very short stabilization with very quick measurements, the position of the liquidus usually does not depend very strongly on the stabilization procedure. The small amount of solid phase at temperatures just below the clear point can relatively easily recrystallize via the liquid phase to the equilibrium solid phase composition. Stabilization strongly influences the position of the solidus.

Proper stabilization requires lengthy schemes of temperature cycling between clear point and softening point. These can take several months to a year.

Often the mixtures are stabilized by long storage at a temperature several degrees below the softening point. This procedure is certainly not sufficient; in this way unstable polymorphic forms are “frozen.” It was shown that they could persist several years (de Bruijne and Reckweg).

9.7.2.1.3 Other Experimental Problems

In older reports, the technique usually applied for measuring phase diagrams is the thaw-melt technique with visual observation of softening and clear points. Visual observation of clear points and especially of softening points is very inaccurate and large errors both in liquidus and solidus may occur.

The method most applied at present is some form of thermal analysis, DTA or DSC. Problems that can occur when using DSC are as follows:

1. Thermal lag because of a large sample size or scan rate. The softening point remains in place, but the observed clear point is shifted to a higher temperature. It becomes more difficult to detect small heat effects.
2. Failure to detect melting peaks. Combination of a large ($>15^{\circ}\text{C}$) difference in melting point, low concentration of one of the components, and some solid solubility leads to broad, diffuse humps rather than sharp melting peaks in the DSC thermogram. The determination of the exact starting and end temperature of these humps is very difficult. The hump itself is easily overlooked. A set of false liquidus and solidus points results.

An alternative method, which is sometimes applied, is measurement of the solid phase content of a set of binary mixtures at different temperatures by wide-range pulse NMR (or before 1970 by dilatometry) (Rossell, 1967). The phase diagram can be constructed from the resulting melting lines or solubility curves (Grootscholten, 1987; Smith, 1988). This method is much more time consuming than the thermal methods. Due to the inaccuracy of the measurements (0.7% solids), the solidus and liquidus are obtained with a relatively large experimental error.

9.7.2.1.4 Illustration

The influence of the experimental problems on the quality of the phase diagram is illustrated in [Figure 9.19](#). Two sets of simulated (Section 9.3.5) DSC curves of the binary POP-PEP are given. The first set was generated using the 2-suffix Margules equation with A/RT of 3, resulting in a mutual solid solubility of about 15%. For the second set the 3-suffix Margules equation was used with $A_{\text{pop-pep}}/RT$ of 0 and $A_{\text{pep-pop}}/RT$ of 6, resulting in zero solubility of PEP in solid POP and 50% solubility of POP in solid PEP. Moreover 3% of impurities, a thermal lag of 0.2°C , and 3% random noise were included. These levels of impurities, thermal lag, and noise are quite normal for literature data on TAGs.

Perfect (i.e., in absence of thermal lag, impurities, etc.) measurements on the first system would result in DSC curves with a sharp spike at the eutectic temperature followed by a broader hump that ends abruptly at the clear point. Due to the presence of impurities and thermal lag the eutectic spike is broadened to $2^{\circ}\text{--}4^{\circ}$.

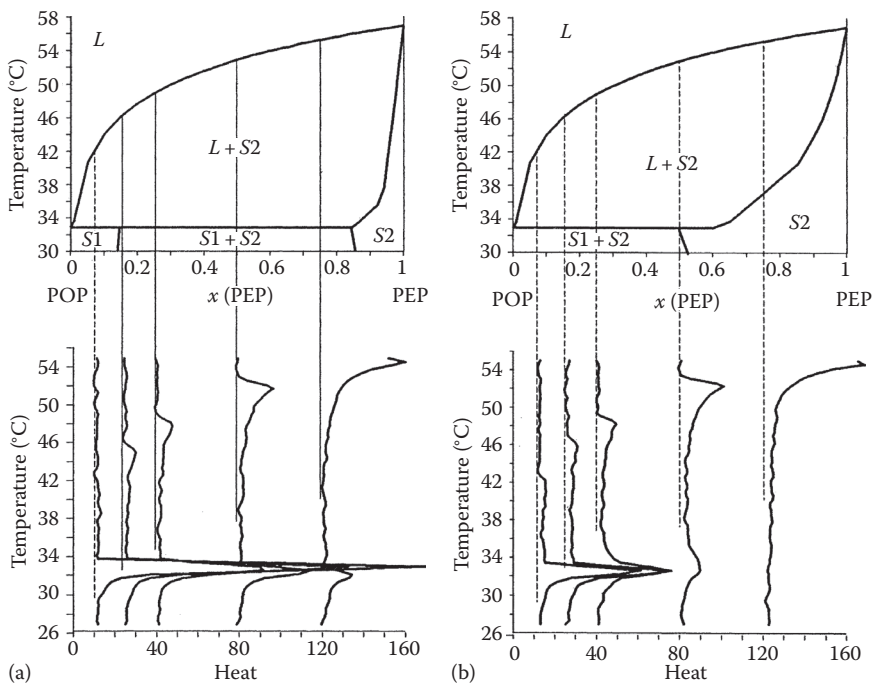


FIGURE 9.19 Simulated DSC melting curves (bottom) and binary phase diagrams (top) for a number of different mixtures of POP and PEP. The trajectory through the binary phase diagram that is followed is indicated for each mixture. (a) simulation with $A_{12} = A_{21} = 3$. (b) simulation with $A_{12} = 0$ and $A_{21} = 6$.

This causes an uncertainty in the position of the solidus of the same size, while the shape of the solidus remains correct.

In the second system, the sharp spike at the eutectic temperature disappears and is replaced by a broad hump at PEP concentrations over 50%. The onset of this hump is hard to determine exactly. At 75% PEP, the hump becomes very broad. In the simulated curve, it is no longer detectable. The softening point of this mixture is 36°C . However, the softening point that one would read from the simulated DSC curve is the onset of the second melting peak, at about 46°C , a difference of 10°C .

The influence that the experimental errors can have the measured phase diagram becomes clear in Figure 9.20. In this figure, the simulated phase diagram is plotted together with pseudoexperimental solidus and liquidus points that are determined from the simulated experimental DSC melting curves. The original simulated liquidus and the experimental liquidus points correspond very well, but the solidus points deviate considerably from the original solidus. At the POP side of the diagram, the experimental points lie far below the original solidus, while they are positioned above the ideal solidus at the PEP side of the phase diagram.

The POP-PEP binary was measured by Lovergren (de Brujne et al., 1972). As in the simulated DSC curve, it is impossible to detect a start melting point between

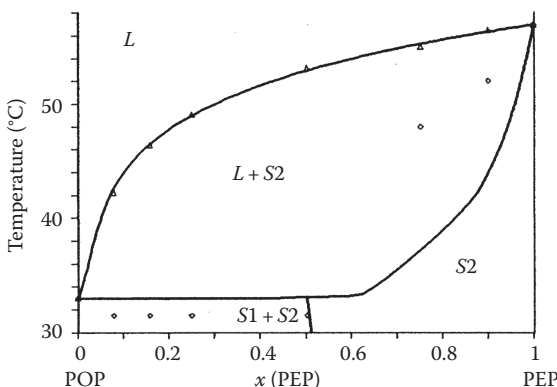


FIGURE 9.20 Solidus and liquidus points read from the simulated DSC curves of Figure 9.19 with the phase diagram that formed the basis for the simulation of the DSC curves.

30°C and 40°C in Lovegren's curve for 75% PEP. Whatever the solubility of POP in PEP would be, the start melting point would have to lie in this temperature range, which implies that the softening point that is read from this curve is wrong.

Solidus points that lie below the eutectic solidus at the side of lowest melting component and suddenly shift to values far above the ideal solidus on the other side of the phase diagram are frequently reported for TAGs with a large difference in melting point (Rossell, 1967). Often, in about half of the cases, contradicting reports exist, showing no solidus points that lie above the ideal solidus. An example from the data of Kerridge for SSS-LLL (Kerridge, 1952), which are in contradiction to the data of Lutton (1955).

A thermodynamic consistency test on the data is not possible. Heats of mixing, which are needed to check if the isobaric, nonisothermal Gibbs–Duhem equation is obeyed, are not available.

Compound formation, which would explain a solidus that lies above the ideal solidus, is very unlikely: compound formation is only known between pairs of TAGs made up of the same fatty acids, but attached to different positions of the glycerol group (like POP and PPO). The binaries for which deviating solidi are reported normally have a large difference in melting point, which stems from large differences in size or shape. It is therefore much more likely that the deviations are caused by impurities, improper stabilization, and failures in detecting the true softening point.

9.7.2.2 Literature Overview

It is clear that the determination of solid–liquid T , x , y phase diagrams is a tedious and unrewarding job, which is probably the reason why since Rossell's review (Rossell, 1967) so few phase diagrams were reported.

De Bruijne et al. (1972) have published the phase diagrams of all binary combinations of TAGs with palmitic (P) and stearic (S) acid. They put much effort in stabilization and purification. Their data seem therefore to be of good quality. They always expected the sharp double-peaked DSC curve that is characteristic for eutectic behavior. Therefore, they missed the solidus in those cases where due to solid solubility the DSC melting curve had another shape.

De Bruijne also determined the phase diagrams of tribehenate (BBB) with tristearate (SSS) and tripalmitate (PPP) (de Bruijne and Reckweg), and of POP with PPO in the β' -modification (de Bruijne and Reckweg). Unfortunately, these diagrams are only of little value as hardly any stabilization was used.

Perron (Perron et al., 1971) and coworkers have also measured the systems of de Bruijne. They do not report any purity of their TAGs and did not stabilize the mixtures at all. Their DSC curves are full of polymorphic transitions, partially overlapping with melting peaks. They report β' -stable PSS and PPS while these TAGs are known to be beta stable (de Bruijne et al., 1972; Gibon, 1984). Consequently, the resulting diagrams can better be disregarded.

In later work, Perron (Ollivon and Perron, 1979) again reports some of these phase diagrams (SSS–PSP, PSP–SPP, and SSS–SPP), but now with very pure components and a longer stabilization procedure.

Gibon (1984) also measured the same systems and those of some of the TAGs occurring in palm oil (POP, PPO, OPO, and POO). Although she worked with very pure samples, she put no effort at all in stabilization. Most of her phase diagrams are therefore, like the early Perron work, useless for our purpose. Gibons work is continued by De Smedt and Gibon (1990) with TAGs that contain elaidic acid (SES, SSE, PEP, PPE, EPE), but unfortunately in the same manner.

Krautwurst (1972) gives the binary diagram of PPP–MMM and some data of the ternary PPP–MMM–LLL. He does not give purities and followed a reasonable stabilization procedure.

The binary SSS-trioctanoate (888) was determined by Barbano and Sherbon (1977) with a stabilization of 23 months and very pure TAGs.

Grootscholten (1987) determined the liquidus of SSS–SES, SSS–SSE, SSE–SES, SSS–SEE, and of PPP and SSS with OOO using a reasonable stabilization procedure.

Smith (1988) reports the only known good quality ternary diagram: a well-stabilized ternary diagram of POP/SOS/POS in their most stable polymorphic form determined by NMR.

Lovegren (de Bruijne et al., 1972) gives the DSC melting curves of the binary POP–PEP after several stabilization procedures, from which a diagram can be constructed.

Norton et al. (1985) gives some liquidus points of PPP and SSS with OOO determined by DSC. His end melting peaks show a strange tail for which the reason is not clear.

Only Rootscholten interpreted his phase diagrams applying an activity coefficient approach (Grootscholten). All other authors only state, if something, whether their data deviate from the Hildebrand equation (eutectic liquidus and solidus).

Also outside the area of edible oils and fats phase diagrams of organic compounds that show similar phase behavior as TAGs, like substituted naphthalenes (Haget et al., 1985) or sulfolane with compounds as dimethylsulfoxide and dioxane (Janelli, 1985) are only interpreted with the Hildebrand equation for pure solids. Solid solutions have not been described quantitatively. Related phase diagrams, between a liquid crystalline phase and a gel phase of phospholipids (e.g., stearyl-palmitoyl-glycero-phosphocholine and dimyristoyl-glycero-phosphocholine, 2 lecithins) have been described quantitatively with the 2-suffix Margules equation. In these systems, stabilization is considerably less important. Values of A/RT between 0 and 1.5 are found (Hagemann, 1975).

9.7.2.3 Fitting Experimental Phase Diagrams

The ability of the 2-suffix and 3-suffix Margules equations to describe non ideal mixing in solid fats was tested by fitting these G^E models to the experimental binary phase diagrams. The Simplex method (Brumbaugh et al., 1990) was used for parameter adjustment. In Section 9.7.2.1, it was concluded that solidus data may be very inaccurate. Therefore, only the liquidus was fitted.

Clear points were calculated using Michelsens' stability test (Section 9.3.2.2). This guaranteed that the solid phase was in the right polymorphic form. Next the solidus data were used to fine-tune the interaction parameters within the error margin that resulted from the fit to the liquidus.

As pointed out in Section 9.7.1.3, accurate values of binary interaction parameters can only be obtained from binaries of components that have a small difference in melting point and a reasonable mutual solid solubility. Typically the requirements are an interaction parameter A/RT less than 3 and a difference in melting point less than 15°C . For all other cases, only rough indications of the values of the interaction parameters can be given, using the solidus points that are available.

The phase diagram was rejected as a whole if

- The reported melting points differ more than 4°C from the accepted values
- The reported liquidus lies on average more than 2°C above the ideal liquidus or more than 2°C below the eutectic liquidus
- The eutectic composition differs 0.08 mol fraction or more from the composition that follows from the melting points alone

Solidus points that lie more than 3°C above the ideal solidus were neglected: as is outlined in Section 15.7.3.1, it is likely that the actual softening point was not detected in the experiments. When published or when a lab journal was still available, the original data were used, but usually the data had to be read from the graphs in the publications (Appendix 9.D).

9.7.2.4 Saturated TAGs

9.7.2.4.1 SSS, SSP, PSP, SPS, PPS, and PPP

These are the TAGs that occur in fully hydrogenated vegetable oils as palm oil, soybean oil, sunflower oil, rape seed oil, and safflower oil (Figures 9.21 through 9.25). The interaction parameters and residual errors in predicted liquidus lines (the square root of the quotient of the sum of squared errors and the number of degrees of freedom) are given in Table 9.20, and the phase diagrams in Figures 9.21 through 9.25.

Taking into account that the experimental error that is claimed is 0.3°C – 0.4°C , the fit to the data is usually most satisfying. In spite of this good fit, the experimental error causes a rather large uncertainty in the interaction parameters. The uncertainty is even larger in the case of PSP. PSP crystallizes in the β' modification, and the phase diagrams are therefore mixed β – β' . Consequently the 3-suffix Margules parameters determined from these diagrams that indicate the solubility in β -PSP and in the β' -modification of the other TAG will show a very large error.

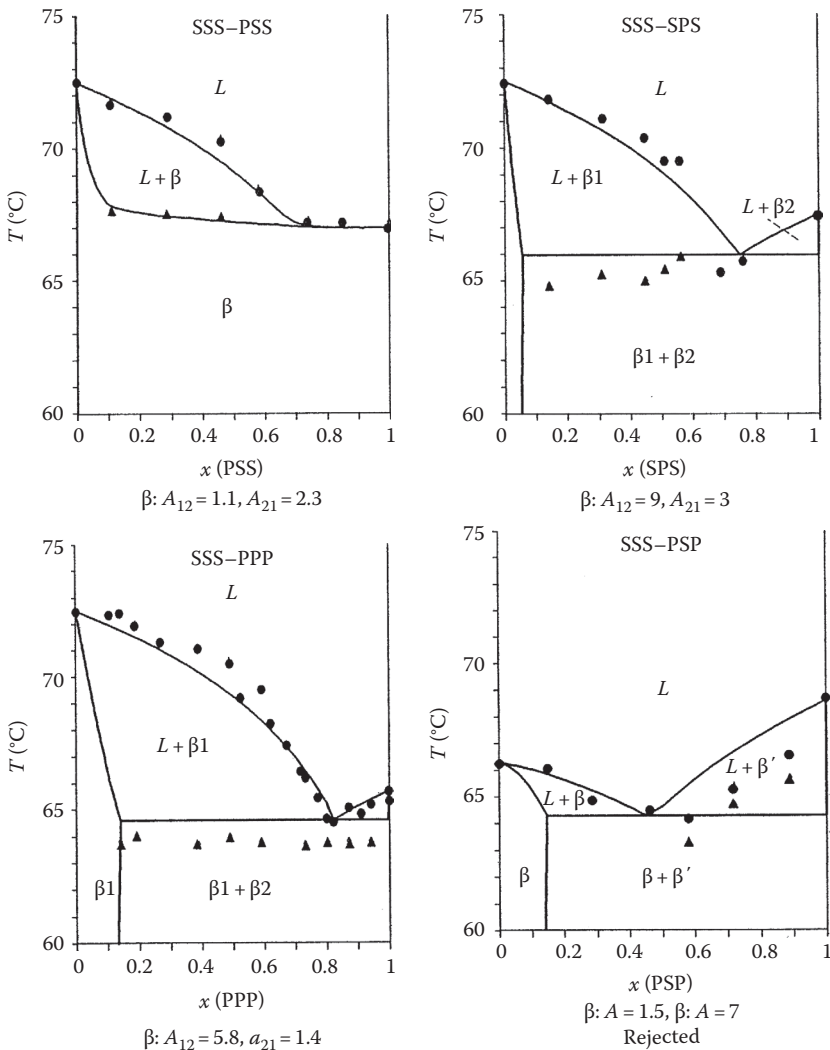


FIGURE 9.21 T, x, y diagrams of TAGs from Table 9.20. Experimental data (circles: clear points; triangles: softening points) and best fit (lines) with the 2- or 3-suffix Margules equation ($a = A/RT$).

The data of Lutton (1955) and de Bruijne and Reckweg for SSS-PPP are in good agreement, while the data of the other authors mentioned by Rossell (Kerridge, Kung, Joglekar) disagree and cannot be fitted at all.

Lutton's and de Bruijne's data for SSS-PSP also agree very well. Both deviate from the data of Perron (Ollivon and Perron, 1979), which show a greater discrepancy between solidus and liquidus. When fitting the G^E models to Perron's data, the residual error is much larger, but similar interaction coefficients are obtained.

The diagrams of SSS-PSS, SSS-PSP, PSS-SPS, PSS-PPS, PSS-PSP, SPS-PSP, and SPS-PPS are perfectly acceptable and are described rather well.

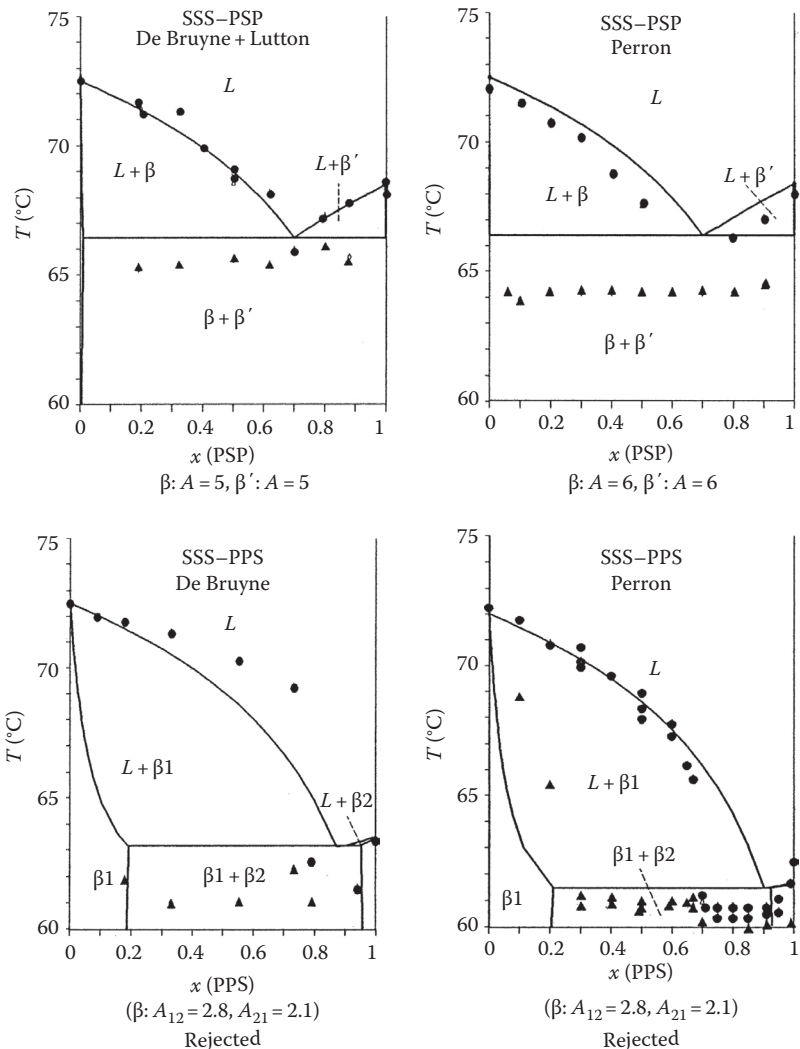


FIGURE 9.22 T, x, y diagrams of TAGs from Table 9.20. Experimental data (circles: clear points; triangles: softening points) and best fit (lines) with the 2- or 3-suffix Margules equation ($a = A/RT$).

The 3-suffix Margules parameter ASSS-SPS is inaccurate, due to lack of data on the SPS side of the diagram. The same holds for the PPP side of the PSP-PPP diagram.

The data for SSS-PPS of de Bruijne are poor; part of the data lies above the ideal liquidus, while the data points on the PPS side of the diagram lie below the eutectic liquidus. The solidus points indicate that the 2-suffix Margules interaction parameter should exceed 2.2. The liquidus of Perron for this binary is somewhat better, although it still does not meet the acceptance criteria of Section 9.7.2.3; on average, the liquidus lies more than 2°C below the eutectic liquidus.

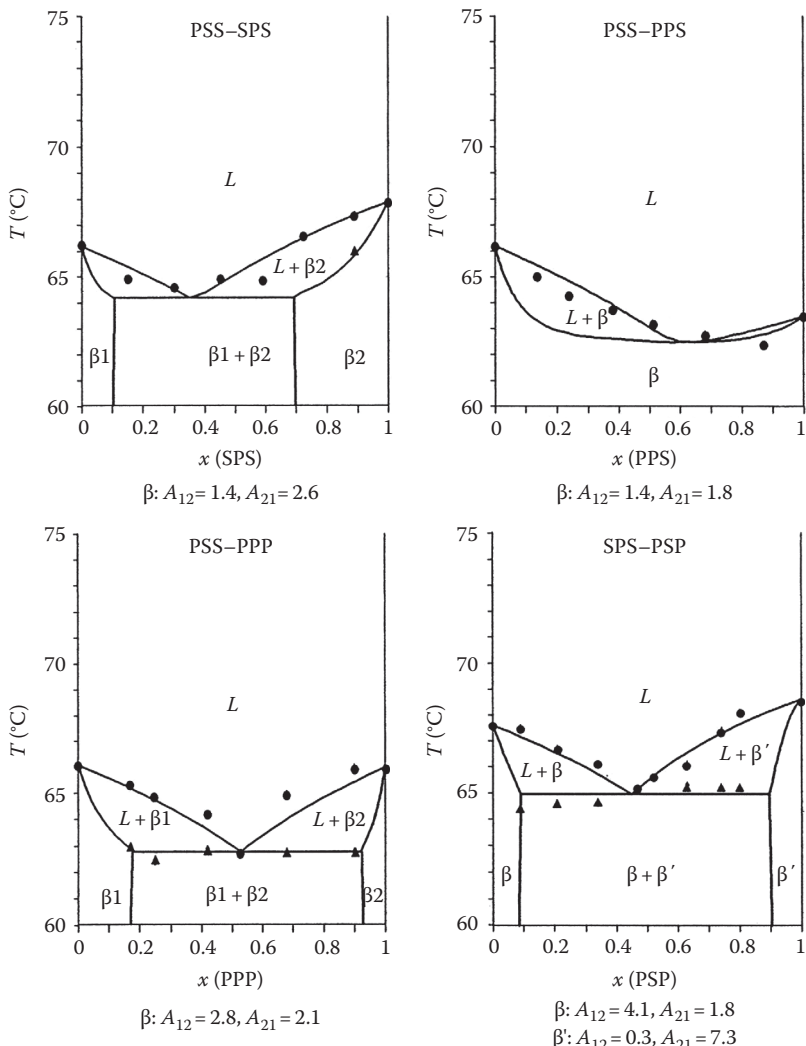


FIGURE 9.23 T, x, y diagrams of TAGs from Table 9.20. Experimental data (circles: clear points; triangles: softening points) and best fit (lines) with the 2- or 3-suffix Margules equation ($a = A/RT$).

At the PSP side of the PSS–PSP diagram, the experimental clear points also lie far below the eutectic liquidus, indicating poor quality of the data. Best fit to the PSS side of the diagram gives an $A(\beta)/RT$ of 1.5 for this system.

The liquidi of Perron and de Bruijne for the system PSP–PPS agree very well, the solidi are in complete disagreement. Best fit to the clear points results in a nearly eutectic solidus, in agreement with de Bruijne's results. The best fit to the complex solidus of Perron, which shows a peritectic and an eutectic, results in a liquidus that fits poorly to the data.

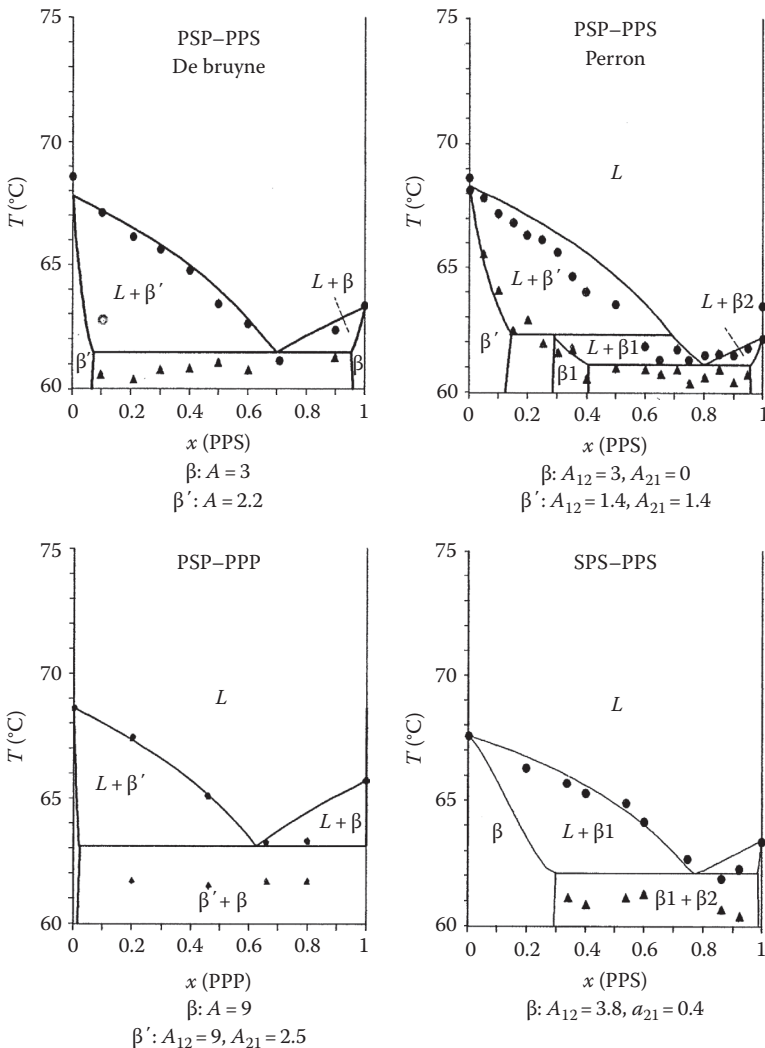


FIGURE 9.24 T, x, y diagrams of TAGs from Table 9.20. Experimental data (circles: clear points; triangles: softening points) and best fit (lines) with the 2- or 3-suffix Margules equation ($a = A/RT$).

In the diagram of PPS-PPP, there are two data points on the PPP side that lie more than 1° below the eutectic liquidus. Those points were given very low weight during fitting. The same occurs in the diagram of SPS-PPP, resulting in a very inaccurate 3-suffix Margules parameter for the solubility of SPS in PPP.

9.7.2.4.2 Saturated Mono-Acid TAGs

The melting points most of these TAGs differ considerably. Therefore no exact values for the interaction parameters can be obtained. In this case fitting is merely

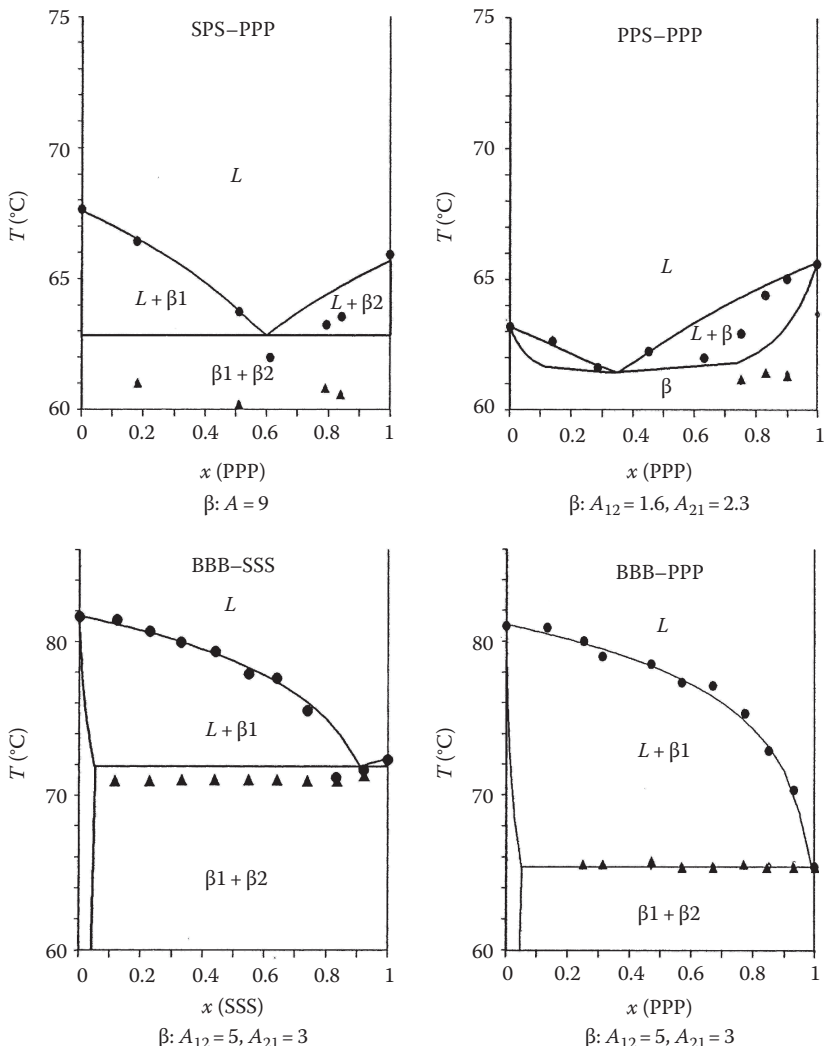


FIGURE 9.25 T, x, y diagrams of TAGs from Tables 9.20 and 9.21. Experimental data (circles: clear points; triangles: softening points) and best fit (lines) with the 2- or 3-suffix Margules equation ($a = A/RT$).

a check whether the reported liquidi agree with expectations (Table 9.21, Figures 9.25 and 9.26).

Indeed all liquidi are described very well. The data of Kerridge and Barbano contain solidus points that lie far above the ideal solidus.

Lutton's data for the systems with LLL confirm that these solidus points are indeed not right. The available solidus points indicate that in all systems solid solubility is only very limited.

TABLE 9.20
Binary Interaction Parameters for the P/S TAGs
and Root Mean Square Error between Experimental
Points and Fitted Liquidus

Binary	2-Suffix Margules		3-Suffix Margules		RMSE	Ref
	A/RT	RMSE	A₁₂/RT	A₂₁/RT		
SSS-PSS	1.6	0.3	1.1	2.3	0.3	A
SSS-PSP	3–7	0.3	3–7	3–7	0.4	A/B
β'	3–7		3–7	3–7		
SSS-SPS	3–9	0.7	3–9	2–4	0.8	A
SSS-PPS	>2.2?	1.7	—	—	—	A
SSS-PPP	3	0.8	5.8	1.4	0.7	A/B
PSS-PSP	1.5?	1.2	—	—	—	A
β'	7?		—	—		
PSS-SPS	2.0	0.4	1.4	2.6	0.3	A
PSS-PPS	1.6	0.4	1.4	1.8	0.5	A
PSS-PPP	2.2	0.5	2.8	2.1	0.5	A
PSP-SPS	1.4	0.3	1.8	1–6	0.3	A
β'	1.0		2–7	0.3		
PSP-PPS	3–9	0.9	3–9	1–9	0.9	A
β'	2.2–9		1–9	2.2–9		
PSP-PPP	3–9	0.7	0–9	3–9	0.8	A
β'	0–9		0–9	0–9		
SPS-PPS	2.0	0.6	3–5	0.4	0.4	A
SPS-PPP	5–9	0.8	5–9	5–9	0.8	A
PPS-PPP	1.9	0.7	1.6	2.3	0.7	A
Perron:						
SSS-PSP	5–9	0.7	5–9	5–9	0.8	C
	5–9		5–9	5–9		
SSS-PPS	2.1?	2.4	—	—	2.4	C
PSP-PPS	—	—	3	0	—	C
			1.4	1.4		

Sources: Data from A: de Bruijne, P. and Reckweg, F., *PDV*, 72, 3275; (B): Lutton, E.S., *JAOCS*, 32, 49, 1955; and (C): Perron, R., Petit, J., and Matthieu, A., *Chem. Phys. Lipids*, 6, 58, 1971.

Note: Standard error in the constants is 0.5. When two sets of constants are given, the first are values for the beta and the second set is for the β' -modification.

9.7.2.5 Saturated TAGs + Trans-TAGs

The similarity between elaidic acid and stearic acid is reflected in the nearly ideal miscibility of SSE and SES with SSS ([Figures 9.27](#) and 9.28).

The interaction parameters for PPP-SSE are very similar to that of PPP and SSS. However, the data of Kung for this system look unreliable: there is a very poor

TABLE 9.21
Binary Interaction Parameters and Root Mean Square Error between Experimental Points and Fitted Liquidus for Saturated Mono-Acid TAGs

Binary	2-Suffix Margules		3-Suffix Margules		RMSE	Ref
	A/RT	RMSE	A₁₂/RT	A₂₁/RT		
BBB–SSS	3–9	1.0	4–9	2–9	1	A
BBB–PPP	3–9	0.5	3–9	2–9	0.5	A
SSS–PPP	3	0.8	5.8	1.4	0.7	A/B
SSS–LLL	3–9	0.9	3–9	3–9	0.9	B/C
SSS–888	3–9	2.4	3–9	0–9	2.4	D
PPP–MMM	3–9	0.3	3–9	2–9	0.3	E
PPP–LLL	3–9	0.3	5–9	2–9	0.3	B/C

Sources: Data from (A) de Bruijne, P. and Reckweg, F., *PVD*, 71, 3637; de Bruijne, P., and Reckweg, F., *PVD*, 72, 3275; (B) Lutton, E.S., *JAOCs*, 32, 49, 1955; (C) Kerridge, R., Unpublished work, Private communication to J.B. Rossel, 1952; (D) Barbano, P. and Sherbon, J.W., *JAOCs*, 55, 478, 1977; (E) Krautwurst, J., *Keiler Milchw. Forsch. Ber.*, 22, 255, 1972.

Note: Standard error in the parameters is 0.5, unless otherwise indicated.

correspondence between liquidus and solidus and the liquidus lies well below the eutectic liquidus near the eutectic point. Therefore the interaction parameters cannot be very reliable either.

Clement's data for PPP–EEE had to be disregarded: the liquidus and solidus lie too far above the ideal liquidus and solidus. Simultaneously, Clements measured the system LLL–EEE, using the same technique and batch of EEE. The data are therefore suspect. The fit to these data is with a residual error of 20%, which is rather poor. The interaction coefficients for EEE–LLL should therefore not be taken too seriously (Table 9.22).

9.7.2.6 Saturated TAGs + Mono- and Di-Unsaturated TAGs

Due to the large differences in melting points, it will only be possible to get a coarse indication of the magnitude of the interaction parameters (Figures 9.28 and 9.29).

A complicating factor in the interpretation of these phase diagrams is the fact that the saturated TAGs crystallize in the β -2 modification, while the *cis*-unsaturated TAGs crystallize in the β -3 modification. Complete miscibility of a saturated and a *cis*-unsaturated TAG is impossible: an intermediate β' -2/ β' -3 structure is not feasible. In thermodynamic calculations, the two β' -forms must therefore be treated as separate modifications, just like the β' - and β -modifications. This requires β -3 melting points and enthalpies of fusion of β -2 stable TAGs and vice versa. In line with the findings of de Jong (1980) and the observations in Section 15.4, the melting point of the β -form

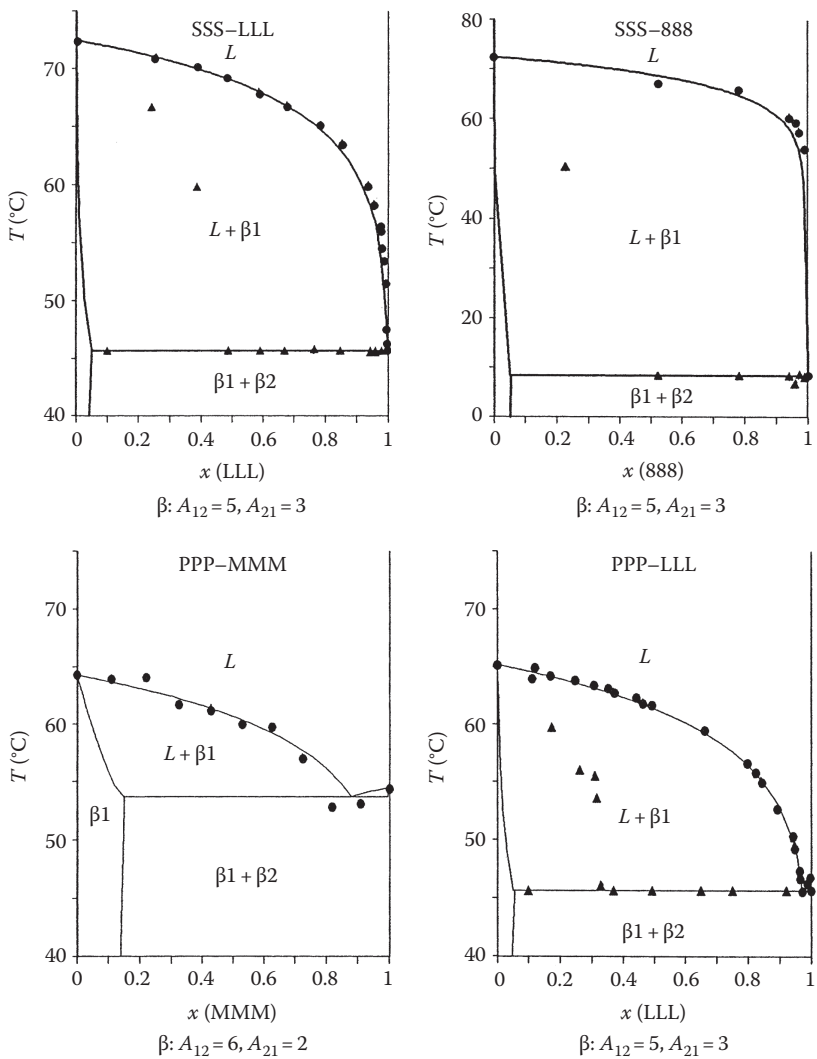


FIGURE 9.26 T, x, y diagrams of TAGs from Table 9.21. Experimental data (circles: clear points; triangles: softening points) and best fit (lines) with the 2- or 3-suffix Margules equation ($a = A/RT$).

that does normally not occur in the pure substance lies 3°C below the normal β melting point, while the enthalpy of fusion is 90% of that of the normal β -enthalpy of fusion.

The liquidi of SSS-SOS (Lutton) and of PPP-POO (Gibon) are described very well. In those cases also, good correspondence with the solidi could be obtained (Table 9.23).

The liquidi of PPP-SOS (Kung, 1950), PPP-POP (Kerridge, 1952), and the data for PPP-POO of Morancelli et al. (1985) are rejected: do not meet the criteria of Section 9.7.2.3: the liquidus lines lie too far below the eutectic liquidus and large parts of the solidus lines are found far above the ideal solidus.

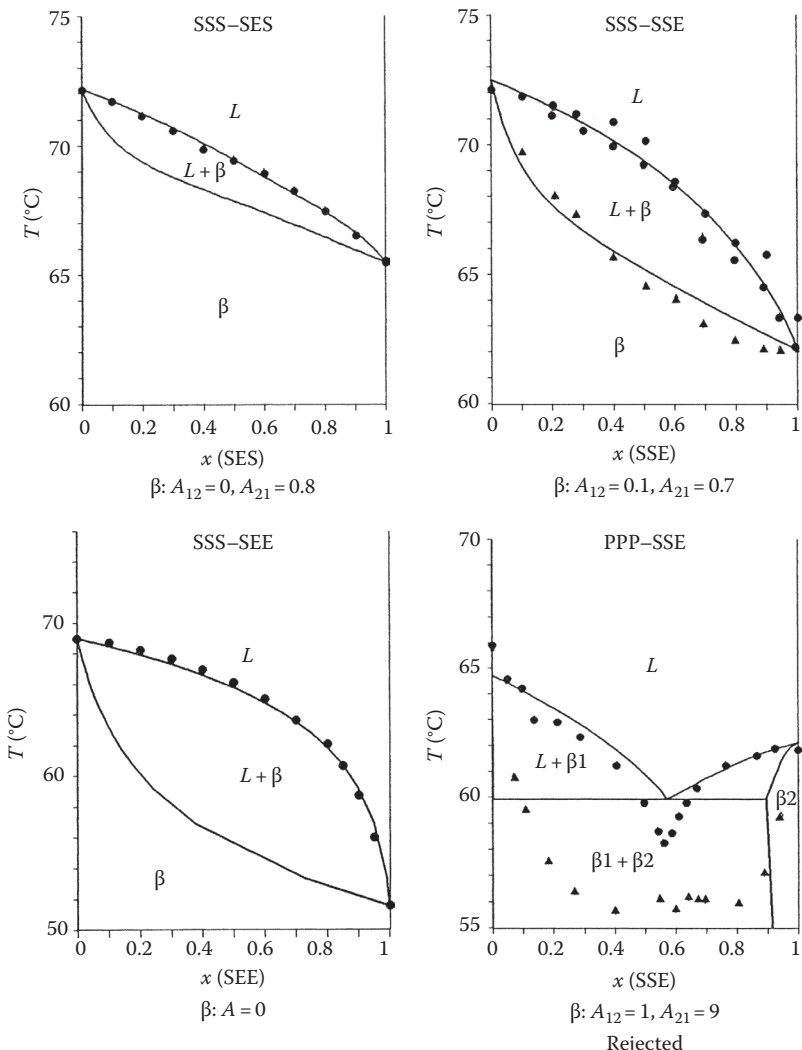


FIGURE 9.27 T, x, y diagrams of TAGs from Table 9.22. Experimental data (circles: clear points; triangles: softening points) and best fit (lines) with the 2- or 3-suffix Margules equation ($a = A/RT$).

9.7.2.7 Unsaturated TAGs

9.7.2.7.1 Mono-Unsaturated TAGs

SSE and SES show ideal miscibility, in line with the good solid solubility of both components in SSS. Elaidic acid behaves like stearic acid (Figures 9.29 and 9.30).

Smith determined solidus and liquidus in independent experiments using NMR. His liquidi of POS–POP, SOS–POP, and SOS–POS, which he obtained after extensive temperature cycling, fit very well. Smith's cycling procedure was less suited for obtaining a reliable solidus, and consequently the correspondence between the solidus and liquidus data is not perfect.

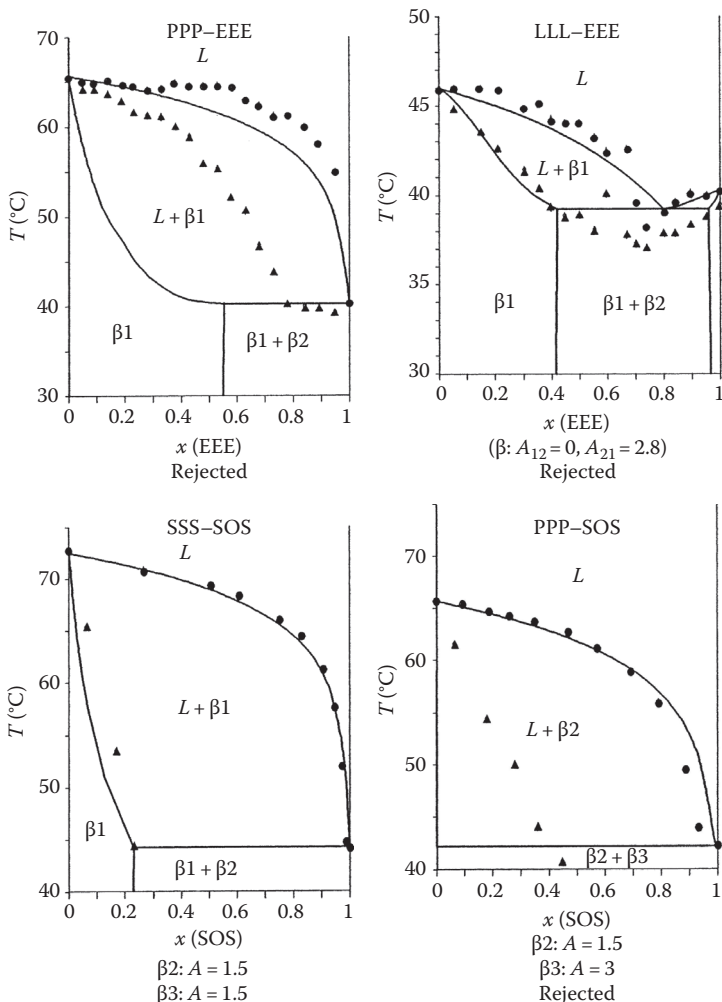


FIGURE 9.28 T, x, y diagrams of TAGs from Tables 9.22 and 9.23. Experimental data (circles: clear points; triangles: softening points) and best fit (lines) with the 2- or 3-suffix Margules equation ($a = A/RT$).

The diagrams of SOS–SSO and POP–PPO could not be fitted. For both systems, there is evidence for formation of a 50–50 compound (Timms, 1984), leading to a maximum in the liquidus lines. The β' -liquid phase diagrams for POP–PPO given by Morancelli et al. (1985) and de Bruijne and Reckweg are in complete disagreement. Morancelli obtained an eutectic at 15% POP, while de Bruijne found an eutectic near 50% POP, in agreement with the eutectic composition that is expected from calculations. Phase diagrams in the unstable β' -modification are suspect: during slow scanning in the DTA or DSC equipment the transition to a more stable modification will occur very easily when a large amount of liquid phase is present. Consequently, not all clear points may be those of the unstable modification.

TABLE 9.22
Binary Interaction Parameters and Root Mean Square
Error between Experimental Points and Fitted
Liquidus for Saturated + *Trans*-Containing TAGs

Binary	2-Suffix Margules		3-Suffix Margules		RMSE	Ref
	A/RT	RMSE	A₁₂/RT	A₂₁/RT		
SSS–SES	0.4	0.2	0	0.8	0.2	A
SSS–SSE	0.4	0.7	0.1	0.7	0.5	A/B
PPP–SSE	—	—	1?	9?	0.9	B
PPP–EEE	—	—	—	—	—	C
LLL–EEE	—	—	2.8?	0?	—	C

Sources: Data from (A): Grootsholten, P.A.M., Unilever Research Vlaardingen, Private communication, 1987; (B): Kung, H.C., Internal Unilever Report LB 113, 1950; (C): Clements, M.S. and Rossell, J.B., Internal Unilever Report P WN 660044, 1966.

Note: Standard error in the constants is 0.5, unless otherwise indicated.

The binary POP–PEP is another example of a phase diagram of two TAGs, which crystallize in different β -forms: PEP crystallizes into the β -2 form, while POP crystallizes into the β -3 form.

9.7.2.7.2 Other Unsaturated TAGs

All phase diagrams reported for these TAGs seem very unreliable (Figures 9.30 and 9.31). Rossell (1967) gives three diagrams of SOS–SOO, from McGowan, Morancelli, and Rossell. The three diagrams all disagree and have liquidus far below the eutectic liquidus. Therefore they are unreliable. There is one similarity: all diagrams have peritectic point at 24% SOS and about 27°C. This peritectic point can be obtained using the values of the interaction parameters given in Tables 9.24 and 9.25.

The liquidus data of Gibon for PPO–POO are described by the eutectic liquidus. The data were obtained after a stabilization at room temperature for a year. The mixtures are still partially liquid at room temperature and it may be assumed that sufficient recrystallization had occurred to render a reasonable liquidus. The solidus was obtained directly after crash cooling and is therefore unreliable. Moran gives for PPO–POO a liquidus far below the eutectic liquidus. His data were therefore not further used.

Both diagrams of Morancelli for POP–POO also have a liquidus below the eutectic liquidus and were therefore disregarded. In Gibon's DSC curves for POP–POO the final melting peak overlapped with a β – β transition. Stabilization has been insufficient.

The data of Morancelli for PPO–OPO are very well described by the eutectic liquidus, but the solidus again lies far above the ideal solidus.

Morancelli reported two diagrams for POO–OPO, of which the one given in Figure 9.14 has an eutectic composition where it is expected, at about 50% POO.

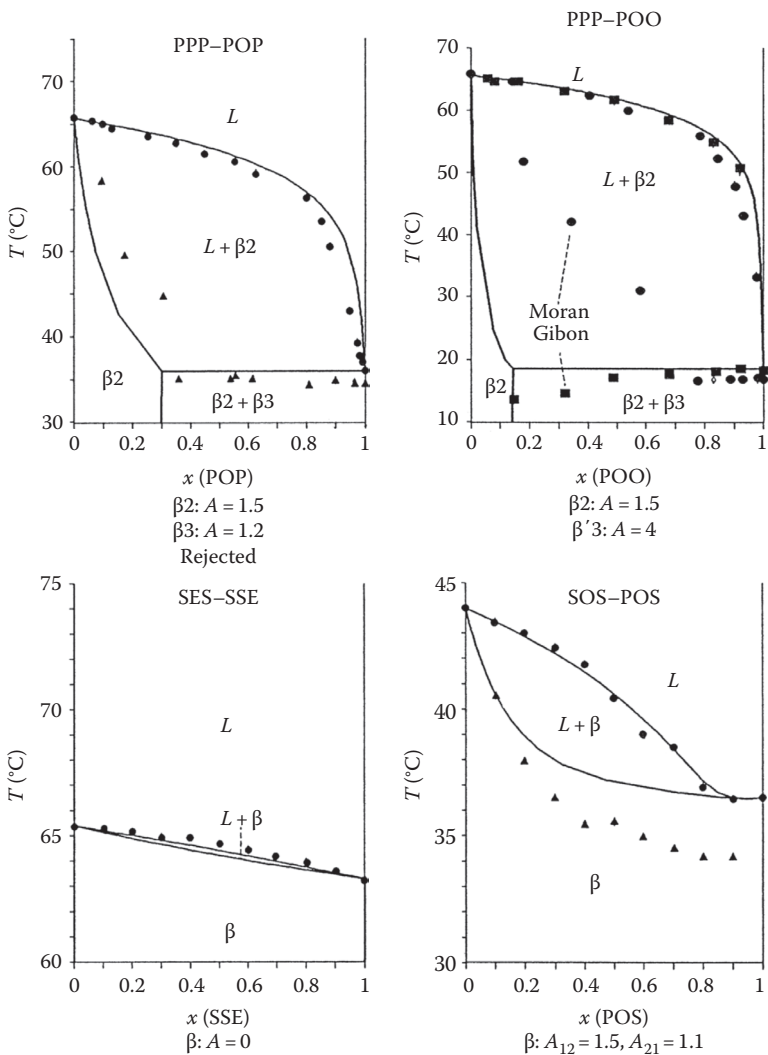


FIGURE 9.29 T , x , y diagrams of TAGs from Tables 9.23 and 9.24. Experimental data (circles: clear points; triangles: softening points) and best fit (lines) with the 2- or 3-suffix Margules equation ($a = A/RT$).

Strangely enough Morancelli judged his other diagram, with a eutectic at 17% POO, more reliable. The correspondence with the solidus is poor in both cases.

Morancelli's diagram for POP-OPO has to be disregarded: the liquidus lies far below the eutectic liquidus. Morancelli explained this by assuming compound formation, but if a compound would have formed, part of the liquidus certainly had to be situated above the eutectic liquidus.

It seems that most of Morancelli's data are not reliable, which arouses doubts about the two diagrams of Morancelli (PPO-OPO and POO-OPO) that did meet the acceptance criteria of Section 9.7.2.3.

TABLE 9.23
Binary Interaction Parameters and Root
Mean Square Error between Experimental
Points and Fitted Liquidus for the
Saturated + Unsaturated TAGs

Binary	2-Suffix Margules		RMSE	Ref
	$A\beta-2/RT$	$A\beta-3/RT$		
SSS–SOS	>1.5	>1	2	A
PPP–SOS	>1	>1	4	B
PPP–POP	>1.3	>1	3.6	C
PPP–POO	1.5	4 ($\beta'-3$)	1	D

Sources: Data from (A): Grootscholten, P.A.M., Unilever Research Vlaardingen, Private communication, 1987; (B): Kung, H.C., Internal Unilever Report LB 113, 1950; (C): Kerridge, R., Unpublished work, Private communication to J.B. Rossel, 1952; (D): Gibon, V., Thesis, Universite Notre Dame de la Paix, Namur, Belgium, 1984.

Note: Standard Error in the Constants is 0.5, unless otherwise indicated.

9.7.2.7.3 *Triolein*

Indeed, all data lie reasonably well on the calculated liquidus, the data of Grootscholten being slightly better than those taken from Rossell (1967; Figures 9.31 and 9.32).

In these diagrams, the difference in melting points is so large that the ideal and eutectic liquidus and solidus almost coincide.

Fitting is in this case merely a test of the quality of the data and does not give much information about the extent of nonideal mixing (Table 9.26).

9.7.2.8 *Summarizing*

Nearly 120 phase diagrams were considered:

- 84 had to be rejected because they were clearly not correct.
- The liquidus lines were fitted very well for 34 of the remaining 36 phase diagrams. The average deviation from the experimental curves was only 7% of the difference between maximal and minimal liquidus temperature.
- In two cases, no fit could be obtained, which was attributed to compound formation that was not accounted for in the thermodynamic modeling.
- The experimental softening points lay far above the ideal solidus at the side of the higher melting component in five of the 34 remaining diagrams. These five binaries all concerned TAGs with a large difference in melting point. It was made plausible that this deviation was due to an experimental error. Experimental evidence that confirmed this exists for two of the five binaries.

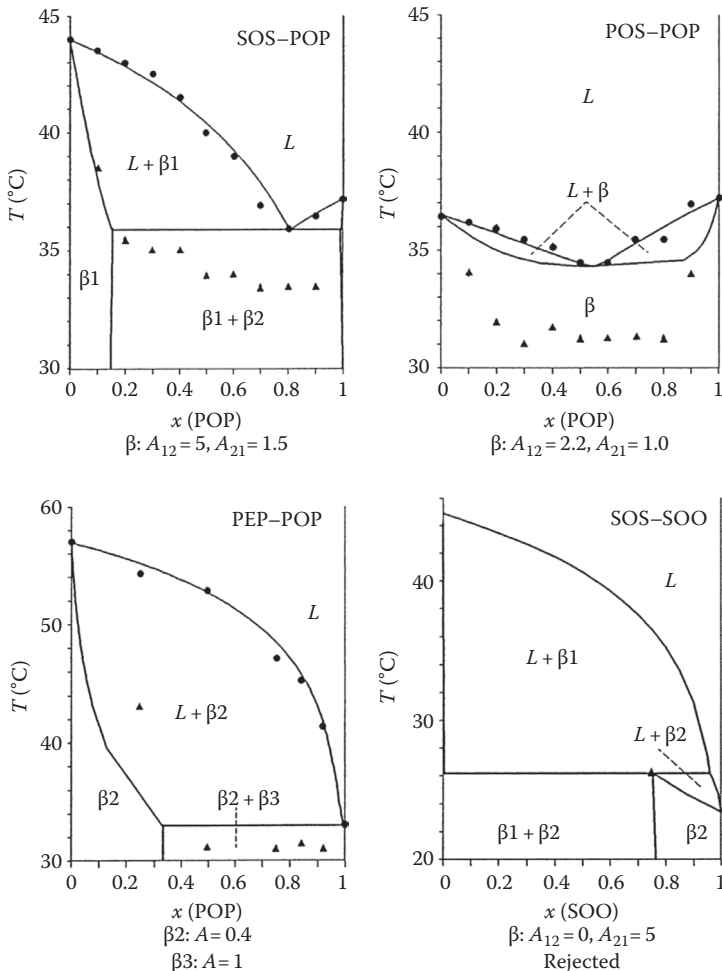


FIGURE 9.30 T, x, y diagrams of TAGs from Tables 9.24 and 9.25. Experimental data (circles: clear points; triangles: softening points) and best fit (lines) with the 2- or 3-suffix Margules equation ($a = A/RT$).

- The difference between the melting points of two components was less than 15°C in 24 of the 34 binaries that remained. Eleven of these 24 diagrams were almost completely eutectic. This implies that only in 13 diagrams the interaction parameters have a clear influence on the shape of the liquidus. Therefore these 13 diagrams are the most demanding test cases for the performance of the excess Gibbs energy models.

The average root mean square error between measured and fitted liquidus for these 13 remaining diagrams is 0.4°C. This is approximately the experimental error that is claimed. It is impossible to obtain very accurate values of the interaction parameters with an experimental error of this magnitude.

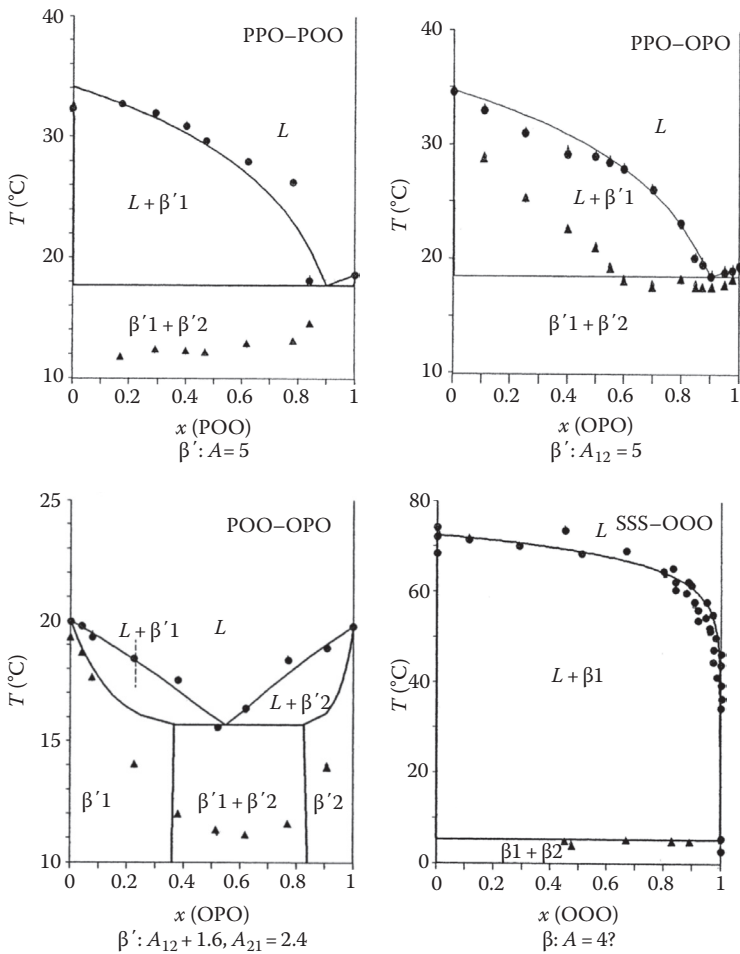


FIGURE 9.31 T , x , y diagrams of TAGs from Tables 9.25 and 9.26. Experimental data (circles: clear points; triangles: softening points) and best fit (lines) with the 2- or 3-suffix Margules equation ($a = A/RT$).

Based on the available data, it is not possible to express a preference for one of the two excess Gibbs energy models used. Hardly any improvement in fit was obtained when the 3-suffix Margules equation was used. Peritectic diagrams that could not be described using the 2-suffix Margules equation, had to be disregarded. Generally the experimental softening points were better described with the 3-suffix Margules equation.

9.7.3 ALTERNATIVE TO PHASE DIAGRAM DETERMINATION

9.7.3.1 How to Proceed?

The evaluation of all available phase diagrams of TAGs in the previous Section (9.7.2.8) has resulted in interaction coefficients for only 35 binaries. The uncertainty in these interaction parameters is considerable, due to the large experimental error in the diagrams.

TABLE 9.24
Binary Interaction Parameters and Root Mean Square Error between Experimental Points and Fitted Liquidus for Mono-Unsaturated TAGs

Binary	2-Suffix Margules		3-Suffix Margules		RMSE	Ref
	<i>A/RT</i>	RMSE	<i>A₁₂/RT</i>	<i>A₂₁/RT</i>		
SES-SSE	0	0.2	0	0	0.2	A
SOS-SSO	—	—	—	—	—	B
SOS-POS	1.3	0.2	1.5	1.1	0.2	C
SOS-POP	3.6–6	0.3	5	1.5	0.3	C
POS-POP	1.6	0.5	2.2	1.0	0.4	C
POP-PPO	—	—	—	—	—	E
POP-PEP	0.4 ± 1	0.9	—	—	—	D
B-3::	1 ± 0.8					

Sources: Data from (A) Grootscholten, P.A.M., *LPVD*, 3074, 84; (B) Freeman, I.P., Internal Unilever Report, Port Sunlight Program, 45, Spring 1957; (C) Smith, K., Unilever Research Colworth, Private communication, 1988; (D) Lovegren, N.V., *JAOCS*, 53, 519, 1976; (E) Morancelli, M., Strauss, H.L., and Snyder, R.G., *J. Phys. Chem.*, 89, 5260, 1985.

Note: Standard Error in the Constants is 0.5, unless otherwise indicated.

TABLE 9.25
Binary Interaction Parameters and Root Mean Square Error between Experimental Points and Fitted Liquidus for Unsaturated TAGs

Binary	2-Suffix Margules		3-Suffix Margules		RMSE	Ref
	<i>A/RT</i>	RMSE	<i>A₁₂/RT</i>	<i>A₂₁/RT</i>		
SOS-SOO	—	—	0?	5?	—	A
PPO-POO(β')	1–9?	1.7	1–9?	1–9?	1.7	C
PPO-OPO(β')	5–9?	0.6	4–9?	2–9?	0.6	B
POO-OPO(β')	2.0?	0.3	1.6?	2.4?	0.3	B

Sources: Data from (A) Rossell, J.B., *Adv. Lip. Res.*, 5, 353, 1967; (B) Morancelli, M., Strauss, H.L., and Snyder, R.G., *J. Phys. Chem.*, 89, 5260, 1985; (C) Gibon, V., Thesis, Universite Notre Dame de la Paix, Namur, Belgium, 1984.

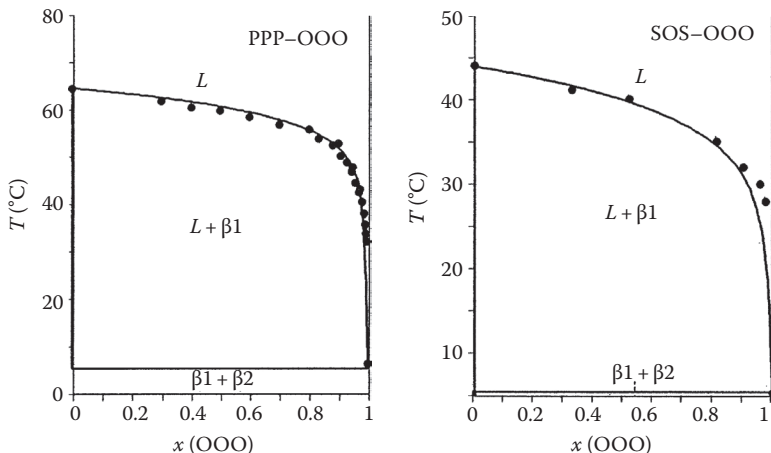


FIGURE 9.32 T, x, y diagrams of TAGs from Table 9.27. Experimental data (circles: clear points, triangles: softening points) and calculated lines.

TABLE 9.26
Binary Interaction Parameters and Root Mean Square Error between Experimental Points and Fitted Liquidus for Triolein

Binary	2-Suffix Margules		3-Suffix Margules		RMSE	Ref
	A/RT	RMSE	A_{12}/RT	A_{21}/RT		
SSS-OOO	0–9	4	—	—		A/B
PPP-OOO	0–9	3	—	—		A/B
SOS-OOO	0–9	2	—	—		A

Sources: Data from (A) Rossell, J.B., *Adv. Lip. Res.*, 5, 353, 1967; (B) Grootscholten, P.A.M., Unilever Research Vlaardingen, Private communication, 1987.

Interaction parameters were almost exclusively obtained for the β -modification. However, it is of much greater importance to know the parameters for the polymorph that is normally found in edible fat products, the β' -modification.

The determination of binary interaction parameters that occur in an excess Gibbs energy model by fitting this model to experimental binary T, x, y solid–liquid phase diagrams has a number of very serious drawbacks:

- It is extremely troublesome, time-consuming, and probably almost impossible to determine accurate phase diagrams. It takes months to years before the samples have been stabilized properly, minor impurities have large effects, and the true start and end melting point of a mixture are very hard to determine.
- Relatively small experimental errors in the position of the liquidus and solidus lead to large uncertainty in the interaction parameters that are

determined from the diagrams. It is questionable whether more accurate β -data can be obtained by determining binary solid–liquid phase diagrams.

- It is not possible to measure reliable phase diagrams of unstable modifications, like a binary β' -phase diagram of β -stable TAGs.
- Determination of binary interaction parameters from phase diagrams is only feasible for TAGs that differ less than about 15°C in melting point. At larger melting point differences, the position of liquidus and solidus becomes too insensitive to the value of the interaction parameters.

Determining phase diagrams of TAGs to obtain binary interaction parameters is therefore not practical and another method has to be defined.

9.7.3.2 Formulation of an Alternative Method

The problem of the extremely long stabilization times can probably be solved. In a solid binary system, diffusion rates are extremely low, so that unstable modifications and crystals with a nonequilibrium composition have been shown to persist for years (Gibon, 1984). But if a surplus of a liquid TAG is added to the binary system, things become different. The phase diagram of such a ternary system (PSP/SEE/OOO) is shown in Figure 9.33. When the temperature is sufficiently above the melting point of the liquid component (OOO), the solidus surface in the diagram coincides with the binary side plane of the two crystallizing TAGs (PSP and SEE), even when ideal mixing in the solid phase occurs. The concentration of the liquid component in the solid phase is then negligible. The solid phase in this ternary system is still a binary mixture.

If the fat is crystallized in very small ($<1\text{ }\mu\text{m}$) crystals, to create a large exchange surface with the liquid phase, then the solid fat can recrystallize relatively easily via

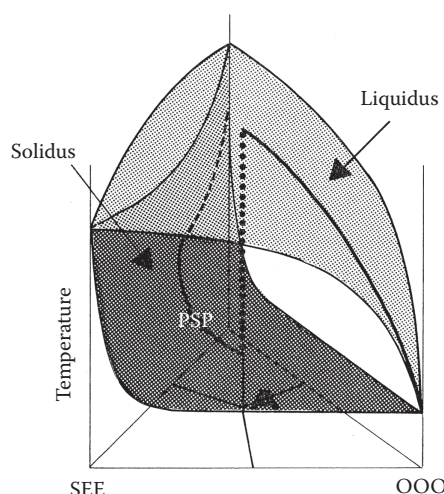


FIGURE 9.33 Schematic ternary phase diagram of the system PSP/SEE/OOO in the β' -modification. The softening point surface is dark shaded, while the clear point surface is light shaded. The lines indicated with solidus and liquidus represent the composition of the solid and liquid phase of a mixture with composition A while it is being melted.

the liquid phase to its equilibrium composition and modification (Zief and Wilcox, 1967; Norton et al., 1985).

Phase diagrams are usually determined by measuring the softening and clear point of a set of mixtures using DSC. Due to impurities and thermal lag that occur both points can only be determined with an accuracy of about 0.2°C–1°C.

In fact, this application of DSC does not use all available information: a DSC curve of a mixture is taken and next the two most undefined points on the curve, its start and end point, are used, while everything in between, that contains lots of information about the phase behavior of the binary system, is wasted. If the complete DSC curve is used for determination of the interaction parameters, rather than only 2 points, it should be possible to increase the accuracy of results with considerably less measurements. In Section 9.3.5, a method to simulate the effect of nonideal mixing in the solid phase on the shape of DSC curves was defined. This method can be applied to fit a complete DSC curve by adapting the binary interaction parameters.

The method for determining interaction parameters that evolve is to fit the complete DSC curve of a binary mixture, to which a surplus of a liquid TAG is added. The liquid TAG assures shorter and better stabilization. The use of the complete curves reduces experimental error reduces the number of measurements and removes the limitation to binary pairs that have a difference in melting point less than 15°C.

9.7.3.3 DSC Curves of Binary Systems Dissolved in a Liquid TAG

Figure 9.34 gives the types of DSC curves that can be obtained for TAGs that differ considerably in melting point by application of the 3-suffix Margules equation. Although in this situation the position of liquidus and solidus in the binary phase diagram is nearly invariant, still considerable differences in curve shape are obtained.

The following aspects feature:

1. All curves contain two melting peaks. The shape of the final melting peak and the start of the first melting peak are hardly influenced by the values of the interaction parameters. This is in line with the invariance of the phase diagram. However, the shape of the first melting peak and the height of the plateau in between the two peaks depend very much on the values of the interaction parameters.
2. The first melting peak ends sharply if demixing in the solid state occurs.
3. If no demixing occurs, the complete shape of the first melting peak is indicative for the value of the interaction parameters, which implies that the interaction parameters can be determined very accurately.
4. If demixing occurs, the height of the plateau just after the first peak is indicative for the magnitude of the interaction parameters. This implies that in these cases, the interaction parameters can be determined less accurately, due to the influence of noise and the uncertainty in the baseline.
5. Above values of $A/RT=4$ the curve shape does not depend on the magnitude of the interaction parameters any more. However, as at $A/RT=4$ already nearly complete solid phase immiscibility occurs, this is not a real problem.
6. For the 2-suffix Margules equation peak shape and peak position are closely related: upon increasing magnitude of the interaction parameters the first

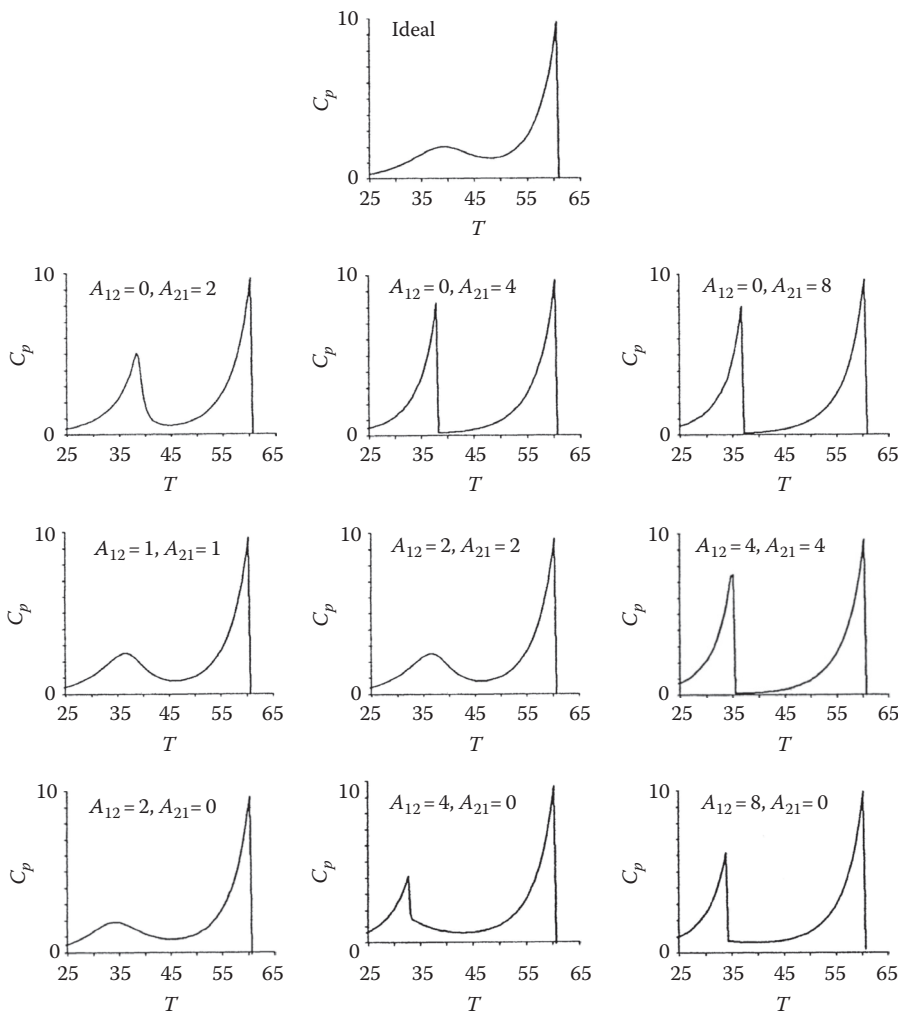


FIGURE 9.34 Theoretically possible DSC melting curves of a ternary mixture of 25% PSP, 25% SOS, and 50% OOO crystallized in the β' -2 modification. The curves are calculated using the 3-suffix Margules equation. The values of the binary interaction parameters are indicated.

melting peak becomes sharper and shifts toward lower temperatures. Therefore 2-suffix Margules parameters can be determined very easily. Bringing in asymmetric behavior with the 3-suffix Margules equation allows shifting of sharp peaks to higher temperatures and of broad humps toward lower temperatures. In fact, if the component with the highest melting point is [1] and the other [2], then the shape of the first melting peak is mainly determined by A_{21} and its position mainly by A_{12} . The 3-suffix Margules parameters determined from the curves will necessarily have a larger error, as the uncertainty in the melting points of 1°C–1.5°C has to be taken into account now.

9.7.3.4 What Experiments?

In most edible fat products, the fat has crystallized into the β' -modification. There are no reliable data available about miscibility in the β' -modification.

For fat fractionation calculations, it is important to know the solubility of mono-unsaturated TAGs in the solid phase of saturated TAGs both in the β' - and β -modifications. It is shown in Section 15.7.3 that the scarce information that exists is unreliable.

In many edible fat products up mostly partially hydrogenated fats were used up to 1995 to provide structure. These are rich in elaidic acid. After 1995 these have been gradually replaced in the industry by palm-oil based fats where structure comes from TAGs of the h2u and h2m type and nowadays elaidic acid rich fats are hardly used (Wesdorp, 1996; Dijkstra et al., 2008).

Of the many systems that can be studied, it seems therefore most relevant to determine interaction parameters of systems where monounsaturated and *trans*-containing TAGs are combined with saturated TAGs.

In order to enable the determination of β' -interaction parameters, assume that during determination of the DSC curve, which must be taken at low scan rates in order to reduce thermal lag, no transition to the β -modification will occur. Near the clear point the solid phase usually almost completely consists of the component with the highest melting point. If this component is β -stable, then a transition is very likely. However, if for this component a β' -stable TAG is taken, the chances of keeping the system sufficiently long into the β' -modification to allow a measurement are much higher. Moreover, even if in this case a solid phase in the β -modification, rich in the crystallizing component with the lower melting point, comes about, the DSC curve will still contain a melting peak of a mixed β' phase that holds information about the miscibility in the β' -modification.

In view of this, the authors have selected a number of systems, of a β' stable saturated TAG and a number of mono- and di-unsaturated TAGs, including some that contain elaidic acid:PSP with SOS, SSO, POP, PPO, PEE, EPE, SEE, ESE, and EEE. MPM with SOS, SSO, POP, PPO, PEE, EPE, SEE, ESE, and EEE.

These systems allow the study of the influence of a difference in size as well as the influence of position and nature of the unsaturated chains. The data themselves are relevant for normal edible fat products.

9.7.4 EXPERIMENTAL

9.7.4.1 Principles of DSC

With DSC, two cups, one containing a few milligrams of the sample to be investigated and the other containing an inert reference material, are placed in two identical microfurnaces. Both furnaces are mounted in cavities of a large aluminum block or heat sink. The aluminum block is kept at a constant temperature, well below the temperature range of the experiment. In the base of each furnace are two identical platinum resistance elements. One is used to provide heat to the furnace, the other that is mounted directly under the furnace base, serves as temperature sensor (Figure 9.35).

The equipment is controlled by two control loops: an average temperature control or scan loop that enables simultaneous heating of both microfurnaces at a constant heating rate (in $^{\circ}\text{C}/\text{min}$). The other loop is a differential temperature control loop from

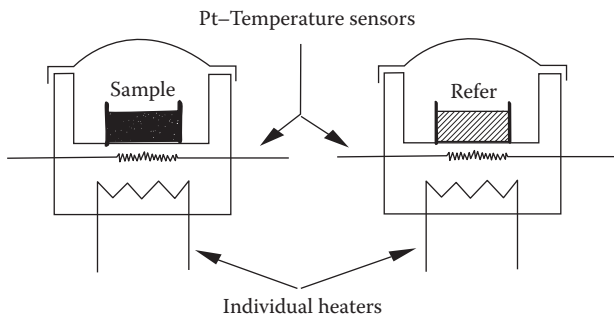


FIGURE 9.35 Schematic view of a DSC apparatus.

which the instrument output signal is obtained. This loop adjusts the heat flow to one of the furnaces if a process in one of the samples takes place that gives out or takes up heat, such that the temperature difference between the two cups always remains zero.

The difference in the amount of energy that must be supplied to the samples to heat both at the same rate plotted as a function of temperature is the DSC curve. It is directly proportional to the apparent heat capacity of the sample as a function of temperature.

DSC is often confused with DTA. In DTA, both samples are heated in the same microfurnace with a constant heat flow. The temperature difference that occurs between the samples, when the sample gives out or takes up heat, is recorded, the DTA curve. The DTA curve contains essentially the same information as the DSC curve. With DTA, fast heating and cooling rates as well as isothermal measurements are not possible and heat effects are derived quantities rather than directly measured quantities. However DTA is technically less complex.

9.7.4.2 Thermal Lag

The main problem in the use of DSC curves is the thermal lag that occurs. During scanning, the temperature of the inner part of the sample lags behind that of the apparatus. This thermal lag can completely disturb the shape of the DSC curve at large sample sizes and scan rates (Figure 9.36).

It is best to check for the presence of thermal lag by obtaining the steepness of the peak at the end melting point. Ideally this should be a straight line perpendicular to the temperature axis. At very low scanning rate or small sample size, thermal lag is negligible, but the DSC signal becomes very weak, leading to noisy DSC curves. In the experimental procedure, the right balance between thermal lag and sensitivity must be found by trial and error.

9.7.4.3 Experimental Procedure

The work was largely carried out using a Perkin Elmer DSC-2, equipped with an IBM-AT for data acquisition and control of the apparatus by means of software developed at the Department for Thermal Analysis of the Unilever Research Vlaardingen. Some work was done on a Perkin Elmer DSC-7, which is mechanically equivalent, but equipped with more advanced Perkin Elmer machinery for data acquisition and control, making it more sensitive. The heat sink was cooled with a solid CO₂/acetone

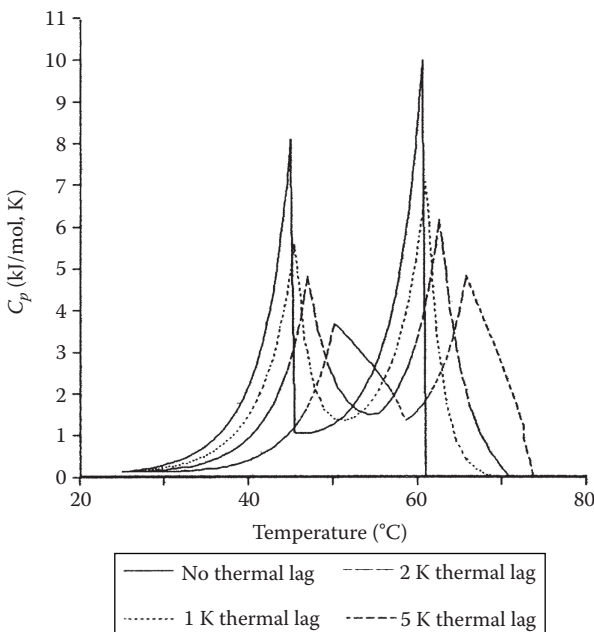


FIGURE 9.36 Influence of thermal lag on the curve shape of the system 25% PSP, 25% SEE, and 50% OOO (simulated curves).

mixture (DSC-2) or liquid nitrogen (DSC-7). The equipment was calibrated using pure indium ($T_f = 156.6^\circ\text{C}$) and gallium ($T_f = 29.8^\circ\text{C}$).

About 10 mg of a sample was weighed into an aluminum cup, which was closed and sealed. The sample was inserted into the apparatus, melted at 80°C and kept for 10 min at that temperature to prevent possible memory effects. Next the sample was cooled at $20^\circ\text{C}/\text{min}$ to 5°C below the temperature where the melting of a fully eutectic β' phase would take place. The sample was stabilized for 1 min at that temperature and subsequently heated at $1^\circ\text{C}–2^\circ\text{C}/\text{min}$. The melting curve was recorded. This procedure is repeated several times with varying stabilization times: 1 min stabilization, 5 min, 15 min, 1 h, 3 h, 24 h, 1 week, and 1 month.

Usually stabilization times less than 1 h resulted in melting curves of the β' -modification, sometimes disturbed by a transition to the β -modification. Longer stabilization times mostly lead to a 3-phase β – β' liquid system.

Stabilization longer than a week usually did not result in changes any more. To verify that indeed crystallization had taken place in the right polymorphic form, x-ray diffractograms were taken after the same cooling and stabilization procedure for some of the mixtures.

The influence of stabilization time on the polymorphic form in which crystallization has taken place is illustrated in Figure 9.37 for the system PSP/SEE/OOO. The shortest stabilization time only shows melting peaks of β' -crystal phases. After somewhat longer stabilization, a β -melting peak starts to appear as a shoulder, while in the completely stabilized sample, a sharp melting peak of a SEE-rich β phase is present next to a melting peak of a PSP-rich β' phase.

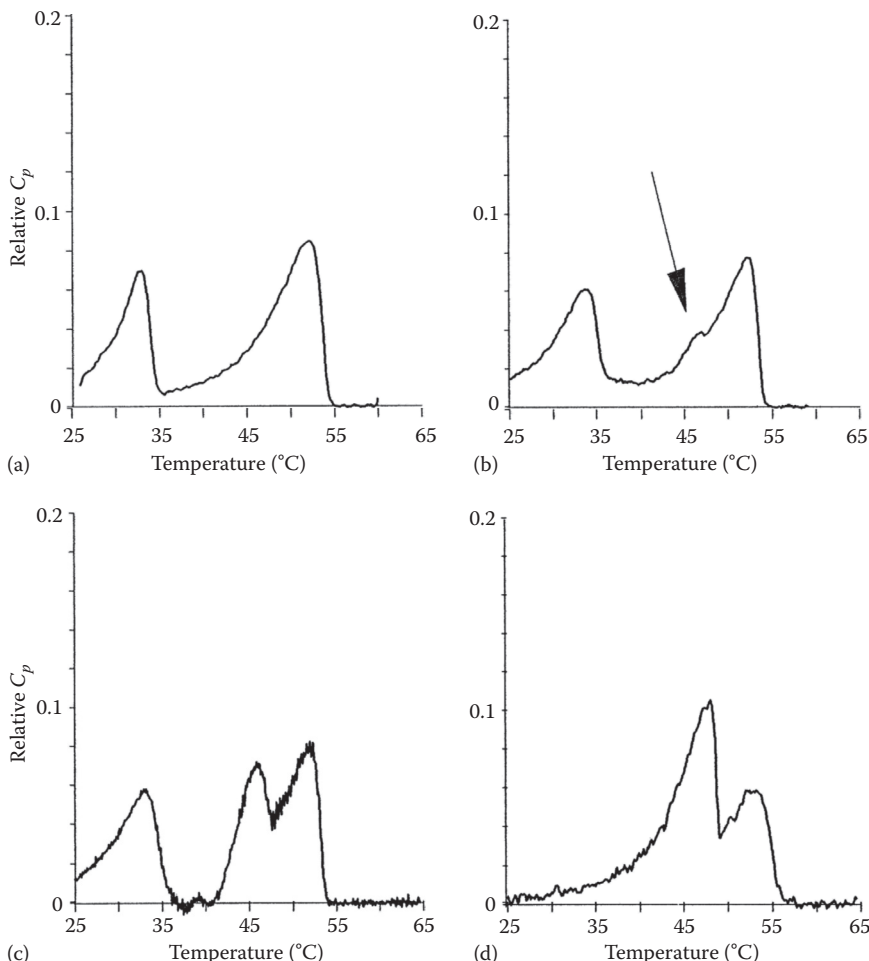


FIGURE 9.37 Measured DSC curves of ternary mixtures of 25% MPM% with $\pm 25\%$ ESE and $\pm 50\%$ OOO. Note the appearance of a melting peak of a separate ESE-rich β phase at 46°C and the disappearance of the melting peak of an ESE-rich β' phase at 34°C upon increasing stabilization time. (a) = 1 min 20°C . (b) = 15 min 20°C . (c) = 60 min 20°C . (d) = 7 days 20°C .

At the sample size and scan rate used, thermal lag maybe neglected: the curve shape does not change significantly when the scan rate is further decreased, while the noise increases. Normally a scan rate of $2.5^\circ\text{C}/\text{min}$ was used, sometimes, if no $\beta'-\beta$ transition occurred and the noise level was acceptable a scan rate of $1.25^\circ\text{C}/\text{min}$ was used.

The TAGs were obtained from Dr. A. Fröhling of the section Organic Chemistry of Unilever Research Vlaardingen. They were pure on TLC. To remove oxidation products and partial glycerides, the unsaturated TAGs were treated over a silica column. The TAGs were as extra purification recrystallized from hexane. To prevent oxidation during measurements and storage, 0.01% of butylhydroxyanisole (BHA) was added as antioxidant. The GLC and HPLC analysis results of the TAGs are given in Appendix 9.C.

9.7.4.3.1 Determination of Interaction Parameters

The interaction parameters were determined from the measured curves by adapting the parameters using a Simplex procedure until the sum of squared errors between the calculated and measured curve are minimal. Heats of fusion and melting points are obtained from the correlations of Section 9.4. As the melting points from the correlations, as well as experimental melting points, have an accuracy of about 1°C, we allowed the fitting procedure to vary the melting point maximally $\pm 1^\circ\text{C}$ around the value from the correlation. Both calculated as well as measured curves are normalized such that the area under the curves from 25°C up to the clear point equals unity. To reduce calculation time, the number of data points was reduced to one per 0.4°C. One iteration required about 40–60 s on a Compaq 386/25 PC under MS-DOS.

9.7.5 RESULTS

9.7.5.1 PSP and MPM with SEE and ESE

The measurements that were carried out and the results of the fitting procedure are given in Table 9.27 and Figures 9.38 and 9.39.

The fit to the measured curves is most satisfactory. The minor overshoot of the calculated curves at the top of sharp peaks must be ascribed to the inertness of the measuring technique, due to factors like thermal lag and the sampling time of the A/D converter in the DSC-2.

Only the 2-suffix Margules parameters are given, as no improvement of fit could be obtained by application of the 3-suffix Margules equation. While the interaction parameters for the β' -modification are indeed very accurate, the interaction

TABLE 9.27
DSC Measurements and 2-Suffix Margules Parameters for the Highest Melting Binary Pair Determined from These Measurements

Modifi- cation	PSP	MPM	SEE	ESE	OOO	Scan Rate (K/min)	Stabi-	Stabi-	A/RT
							zation Time (min)	zation Temp. (°C)	
β'	0.26		0.25		0.49	2.5	15–180	20	0 ± 0.2
β'		0.28	0.24		0.48	2.5	1–15	20	3.0 ± 0.2
β'	0.26			0.24		2.5	1–180	20–25	0 ± 0.2
β'						2.5	1–15	20	3.0 ± 0.2
β	0.26		0.25			2.5	14d	20	≥ 2.5
2.5β						2.5	1d–3d	20	≥ 2.5
β	0.26		0.24			1.25	5d–28d	20–25	≥ 2.0
β						1.25	1m–7d	20	2 ± 1

Note: Composition in mole fractions, temperatures in °C, time in minutes, unless otherwise indicated: d \triangleq days.

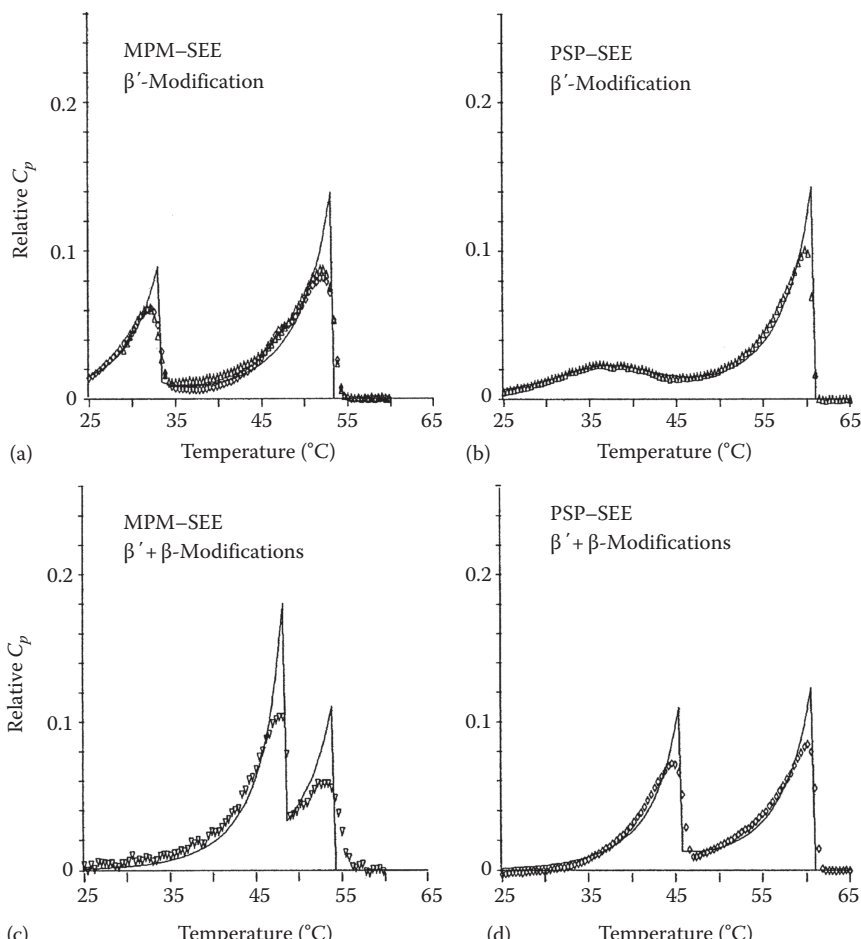


FIGURE 9.38 Measured (dots) and fitted (lines) DSC curves of ternary mixtures of $\pm 25\%$ PSP or MPM% with $\pm 25\%$ SEE and $\pm 50\%$ OOO. The modification(s) in which crystallization has taken place is indicated.

parameters for the β' -modification are only rough estimates. In combination with a β' -stable TAG, a solid phase split, leading to a DSC curve with two sharp peaks, will always occur. Only the position of the peak at the lower temperature end of the curve is indicative of the magnitude of β -interaction parameter, while its shape does not change.

The behavior of ESE and SEE is exactly the same, which is in correspondence to the close similarity of elaidic and stearic acid. Both mix ideally with PSP in the β' -modification, but show a solid solubility less than 15% in the β' -modification. With MPM, the solubility in the β' -modification is reduced to only 7%, showing the influence the increased difference in molecular size.

X-ray diffractograms for PSP-SEE-OOO are in line with these DSC observations: initially a typical β' diffraction pattern is obtained, with two strong maxima

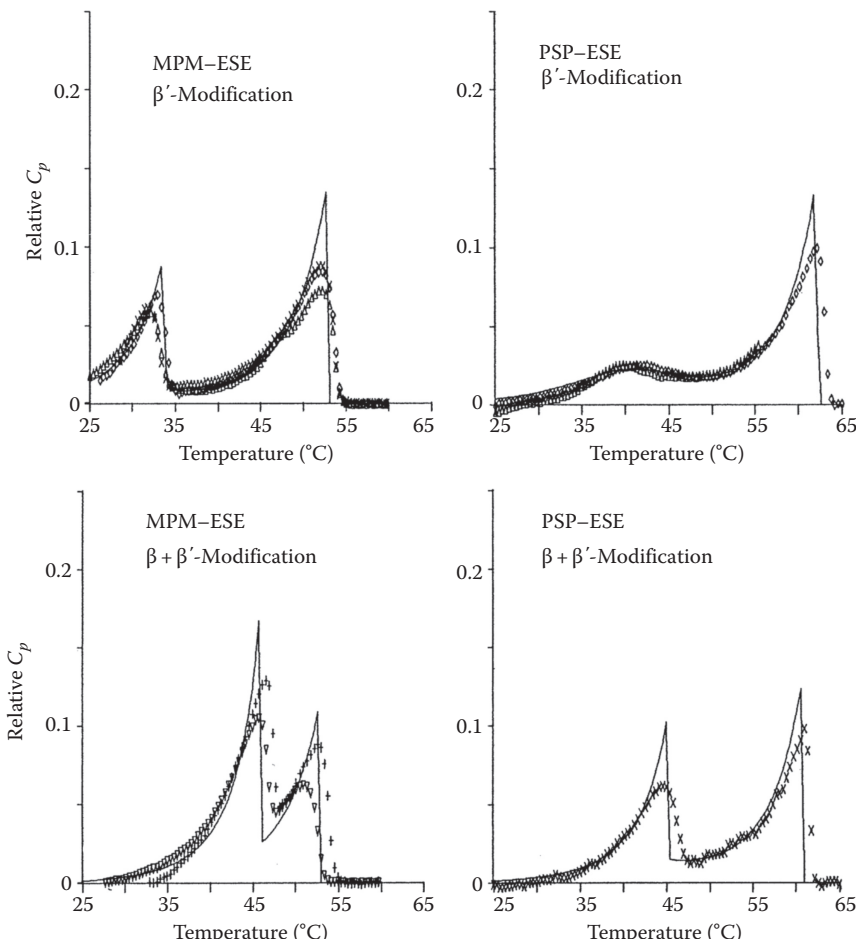


FIGURE 9.39 Measured (dots) and fitted (lines) DSC curves of ternary mixtures of $\pm 25\%$ PSP or MPM% with $\pm 25\%$ ESE and $\pm 50\%$ OOO. The modification(s) in which crystallization has taken place is indicated.

at 3.80 and 4.20 \AA , which are characteristic of the β' -modification and a single long spacing, indicating the existence of only one crystalline phase. The diffraction pattern differs from that of pure PSP, indicating that a single mixed β' phase indeed exists, in agreement with the complete miscibility derived from the DSC results (Figure 9.40).

After one day, the diffraction pattern has changed. The β' -short spacings are still present, but also a short spacing at 4.55 \AA has come up, which is characteristic of the β -modification. The long spacing has doubled, indicating the presence of a second crystalline phase. The DSC results are confirmed again: after long stabilization, a β phase coexists with a β' phase. The positions of the extra β -diffraction peaks correspond closely to those of pure SEE, in agreement with the prediction of a nearly pure β -SEE phase, which can be derived from the DSC curve.

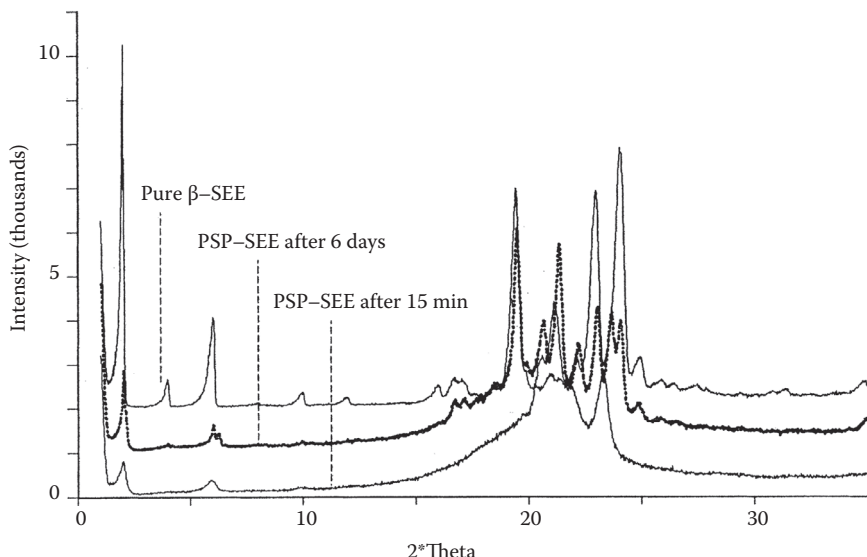


FIGURE 9.40 X-ray diffractograms of the mixture 25% PSP, 25% SEE, and 50% OOO, after 15 min and 6 days of stabilization at 20°C. The diffractogram of pure SEE is also given.

9.7.5.2 PSP and MPM with EPE and PEE

The measurements that were carried out and the results of the fitting procedure are given in Table 9.28 and Figures 9.41 and 9.42.

Naturally palmitic and elaidic acids do not show the similarity in behavior that elaidic and stearic acids do. Consequently PEE and EPE can be expected to show differences

TABLE 9.28
DSC Measurements and 2-Suffix Margules Parameters for the Highest Melting Binary Pair Determined from These Measurements

Modifi- cation	PSP	MPM	PEE	EPE	OOO	Scan Rate (K/min)	Stabili- zation Time (min)	Stabili- zation Temp. (°C)	A/RT
β'	0.26		0.25		0.49	0.62	14d	15	0 ± 0.2
β'		0.28	0.24		0.48	2.5	1–5	5–15	1.8 ± 0.5
β'	0.26			0.25	0.49	2.5	7d	15	2.0 ± 0.5
β'		0.27		0.25	0.48	1.25	3d	20	2.3 ± 0.5
β	0.26		0.25		0.49	0.62	30d	15	no β
β		0.28	0.24		0.48	2.5	15–10d	15	≥2.5
β	0.26			0.25	0.49	2.5	7d	15	≥2.5
β		0.27		0.25	0.48	1.25	3d	20	≥3

d, days.

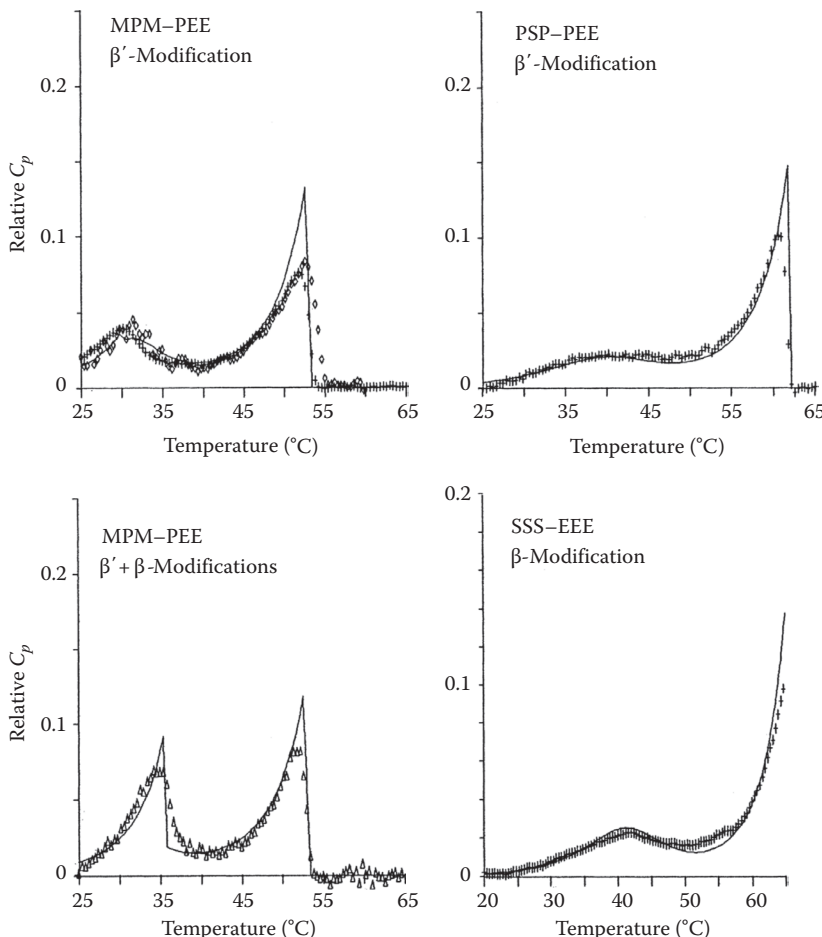


FIGURE 9.41 Measured (dots) and fitted (lines) DSC curves of ternary mixtures of $\pm 25\%$ PSP or MPM% with $\pm 25\%$ PEE and $\pm 50\%$ OOO and of a mixture of 25% SSS, 25% EEE, and 50% OOO. The modification(s) in which crystallization has taken place is indicated.

in mixing behavior. This is indeed observed: while PEE shows a complete miscibility with both PSP and MPM in the β' -modification, EPE shows only limited solubility.

PEE shows a very interesting behavior. The system PSP/PEE/OOO has remained in the β -modification, even after a month of stabilization. This is confirmed by the x-ray results for this system. Looking at the results obtained for SEE, ESE, and EPE, a realistic estimate for the PSP-PEE β -interaction parameter is $A/RT = 3$. In that case, calculations show that this system is β' -stable at all temperatures, although PEE itself is β -stable: the extra stability of the β -modification is not enough to compensate for the large excess Gibbs energy of a solid phase in that modification. A nearly pure β -PEE phase will only crystallize when the ratio PSP/PEE in the system drops below 0.5. But even for such mixtures the driving force to β is very low, making a speedy recrystallization unlikely. After 1 week of stabilization of such a mixture, only a

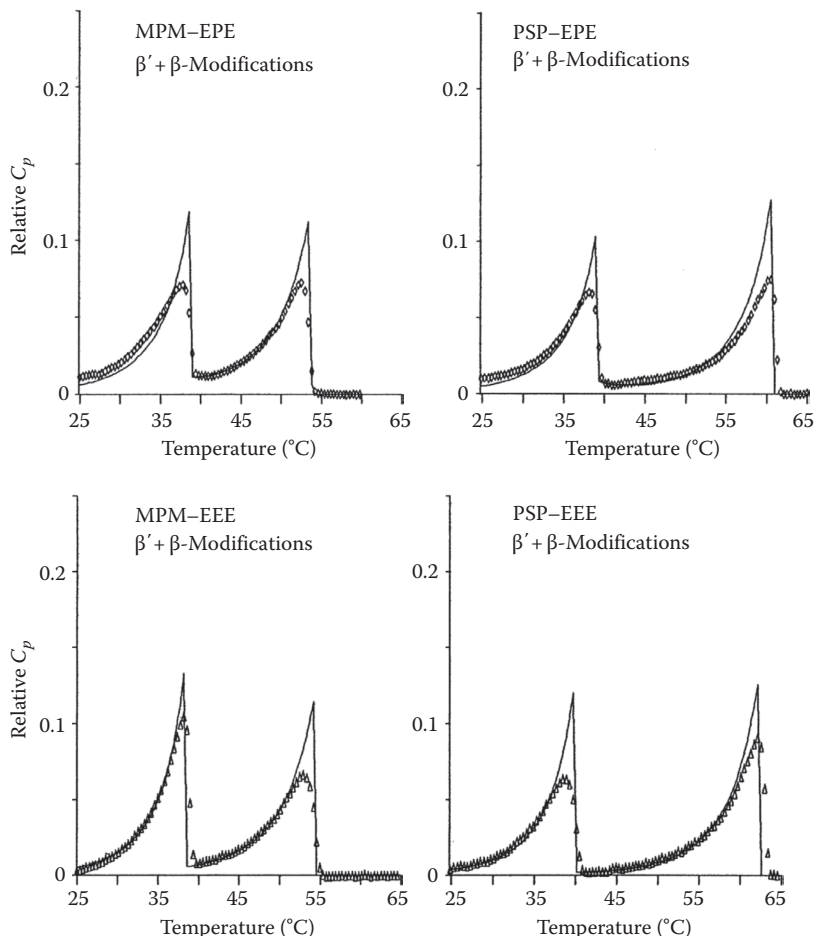


FIGURE 9.42 Measured (dots) and fitted (lines) DSC curves of ternary mixtures of $\pm 25\%$ PSP or MPM% with $\pm 25\%$ EPE or EEE and $\pm 50\%$ OOO. The modification(s) in which crystallization has taken place is indicated.

minor broadening of the first β' -melting peak at the position, where a β -melting peak would occur, was observed.

The system MPM/PEE/OOO does crystallize into the β -modification. Contrary to PSP and PEE, MPM and PEE show nonideal mixing in the β' -modification, and therefore the difference in excess Gibbs energy between the two modifications is not large enough to counterbalance the stability difference. The same holds for the PSP/EPE/OOO system that was studied.

Even without stabilization, the DSC curves of the systems with EPE showed exothermic peaks of the β' - β transition. A complete β' -melting curve can therefore not be obtained. The estimate for the β' -interaction parameter is based on the shape and height of the plateau just after the first melting peak in the curve of a completely stabilized sample.

9.7.5.3 PSP and MPM with EEE

The measurements that were carried out and the results of the fitting procedure are given in Table 9.29 and Figures 9.41 and 9.42.

These systems all recrystallized quickly into the β -modification. Even without stabilization, the melting curves of the β' -modification were disturbed by exothermic peaks of the $\beta' \rightarrow \beta$ transition. Therefore the values of the β' -interaction parameters had to be estimated from the height of the plateau just after the first melting peak. The plateau height is nearly zero.

For a reliable determination of the β' -interaction parameter, the β' -melting point of EEE is required. The authors were not able to determine a β' -melting point of their EEE sample, only α - and a β -melting points were found. This is in line with the findings of Hagemann (1975) and earlier authors (Vazquez Ladron and Castro Ramos, 1971), who also could not detect a β' -melting point of EEE. A very old report of Malkin and Carter (1947) gives 37°C for the β' -melting point. This value does not compare well with the data of Hagemann (1975) for a number of glycerol tri-*trans*-octadecenoates. Hagemann found a steady decrease in the β' -melting point from 43°C for *trans*-17-octadecenoic acid to 28°C for *trans*-11-octadecenoic acid. Extrapolating the data of Hagemann to 9-octadecenoic acid (E) results in a β' -melting point of 27°C–28°C for EEE.

If 37°C is used as β' -melting point of EEE, than the 2-suffix Margules interaction parameter for PSP-EEE in the β' -modification must be greater than 2.5 in order to explain a zero plateau height. If a melting point of 27°C is used, A/RT (PSP-EEE) = 0 ± 1 .

From binary phase diagrams, we concluded that SSS mixes nearly ideally with SES, SSE, and SEE in the β -modification (Section 9.7.3). In addition to the DSC curve of PSP-EEE-OOO, we also determined the curve of SSS-EEE-OOO in the β -modification (Figure 9.43). The result is not very surprising: SSS and EEE also mix ideally in the β -modification. Clearly the elaidic and stearic acid chains

TABLE 9.29
DSC Measurements and 2-Suffix Margules Parameters
for the Highest Melting Binary Pair Determined from These
Measurements

Modifi- cation	PSP	MPM	PEE	OOO	Scan Rate (K/min)	Stabi- lization Time (min)	Stabi- lization Temp. (°C)	A/RT
β'	0.26		0.25	0.49	2.5	1–7d	15	0 ± 1
β'		0.27	0.25	0.48	2.5	30–70	15–20	$\geq 2?$
β	0.26		0.25	0.49	2.5	1–7d	20	≥ 2.0
β		0.27	0.25	0.48	2.5	30–70	15–20	≥ 2.0

Note: Composition in mole fractions, temperatures in °C, time in minutes, unless otherwise indicated: d Δ days.

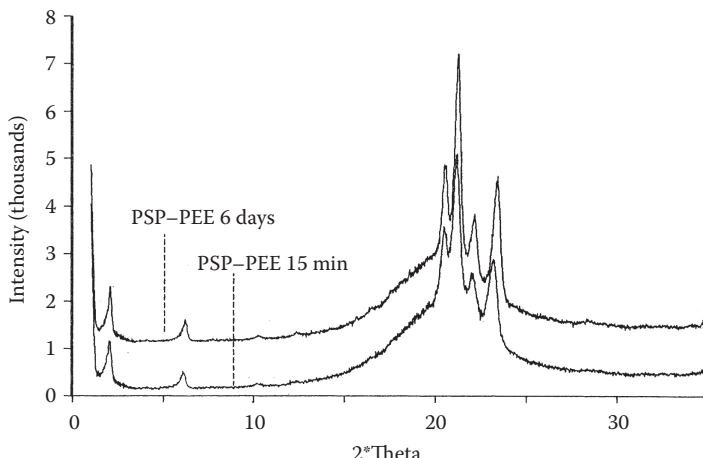


FIGURE 9.43 X-ray diffractograms of the mixture of 25% PSP, 25% PEE, and 50% 000, after 15 min and 6 days of stabilization at 20°C.

behave more or less equivalent, which is confirmed by our findings for PSP-SEE and PSP-ESE for both β' - and β -modifications.

If S and E behave equivalent, then the interaction parameter for the binary PSP-EEE should be equal to those of PSP-SEE and PSP-ESE. As the latter parameters both equal zero, expect that A/RT (PSP-EEE) will also be zero. This implies that the β' -melting point of EEE must be $27^\circ\text{C} \pm 2^\circ\text{C}$, and that Malkins' value for the β' -melting point of EEE, 37°C , is not right.

9.7.5.4 PSP and MPM with *cis*-Unsaturated TAGs

The measurements of mixtures of PSP and MPM with SSO, PPO, SOS, and POP resulted in more complicated curves than those of the previous mixtures. Contrary to the previous TAGs, which all crystallized into the β' -2 and β -2 modifications, most *cis*-unsaturated TAGS crystallize into the β' and β -3 modifications. Only POP crystallizes into the β' -2 form (Table 9.30).

TABLE 9.30
Polymorphic Forms of the
Cis-Unsaturated TAGs

PSP			
PSP	β' -2	MPM	β' -2
SOS	β' -3	β -3	PPO
SSO	β' -3	POP	β' -2 β' -3

Sources: Sato, K. et al., *JAOCS*, 66, 664, 1989; Vazquez Ladron, R. and Castro Ramos, R., *Gracas y Aceites*, 22, 401, 1971.

The formation of a continuous solid solution between a component that crystallizes into the β' -2 form and a component that crystallizes into the β' -3 form seems on structural grounds impossible: an intermediate β' -2/ β' -3 structure is not feasible. In thermodynamic calculations, the two β' -forms must therefore be treated as separate modifications, just like the β' - and β -modifications.

This has two implications:

1. The DSC curve of the β' -modification of a mixture of a β' -2 and a β' -3 forming TAG must always contain two sharp peaks, because demixing in the solid phase will occur even when the components mix ideally both in the β' -2 as in the β' -3 phase.
2. For calculation of the interaction parameters, the heat of fusion and the melting point of a hypothetical β' -2 form of the β' -3 forming TAG and of the hypothetical β -3 form of the β' -2 forming TAG must be known. These hypothetical pure component properties cannot be measured. They must be estimated, which will cause a considerable uncertainty in the value of the interaction parameters.

Quite surprisingly, after short stabilization of the MPM–SSO–OOO and MPM–PPO–OOO mixtures, DSC curves in which the first melting peak is a broad hump were obtained, rather than the sharp peak that was expected for these β' -2/ β' -3 mixtures. After prolonged stabilization, a clear polymorphic transition was observed, and finally the expected DSC curves with two sharp peaks were obtained. The final melting peak remained in place during this transition. The broad hump indicates that initially crystallization must have taken place into a single, mixed solid phase, which has to be in the β' -2 modification. The final, stable, separate PPO- or SSO-rich β' -3 phase is only formed later. This behavior confirms the assumption that the 2-layer and 3-layer forms of the same modification must be treated thermodynamically as separate, independent ‘states’, that need not always occur in pure components. The order of the polymorphic transitions that is observed is therefore:



From the work of de Jong (1980), it can be concluded that the melting point of a hypothetical β' -3 modification of PSP and MPM is about 3°C less than the melting point of a hypothetical β' -2 form of these TAGS. In analogy to the β -modification, assume that the β' -3 melting points of MPM and PSP also lie 3°C below their experimental β' -2 melting points. Based on the enthalpy of fusion data of Chapter 4, we conclude that the heat of fusion of the β' -3 form is about 90% of that of the β' -2 modification.

Similarly, it is assumed that the heat of fusion of the hypothetical β' -2 form of SSO, PPO and SOS is 90% of that of the β' -3 modification. If the 2-suffix Margules equation is used, the melting points of the β' -2 modification of these TAGs can be calculated from the β' -2 DSC curves of the mixtures with MPM:

$$\text{SSO: } T_f(\beta'-2) = 39 \pm 0.5^\circ\text{C} \quad (T_f(\beta'-3) = 42^\circ\text{C})$$

$$\text{SOS: } T_f(\beta'-2) = 29 \pm 2^\circ\text{C} \quad (T_f(\beta'-3) = 36.5^\circ\text{C})$$

$$\text{PPO: } T_f(13'-2) = 31 \pm 0.5^\circ\text{C} \quad (T_f(\beta'-3) = 34^\circ\text{C})$$

TABLE 9.31
DSC Measurements and 2-Suffix Margules Parameters for the Highest Melting Binary Pair Determined from These Measurements

Modifi- cation	PSP	MPM	SOS	SSO	OOO	Scan Rate (K/min)	Stabili-	Stabili-	A/RT
							zation (min)	zation (°C)	
β' -2	0.32		0.19		0.49	2.5	15	5	0 ± 0.3
β' -2		0.29	0.23		0.48	2.5	1	5	2 ± 0.7
β' -2	0.26			0.24	0.50	2.5	1–7d	10	No fit
β' -2		0.28		0.24	0.48	1.25	1–60	15	2 ± 0.2
β' -3	0.32		0.19		0.49	2.5	15	5	0 ± 0.5
β' -3		0.29	0.23		0.48	1.25	8d	10	1.7 ± 0.7
β' -3		0.28		0.24	0.48	1.25	3d	15	2 ± 0.5
β	0.32		0.19		0.49	1.25	1d	28	1.5 ± 0.5
β		0.29	0.23		0.48	1.25	8d	10	1.0 ± 0.5

d, days.

The measurements that were carried out and the results of the fitting procedure are given in Tables 9.31 and 9.32 and Figures 9.44 through 9.47.

The broad first melting peaks in the β' -2 DSC curves of PSP–POP and PSP–SSO have maxima that lie several degrees above the temperature where these maxima should be situated when $A/RT = 0$. These DSC curves could only be fitted with the 3-suffix Margules equation, using negative values for $A_{\text{PSP-POP}}$ and $A_{\text{PSP-SSO}}$ (Table 9.33).

TABLE 9.32
DSC Measurements and 2-Suffix Margules Parameters for the Highest Melting Binary Pair Determined from These Measurements

Modifi- cation	PSP	MPM	POP	PPO	OOO	Scan Rate (K/min)	Stabili-	Stabili-	A/RT
							zation (min)	zation (°C)	
β' -2	0.26		0.26		0.48	1.25	15–7d	10	No fit
β' -2	—	0.29	0.23		0.48	2.5	1	5	0.8 ± 0.2
β' -2	0.25			0.28	0.47	1.25	7d	15	–1.5?
β' -2		0.28		0.25	0.47	1.25–2.5	1–60	10	0.8 ± 0.4
β' -3	0.25			0.28	0.47	1.25	26d	5	—
β' -3		0.28		0.25	0.47	1.25–2.5	7d	10	-0.2 ± 0.4
β	0.26		0.26		0.48	—	—	15	No
β		0.29	0.23		0.48	1.25	7d	5	3.5 ± 1

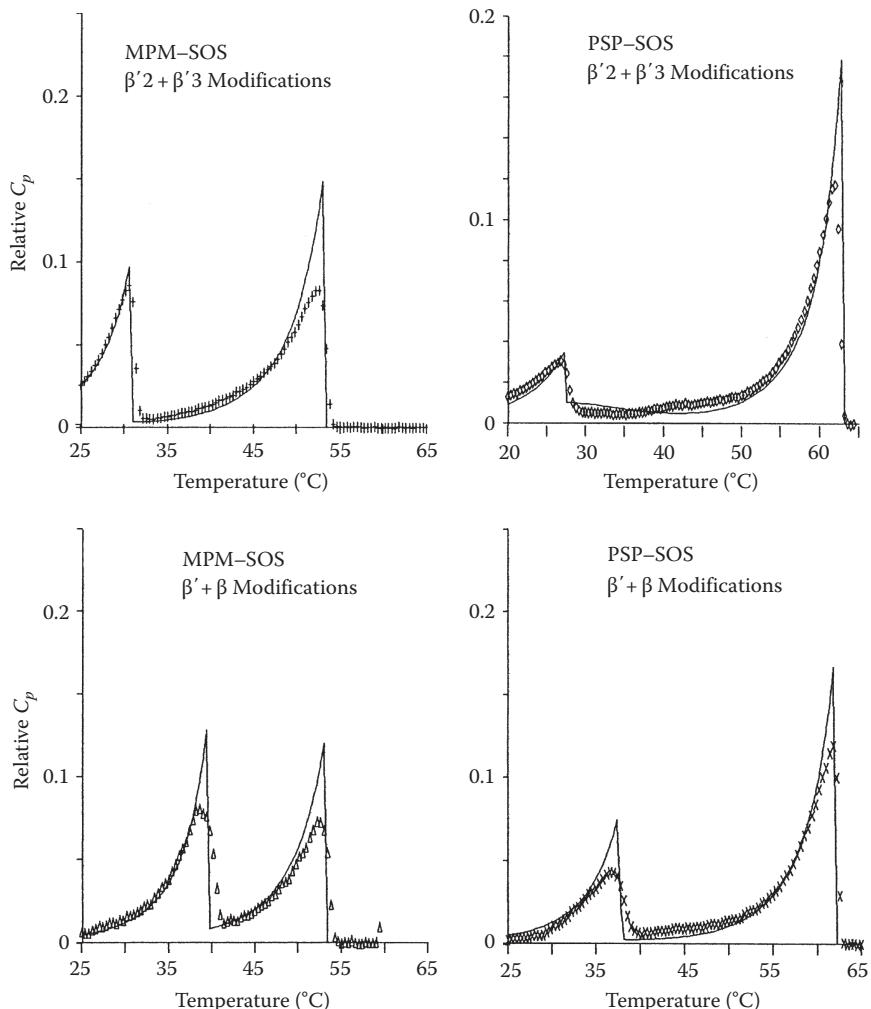


FIGURE 9.44 Measured (dots) and fitted (lines) DSC curves of ternary mixtures of $\pm 25\%$ PSP or MPM% with $\pm 25\%$ SOS and $\pm 50\%$ OOO. The modification(s) in which crystallization has taken place is indicated.

Apparently the β' -2 form of POP and SSO is enormously stabilized by the presence of PSP, their almost exact saturated counterpart. Calculations show that this stabilizing effect makes the mixture β' -2 stable. Indeed, no transition to the β -modification (POP) or the β' -3 modification (SOS) was observed even after long stabilization.

The stabilizing effect seems also present in the curves of PSP-PPO and PSP-SOS. In these cases, an exact determination of the β' -2 state was not possible: a β' -2/ β' -3 transition always disturbed the DSC curve. The shape of the PSP-PPO-OOO melting curves above 35°C suggest $A/RT = -1.5$.

The 2-suffix parameters for the β -modification of the mixtures with SOS are very low, compared to those for the β' -modification. It is possible to use 3-suffix

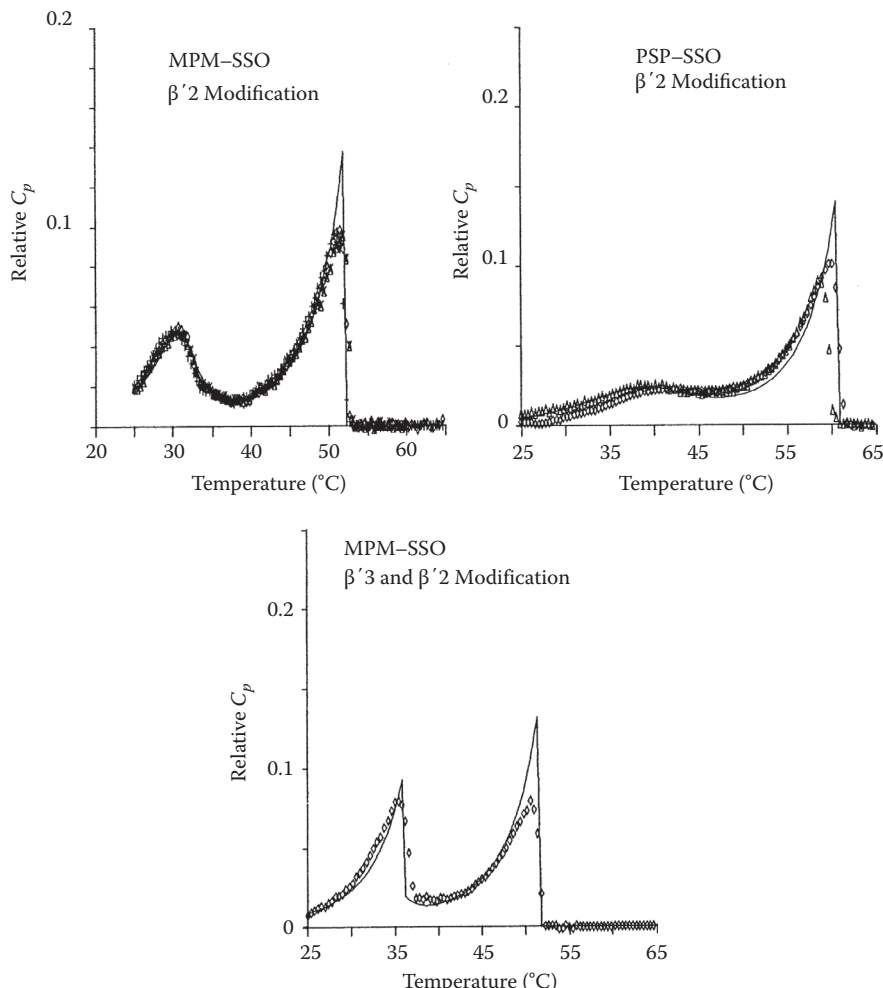


FIGURE 9.45 Measured (dots) and fitted (lines) DSC curves of ternary mixtures of $\pm 25\%$ PSP or MPM% with $\pm 25\%$ SSO and $\pm 50\%$ OOO. The modification(s) in which crystallization has taken place is indicated.

Margules β' -interaction parameters that are more in line with the results for the β' -modification for the description of the curve (Table 9.33). However, they have no statistical significance.

9.7.6 DISCUSSION

9.7.6.1 Use of DSC Melting Curves

The results show that it is possible to use DSC melting curves of ternary mixtures to determine binary interaction parameters. This method is much quicker and more reliable than the determination of a phase diagram. It allows the study of phase

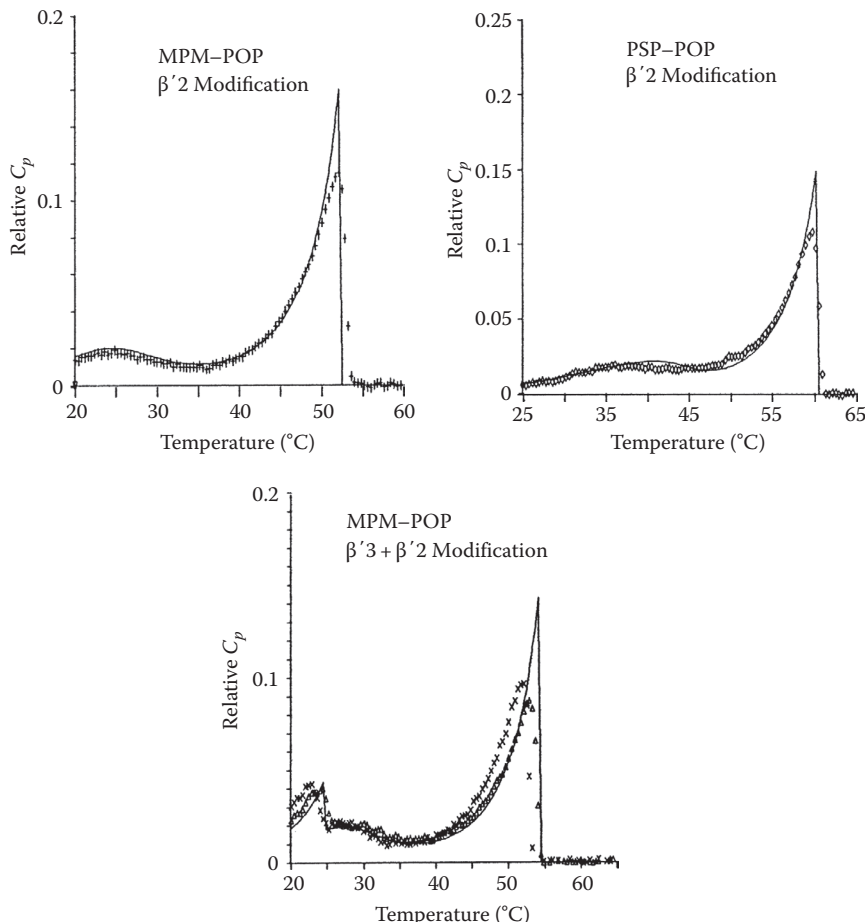


FIGURE 9.46 Measured (dots) and fitted (lines) DSC curves of ternary mixtures of $\pm 25\%$ PSP or MPM% with $\pm 25\%$ POP and $\pm 50\%$ OOO. The modification(s) in which crystallization has taken place is indicated.

behavior in unstable modifications. Thus we have obtained a new, powerful, and versatile method for studying the solid–liquid phase behavior.

9.7.6.1.1 3-Suffix Margules Equation

The 3-suffix Margules interaction parameters can be obtained from the combination of peak shape and peak position in the DSC melting curve. This dependency on exact peak position implies that the uncertainty in the melting points of the pure components of about 1°C will translate itself into an error in the 3-suffix Margules parameters of about 0.5. Due to this uncertainty in the parameters, asymmetric behavior in systems that show only small differences in the two parameters cannot be detected. In those cases, the 2-suffix Margules equation performs equally well. In this work, TAGs were studied that show considerable differences in stereochemical nature.

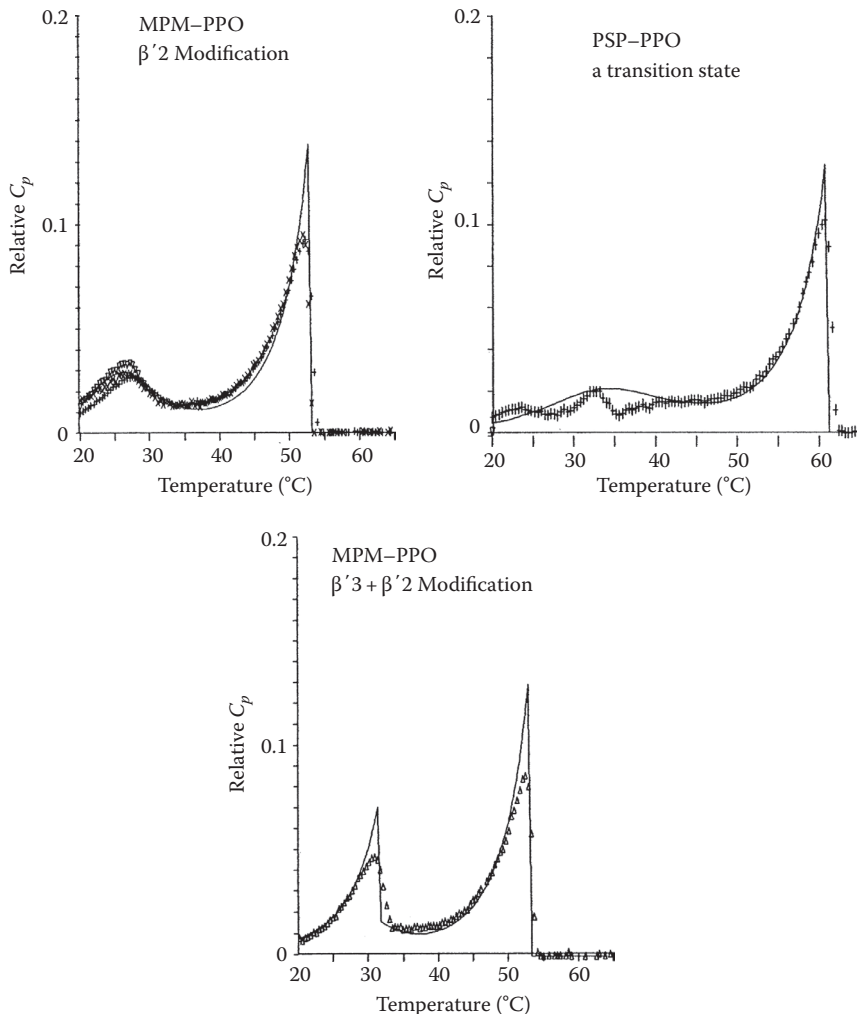


FIGURE 9.47 Measured (dots) and fitted (lines) DSC curves of ternary mixtures of $\pm 25\%$ PSP or MPM% with $\pm 25\%$ PPO and $\pm 50\%$ OOO. The modification(s) in which crystallization has taken place is indicated.

Yet only in the most extreme case, for TAGs with oleic acid, which crystallize in very different lattices, clear asymmetric behavior and the need for using the 3-suffix Margules equation were apparent.

9.7.6.2 Binary Interaction Parameters

9.7.6.2.1 β' -Modification

For the first time, reliable information about mixing behavior in the β' -modification has been obtained. On average, solid solubility in the β' -modification is higher than in the β -modification, but contrary to the α -modification, nonideal mixing can occur.

TABLE 9.33
2- and 3-Suffix Margules Parameters for Some
of the Systems of Tables 9.31 and 9.32

System	Modification	A/RT	A_{12}/RT	A_{21}/RT
PSP–POP	β' -2	—	-3 ± 1	0 ± 0.5
PSP–SSO	β' -2	—	-2 ± 1	0 ± 0.5
PSP–SOS	β	1.5 ± 0.5	1.5 ± 0.5	3 ± 1.5
MPM–SOS	β	1.0 ± 0.5	0.5 ± 1	3 ± 2

The influence of size differences is clear: none of the unsaturated TAGs mixes very well with the smaller TAG MPM, while often even ideal miscibility is found with PSP, which is about similar in size. The position of the fatty acid chains on the glycerol influences the mixing behavior with MPM only very slightly, and the size difference dominates. But when the size difference is small, the chain position is of great influence, as can be seen from the data on PSP–PEE vs. PSP–EPE, PSP–SSO vs. PSP–SOS, and PSP–PPO vs. PSP–POP. It is not clear why these relatively small differences can have such large effects on mixing behavior. Simulation of the disturbance of a crystal lattice by insertion of another TAG using molecular mechanics may help to create understanding. This will be attempted in Section 15.8.

9.7.6.2.2 β -Modification

Due to the use of β' -stable TAGs as the highest melting component in the systems that were studied by DSC, β -interaction parameters could only be determined very roughly from the position of the first melting peak. That means that the uncertainty in the melting points already has to be taken into account in the 2-suffix Margules parameters, while the determination of statistically significant 3-suffix Margules parameters is impossible.

However, as illustrated for the system SSS and EEE, determination of accurate interaction parameters for the β -modification from DSC-curves is very well possible if a β -stable TAG is used as highest melting component.

In the survey of the binary phase diagrams, complete solid miscibility was only found for pairs of TAGs that are very similar in size, like SSS and PSS. Our DSC results are in line with this finding. In Section 9.8, the data will be used in an attempt to find a relation between the influence of structural differences of TAGs and the magnitude of the interaction parameters.

9.7.6.3 Kinetics

It is striking how strongly the kinetics of transformation from β' to β depend on the miscibility in the β' -modification: if the components mix very well in the β' -modification, the transformation takes at least several days, while if solid phase immiscibility occurs, it takes only a few seconds to an hour to complete the transformation.

The explanation is twofold:

The combination of poor β' -phase miscibility and nearly ideal mixing in the β' -modification reduces the Gibbs energy difference between the two modifications, which is the driving force for recrystallization.

It also leads to a β' -solid phase composition that is completely different from that in the demixed β -modification, which makes the transformation kinetically much more difficult. In the case of poor β' -phase miscibility, the solid phase composition is nearly equal to that in the β -modification, so that the barrier for the transformation is much smaller.

9.7.7 TERNARY SOLIDS

Although the DSC melting curves of Section 15.7.6 were measured using ternary mixtures, the composition of the mixture and the temperature range of the experiment were selected such that only a binary solid phase was present. This enabled the determination of binary interaction parameters in the solid phase.

Crystallized fats are normally multicomponent solid phases. The binary interaction parameters that were determined in this work can only be used for prediction of multicomponent phase behavior if ternary, quaternary, and higher interaction terms can be neglected. A way of checking this is comparing measured ternary phase diagrams with phase diagrams predicted from binary interaction parameters. In the literature, there are only a few ternary phase diagrams available: that of the cocoa butter (CB) TAGs SOS/POS/POP from Smith (1988) and those of the palm oil TAGs PPP/POP/POO and PPP/PPO/POO from Gibon (1984). The data from Gibon are not very reliable, due to the very poor stabilization procedure and the high DSC scan rates that were used (Section 15.7.2). Calculated and measured ternary clear point curves for the three systems are given in Figures 9.48 and 9.49. For SOS–POS–POP also, a diagram is given with the isotherms for 25% solids.

As can be seen, the agreement between theory and experiment is very good for the SOS/POS/POP ternary, taking into account the error in the measurements of 1°C. Also the temperatures at which a mixture contains 25% solids are predicted within 1°C.

The PPP/POP/POO and PPP/PPO/POO ternaries also show good agreement between measurements and calculations. The agreement near the PPP corner at the PPP–POO side of the diagrams is somewhat less good. However, the clear points that are given by Gibon for this PPP/POO binary are probably not correct as they lie well below the eutectic liquidus.

The results suggest that the use of binary interaction parameters is indeed sufficient for the description of multicomponent TAG systems. Later in this chapter it is shown that also in multicomponent systems excellent results can be obtained using only binary interaction parameters (Section 9.9).

The clear point diagram for the CB-TAGs SOS/POS/POP may be used to define the possible compositions of CBEs (cocoa butter equivalents). CBEs must have the same clear point as CB, and so all possible CBE compositions will be restricted to the isotherm through the CB composition. The 25% isosolids diagram demonstrates

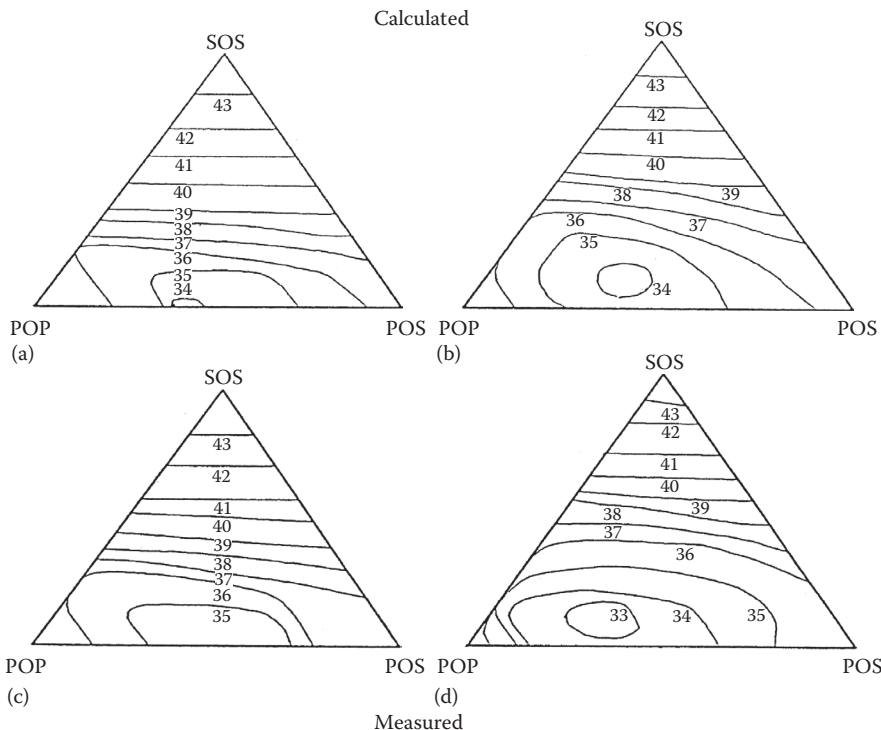


FIGURE 9.48 Calculated and measured ternary isosolids diagrams of SOS–POS–POP. Measured by Smith (1988). (a) and (c): clear point diagrams; (b) and (d): isotherms with 25% solid fat. (From Smith, K., Unilever Research Colworth, Private communication, 1988.)

that even for such difficult systems as SOS–POS–POP solids content can be predicted by application of solid–liquid equilibrium thermodynamics.

9.7.8 CONCLUSION

In the β - and β' -modifications, TAGs show limited solid miscibility that can be described with rather simple models for the excess Gibbs energy: the 2- and 3-suffix Margules equation.

Eighty-four of the 120 binary phase diagrams of TAGs, which are available in the literature, are rejected because they are clearly not correct. The solidus lines of most of the remaining 36 phase diagrams show large inconsistencies. The majority of these phase diagrams were measured after 1971. The 36 phase diagrams can be described within experimental error both by the 2- and by the 3-suffix Margules equations.

The excess Gibbs energy models contain binary interaction parameters. The large experimental errors in the binary phase diagrams lead to a very large inaccuracy in the interaction parameters that are determined from these diagrams.

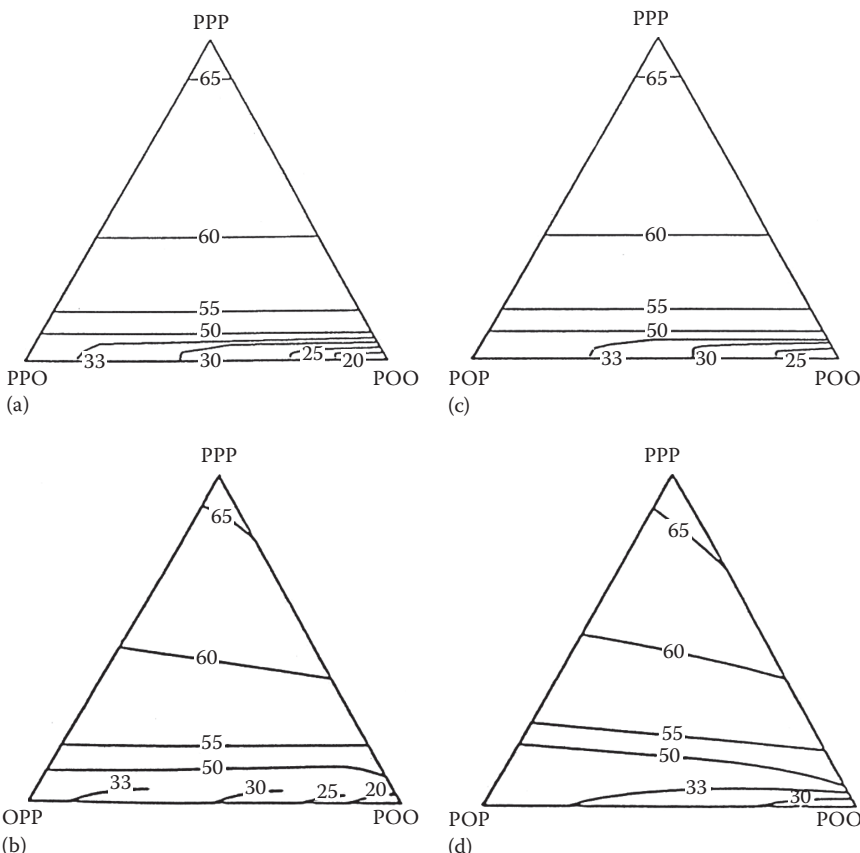


FIGURE 9.49 Calculated and experimental clear point diagrams of TAGS from palm oil. (a) and (c): calculated; (b) and (d): measured by Gibon (1984). (From Gibon, V., Thesis, Universite Notre Dame de la Paix, Namur, Belgium, 1984.)

Due to the serious drawbacks in the use and determination of binary phase diagrams, a new method for the study of solid–liquid phase behavior has been defined. It is possible to obtain quantitative information about mixed crystal formation from a single, complete DSC melting curve of a ternary system, consisting of two crystallizing TAGs and one liquid TAG.

The method is much quicker, more reliable, and more versatile than the traditional study of phase behavior of TAGs via binary phase diagrams.

For the first time, accurate information was obtained about the degree of mixed crystal formation in the β' -modification. Generally solid phase miscibility is higher in the β' -modification than in the β -modification. Large differences in molecular size reduce solid phase miscibility. Also the position of the fatty acid on the glycerol group has a great influence on solid phase miscibility.

Surprisingly the mixing behavior of TAGs in the solid phase can usually be described with sufficient accuracy by the very simple regular solution model or

2-suffix Margules equation. Only in a few cases, the use of the more complex 3-suffix Margules equation was required.

Ternary systems could be described with binary interaction parameters only.

Kinetics of recrystallization showed a clear relation with the calculated thermodynamic driving force and the degree of rearrangement of the solid phase that is required.

9.8 PREDICTING INTERACTION PARAMETERS

Now that it has been shown that the mixing behavior of TAGs in the α -, β' -, and β -modifications can be described with rather simple excess Gibbs energy models, there remains only one step to be taken: finding a procedure for predicting the binary interaction parameters for any pair of TAGs. Therefore, the relation between geometrical differences and the magnitude of the interaction parameter is studied. Molecular mechanics are used to obtain an impression of the lattice distortions that are brought about by incorporation of guest TAGs in a lattice of a host TAG. Finally a first, empirical, set of rules is given for prediction of the binary interaction parameters.

9.8.1 ARE INTERACTION PARAMETERS RELATED TO STRUCTURAL DIFFERENCES?

In the conclusion of Section 9.2, four steps were mentioned that had to be taken to obtain a description of the liquid–multiple solid phase equilibria in fats. Those four steps were the subject of the preceding sections. It was concluded that the solid–liquid phase equilibrium in a TAG mixture can be described, provided the binary interaction parameters for all possible pairs of TAGs in the mixture are known. The large number of TAGs in a natural oil makes it impossible to determine the parameters experimentally. Therefore a method must be developed for predicting these binary parameters. Fortunately TAGs are chemically very similar, so the degree of nonideal mixing will only be determined by sterical effects. In the next sections, a relation between the binary interaction parameters and structural differences will be discussed.

9.8.1.1 Degree of Isomorphism

In his work on mixed crystals, Kitaigorodskii (1984) investigated the solid miscibility of several hundreds of pairs of organic compounds. Based on this investigation, he formulated his “major rule of substitutional solid solubility” of organic compounds:

1. Solid solubility is determined by geometric factors if
 - There is no electron transfer between the two components to be mixed
 - The components to be mixed have no permanent dipole moments
 - The components to be mixed do not form strong hydrogen bridges
2. If solid solubility is solely determined by geometrical factors, then two components will only mix in the solid state if their “degree of isomorphism” exceeds 0.85.

The degree of isomorphism ϵ is defined as follows: superimpose the molecules of the components so as to maximize the intermolecular overlap.

Let the volume of the non-overlapping parts be V_{non} and the volume of the overlapping parts v_0 . Then the degree of isomorphism or coefficient of geometrical similarity is given by

$$\epsilon = 1 - \frac{V_{\text{non}}}{v_0} \quad (9.94)$$

3. In addition to this second condition, complete solid state miscibility in any proportion is only possible if the molecular packing in the crystal of the pure components is similar, the crystals have the same symmetry and the atoms occupy the same crystallographic positions.

Generally, Kitaigorodskii's rule gives a correct prediction of the occurrence of fully eutectic behavior and the presence of a miscibility gap. However, the reverse is not true: sometimes a miscibility gap is found, even though Kitaigorodskii's rule has predicted a good solid state miscibility. The reason for this is that when a guest molecule is inserted in a host lattice, then, depending on the nature of the guest molecule, its protruding part may occupy a lattice site in an area where packing is very dense. Obviously, solid solubility will be considerably less than in the case of a guest molecule of the same size that protrudes into a loosely packed area. Therefore, generally, Kitaigorodskii's rule can only be used for qualitative statements on solid phase miscibility.

According to Kitaigorodskii, quantitative predictions of solid solubility can be obtained by calculating the lattice distortion:

1. An impurity is placed in an undistorted lattice of the pure component.
2. The difference in interaction energy of the impurity with the lattice and of the host with the lattice is calculated.

The simplest approach is to leave the host lattice completely undisturbed and calculate the conformation of the impurity that gives minimal interaction energy. A more sophisticated approach is to allow also some conformational changes in the host lattice near the impurity ("crystal elasticity"). Unfortunately, this increases computing time enormously.

The lattice distortion obtained in this way can be used to calculate the excess Gibbs energy and hence the maximum solid solubility. The results are reasonable estimates of the maximum solid solubility. Surprisingly, Kitaigorodskii only calculates the maximal solid solubility and does not use this information to calculate a complete binary phase diagram. Most of these complex computer calculations were carried out for relatively simple atomic crystals. Only one example of molecular crystals is mentioned (diphenyl-dipyridyl).

In mixtures of TAGs, the lattice distortion always occurs on the same lattice sites, the methyl-end-plane region, and is always caused by the same functional group: CH_2-CH_3 . Because of this, it may very well be that the degree of isomorphism correlates much better with the solid solubility of TAGs than with that of an arbitrary pair of organic substances.

The condition for complete solid state miscibility of Kitaigorodskii's rule implies that complete solid solubility in the equilibrium state cannot occur when two TAGs differ in their most stable polymorphic form, like PSP and SSS. This was already implicitly assumed in all previous calculations by treating the polymorphic forms

as different states of the substance, equivalent to the liquid and gas state. However, this condition also implies that complete miscibility cannot occur in mixtures of two TAGs that crystallize in different submodifications, as is the case in a mixture of a β -3 forming TAG and a β -2 forming TAG.

In the next sections, the following is discussed: the extent to which the simple parameter ϵ correlates with the interaction parameters of TAGs, whether it is possible to calculate the lattice distortion by impurities in TAG crystals, and whether this lattice distortion can be used for prediction of interaction coefficients will be discussed.

9.8.1.2 TAGs and the Degree of Isomorphism ϵ

There are two major lattice distortions that occur in TAG mixtures: those caused by differences in chain length and those caused by *cis*-unsaturated double bonds. Assume that the distortion in the lattice of a saturated TAG that is caused by a *trans*-double bond is negligible, in line with the nearly ideal miscibility that was found for SSS, SES, SSE, SEE, and EEE. The two major distortions will be considered separately.

9.8.1.2.1 β' -Modification

In Table 9.34, the binary interaction parameters for the β' -modification of saturated and *trans*-unsaturated TAGs are listed together with the degree of isomorphism. As a matter of convenience, v_{non} is the sum of the absolute differences in carbon number of each of three chains and for v_0 the sum of the carbon numbers of the smallest chain on each glycerol position.

The correlation between the degree of isomorphism ϵ and the binary interaction parameter is striking. In agreement with the results of Kitaigorodskii, the limit of complete miscibility, corresponding to $A/RT = 2$, is reached at $\epsilon = 0.85$. Moreover, ideal miscibility is found if $\epsilon > 0.92$. The degree of isomorphism explains the large

TABLE 9.34
2-Suffix Margules Parameters
for the β' -Modification and the
Degree of Isomorphism of
Saturated and *Trans*-Unsaturated
TAGs (from Section 9.7.5)

Binary Pair	A/RT	ϵ
PSP–PEE	0 ± 0.2	0.96
PSP–SEE	0 ± 0.2	0.92
PSP–ESE	0 ± 0.2	0.92
PSP–EEE	0 ± 2	0.92
PSP–EPE	2 ± 0.5	0.88
MPM–PEE	1.8 ± 0.5	0.82
MPM–EPE	2.3 ± 0.5	0.82
MPM–SEE	3 ± 0.2	0.77
MPM–ESE	3 ± 0.2	0.77
MPM–EEE	3 ± 2	0.77

TABLE 9.35
**2- or 3-Suffix Margules Parameters for the
 β' -Modification and the Degree of Isomorphism
of Saturated and *Cis*-Unsaturated TAGs**

Binary Pair	Modification	A_{12}/RT	A_{21}/RT	ϵ
PSP-POP	β' -2	-3 ± 1	0 ± 0.5	1-
PSP-PPO	β' -2	-1.5 ± 1.5	-1.5 ± 2	0.92-
PSP-SSO	β' -2	-2 ± 1	0 ± 0.5	0.92-
MPM-POP	β' -2	0.8 ± 0.4	0.8 ± 0.2	0.86-
MPM-PPO	β' -2	0.8 ± 0.5	0.8 ± 0.3	0.86-
MPM-SSO	β' -2	2 ± 0.7	2 ± 0.2	0.77-
Binary Pair	Modification	A/RT		
PSP-SOS	β' -3	0 ± 0.5		
MPM-PPO	β' -3	-0.2 ± 0.4		
MPM-SOS	β' -3	1.7 ± 0.7		
MPM-SSO	β' -3	2 ± 0.5		

Note: The modification in which the *cis*-unsaturated tag has crystallized is given. A – behind the value of ϵ indicates that the contribution of the *cis*-double bond to ϵ is not incorporated in the value of ϵ .

difference in miscibility with PSP that has been found for PEE and EPE in Section 15.7. Although the number of data is too small for a decisive statement, it seems possible to use ϵ for predicting the binary interaction parameters of pairs of these TAGs.

The correlation for *cis*-unsaturated TAGs will be less simple, as the *cis*-double bond disturbs the regular zigzag (*trans* configuration) of the saturated chains in the crystal lattice. From the *cis*-unsaturated TAGs that were studied in Section 9.7.6, only POP crystallizes in the β' -2 modification, while SOS, SSO, and PPO are reported to crystallize in the β' -3 modification (Vazquez Ladron and Castro Ramos, 1971; Gibon, 1984; Sato et al., 1989). In Section 9.7, SSO and PPO initially seem to crystallize in a β' -2 form that does not exist in pure PPO and SSO. The values of the 2- or 3-suffix Margules equation interaction parameters for the β' -2 and β' -3 forms are listed in Table 9.35 together with ϵ . The extra contribution of a *cis*-double bond to ∞ is not incorporated in the number, but indicated by a – (minus).

Here again, the limited amount of data for both β' -forms indicate that the degree of isomorphism is related to the magnitude of the binary interaction parameters. Surprisingly the miscibility of saturated and *cis*-unsaturated TAGs seems to be slightly better than that of saturated and *trans*-unsaturated TAGs with the same degree of isomorphism.

9.8.1.2.2 β -Modification

Most data for the β -modification that are available have a considerable error margin. Yet, as appears from Table 9.36, a correlation between degree of isomorphism and the binary interaction parameters seems present.

TABLE 9.36
2- and 3-Suffix Margules Interaction Parameters and
the Degree of Isomorphism for Binary Pairs of -2 or -3
Forming TAGs

Binary Pair	Modification	A/RT	A_{12}/RT	A_{21}/RT	ϵ
SSS–SES	β -2	0.4 ± 0.5	0 ± 0.5	0.8 ± 0.5	1
SSS–SSE	β -2	0.4 ± 0.5	0.1 ± 0.5	0.7 ± 0.5	1
SSS–SEE	β -2	0 ± 1	0 ± 1	0 ± 1	1
SSS–EEE	β -2	0 ± 0.2	0 ± 0.2	0 ± 0.2	1
SES–SSE	β -2	0 ± 0.5	0 ± 0.5	0 ± 0.5	1
SSS–PSS	β -2	1.6 ± 0.5	1.1 ± 0.5	2.3 ± 0.5	0.96
SSS–SPS	β -2	>3	>3	>2	0.96
PSS–PPS	β -2	1.6 ± 0.5	1.4 ± 0.5	1.8 ± 0.5	0.96
SPS–PPS	β -2	2 ± 0.5	3–5	0.4	0.96
PSP–PPP	β -2	>3	>3	>1	0.96
PPS–PPP	β -2	1.9 ± 0.5	1.6 ± 0.5	2.3 ± 0.5	0.96
SSS–PSP	β -2	>3	—	—	0.92
SSS–PPS	β -2	>2.2?	—	—	0.92
PSS–SPS	β -2	2 ± 0.5	1.4 ± 0.5	2.6 ± 0.5	0.92
PSS–PPP	β -2	2.2 ± 0.5	2.8 ± 0.5	2.1 ± 0.5	0.92
SPS–PPP	β -2	>5	>5	>5	0.92
PSP–PPS	β -2	>3	>3	>1	0.92
PSP–SEE	β -2	>2.5	—	—	0.92
PSP–ESE	β -2	>2	—	—	0.92
PSP–EEE	β -2	>2	—	—	0.92
SSS–PPP	β -2	3 ± 0.5	5.8 ± 1	1.4 ± 1	0.88
SPS–PSP	β -2	1.4 ± 0.5	1	1.8 ± 0.5	0.88
PSP–EPE	β -2	>2.5	—	—	0.88
PPP–MMM	β -2	>3	—	—	0.86
MPM–PEE	β -2	>2.5	—	—	0.82
MPM–EPE	β -2	>3	—	—	0.82
BBB–SSS	β -2	>3	—	—	0.77
MPM–SEE	β -2	>2.5	—	—	0.77
MPM–ESE	β -2	2 ± 1	—	—	0.77
PPP–LLL	β -2	>3	—	—	0.67
BBB–PPP	β -2	3	—	—	0.63
SSS–LLL	β -2	>3	—	—	0.50
SSS–888	β -2	>3	—	—	0
SOS–POS	β -3	1.3 ± 0.5	1.5 ± 0.5	1.1 ± 0.5	0.96
POS–POP	β -3	1.6 ± 0.5	2.2 ± 0.5	1.0 ± 0.5	0.96
SOS–POP	β -3	>3.6	5 ± 1	1.5 ± 1	0.92

In line with expectations, the degree of isomorphism that is required for complete miscibility in the β -modification is higher than for the less densely packed β' -modification: in the β' -modification $A/RT = 2$ is already reached when $\epsilon = 0.94$, while miscibility in the β' -modification at $\epsilon = 0.94$ is still ideal. The few data for the β -3 modification agree with those for the β -2 modification.

There are a few noticeable exceptions in the data set, all concerning SPS and PSP: in combination with each other, the miscibility is better than could be expected from their low degree of isomorphism, while in combination with other saturated TAGs that have a high degree of isomorphism with these two TAGs, miscibility seems much less than expected.

Although SSS and SPS both crystallize in a β -2 lattice, according to de Jong (1980), they crystallize into different β -2 submodifications. SSS, PSS, PPS, and PPP crystallize into the β -2A submodification, while PSP and SPS both crystallize into the β -2B submodification. Although these submodifications are very similar, apparently the condition for complete solid miscibility of Kitaigorodskii's rule is not fulfilled. The β -2 submodifications should have been treated as independent polymorphs. The effect of treating the submodifications as independent polymorphs is illustrated in [Figure 9.50](#) for $A/RT = 1.8$, a value in agreement with the other data of TAGs with a degree of isomorphism $\epsilon = 0.96$. It is clear that the treatment as independent polymorphs gives a much better fit to the data.

Out of the four β -2 submodifications that occur, the β -2B submodification has the lowest packing density in the methyl terrace area. This could explain the "too large" miscibility that was experimentally found for SPS–PSP.

9.8.1.2.3 Conclusions

Kitaigorodskii's major rule of substitutional solubility applies to TAGs. Within one submodification, the degree of isomorphism correlates very well with the binary interaction parameters. Contrary to the general case of organic compounds, the use of the degree of isomorphism for an empirical prediction of interaction parameters between TAGs seems feasible.

It turns out that in the description of phase equilibria in TAGs not only the three basic modifications have to be considered as separate states, but also each subform of these three modifications. A practical problem in doing so is the fact that only the heat of fusion and melting point of the most stable subform can be determined experimentally.

9.8.2 CALCULATION OF LATTICE DISTORTION

When the degree of isomorphism is used for predicting binary interaction parameters, it is implicitly assumed that the two suffix Margules equation gives an adequate description of the phase behavior of TAGs. Although this is quite often true, it is not always the case. Moreover, the validity of the 2-suffix Margules equation is theoretically unlikely. There is no reason why an impurity with a protuberance will lead to a lattice distortion of the same magnitude as an impurity that causes a hole in the lattice, or why a protuberance of a constant size should cause a lattice distortion of the same magnitude regardless whether it is a protuberance of the fatty acid on 1,

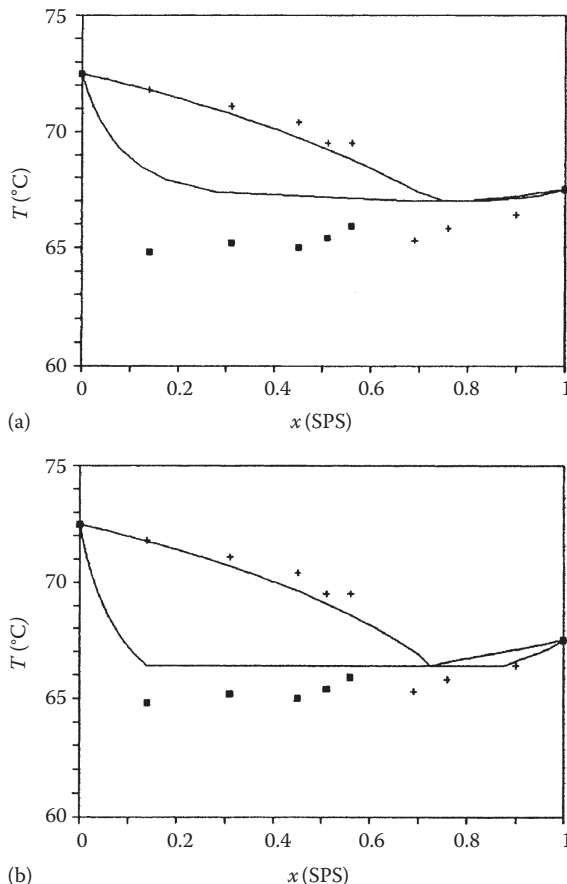


FIGURE 9.50 The influence of discontinuous miscibility in the β -2A and β -2B submodifications on the phase diagram of SSS–SPS. (a) continuous miscibility with $A/RT = 1.8$ and (b) discontinuous miscibility with $A/RT = 1.8$ for both submodifications.

2, or 3 position of the glycerol group. To get a clearer insight into this matter, more sophisticated molecular considerations are required.

9.8.2.1 Equivalent Distortions in the β -2 Modification

All saturated TAGs and *trans*-unsaturated TAGs that were considered in this work crystallize in the β -2 modification. According to de Jong (1980) and using his nomenclature, all mono-acid TAGs—PSS, PPS, SES, SSE, SEE, and EEE—crystallize in the β -2A submodification, while PSP, SPS, and probably also PEP crystallize into the β -2B submodification. These two submodifications have the same angle of tilt, 60° of the fatty acid chains, but differ in the shape of their methyl end plane. The β -2B modification is somewhat less densely packed in this area. Within one submodification the shape of the methyl terrace does not change, but the position of the “steps” in the terrace is shifted (Figure 9.51).

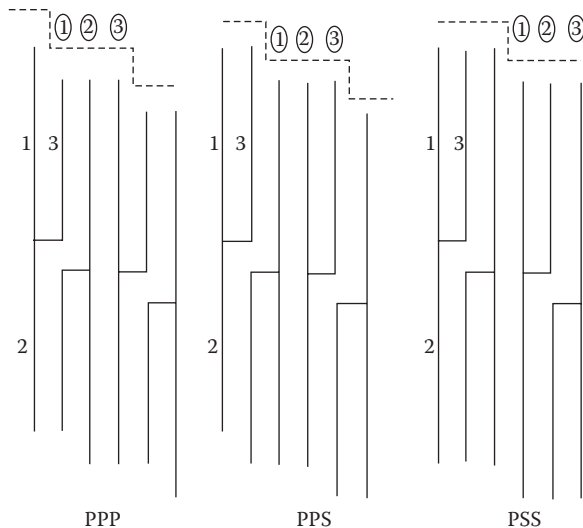


FIGURE 9.51 Equivalent positions on the methyl terraces of PPP, PPS, and PSS (marked by a circled number).

In Figure 9.51, equivalent positions on the methyl terrace are marked by a circled 1, 2, or 3. Exchanging a molecule by a molecule of another TAG will corrupt the methyl end plane. If a PPP molecule is exchanged by PPS, then an ethyl group is added to the first chain of a “step” of the methyl terrace. The distortion of the lattice caused by this addition will be called a (1,0,0) distortion, while that caused by removing an ethyl group from the same chain will be denoted as a (-1,0,0) distortion. A (0,1,0) distortion is in this nomenclature the addition of an ethyl group to the chain in the middle of a “step” in the methyl terrace. It is also possible to bring about a (1,0,0) distortion in a PPS crystal: by exchanging PPS with PSS. As the distortion to the lattice is exactly the same, the activity coefficients at infinite dilution of PPS in PPP and PSS in PPS must be equal. Therefore, according to Equation 9.88, the 3-suffix Margules parameters $A_{\text{PPS-PPP}}$ and $A_{\text{PSS-PPS}}$ should be identical as well, which was found indeed ($A_{\text{PPS-PPP}} = 1.6$, $A_{\text{PSS-PPS}} = 1.43$). Table 9.37 lists all 26 different distortions to the lattice of β -2A and β -2B TAGs that can be caused by addition or removal of ethyl groups.

These 26 different distortions occur at only three levels of the degree of isomorphism.

A complicating factor is the asymmetry of the TAGs PPS and PSS: PPS causes a (1,0,0) distortion in PPP, while its mirror image SPP leads to a (0,0,1) disturbance. These two distortions are not necessarily equivalent.

Notwithstanding the fact that sometimes asymmetric TAGs are involved, a good agreement is found between the values of the three suffix Margules parameters of equivalent distortions (Table 9.38).

The 3-suffix Margules parameters for the binary SSS-PPS could not be determined because of poor data quality. If the effects of chirality are negligible, they should be the same as those of PSS-PPP.

TABLE 9.37

**TAGs That Cause Equivalent Distortions When Inserted
in the Crystal Lattice of the Six TAGs That Can Be Formed
from P and S**

Disturbance of Methyl Terrace	TAGs Crystallizing in the -2A Modification				TAGs in the -2B Modification		
	PPP	SSS	PPS	PSS	PSP	SPS	ϵ
A -1 -1 -1	MMM	PPP	MMP	MPP	MPM	PMP	0.88
B -1 -10	PMM	SPP	MMS	MSP	MPP	PPP	0.92
C -1 -11	SMM	APP	MMA	MAP	MPS	PSP	0.88
D -10 -1	MPM	PSP	PMP	MPS	PPM	PMS	0.92
E -10 0	PPM	SSP	PMS	MSS	PPP	PPS	0.96
F -10 1	SPM	ASP	PMA	MAS	PPS	PSS	0.92
G -11 -1	MSM	PAP	SMP	MPA	SPM	PMA	0.88
H -11 0	PSM	SAP	SMS	MSA	SPP	PPA	0.92
I -11 1	SSM	AAP	SMA	MAA	SPS	PSA	0.88
J 0 -1 -1	MMP	PPS	MPP	PPP	MSM	SMP	0.92
K 0 -10	PMP	SPS	MPS	PSP	MSP	SPP	0.96
L 0 -11	SMP	APS	MPA	PAP	MSS	SSP	0.92
M 0 0 -1	MPP	PSS	PPP	PPS	PSM	SMS	0.96
N 0 0 1	SPP	ASS	PPA	PAS	PSS	SSS	0.96
O 0 1 -1	MSP	PAS	SPP	PPA	SSM	SMA	0.92
P 0 1 0	PSP	SAS	SPS	PSA	SSP	SPA	0.96
Q 0 1 1	SSP	AAS	SPA	PAA	SSS	SSA	0.92
R 1 -1 -1	MMS	PPA	MSP	SPP	MAM	AMP	0.88
S 1 -10	PMS	SPA	MSS	SSP	MAP	APP	0.92
T 1 -11	SMS	APA	MSA	SAP	MAS	ASP	0.88
U 1 0 -1	MPS	PSA	PSP	SPS	PAM	AMS	0.92
V 1 0 0	PPS	SSA	PSS	SSS	PAP	APS	0.96
W 1 0 1	SPS	ASA	PSA	SAS	PAS	ASS	0.92
X 1 1 -1	MSS	PAA	SSP	SPA	SAM	AMA	0.88
Y 1 1 0	PSS	SAA	SSS	SSA	SAP	APA	0.92
Z 1 1 1	SSS	AAA	SSA	SAA	SAS	ASA	0.88

The distortions of Table 9.38 are arbitrarily marked from A–Z for the β -2A submodification and from A'–Z' for the β -2B submodification. Using these markers, the phase diagrams can be classified: for example, SSS–PPP is a Z/A phase diagram. The binary interaction parameters for all Z/A phase diagrams should be the same, regardless of the excess Gibbs energy model used.

If chirality is neglected, the 15 phase diagrams can be classified into nine different groups. The value of the binary interaction parameter within a group seems to be constant.

These structural considerations show clearly that there is no reason at all for the assumption that the interaction parameters for the binary pairs PSP–PPP (type P/E')

TABLE 9.38
3-Suffix Margules Parameters for Some Equivalent Distortions ($a \triangleq A/RT$)

Code	Distortion	$\alpha_{PSP-PPP} = >3$	$\alpha_{SPS-PPS} = >3$
P	(0,1,0)	$\alpha_{PSP-PPS} = >3$	$\alpha_{SPS-PPS} = >3$
U	(1,0,-1)	$\alpha_{PSP-PPS} = >3$	$\alpha_{SPS-PPS} = 2.6$
J	(0,-1,-1)	$\alpha_{PPS-SSS} = 2.3$	$\alpha_{PPP-PSS} = 2.1$
M	(0,0,-1)	$\alpha_{PSS-SSS} = 2.3?$	$\alpha_{PPP-PPS} = 2.3$
V	(1,0,0)	$\alpha_{SSS-PSS} = 1.1$	$\alpha_{PPS-PPP} = 1.6$
Y	(1,1,0)	$\alpha_{PSS-PPP} = 2.8$	$\alpha_{SSS-PPS} = 2.3?$

and PPS–PPP (type VN/M) should be the same, in spite of the fact that the degree of isomorphism of both pairs is 0.96. In the previous section, it was found that the binaries with PSP and SPS are exceptions to the empirical “rule” that the degree of isomorphism is related to the magnitude of the 2-suffix Margules parameter. This was explained by assuming that continuous miscibility cannot exist between the β -2A and β -2B modification, in spite of the close resemblance between the two β -modifications. An alternative explanation is simply that the (0,1,0) distortion caused by PSP in PPP is not equivalent to the (1,0,0) distortion of PPS in PPP. This alternative explanation implies that the degree of isomorphism is too coarse a measure to correlate the interaction parameters.

Only calculation of the magnitude of the lattice distortions can decide which of the explanations is most likely (Table 9.39).

9.8.2.2 β -2A Lattice Distortion Calculations

The calculations were carried out using the programs Insight and Discover from Biosym. The program calculates the molecular configuration with minimal energy. The molecular energy is the sum of the internal energy from bond length stretching, bond angle stretching, and torsion, and the nonbond-associated energy due to Coulomb and van der Waals forces.

The magnitude of a (1,0,0), a (0,1,0), and a (0,0,1) distortion to LLL have been calculated by comparison of the lattice energy of a pure LLL crystal with the lattice energy of an LLL crystal in which one molecule of an impurity [I] has been inserted per 54 molecules of LLL.

In the latter calculations, we allowed the impurity to obtain the conformation with minimal energy, while the LLL molecules were fixed to the conformation that they have in a pure crystal. Calculations in which the complete impure crystal was allowed to rearrange went beyond the capacity of the program. The results are given in Table 9.40.

The order of magnitude of the crystal energy corresponds very well with the data of de Jong (1980) for CCC.

The (0,1,0) lattice distortion, which is brought about by the β -2B-forming TAG LML, has the same order of magnitude as those caused by the two β -2A forming TAGs LLM and MLL. The very poor miscibility in the solid phase that was found

TABLE 9.39
The P/S Binaries Classified in the Types Defined in
Table 9.37, Together with the 2-Suffix Margules
Parameters

Binary	Type	A/RT	Binary	Type	A/RT
SSS–PSS	V/ME	1.6	SSS–PPP	Z/A	3
PSS–PPS	VX/MS	1.6			
PPS–PPP	VN/M	1.9	PSP–SPS	C/I	1.4
SSS–PSP	Q'/D	>3	PSS–SPS	F'L/U	2
			PSP–PPS	U/F'H'	β'
SSS–SPS	N'/K	>3			
PSS–PSP	N'/K		PSP–PPP	P/E'	β'
			SPS–PPS	P/E'	2
SSS–PPS	Y/BJ	>2.3?			
PSS–PPP	QY/J	2.2	SPS–PPP	W/B'	>5

Note: Where asymmetric tags are involved, a three- or four-letter code is used, indicating the distortions caused by both mirror images.

TABLE 9.40
Lattice Distortions U/RT to a β -2A Crystal of LLL Caused by Impurities at Infinite Dilution in LLL

Type	Caused by	Distortion U/RT	U (Distorted Crystal) kJ/mol	U (Pure “Impurity”) kJ/mol
(1, 0, 0)	LLM	1.0	258.9	270.1
(0, 1, 0)	LML	1.9	251.9	268.8
(0, 0, 1)	MML	3.6	255.0	270.1
(0, 0, 0)	LLL	0	253.8	253.8

experimentally for TAGs equivalent to LML and LLL can therefore only be explained by assuming that continuous miscibility between the β -2A and β -2B submodification is not possible, in line with the findings in the previous section. The magnitude of the lattice distortion U/RT agrees strikingly well with the magnitude of the interaction parameter $A/RT = 1.8$ that we obtained from the experimental data (Figure 9.50).

The (1,0,0) distortion caused by LLM is much smaller than the (0,0,1) distortion caused by its mirror image MLL. The effects of chirality may clearly not be disregarded. Here again, the average value of the distortions U/RT corresponds reasonably well to the values of the interaction parameter A/RT of 1.6–2.3 that were found experimentally.

The order of magnitude of the calculated distortions corresponds with that expected from the value of the interaction parameters. However, we would expect that the distortions calculated in this way would lead to a systematic overestimate of

the interaction parameters. The actual distortion is smaller, because in reality some relaxation of the LLL lattice near the distortion will occur. Moreover, entropy effects are neglected. Apparently both effects are relatively small.

It has become evident that the lattice distortion calculations can be used to obtain good insight into the influence of structural differences on the solid state miscibility. We will continue this approach in future work. In view of the results obtained, the good performance of the 2-suffix Margules equation and the good correlation of the interaction parameter with the degree of isomorphism remain very surprising.

9.8.3 EMPIRICAL METHOD

Although Larsson and Hernqvist (1982) have announced a detailed analysis of the crystal structure of the β' -modification, similar to that of de Jong (1980) for the 13-modification, at present the β' -crystal structure of TAGs is still not exactly known. The instability of the β' -modification and the inability to grow large single crystals are the main obstacles. The crystal structure of *cis*-unsaturated TAGs has not been unambiguously revealed either. This implies that it is not yet possible to study the influence of impurities on the β' -crystal lattice by molecular modeling. The fundamental insight into the relation between nonideal miscibility of TAGs and structural differences can probably best be obtained from these lattice distortion calculations. While this is impossible, a semiempirical approach to the problem of this chapter, finding a method to predict binary interaction parameters, has to be followed.

9.8.3.1 Method

The correlation between the degree of isomorphism, ϵ , and the 2-suffix Margules parameter within one submodification can serve as basis for such a semiempirical predictive method. The following are assumed:

1. Within one submodification, the 2-suffix Margules binary interaction parameter A/RT is

For a β' -modification:

$$\epsilon > 0.93: \frac{A}{RT} = 0 \quad (9.95)$$

$$\epsilon \leq 0.93: \frac{A}{RT} = -19.5 \epsilon + 18.2 \quad (9.96)$$

and for a β -modification:

$$\epsilon > 0.98: \frac{A}{RT} = 0 \quad (9.97)$$

$$\epsilon \leq 0.98: \frac{A}{RT} = -35.8 \epsilon + 35.9 \quad (9.98)$$

2. Both 3-suffix Margules parameters are also given by Equations 9.92 through 9.95, except for the β' -2 modification of a binary pair of which one of the TAGs belongs to the h_2u TAG-group. If the h_2u -type TAG is indicated by 2, then A_{21} is given by Equations 9.92 and 9.93, while A_{12} follows from

$$\frac{A_{12}}{RT} = -21.7 \in +18.7 \quad (9.99)$$

3. If $A/RT > 8$, $A/RT = 8$ can be used in calculations.

The relations in Equations 9.95–9.99 were obtained by linear regression through the data of Tables 9.34 through 9.36. The correlation coefficient is 0.9, while the standard error in the estimated interaction parameters is 0.3–0.5. The values of the regression constants clearly illustrate the better solid miscibility in the less densely packed β' - modification.

Interaction parameters within a submodification are useless if the pure component properties of the TAG, crystallized in that submodification, are not known. Often these properties cannot be measured, because the pure components do not occur in the desired submodification. Therefore the following additional assumptions are made in line with our observations in Section 9.4 and those of de Jong (1980).

4. The melting point of a hypothetical -3 form of a TAG that crystallizes into the β' -2 or β -2 form is 3°C less than the melting point of the corresponding -2 form. The heat of fusion is 90% of that of the corresponding -2 form. Similarly the melting point of a hypothetical -2 forms of a TAG that crystallizes into β' -3 or β -3 form is 3°C less than that of the corresponding -3 form, while the heat of fusion is 90% of that of the -3 form.
5. Submodifications in the β' -modification are, if they exist, continuously miscible.
6. It is only possible to form continuous solid solutions of two TAGs in the β -2 modification when they both crystallize in the same β -2 submodification. Table 9.41 lists the four different β -2 submodifications that occur in

TABLE 9.41
Summary of the β -2 Submodifications
in Which Different TAG Families (x,y)
Crystallize

β -2 Submodification			
A	B	C	D
(0, 0)	(-2, 0)	(4, 2)	(2, 2)
(0, 2)	(2, 0)	(4, 4)	
(2, 2)	(2, 4)		

practice, using de Jong's nomenclature, representing a TAG according to the method defined in Section 9.4 as $(p \cdot p + x \cdot p + y)$ and thus indicating TAG families by (x, y) .

7. The melting point and heat of fusion of the hypothetical β -2 forms, which do not occur in the pure TAG, are assumed to lie 3°C below that of the stable β -2 form, while the heat of fusion is 90% of that of the stable form.

Thermodynamic calculations now become extremely complicated, as the number of independent polymorphs that have to be considered, has increased with each extra assumption from 3 to 8. Because most binary pairs of TAGs that crystallize into different β -2 modifications are not completely miscible even when they would crystallize in the same submodification, often equivalent calculation results are obtained if assumption 7 is replaced by the following assumption.

8. In calculations, only one β -2 polymorph can be used. However, if the two TAGs of a binary crystallize in different submodifications, the two suffix Margules parameter that is obtained from Equations 9.94 and 9.95 is augmented by 1.

The phase diagram of SSS–SPS (Figure 9.50) that was calculated allowing the occurrence of 2 β -2 modifications and $A/RT = 1.8$ in each submodification is nearly the same as the phase diagram given in Section 9.7.2.4.1 using only one β -modification and $A/RT = 3$.

The difference of 3°C between the melting point of the stable and hypothetical β' - and β -forms is a best guess, based on de Jong's findings for the melting points of saturated mono-acid TAGs in different submodifications. The value of 90% for the heat of fusion of hypothetical submodifications is a best guess that is based on the data given in Section 9.4.

9.8.3.2 Discussion

It is obvious that the empirical method given is far from perfect, as it is based on a small number of data, which necessitated a number of speculative assumptions. However, the underlying notion that only TAGs with a high degree of geometric similarity will mix well in a densely packed solid phase is most likely correct. Therefore, the main effects of structural differences on solid phase miscibility are covered by the method, although not always very precise. In order to improve the method, more data are required and a number of issues need to be solved:

1. There is still a lack of reliable data on binary interaction parameters of TAGs, both for the β' -modification and for the β -modification. Especially on mixtures with *cis*-mono- and di-unsaturated TAGs more information is required.
2. The crystal structure of the β' -modification and its possible submodifications as well as the structure of the polymorphic forms of *cis*-unsaturated TAGs have to be known.
3. It must be established to what extent the structure of two submodifications must be different before continuous miscibility of the two submodifications cannot occur, so that treatment as independent polymorphs is necessary.

4. If two submodifications need to be treated as independent polymorphs, a method must be developed to estimate the thermodynamic properties of those polymorphs that do not occur in the pure component.
5. To obtain insight in the magnitude of different lattice distortions, more mixtures have to be studied by molecular modeling, not only in the β -modification, but also in the β' -modification.

In spite of its serious limitations, in Section 9.9 this empirical method will be tested to see how it performs in practical situations.

9.8.4 CONCLUSION

The nonideal mixing behavior of TAGs in the solid phase can be explained by geometrical considerations.

Within one (sub)modification the binary interaction parameters show a clear correlation with the degree of isomorphism, as defined by Kitaigorodskii (1984).

Based on the good correlation between degree of isomorphism and the 2-suffix Margules interaction parameter, a method has been defined that predicts the binary interaction parameters from structural differences.

The work that is required to improve this predictive method was outlined.

9.9 PRACTICAL APPLICATIONS

In the previous sections, all steps that are required to meet the objective of this work (prediction of melting ranges and solid phase composition of fats) have been taken. In this section, the method developed will be used for predictions in a number of practical situations: the prediction of melting ranges of margarine fat blends, the prediction of the composition of fat fractions obtained from fractional crystallization, and the understanding of recrystallization phenomena. Some examples outside the area of edible fats are considered as well. Finally the conclusions of this chapter are summarized.

9.9.1 PREDICTION OF MELTING RANGES

The primary objective of this chapter is the development of a general method to predict the melting range of a fat blend from its composition. In this section, we will investigate to what extent this objective has been attained.

In Section 9.6, it was shown that the α -melting ranges, or “ α -lines” of the fat blends of nine different commercial fat spreads could be predicted very well.

If the binary interaction parameters for the β' -modification are estimated with the procedure outlined in Section 9.8.3, it is in principle possible to calculate the β' -melting ranges of these fats as well. A complicating factor in the calculations is the large number of components, usually between 30 and 400 in these fats. Even if only four coexisting β' phases are formed, the flash calculation of Section 9.3 must already handle matrices with a 2000×2000 dimension, which will make the calculation procedure too slow for practical use.

To keep the calculations manageable, pseudocomponents are defined as follows: all components that are nearly isomorphous ($\in > 0.95$) and that differ 5°C or less in their β' -2 melting point are taken together as a new pseudocomponent that has the polymorphic behavior and the size of the component that contributes most to the pseudocomponent. Components and pseudocomponents with a concentration less than 0.1% are neglected.

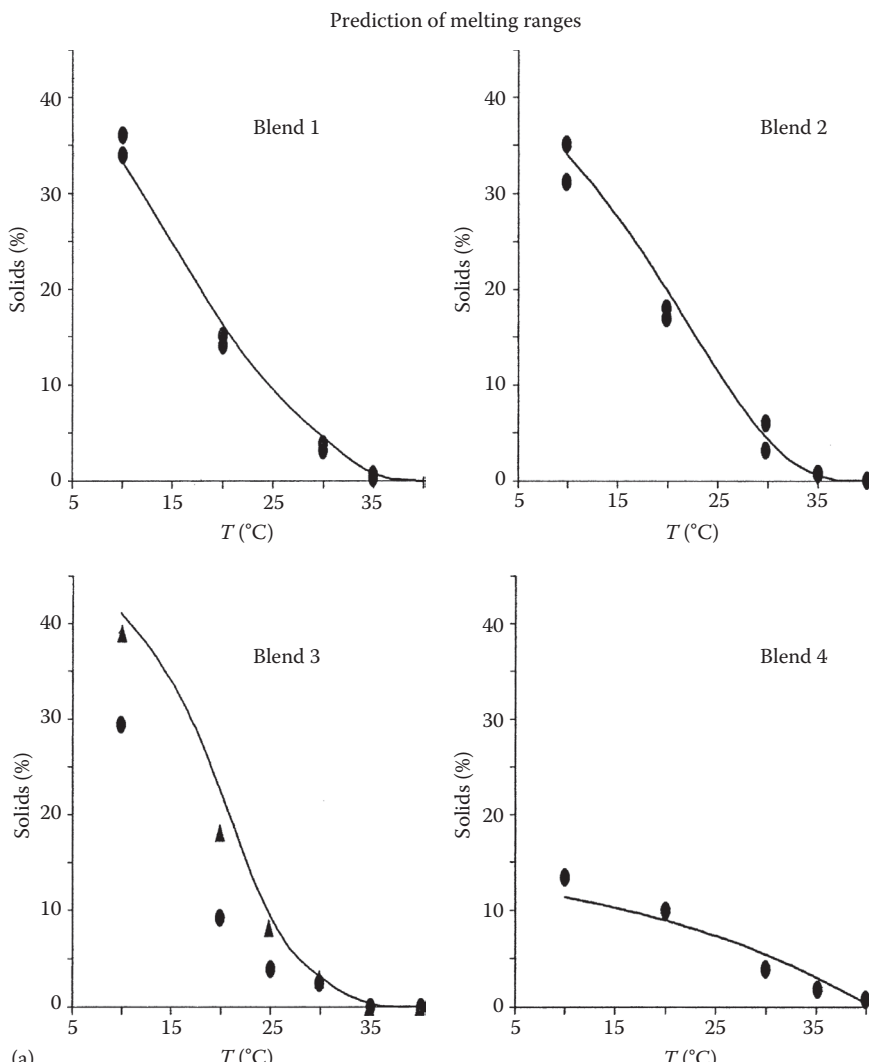


FIGURE 9.52 (a) Predicted (lines) and experimental (points) β' -melting ranges of several commercial fat blends. The numbers refer to the composition of the fat blend, given in Table 9.19. The 2-suffix Margules equation was used for the excess Gibbs energy. dots: solid phase measured with standard procedure triangles (blend 3 only): determined in a week-old margarine.

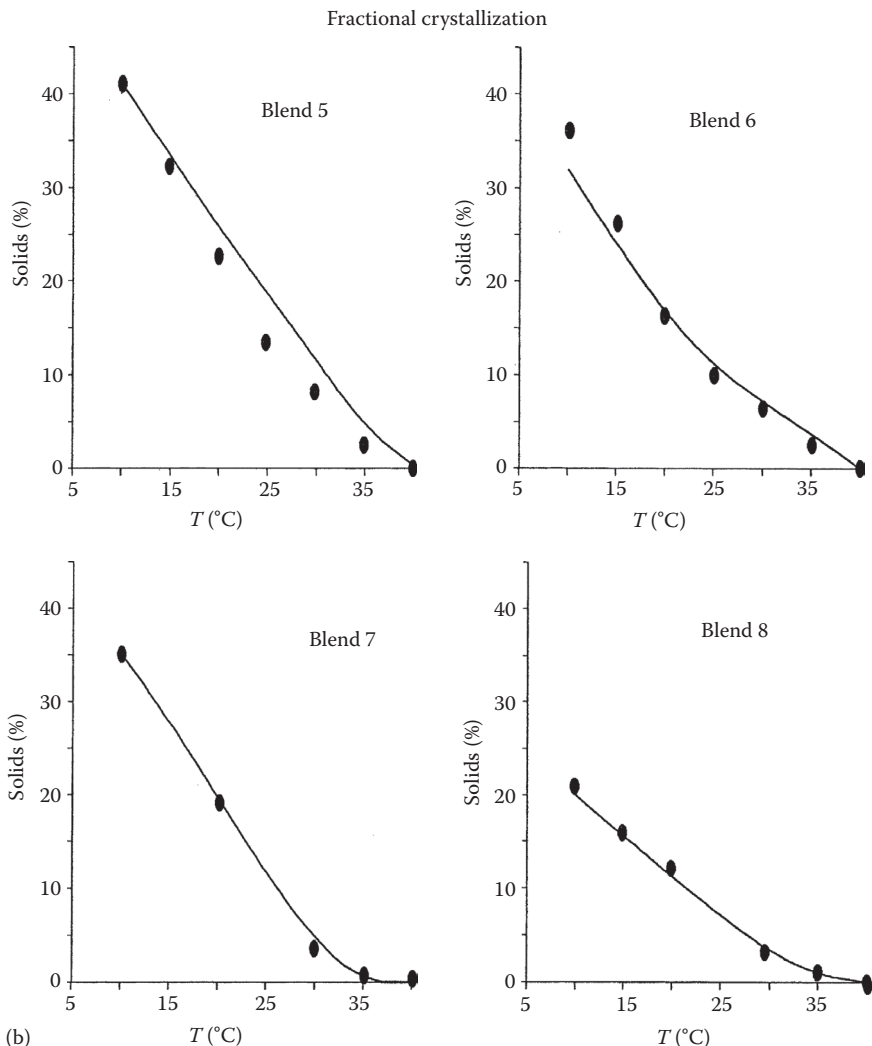


FIGURE 9.52 (continued) (b) Predicted (lines) and experimental (points) β' -melting ranges of several commercial fat blends. The numbers refer to the composition of the fat blend, given in Table 9.19. The 2-suffix Margules equation was used for the excess Gibbs energy.

In this way blend 1–8 from Table 9.19 were reduced to 15–20 component mixtures. Only blend 9 remained too complex. The β' -melting ranges of these 15–20 component mixtures were calculated and plotted in Figure 9.52, together with the experimental values. The experimental values were obtained with wide range NMR of samples that were molten, kept for 1 h at 80°C, rapidly cooled to 0°C, stabilized for 16 h at 0°C and for 30 min at the temperature of measurement. With this procedure, one of the Unilever standard methods, most normal fat blends have crystallized completely.

Although the predictions show a larger deviation than those for the α -melting ranges, the agreement with the experimental data is still very good, in spite of the large simplifications that were made in the composition and in the estimation of the interaction parameters. The standard error of 3% solids compares well with the experimental error of 1% solids and the effects of kinetics of crystallization, that are normally estimated to be in the order of a few percent of solids.

Out of the empirical methods, mentioned in Section 9.1, only the multiple linear regression/linear programming method performs better, but only within the limited range of compositions for which this method is valid. As it is based on interpolations within a finely meshed raster of experimental data points, this is not too surprising.

Only for blend 3, which contains 23% of POP, the experimental points, determined with the standard method, lie far below the calculated line. Blend 3 is a typical example of a fat blend that shows extreme “postcrystallization.” Postcrystallization means that in the first week after production still a considerable amount of solid fat crystallizes. The solid fat content that was determined in a margarine sample of a week old is also plotted in Figure 9.52. Now the agreement with the calculated data is very good. Obviously, blend 3 has not crystallized completely when the standard procedure is used.

Thus it has been demonstrated that melting ranges of the practically relevant polymorphic forms of fat blends can be predicted by application of solid–liquid phase equilibrium thermodynamics.

9.9.2 FRACTIONAL CRYSTALLIZATION

The second objective of this chapter is the development of a method that predicts the solid phase composition of a fat at a certain temperature, in order to enable modeling of a fractional crystallization process. At present fractional crystallization is primarily used for fractionation of palm oil into palm olein, a liquid fraction of palm oil and palm stearin, a solid fraction.

Palm oil was heated to 80°C for 1 h and subsequently cooled to the fractionation temperature. Five hours after the appearance of the first turbidity the palm olein was filtered off in a filter press at 12 bar. The separation efficiency (amount of olein that is obtained over the total amount of liquid phase that is present in palm oil) was determined. NMR showed that crystallization had taken place into the β' -modification. The TAG compositions of the palm oil, the olein, and the stearin were analyzed by A_gNO_3 -HPLC (Kitaigorodskii, 1984). The results are given in Table 9.42, together with the composition that was calculated, using the procedure as outlined earlier and the measured separation efficiency.

The calculated data agree very well with the experimental ones. Van Putte and Bakker (1987) states that palm oil crystallizes into the β' -modification when the crystallization takes place at 27° or less, while above this temperature the β -modification is observed. In line with this observation, calculations show that in palm oil up to 25°C–26°C a stable β' -solid phase coexists with two β -solid phases, while above this temperature only β -solid phases remain.

This example shows clearly that application of solid–liquid phase equilibrium thermodynamics to fat fractionation processes is feasible.

TABLE 9.42
Experimental and Predicted Compositions
of Palm Oil Fractions (Calculated for the
Most Stable State, the β -Modification)

	Fract. at 29°C		Fract. at 32°C	
	Measured	Calc.	Measured	Calc.
Palm oil				
h ₃	8.8			
hOh	33.0			
hhO	7.1			
hlh	9.5			
Rest	41.7			
Stearin				
h ₃	45.3	46.2	54.7	53.3
hOh	25.4	29.3	21.5	17.2
hhO	6.1	4.1	5.5	4.3
hlh	5.3	4.9	4.3	4.7
Rest	17.9	15.4	14.0	20.1
Olein				
h ₃	2.2	0.1	2.8	0.2
hOh	34.4	33.7	34.7	35.8
hhO	6.1	7.8	5.9	7.6
hlh	10.6	10.5	10.1	10.3
Rest	46.7	47.7	46.4	46.0

9.9.3 RECRYSTALLIZATION PHENOMENA

9.9.3.1 Influence of Precrystallization and Temperature Cycling

In Section 9.7.4, DSC curves of mixtures of a crystallizing binary pair of TAGs in a surplus of a liquid TAG were determined. The samples were stabilized by rapid cooling to a stabilization temperature. In those experiments, stabilization at temperatures below the onset of the first melting peak in the DSC thermogram in the end always resulted in the same DSC curve, regardless of the stabilization procedure that was followed. However, if a well-stabilized sample was subjected to temperature cyclization by increasing the temperature from the stabilization temperature to a cycling temperature well above the onset of the first melting peak and backward, then the DSC curves that were measured directly after the cycling step often had a completely different shape. The effect even occurred at cycling rates as low as 0.6°C/min. It was not possible to fit such DSC curves with the 2- or the 3-suffix Margules equation.

The shape of the curves of the cycled samples could be obtained using the well-known concept of shell formation (Zief and Wilcox, 1967), which was already mentioned in Section 9.2. Upon heating, the sample part of the solid phase dissolves. It is assumed that upon cooling the remaining crystals are covered with a layer of solid

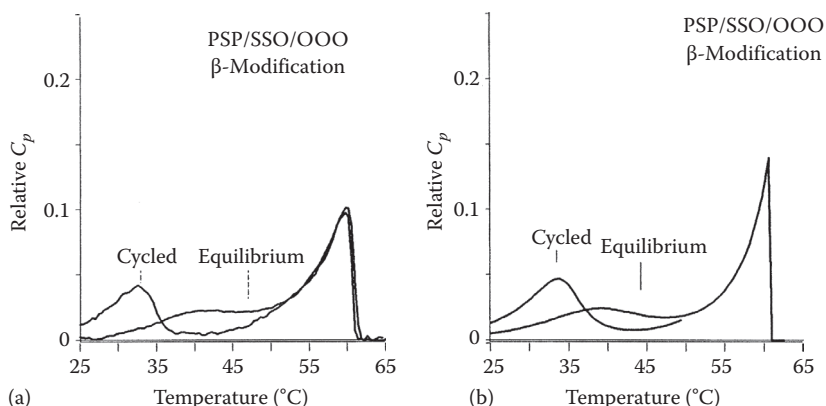


FIGURE 9.53 (a) 25% PSP/25% SSO/50% OOO. Effect of cycling to 50°C on the DSC melting curve. Experimental curves, taken at 2.5°C/min. (b) Simulation of the effect of cycling to 50°C on the DSC melting curve of the system of Figure 9.30.

fat that is in equilibrium with the liquid phase that is present. This shell effectively keeps the inner part of the crystals from gaining the equilibrium composition.

The resulting DSC melting curve will be the sum of that a sample that has an overall composition equal to that of the liquid phase at the cyclization temperature and the curve of the solid phase that remained at the cyclization temperature. This DSC curve will deviate from the equilibrium curve at temperature below the cyclization temperature. Figure 9.53a shows that this is exactly what is observed, while the curves in Figure 9.53b, which are calculated assuming shell formation, confirm that shell formation can describe the observations.

Shell formation is much less likely with the isothermal stabilization procedure that is followed in this work: always a completely liquid sample is very quickly supercooled to the stabilization temperature. Therefore all solids are formed at the stabilization temperature.

Elaborate cyclization procedures were followed in order to obtain the binary phase diagrams given in Section 9.7.2. The cycling effect described here offers another explanation for the large discrepancies between solidus and liquidus that were found: cyclization leads to the formation of a solid phase that starts to melt off at lower temperatures. After initial melting, a solid phase that is enriched in the highest melting component remains.

Shell formation also offers the explanation for the differences in fraction composition that are obtained with fractional crystallization of oils and fats when different cooling rates are used (Keulemans, 1986): slow cooling to the fractionation temperature causes shell formation and so results in a solid phase that is enriched in the higher melting components, while quick cooling results in the equilibrium composition. This work enables the quantification of the magnitude of these effects.

Shell formation also plays a role in the normal margarine “votator” process. Fat spreads are usually prepared by quickly cooling and emulsifying a mixture of a molten fat blend and milk or water in a scraped surface heat exchanger or “A-unit.” The supercooled emulsion is subsequently crystallized in a pin stirrer, or “C-unit.” In many cases, this is followed by further cooling and crystallization in second series of A and C-units, so that the complete votator process sequence becomes A–C₁–A–C₂. It is

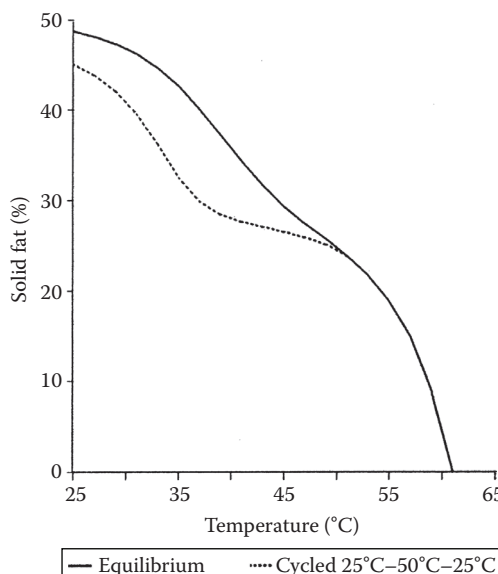


FIGURE 9.54 Calculated solids temperature lines of the TAG blend of Figure 9.53 (25% PSP/25% SSO/50% 000). Solid line = equilibrium line, dashed line = after precrystallization at 50°C.

often impossible to complete crystallization in this second C-unit to the β' -equilibrium, even when a very long residence time is provided. Upon storage, the equilibrium solids content will eventually be reached, resulting in a considerable posthardening and change of rheological properties. In fact, the two-step crystallization in this vortator process is a build in cyclization step: in the first C-unit a solid phase is formed, which is encapsulated in the second C-unit with a solid phase of different composition.

The effect of this precrystallization on solids content can be quite dramatic, as is illustrated in Figure 9.54 for the PSP/SSO/000 model blend that was used in Section 9.7.5.4: the difference in solid content between precrystallized and equilibrium situation can be as large as 10%–15% solids. After the A–C₁–A–C₂ vortator process the fat can only crystallize to a point on the lower solids line. But upon storage, it will recrystallize to the equilibrium composition in several weeks, which explains the increase in solids content and the rise in product hardness.

Fat blends in which the TAGs show considerable solid phase miscibility will be more sensitive to precrystallization effects than blends in which the TAGs show no solid phase miscibility.

9.9.3.2 Sandiness

A well-known phenomenon is the development of sandiness in fat spreads with a fat blend containing only liquid oils and hydrogenated low erucic acid rape seed oil (Hernqvist et al., 1981; Hernqvist and Anjou). Sandiness is the development upon storage of large β -fat crystals in a product that initially had crystallized into the β' -modification. Those large crystals give a sensation to the consumer as if sand has been erroneously added to the product.

Hydrogenated rape seed oil consists for 95% out of TAGs from C18 fatty acids (E, O, and S). The degree of isomorphism between these TAGs is 1, which implies ideal solid solubility both in the β' - and β -modifications. In Section 9.7.6.3 it was found that the rate recrystallization from β' to the β -modification depends on the thermodynamic driving force and on the degree of rearrangement of the solid phase that is required. Because the rape seed TAGs mix ideally in both modifications, the thermodynamic driving force is the full stability difference between the two modifications, while virtually no change in solid phase composition has to take place.

In this reasoning, the tendency to develop sandiness can be reduced by additions of TAGs that reduce the thermodynamic driving force and increase the degree of rearrangement in the solid phase that is required. Such TAGs should mix nearly ideally with the TAGs from rape seed oil in the β' -modification, but must demix in the β -modification. TAGs that have a degree of isomorphism with the rape seed TAGs of about 0.92 and a melting point above 30°C fulfill this criterion. Candidates are therefore the TAGs P₂S, P₂E, P₂O, A₂S, A₂S, A₂O, and also BS₂, B₂E, and B₂O. The solubility of these inhibiting TAGs in the β -modification of the rape seed TAGs is according to the findings in Section 8 nearly 10%. Therefore, expect that the β' - β transition in hydrogenated rape seed oil mixtures will be retarded considerably if the crystallizing TAGs in the fat blend consist for more than 10% of inhibiting TAGs. Hydrogenated rape seed oil already contains 5% of those TAGs, so that addition of only 5% of an inhibiting fat is required to retard sandiness.

TAGs with a degree of isomorphism with the rape seed TAGs of less than 0.86 are expected to have much less effect: they do not even cocrystallize with the rape seed TAGs in the β' -modification, so that still hardly any solid phase rearrangement is required for the formation of the β -modification.

Hydrogenated soybean oil has a TAG composition that is very similar to that of hydrogenated rape seed oils, but the concentration of sandiness inhibiting TAGs is higher: it varies from batch to batch around the critical value of 10%, which implies that depending on the batch of oil sandiness can occur. And indeed from time to time, we have observed sandiness in products based on hydrogenated soybean oil.

Hydrogenated high erucic rape seed oil, contains depending on the hydrogenation procedure followed, more than 10% of inhibiting TAGs. Therefore sandiness is not so often observed in products of this rape seed oil breed (Hernqvist et al., 1981; Hernqvist and Anjou).

Hernqvist already mentioned the possibility of addition of inhibiting TAGs, but he followed another reasoning and is not able to specify which TAGs and what amounts are required. By trial and error, Hernqvist found no sandiness in a mixture of TAGs from rape seed and 20% PSP and he suggests that other inhibiting TAGs may exist. Indeed PSP belongs to the inhibiting TAGs mentioned.

9.9.3.3 Conclusion

The examples in this section have made clear that, although quantitative predictions are not always possible, the methods of this work help create understanding of recrystallization phenomena, which can directly be translated into practical methods to influence recrystallization.

9.9.4 APPLICATIONS OUTSIDE EDIBLE OILS AND FATS

9.9.4.1 Solid–Liquid Phase Behavior of *n*-Alkanes

Contrary to TAGs, which have only one thermodynamically stable polymorph (“monotropic polymorphism”), each polymorphic form of medium to long chain odd numbered *n*-alkanes is stable within a certain temperature and pressure region (“enantiotropic polymorphism”). Far below the melting point the β' -form is stable. However, from about 10°C below to the melting point upward the α -modification (“rotator phase”) is the stable polymorph. Upon heating a β' -form of an odd numbered *n*-alkane, it will first transform to the α -modification at the so-called transition temperature and finally melt at the α -melting point.

The enantiotropic polymorphism gives rise to most peculiar solid–liquid phase diagrams, of which an example is depicted in Figure 9.55. The phase diagram consists of three single-phase regions, a liquid, an α - and a β -region. The regions are separated by two phase domains, a cigar-shaped α -L and a β' - α region with a minimum transition temperature (Wurflinger, 1972; Morancelli et al., 1985). Although on first sight the phase behavior seems completely different, remarkable agreement exists between the phase behavior of TAGs and these *n*-alkanes.

The cigar-shape of the α -L region indicates that miscibility in the α -modification of these *n*-alkanes must be nearly ideal. This is in agreement with our findings for the α -modification of TAGs.

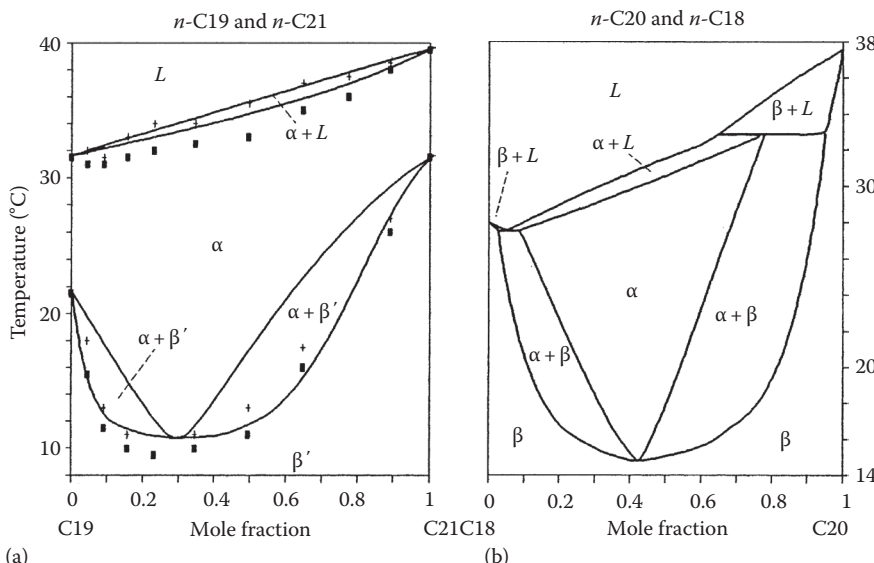


FIGURE 9.55 Phase diagrams of binary *n*-alkane mixtures. (a) *n*-C19 with *n*-C21, points: data from Würflinger (1972) lines: calculated with ideal α and liquid phase miscibility and nonideal mixing in the β' -modification with 3-suffix Margules parameters $A_{19_21}/RT = 0.4$ and $A_{21_19}/RT = 1.7$. (b) *n*-C18 with *n*-C20. Calculated assuming ideal miscibility in the α -modification and liquid phase and nonideal miscibility in the β' -modification with regular solution parameter $A/RT = 1.6$. The α -melting points were taken 1.5°C below the β -melting points. (From Würflinger, A., Thesis, University of Bochum, Bochum, Germany, 1972.)

The shape of the β' - α region and the existence of a single phase β' -region suggest non ideal mixing in the β' -modification, with a value for a regular solution binary interaction parameter in the β' -modification around 1.3–1.8. This is the same order of magnitude of the interaction parameters that have been found for the β' -modification of a binary pair of TAGs with a degree of isomorphism of 0.89.

When these values are used to describe the mixing behavior in the α - and β' -modification, the phase diagram of Figure 9.55 is obtained easily, applying the models and techniques used in this work for TAGs.

The main problem in the calculations is the absence of values for the β' -melting points. The enantiotropic behavior of these *n*-alkanes makes an experimental determination of β' -melting point impossible. However, they can be calculated from the measured β' - α -transition temperatures using the following expression:

$$T_{f,\beta'} = T_{\text{transition}} \cdot \frac{\Delta H_{\beta'}}{\Delta H_{\beta'} + \Delta H_{\alpha} \left(\frac{T_{\text{transition}}}{T_{f,\alpha}} - 1 \right)} \quad (9.100)$$

The expression follows from the fact that at the transition temperature the Gibbs energy of the two polymorphs must be equal. The differences in heat capacity are neglected. Calculated β' -melting points are listed in Table 9.42. Although the transition temperatures lie 10°C or more below the α -melting point, the calculated β' -melting points lie only 1°C or 2°C below the α -melting point.

The table also shows that, in spite of the higher melting point, entropy and heat of fusion of the α -modification are only 70% of the β -values, which is in agreement with the values found for TAGs. In fact, a rise of only 5% in α -melting entropy would change the enantiotropic polymorphism into the normal monotropic behavior that is observed for TAGs.

The phase diagram that is calculated from the values of Table 9.43 and the assumptions about the mixing behavior in the various polymorphic forms is plotted in Figure 9.55a, together with the data of Würflinger. The agreement is striking, especially when taking into account that it must be almost impossible to determine the equilibrium α - β' coexistence region correctly by experiment. It would require large rearrangements in the solid state within the time of measurement, while solid state diffusion is extremely slow.

Some even-chain *n*-alkanes are just monotropic: the α -melting point lies just below the β -melting point. Binary mixtures of those components are enantiotropic, which gives rise to interesting phase diagrams (Würflinger, 1972). This type of phase diagrams, too, is obtained without problems, assuming ideal mixing in the α -modification and non ideal mixing in the β' -modification with $A_{12}/RT = 1.3$ –1.8 (Figure 9.55b).

Thus it is illustrated that very simple excess Gibbs energy models, when combined with a proper treatment of polymorphism, can describe the main features of the complex solid–liquid phase behavior of *n*-alkanes.

9.9.4.2 Petroleum Waxes

In parallel with this chapter, a number of articles appeared from Won (1986, 1989) and Hansen (1987) on petroleum waxes. If mineral oils are brought from reservoir

TABLE 9.43
Thermodynamic Data of Some Odd-Chain *n*-Alkanes

Carbon Number	$T_f \alpha$	$T_{f\beta'}$	ΔH_α	ΔH_β	ΔS_α	ΔS_β	T_{trans}
9	-53.5	-54.2	16	22	71	100	-56.0
11	-25.5	-28.1	22	29	90	118	-36.5
13	-5.4	-8.1	28	36	106	136	-18.0
15	9.9	7.3	35	44	123	157	-2.3
17	21.9	19.4	41	52	138	176	10.5
19	32.0	29.6	46	59	150	197	22.0
21	40.2	38.3	48	63	152	203	32.5
23	47.5	45.5	54	76	169	238	40.5
25	53.5	51.5	58	84	177	258	47.0
27	58.8	56.9	60	89	182	270	53.0
29	61.2	60.2	66	98	198	293	58.0

Sources: Wurflinger, A., Thesis, University of Bochum, Bochum, Germany, 1972.

Note: T in °C, H in kJ/mol and S in J/K, mol.

temperature and pressure to atmospheric conditions, sometimes a solid wax phase crystallizes, which causes fouling of the equipment and pipelines.

This wax phase is amorphous, so it is in complete rotational disorder. In line with our findings for the α -modification of TAGs and the rotator phase of alkanes, it can be expected that these wax phases behave like ideal solid solutions. Consequently it is possible to calculate the wax appearance point of these oils.

Indeed, Won and Hansen found that the melting range of these complex petroleum waxes was predicted correctly by assuming ideal solid phase miscibility.

9.9.4.3 β -Substituted Naphthalenes

Another class of components that show polymorphism are the β -substituted naphthalenes. Like the odd-chain alkanes, the polymorphism is enantiotropic, with a high-temperature polymorph that shows some rotational disorder and more densely packed lower temperature polymorphs. Consequently, the phase diagrams are very similar to those of the enantiotropic odd-chain *n*-alkanes. An extensive study of binary phase diagrams of these components has been made by Chanh and Haget (Chanh and Haget, 1972, 1975; Haget et al., 1985). Contrary to the *n*-alkanes, the rotational disorder in the high temperature α -polymorph is not very large, so that a fairly high degree of isomorphism is required for ideal α -miscibility. In the more densely packed lower temperature polymorphs miscibility is even less ideal than in the α -modification, which in mixtures will lead to an extension toward lower temperatures of the region where the α -modification is stable. This is illustrated in Figure 9.56 for β -thionaphthalene and β -bromonaphthalene with a degree of isomorphism of 0.97. These components mix nearly ideally in the α -modification and highly nonideal in the other modifications. β -Thionaphthalene and β -fluoronaphthalene, with a degree isomorphism of only 0.87, already show nonideal mixing in the α -modification.

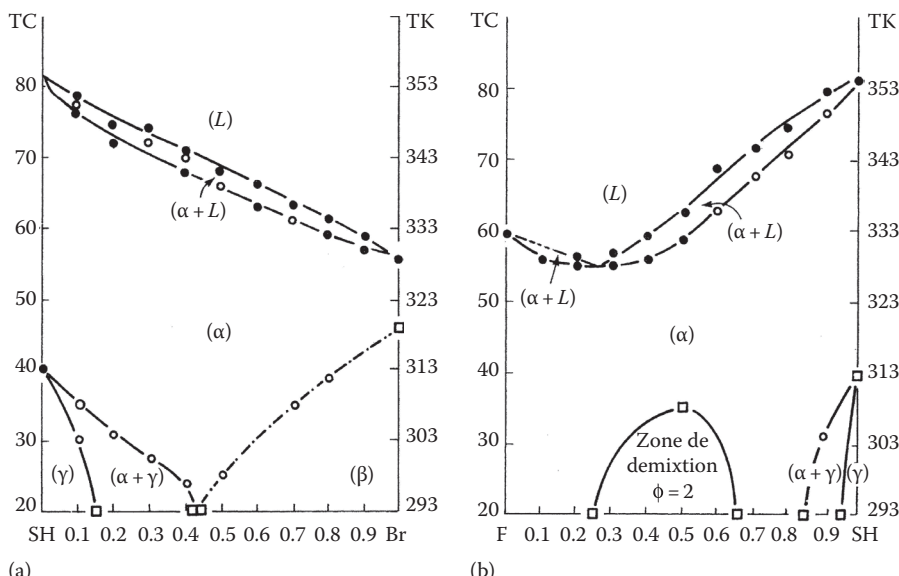


FIGURE 9.56 T, x, y binary phase diagrams of some β -substituted naphthalenes. (a) β -thionaphthalene and β -bromonaphthalene. (b) β -thionaphthalene and β -fluoronaphthalene.

Although Chanh et al. do not report pure component properties for each polymorphic form, so that calculation of the phase diagrams from their data is not possible, it is clear that the approach of this work offers a good starting point for the development of a description of the complex solid phase behavior of this class of compounds.

9.9.5 CONCLUSIONS OF THIS CHAPTER

The objective of this chapter is the development of a predictive method for the melting range and the solid phase composition of edible oils and fats. We have shown that this objective can be attained by application of solid–liquid phase equilibrium thermodynamics to all three basic polymorphic forms in which TAGs crystallize.

In order to develop this thermodynamic description:

- Existing multicomponent multiphase vapor liquid flash calculation algorithms have been adapted to deal with a number of mixed solid phases that show polymorphism.
- The heat of fusion and the melting points of TAGs have been correlated with a number of structural parameters.
- Liquid TAG mixtures and TAG mixtures in the α -modification have been treated as ideal mixtures.
- The deviation from ideal miscibility in the β' - and β -modifications has been described by the 2- and the 3-suffix Margules equations.
- A new method for the determination of the binary interaction parameters that occur in the 2- or 3-suffix Margules equation has been developed. The method

is based upon the interpretation of the complete DSC melting curve of a mixture of the binary pair and a surplus of a liquid TAG. It is quicker, more versatile and more reliable than the use of binary T, x, y solid–liquid phase diagrams.

- The binary interaction parameters that occur in the 2- or the 3-suffix Margules equation have been correlated with the degree of isomorphism of the binary pair, a parameter that indicates geometrical similarity.

Now the thermodynamic framework has been set up, the main scope of future research in this area should be the development of a more refined method to predict binary interaction parameters from structural differences.

9.10 SUMMARY

The properties of many food products, like margarine, reduced fat spreads, bakery products, snacks, cake, ice cream, and chocolate, are to a large extent determined by the melting range of the fat that they contain.

This chapter gives a general method to predict the melting range and solid-phase behavior of fats from their overall composition. It appears that solid fats are complex mixtures of several mixed crystalline solid phases in several polymorphic forms.

The ultimate amount, polymorphic form, and composition of the solid phase in a fat are determined by the position of the thermodynamic equilibrium solely. However, the crystallization process may lead to significant deviations from the equilibrium composition in practical situations. Yet, the starting point for any general predictive method of the solid-phase content and polymorphic behavior is an understanding of the solid–liquid phase equilibrium.

Fats consist of hundreds of different triacylglycerols (TAGs) that, like other long-chain hydrocarbons, can basically crystallize in three main forms:

1. The unstable α -modification
2. The metastable β' -modification
3. The stable β -modification

The thermodynamic framework describing the solid–liquid phase equilibrium for all three polymorphic forms of TAGs is given. The thermodynamic equations that determine these equilibria are worked out. Methods are developed that generate the information needed to solve this set of equations.

1. Calculation methods for gas–liquid systems are adapted to work for complex multicomponent liquid oil–solid fat systems that show polymorphism. Michelsen's method for the initial estimate combined with a Gibbs free energy minimization according to Murray is recommended as the best solution method for the thermodynamic equations.
2. The melting enthalpies and melting points of pure TAGs are obtained from correlations of the TAG structure with existing and new experimental data.
3. In the liquid (oil) phase TAGs are found to exhibit ideal mixing.
4. The degree of mixed crystal formation of TAGs in the solid fat phases can be described by simple excess Gibbs energy models: the 2- and 3-suffix

Margules equations. Binary interaction parameters of the Margules model are determined from existing and newly determined phase diagrams. Miscibility of TAGs in the solid phase is found to be governed by size differences of TAGs only. An empirical correlation is developed that predicts Margules binary parameters from the difference in structure of the two TAGs.

A large part of published binary phase diagrams of TAGs appears to be inaccurate due to experimental errors and stabilization issues.

A simple, fast, and accurate DSC method using a ternary system is given that allows easy determination of binary phase diagrams of two TAGs. It also uniquely allows the determination of phase diagrams of the unstable polymorphic forms.

The experimental data of multicomponent solid-phase behavior of fats and oils show that

- TAGs form ideal mixed crystals in the unstable α -modification. Chain mobility and space in the methyl end plane of the crystals is apparently sufficient to accommodate differences in size between TAGs. α -Melting ranges of a large number of commercial fats are predicted very well assuming complete and ideal mixed crystal formation.
- In the β' -form still a large extent of mixed crystal formation is found; however at chain length differences of 4 or more mixed crystal formation is only limited and TAGs start to crystallize into two separate partially mixed solid phases.
- In the most densely packed β -modification, TAGs only form perfect mixed crystals when there are no chain length differences. Any difference in chain length leads to crystallization in two separate partially mixed solid phases, and at differences in chain length exceeding 4, co-crystallization has virtually ceased.
- Applying the prediction of binary interaction parameters from differences in structure to all binary pairs of TAGs in a commercial fat, it is possible to calculate the β' - and β -melting ranges, the polymorphic behavior, and the solid fat and liquid oil compositions of the commercial fat surprisingly accurately from the composition of the fat blend.

This can be used for optimization of blend composition, fractionation processes, and understanding of product defects upon storage and storage temperature cycling. A better insight is obtained into the occurrence and prevention of undesired recrystallization phenomena that occur in fats. Also applications outside the world of edible fats are shown to be feasible.

LIST OF SYMBOLS

A	Interaction coefficient
A	Interaction parameter
A	Interaction parameter
a	A/RT
B_{11}	Second virial coefficient
c_p	Heat capacity (J/mol, K)

f	A function
G	Gibbs free energy (J)
g	Molar Gibbs free energy (J/mol)
K	Molar distribution coefficient
k, K	A constant
K^{AB}	Distribution constant
L	Long spacing
M	Molar weight (kg/mol)
m	Mass (kg)
N	Number of components
n	Number of moles (mol)
$n_{o,1,e}$	Number of o, 1, or e chains
P	Number of phases
P	Pressure (Pa)
p	Shortest outer TAG chain
P^*	Vapor pressure of pure component
q	Middle TAG chain
R	Gas constant (J/K, mol)
r	Longest outer TAG chain
T	Temperature (K)
T_f	Normal melting point (K)
T_∞	Hypothetical melting point of polyethylene (K)
V	Volume (m^3)
v	Volume of a molecule
v	Liquid molar volume (m^3/mol)
x	Interaction parameter
x	Mole fraction (mol/mol)
x	$P - q$
Y	Activity coefficient
y	$P - r$
z	Overall mole fraction
Δ	Number of double bonds
ΔH_f	Heat of fusion (kJ/mol)
ΔH_f	Heat of fusion (kJ/mol) at T_f
ΔS_f	Melting entropy (J/K, mol)
δ, θ	Constants
γ	Activity coefficient
Φ	Phase fraction
Φ_v	Volume flow rate (m^3/s)
ϕ	Volume fraction
μ	Chemical potential (J/mol)
τ	Angle of tilt
ϵ	Degree of isomorphism
$\%S$	Solid phase content
\times	Mole fraction

APPENDIX 9.A: PURE COMPONENT DATA

9.A.1 SATURATED TAGs

TABLE 9.A.1
Enthalpy of Fusion for the α -Modification of Saturated TAGs

X	Y	TAG	n	ΔH_f (kJ/mol)	Predicted	Residual	FREQ
-6	0	SLS	48	70.0	85.1	-15.1	1*
-6	2	PCS	44	80.0	71.8	8.2	1*
-4	0	PLP	44	65.0	76.6	-11.6	1*
-4	0	SMS	50	90.0	92.8	-2.8	1*
-4	2	PLS	46	70.0	79.5	-9.5	1*
-4	4	MCS	42	67.0	63.7	3.3	1*
-2	0	PMP	46	79.0	86.5	-7.5	1*
-2	0	SPS	52	103.0	102.7	0.3	
-2	2	PMS	48	93.0	89.4	3.6	1*
0	0	888	24	18.4	31.8	-13.4	3*
0	0	CCC	30	57.3	47.9	9.4	2*
0	0	LLL	36	69.8	64.1	5.7	3*
0	0	MMM	42	81.9	80.3	1.6	3*
0	0	PPP	48	95.8	96.5	-0.7	3*
0	0	SSS	54	108.5	112.7	-4.2	3*
0	0	BBB	66	143.2	145.1	-1.9	1
0	0	24.24.24	72	160.9	161.3	-0.4	1
0	2	88C	26	26.0	34.7	-8.7	1*
0	2	MMP	44	82.0	83.2	-1.2	1*
0	2	PPS	50	100.0	99.4	0.6	1*
0	4	LLP	40	67.0	67.4	-0.4	1*
0	4	MMS	46	87.0	83.6	3.4	1*
2	0	8C8	26	51.0	37.8	13.2	1*
2	0	CLC	32	67.0	54.0	13.0	1*
2	0	LML	38	83.0	70.2	12.8	1*
2	0	MPM	44	93.0	86.4	6.6	1*
2	0	PSP	50	112.2	102.6	9.7	2*
2	2	MPP	46	89.0	89.3	-0.3	1*
2	2	PSS	52	106.0	105.5	0.5	1*
2	4	LMP	42	74.0	73.5	0.5	1*
2	4	MPS	48	86.0	89.7	-3.7	1*
2	6	CLP	38	57.0	59.0	-2.0	1*
2	6	MPA	50	72.0	91.3	-19.3	1
4	0	MSM	46	99.0	87.8	11.2	1*
4	0	SBS	58	128.0	120.2	7.8	1*
4	2	MSP	48	91.0	90.7	0.3	1*
4	4	LPP	44	83.0	75.0	8.0	1*
6	0	LSL	42	66.0	72.2	-6.2	1*
6	0	LSL	42	66.0	72.2	-6.2	1*

TABLE 9.A.1 (continued)**Enthalpy of Fusion for the α -Modification of Saturated TAGs**

X	Y	TAG	n	ΔH_f (kJ/mol)	Predicted	Residual	FREQ
6	0	MAM	48	88.0	88.4	-0.4	1*
6	4	LSP	46	76.0	75.5	0.5	1*
6	6	CPP	42	53.0	61.0	-8.0	1*
6	6	LSS	48	70.0	77.2	-7.2	1*

Note: Data Marked by a * include measurements from this chapter. FREQ indicates the number of measurements that has been averaged.

TABLE 9.A.2**Enthalpy of Fusion for the β' -Modification of Saturated TAGs**

X	Y	TAG	n	ΔH_f (kJ/mol)	Predicted	Residual	FREQ
0	0	LLL	36	86.0	88.0	-2.0	1
0	0	MMM	42	106.0	111.1	-5.1	3*
0	0	PPP	48	126.5	134.3	-7.8	2*
0	0	SSS	54	156.5	157.5	-1.0	2*
0	2	MMP	44	100.0	106.5	-6.5	1*
0	2	PPS	50	124.0	129.7	-5.7	1*
0	4	LLP	40	90.0	84.4	5.6	1*
0	4	MMS	46	93.0	107.6	-14.6	1*
2	0	8C8	26	62.0	63.5	-1.5	1*
2	0	CLC	32	87.5	86.7	0.8	2*
2	0	LML	38	112.0	109.9	2.1	1*
2	0	MPM	44	127.0	133.0	-6.0	1*
2	0	PSP	50	165.5	156.2	9.3	4*
2	4	LMP	42	94.0	106.3	-12.3	1*
2	4	MPS	48	111.0	129.5	-18.5	1*
4	0	MSM	46	148.0	133.0	15.0	1*
4	0	SBS	58	189.0	179.4	9.6	1*
4	2	MSP	48	143.5	128.4	15.1	2*
4	4	LPP	44	110.0	106.3	3.7	1*
4	4	MSS	50	128.0	129.5	-1.5	1*
6	0	LSL	42	87.0	107.8	-20.8	0*
6	0	MAM	48	117.0	130.9	-13.9	1*
6	4	LSP	46	107.0	104.2	2.8	1*
6	6	LSS	48	104.0	111.6	-7.6	1*

Note: Data marked by a * include measurements from this work. FREQ indicates the number of measurements that has been averaged.

TABLE 9.A.3
**Enthalpy of Fusion for the β -Modification
of Saturated TAGs**

X	Y	TAG	n	ΔH_f (kJ/mol)	Predicted	Residual	FREQ
-10	0	S8S	44	141.0	131.7	9.3	1
-8	0	P8P	40	122.0	116.2	5.8	3
-8	0	SCS	46	143.0	139.5	3.5	2
-6	0	PCP	42	122.5	124.0	-1.5	2
-6	0	SLS	48	132.0	147.4	-15.4	2*
-6	2	PCS	44	125.0	123.3	1.7	1*
-4	0	PLP	44	121.5	133.1	-11.6	2*
-4	0	SMS	50	146.5	156.5	-10.0	2*
-4	2	PLS	46	123.0	132.4	-9.4	1*
-4	4	MCS	42	88.0	106.3	-18.3	1*
-2	0	PMP	46	137.0	148.3	-11.3	2*
-2	0	SPS	52	170.3	171.7	-1.4	4*
-2	2	PMS	48	152.0	147.6	4.4	1*
0	0	888	24	69.2	74.7	-5.4	4*
0	0	CCC	30	95.0	98.0	-3.0	5*
0	0	LLL	36	122.2	121.3	0.9	9*
0	0	MMM	42	146.8	144.7	2.1	8*
0	0	PPP	48	171.3	168.0	3.3	16*
0	0	SSS	54	194.2	191.3	2.8	20*
0	2	88C	26	59.0	73.9	-14.9	1*
0	2	LLM	38	116.0	120.6	-4.6	1
0	2	MMP	44	131.0	143.9	-12.9	1*
0	2	PPS	50	166.3	167.3	-1.0	4*
0	4	LLP	40	117.0	117.8	-0.8	1*
0	4	MMS	46	145.0	141.2	3.8	1*
2	0	PSP	50	166.0	173.6	-7.6	1
2	2	LMM	40	118.0	126.2	-8.2	1
2	2	MPP	46	140.0	149.6	-9.6	1*
2	2	PSS	52	175.0	172.9	2.1	3*
2	4	LMP	42	125.0	123.5	1.5	1*
2	4	MPS	48	137.0	146.8	-9.8	1*
2	6	CLP	38	95.0	105.0	-10.0	1*
2	6	MPA	50	122.0	151.6	-29.6	0*
4	4	LPP	44	146.0	119.0	27.0	0*
4	4	MSS	50	139.0	142.4	-3.4	1*
6	0	LSL	42	131.0	124.8	6.2	1*
6	0	MAM	48	157.0	148.1	8.9	1*
6	4	LSP	46	124.0	121.3	2.7	1*
6	6	CPP	42	89.0	102.8	-13.8	1*
6	6	LSS	48	123.0	126.1	-3.1	1*

Note: Data marked by a * include measurements from this work. FREQ indicates the number of measurements that has been averaged.

TABLE 9.A.4
Melting Points of the α -Modification of Saturated TAGs

X	Y	TAG	n	T_f (oC)	Predicted (oC)	Residual	FREQ
-12	0	S6S	42	27.8	23.7	4.1	2
-10	0	P6P	38	14.6	10.2	4.4	2
-8	0	SCS	46	30.0	34.4	-4.4	2
-6	0	PCP	42	20.0	24.3	-4.3	2
-6	0	SLS	48	36.0	39.3	-3.3	2
-4	0	MCM	38	16.0	13.4	2.6	1
-4	0	PLP	44	32.6	31.4	1.2	2
-4	0	SMS	50	43.8	44.3	-0.5	4
-4	0	BSB	62	61.1	61.7	-0.6	1
-2	0	LCL	34	5.0	2.9	2.1	2
-2	0	MLM	40	24.0	23.7	0.3	1
-2	0	PMP	46	39.1	38.5	0.6	5
-2	0	SPS	52	50.7	49.4	1.3	6
-2	2	PMS	48	40.9	41.3	-0.4	2
-1	0	P.15.P	47	43.4	41.7	1.7	1
-1	0	s.17.s	53	53.1	51.8	1.3	1
0	0	888	24	-51.0	-47.8	-3.2	1
0	0	9.9.9	27	-26.0	-26.1	0.1	1
0	0	CCC	30	-11.5	-9.3	-2.2	2
0	0	11.11.11	33	2.0	4.2	-2.2	2
0	0	LLL	36	15.6	15.2	0.4	4
0	0	13.13.13	39	24.5	24.3	0.2	3
0	0	MMM	42	32.6	32.0	0.6	6
0	0	15.15.15	45	39.5	38.7	0.8	4
0	0	PPP	48	44.7	44.4	0.3	5
0	0	17.17.17	51	49.9	49.4	0.5	4
0	0	SSS	54	54.7	53.8	0.9	8
0	0	19.19.19	57	59.1	57.7	1.4	2
0	0	AAA	60	62.9	61.3	1.6	2
0	0	21.21.21	63	65.0	64.4	0.6	1
0	0	BBB	66	69.1	67.3	1.8	2
0	1	11.11.L	34	7.5	7.3	0.2	1
0	2	CCL	32	0.0	-3.2	3.2	1
0	2	LLM	38	19.0	19.4	-0.4	1
0	2	MMP	44	34.5	35.2	-0.7	3
0	2	PPS	50	46.4	46.9	-0.5	5
0	4	CCM	34	3.0	-0.8	3.8	2
0	4	LLP	40	20.0	21.4	-1.4	1
0	4	MMS	46	35.6	37.0	-1.4	3
0	4	SSB	58	56.7	57.2	-0.5	2
0	6	CCP	36	2.0	3.2	-1.2	1

(continued)

TABLE 9.A.4 (continued)
Melting Points of the α -Modification of Saturated TAGs

X	Y	TAG	n	T_f (oC)	Predicted (oC)	Residual	FREQ
0	6	LLS	42	20.5	24.5	-4.0	2
0	8	CCS	38	32.0	9.6	22.4	0
0	10	66P	28	-7.4	-50.2	42.8	0
0	10	88S	34	5.0	-9.0	14.0	0
0	12	66S	30	6.8	-34.1	40.9	0
0	14	88B	38	26.0	9.0	17.0	0
0	16	66B	34	31.0	-9.1	40.1	0
1	0	P.17.P	49	48.2	46.5	1.7	1
1	0	S.19.S	55	55.5	55.4	0.1	1
2	0	CLC	32	6.0	0.8	5.2	1
2	0	LML	38	24.0	22.0	2.0	1
2	0	MPM	44	36.2	36.9	-0.7	3
2	0	PSP	50	47.2	48.0	-0.8	5
2	2	CLL	34	5.0	6.1	-1.1	1
2	2	LMM	40	22.0	25.7	-3.7	1
2	2	MPP	46	36.0	39.8	-3.8	1
2	2	PSS	52	50.1	50.4	-0.3	5
2	4	MPS	48	41.9	41.5	0.4	3
4	0	CMC	34	3.0	4.4	-1.4	1
4	0	LPL	40	19.0	24.7	-5.7	1
4	0	MSM	46	33.0	39.1	-6.1	1
4	0	SBS	58	56.0	58.2	-2.2	1
4	4	CMM	38	15.0	11.7	3.3	1
4	4	LPP	44	32.0	30.3	1.7	1
4	4	MSS	50	44.0	43.6	0.4	1
4	4	SBB	62	61.3	61.4	-0.1	1
6	0	CPC	36	6.0	6.9	-0.9	1
6	0	LSL	42	21.0	26.8	-5.8	1
6	0	PBP	54	47.4	51.4	-4.0	1
6	6	CPP	42	23.0	17.6	5.4	1
6	6	LSS	48	36.0	34.9	1.1	1
6	6	PBB	60	55.9	56.8	-0.9	1
8	0	CSC	38	34.0	11.5	22.5	0
8	8	CSS	46	42.5	26.6	15.9	0
12	0	6S6	30	0.0	-31.6	31.6	0

Note: FREQ indicates the number of measurements that has been averaged.

TABLE 9.A.5
Melting Points of the β' -Modification of Saturated TAGs

X	Y	TAG	n	T_f (oC)	Predicted (oC)	Residual	FREQ
-8	0	SCS	46	53.0	54.3	-1.3	1
-6	0	PCP	42	44.5	47.7	-3.2	2
-6	0	SLS	48	57.3	57.0	0.3	2
-4	0	MCM	38	40.0	39.4	0.6	1
-4	0	PLP	44	49.6	51.2	-1.6	2
-4	0	SMS	50	58.8	59.5	-0.7	3
-4	0	BSB	62	71.8	70.5	1.3	2
-2	2	PMS	48	56.1	53.5	2.6	1
0	0	888	24	-19.5	-16.7	-2.8	2
0	0	9.9.9	27	4.0	3.0	1.0	1
0	0	CCC	30	16.8	17.3	-0.5	2
0	0	11.11.11	33	27.9	28.2	-0.3	4
0	0	LLL	36	35.1	36.7	-1.6	9
0	0	13.13.13	39	41.8	43.6	-1.8	4
0	0	MMM	42	45.9	49.3	-3.4	5
0	0	15.15.15	45	50.8	54.1	-3.3	2
0	0	PPP	48	55.7	58.1	-2.4	6
0	0	17.17.17	51	61.5	61.6	-0.1	4
0	0	SSS	54	64.3	64.6	-0.3	7
0	0	19.19.19	57	65.6	67.3	-1.7	2
0	0	AAA	60	69.5	69.6	-0.1	2
0	0	21.21.21	63	71.0	71.7	-0.7	1
0	0	BBB	66	74.8	73.6	1.2	2
0	1	11.11.L	34	28.5	28.3	0.2	1
0	2	88C	26	5.5	-24.9	30.4	0
0	2	CCL	32	26.0	13.6	12.4	0
0	2	LLM	38	37.8	34.8	3.0	3
0	2	MMP	44	48.5	48.2	0.3	2
0	2	PPS	50	58.7	57.5	1.2	3
0	4	CCM	34	31.0	15.6	15.4	0
0	4	LLP	40	43.0	36.2	6.8	1
0	4	MMS	46	49.3	49.3	0.0	2
0	4	SSB	58	69.7	65.0	4.7	1
0	6	LLS	42	39.8	41.0	-1.2	2
0	8	CCS	38	38.0	30.2	7.8	1
0	10	66P	28	12.0	-22.2	34.2	0
0	10	88S	34	25.0	15.3	9.7	1
0	12	66S	30	17.0	-6.7	23.7	0
1	0	P17P	49	61.2	60.9	0.3	2
1	0	S19S	55	69.8	66.7	3.1	1
2	0	8C8	26	18.5	14.3	4.2	1

(continued)

TABLE 9.A.5 (continued)
Melting Points of the β' -Modification of Saturated TAGs

X	Y	TAG	n	T_f (oC)	Predicted (oC)	Residual	FREQ
2	0	CLC	32	37.7	34.5	3.2	2
2	0	LML	38	49.8	47.5	2.3	3
2	0	MPM	44	59.5	56.6	2.9	5
2	0	PSP	50	67.7	63.4	4.3	10
2	0	11.13.11	35	42.6	41.6	1.0	1
2	2	8CC	28	12.8	10.3	2.5	2
2	2	CLL	34	31.0	32.4	-1.4	1
2	2	LMM	40	42.0	46.4	-4.4	1
2	2	MPP	46	52.0	56.0	-4.0	1
2	2	PSS	52	61.8	63.0	-1.2	3
2	4	CLM	36	36.7	33.9	2.8	1
2	6	LMS	44	45.5	50.8	-5.3	1
2	8	CLS	40	40.0	43.4	-3.4	1
4	0	CMC	34	30.0	35.2	-5.2	1
4	0	LPL	40	46.7	48.2	-1.5	2
4	0	LPL	40	42.5	48.2	-5.7	1
4	0	MSM	46	55.2	57.2	-2.0	3
4	0	SBS	58	64.0	69.0	-5.0	1
4	4	CMM	38	38.0	34.7	3.3	1
4	4	LPP	44	49.5	48.1	1.4	1
4	4	MSS	50	58.3	57.4	0.9	2
4	4	SBB	62	71.5	69.4	2.1	1
4	6	LPS	46	47.0	51.5	-4.5	1
4	8	CMS	42	42.0	44.1	-2.1	1
6	0	CPC	36	36.0	34.8	1.2	1
6	0	LSL	42	43.0	48.0	-5.0	1
6	0	PBP	54	61.5	64.0	-2.5	1
6	6	CPP	42	41.0	39.3	1.7	1
6	6	LSS	48	51.4	51.4	0.0	8
6	6	PBB	60	66.1	66.2	-0.1	1
8	0	CSC	38	40.0	39.4	0.6	1
8	8	CSS	46	46.0	47.6	-1.6	1

Note: FREQ indicates the number of measurements that has been averaged.

TABLE 9.A.6
Melting Points of the β -Modification of Saturated TAGs

X	Y	TAG	n	T_f (oC)	Predicted (oC)	Residual	FREQ
-12	0	S6S	42	53.1	53.6	-0.5	2
-10	0	P6P	38	45.4	45.7	-0.3	3
-10	0	S8S	44	54.0	57.0	-3.0	5
-8	0	P8P	40	48.5	49.9	-1.4	1
-8	0	SCS	46	57.4	60.1	-2.7	4
-6	0	PCP	42	51.8	53.7	-1.9	2
-6	0	SLS	48	60.3	62.9	-2.6	3
-6	2	PCS	44	54.2	51.2	3.0	3
-4	0	MCM	38	43.5	46.0	-2.5	1
-4	0	PLP	44	53.9	57.2	-3.3	4
-4	0	SMS	50	63.3	65.6	-2.3	9
-4	2	PLS	46	57.0	54.9	2.1	2
-4	4	MCS	42	51.7	45.3	6.4	3
-2	0	C8C	28	20.0	19.9	0.1	1
-2	0	LCL	34	37.4	38.5	-1.1	3
-2	0	MLM	40	49.8	51.4	-1.6	2
-2	0	PMP	46	59.9	60.8	-0.9	6
-2	0	SPS	52	68.0	68.1	-0.1	8
-2	2	PMS	48	59.6	58.7	0.9	3
-2	4	MLS	44	54.5	50.9	3.6	2
-2	6	LCS	40	41.8	41.7	0.1	1
-1	0	P.15.P	47	56.5	57.7	-1.2	1
-1	0	S.17.S	53	65.7	64.9	0.8	2
0	0	888	24	9.1	11.4	-2.3	6
0	0	CCC	30	31.6	31.8	-0.2	8
0	0	LLL	36	45.7	45.9	-0.2	9
0	0	13.13.13	39	44.1	45.8	-1.7	5
0	0	MMM	42	57.1	56.2	0.9	10
0	0	15.15.15	45	54.6	55.5	-0.9	4
0	0	PPP	48	65.9	64.0	1.9	9
0	0	17.17.17	51	63.9	63.0	0.9	6
0	0	SSS	54	72.5	70.2	2.3	9
0	0	19.19.19	57	70.6	69.0	1.6	3
0	0	AAA	60	77.8	75.3	2.5	4
0	0	21.21.21	63	77.0	73.9	3.1	2
0	0	BBB	66	81.7	79.4	2.3	7
0	0	24.24.24	72	86.0	82.9	3.1	1
0	1	11.11.L	34	29.2	29.8	-0.6	2
0	2	88C	26	11.5	7.9	3.6	1
0	2	CCL	32	30.0	28.9	1.1	1
0	2	88C	26	11.5	7.9	3.6	1
0	2	CCL	32	30.0	28.9	1.1	1
0	2	LLM	38	42.3	43.4	-1.1	4
0	2	MMP	44	53.3	54.1	-0.8	5

(continued)

TABLE 9.A.6 (continued)
Melting Points of the β -Modification of Saturated TAGs

X	Y	TAG	n	T_f (oC)	Predicted (oC)	Residual	FREQ
0	2	PPS	50	62.6	62.2	0.4	10
0	2	15.15.17	47	54.0	53.5	0.5	1
0	4	CCM	34	34.5	30.6	3.9	1
0	4	LLP	40	45.6	45.3	0.3	5
0	4	MMS	46	56.6	55.9	0.7	4
0	4	SSB	58	70.7	70.3	0.4	1
0	6	CCP	36	35.0	35.1	-0.1	1
0	6	LLS	42	45.1	48.7	-3.6	8
0	8	CCS	38	42.5	40.1	2.4	2
0	10	88S	34	31.0	29.3	1.7	2
0	12	66S	30	22.6	15.4	7.2	2
0	14	88B	38	38.0	40.1	-2.1	1
0	16	66B	34	34.0	29.3	4.7	1
2	0	8C8	26	20.5	17.9	2.6	1
2	0	CLC	32	34.0	36.4	-2.4	1
2	0	MPM	44	55.0	58.8	-3.8	1
2	0	PSP	50	65.3	66.2	-0.9	2
2	2	8CC	28	19.0	14.6	4.4	2
2	2	CLL	34	34.1	33.6	0.5	2
2	2	LMM	40	47.5	46.9	0.6	2
2	2	MPP	46	55.8	56.8	-1.0	4
2	2	PSS	52	64.4	64.4	0.0	9
2	4	LMP	42	48.5	48.8	-0.3	3
2	4	MPS	48	58.5	58.7	-0.2	5
2	6	LMS	44	49.0	52.0	-3.0	2
2	8	CLS	40	44.0	44.1	-0.1	1
4	0	CMC	34	34.0	37.7	-3.7	1
4	0	SBS	58	69.9	73.8	-3.9	2
4	4	CMM	38	43.5	36.7	6.8	1
4	4	LPP	44	54.4	50.5	3.9	4
4	4	MSS	50	60.9	60.5	0.4	6
4	4	SBB	62	73.5	73.9	-0.4	1
4	6	LPS	46	52.0	53.8	-1.8	1
4	8	CMS	42	45.0	45.7	-0.7	1
6	0	CPC	36	40.0	41.2	-1.2	1
6	0	LSL	42	49.8	53.8	-4.0	3
6	0	MAM	48	59.0	63.0	-4.0	1
6	0	PBP	54	65.5	70.0	-4.5	2
6	6	CPP	42	45.5	44.5	1.0	1
8	0	CSC	38	44.5	45.7	-1.2	1
8	8	CSS	46	48.3	52.8	-4.5	3
10	0	8S8	34	41.0	35.6	5.4	1
12	0	6S6	30	32.0	22.5	9.5	1

Note: FREQ indicates the number of measurements that has been averaged.

9.A.2 UNSATURATED TAGs

TABLE 9.A.7
**Enthalpy of Fusion for the α -Modification
of Unsaturated TAGs**

X	Y	TAG	N	ΔH_f (kJ/mol)	Predicted	Residual	FREQ
-2	0	EPE	52	79	79	0	2*
0	0	SSO	54	71	81	-10	2*
0	0	SOS	54	73	81	-8	1
0	0	OOO	54	37	18	19	1
0	0	SEE	54	89	89	0	1*
0	0	EEE	54	78	78	0	1*
0	0	ESE	54	92	89	3	2*
0	2	PPE	50	118	88	30	0
0	2	PPO	50	53	68	-15	2*
2	0	PEP	50	122	91	31	0
2	0	POP	50	70	71	1	4*
2	2	POS	52	78	74	4	2
2	2	PEE	52	81	82	-1	2*

Note: Data marked by a * include measurements from this chapter. FREQ indicates the number of measurements that has been averaged.

TABLE 9.A.8
**Enthalpy of Fusion for the β' -Modification
of Unsaturated TAGs**

X	Y	TAG	n	ΔH_f (kJ/mol)	Predicted	Residual	FREQ
-2	0	SPO	52	126	117	9	1
0	0	SOS	54	111	129	-18	2
0	0	SOO	54	110	101	9	1
0	0	SSO	54	125	129	-4	2*
0	0	OOO	54	79	73	6	1
0	2	PPO	50	111	101	10	2*
2	0	PEP	50	135	140	-5	1*
2	0	POP	50	104	128	-24	6
2	2	PSO	52	111	123	-12	1
2	2	POS	52	114	123	-9	1
2	2	POO	52	95	95	0	1

Note: Data marked by a * include measurements from this chapter. FREQ indicates the number of measurements that has been averaged.

TABLE 9.A.9
**Enthalpy of Fusion for the β -Modification
of Unsaturated TAGs**

X	Y	TAG	n	ΔH_f (kJ/mol)	Predicted	Residual	FREQ
-2	0	SPO	52	126	117	9	1
-2	0	EPE	52	130	140	10	2
-2	0	OPO	52	126	111	14	1
0	0	EEE	54	148	144	4	11
0	0	ESE	54	155	160	-5	3
0	0	III	54	84	78	6	1
0	0	SES	54	163	175	-12	2
0	0	SEE	54	155	160	-5	1
0	0	SOS	54	154	161	-7	5
0	0	OOO	54	100	101	1	5
0	2	PPE	50	157	151	6	3
0	2	SOA	56	158	160	-2	1
2	0	POP	50	140	143	-3	4
2	0	PIP	50	100	136	-36	0
2	0	PEP	50	150	158	-8	1
2	2	POS	52	150	143	7	2
2	2	PEE	52	134	141	-7	2

Note: Data marked by a * include measurements from this chapter. FREQ indicates the number of measurements that has been averaged.

TABLE 9.A.10
Melting Points of the α -Modification of Unsaturated TAGs

TAG	T_f (°C)	Predicted (°C)	Residual	FREQ	OMOD
CCE	15	8.9	6.1	1	?
CO _C	-16.4	-22.8	6.4	1	Alpha
LLI	15.5	17	-1.5	1	?
LII	-11.5	-15.6	4.1	1	?
MMI	20.5	22.2	-1.7	1	?
MI _{II}	-8.5	-7.6	-0.9	1	?
MOM	11.7	4.8	6.9	2	Alpha
PPO	18.4	16.8	1.6	4	Alpha
PSI	36.5	32.6	3.9	1	?
PSO	25.9	21.3	4.6	2	Alpha
PEP	39.4	35.6	3.8	2	Alpha
PEE	22.8	26.1	-3.3	1	?
PIO	13.2	11.2	2	1	?
POP	16.6	17.6	-1	6	Alpha
POS	19.6	21.3	-1.7	4	Alpha
POI	13.3	11.2	2.1	1	?
SES	41.5	44	-2.5	2	Alpha
SES	46.5	44	2.5	0	
SIS	37.9	37.3	0.6	3	?
SOS	22.9	27.2	-4.3	8	Alpha
88E	3	5.4	-2.4	1	?
EPE	26	27	-1	1	Alpha
EPE	32	27	5	0	
ESS	43	44	-1	1	?
ESE	34	32	2	1	Alpha
EES	28.8	32	-3.2	1	Alpha
EEE	15.8	19.1	-3.3	4	Alpha

(continued)

TABLE 9.A.10 (continued)
Melting Points of the α -Modification of Unsaturated TAGs

TAG	T_f (oC)	Predicted (oC)	Residual	FREQ	OMOD
IPS	34.2	33.1	1.1	1	?
IPO	11.7	11.1	0.6	1	?
ISI	-3	0.2	-3.2	1	?
ISO	16.5	15.8	0.7	1	?
IlO	-16.4	-15.6	-0.8	2	?
IlleO	-24.7	-22.5	-2.2	1	?
lOO	-2.2	-5.7	3.5	1	?
leSl	-9.2	-7.9	-1.3	1	?
leSO	5.2	6.1	-0.9	1	?
leIS	-8.3	-7.9	-0.4	2	?
lelO	-22.4	-22.5	0.1	2	?
lelele	-44.6	-42.8	-1.8	1	al-
phaleleO	-17.8	-19.9	2.1	2	?
leOS	-2.5	6.1	-8.6	1	?
OPS	17.9	22.1	-4.2	2	Alpha
OSS	30.3	27.2	3.1	6	Alpha
OSO	1	-0.7	1.7	1	Alpha
OleO	-15	-14.3	-0.7	1	?
OOO	-33.7	-28.8	-4.9	4	Alpha

Note: FREQ indicates the number of measurements that has been averaged,
 OMOD indicates the modification that was originally reported for the
 melting point.

TABLE 9.A.11
**Melting Points of the β' -Modification
of Unsaturated TAGs**

TAG	T_f (oC)	Predicted (oC)	Residual	FREQ	OMOD
CCO	4.4	2.7	1.7	2	?
CEE	25	20.1	4.9	1	?
LLO	18	15.7	2.3	2	?
MOM	26.4	26.4	0	2	β
PPI	26.5	24.9	1.6	1	?
PPO	34.6	34.2	0.4	8	β
PSO	40	38	2	6	β
PES	48.5	51.4	-2.9	1	?
Pll	-4.2	-2.9	-1.3	3	?
Plel	-7.5	-6.2	-1.3	1	?
Plele	-10.5	-10.2	-0.3	1	?
POP	33.2	34.8	-1.6	8	β
SOS	37	42.2	-5.2	9	β
SOS	43	42.2	0.8	0	β
ESS	56.7	54.9	1.8	1	?
ESE	43.2	45.1	-1.9	0	β
EEE	37	35.7	1.3	1 β	
IPl	-3	-2.3	-0.7	1	?
llS	2.5	3.8	-1.3	2	?
lll	-25.3	-25	-0.3	3	β
IOS	-3.5	-1.2	-2.3	1	?
lOl	-39	-46.5	7.5	1	?
lePl	-4	-4	0	1	?
leSS	27.8	28.1	-0.3	2	?
lelle	-15.5	-15.5	0	1	?
lelel	-16.5	-15.5	-1	1	?
leOl	-28.5	-31.7	3.2	1	?
leOle	-11.1	-14.9	3.8	2	?
OSS	41.9	42.2	-0.3	10	β
OSO	20.5	19.3	1.2	1	β
OlS	-10.4	-1.2	-9.2	2	?
OleS	14.2	7.6	6.6	1	?
OOA	29.2	23	6.2	1	?
OOB	33.3	25.8	7.5	1	?
0.024	36.1	27.4	8.7	1	?
OOO	-10	-3.4	-6.6	5	β

Note: FREQ indicates the number of measurements that has been averaged,
OMOD indicates the modification that was originally reported for the
melting point.

TABLE 9.A.12
**Melting Points of the β -Modification
of Unsaturated TAGs**

TAG	T_f (oC)	Predicted (oC)	Residual	FREQ	OMOD
CCI	-0.5	-9.7	9.2	1	?
CMO	13.9	16.8	-2.9	1	?
COC	-4.8	1.6	-6.4	0	β
COC	5.9	1.6	4.3	2	β
COO	-0.3	5	-5.3	2	?
LLE	27	31.6	-4.6	1	?
LPO	29.5	24.6	4.9	1	?
LEE	35.5	38	-2.5	1	?
LOL	16.5	15.8	0.7	0	β
LOO	5.1	4.7	0.4	3	?
MME	39.5	40.9	-1.4	1	?
MMO	23.9	22.4	1.5	2	?
MEE	40	39.8	0.2	1	?
MOM	28	28	0	2	β
MOP	27	30	-3	1	?
MOS	27	32.7	-5.7	1	?
MOO	12.8	8.3	4.5	4	?
PPE	50.2	50.1	0.1	3	?
PEP	55.3	53.7	1.6	4	β
PEP	53.9	53.7	0.2	0	β
PEE	44.2	44.1	0.1	3	?
PIP	27.1	27.6	-0.5	2	β
PIS	24.5	28.8	-4.3	1	?
POP	37.2	37.6	-0.4	10	β
POS	31	38	-7	0	β
POS	37.1	38	-0.9	8	β
POO	18.5	14.6	3.9	0	β
SES	60.5	59.3	1.2	3	β
SleS	35.8	31.4	4.4	2	?
SOA	41.5	44	-2.5	1	β
EPE	44.5	46.9	-2.4	1	β
ESS	61.1	59.3	1.8	4	β
ESE	49.7	50.2	-0.5	2	β
EES	49.7	50.2	-0.5	5	β
EEE	42.2	44	-1.8	9	β
ISS	35.8	35.4	0.4	4	?
III	-12.3	-14	1.7	6	β

TABLE 9.A.12 (continued)
Melting Points of the β -Modification
of Unsaturated TAGs

TAG	T_f (°C)	Predicted (°C)	Residual	FREQ	OMOD
leleS	-0.5	-0.5	0	1	?
lelele	-24.2	-23.5	-0.7	3	β
leOO	-13.1	-12	-1.1	2	?
OPS	40.2	41	-0.8	0	β
OPO	19.6	17.9	1.7	3	β
OSO	23.9	22.7	1.2	4	β
OIO	-9.5	-7	-2.5	1	?
OOS	23.5	22.7	0.8	0	β
OOO	4.8	6.1	-1.3	9	β
PEP	54	51.2	2.8	0	?

Note: FREQ indicates the number of measurements that has been averaged, OMOD indicates the modification that was originally reported for the melting point.

APPENDIX 9.B: SPECIFIC RETENTION VOLUMES OF SEVERAL PROBES IN STATIONARY PHASES OF LIQUID TAGs

TABLE 9.B.1
Specific Retention Volume in mL/g

T (°C)	82	92	102	112	123	133
<i>n</i> -Pentane	16.856	13.332	10.611	8.567		
<i>n</i> -Hexane	38.053	29.16	22.595	18.307	14.618	11.571
<i>n</i> -Heptane	88.048	64.449	48.319	39.669	29.083	22.295
2-Methyl-pentane	28.852	23.087	18.014	14.722	11.722	9.36
3-Methyl-pentane	33.438	26.465	20.88	16.188	13.428	10.789
Benzene	88.658	65.532	50.591	39.684	31.332	24.767
Toluene	218.379	154.476	114.394	85.939	64.479	50.534
Cyclohexane	73.4	55.932	42.915	33.832	26.582	20.903

Note: Stationary phase: SSS.

TABLE 9.B.2
Specific Retention Volume in mL/g

T (°C)	82	92	102	112	123	133
<i>n</i> -Pentane	16.448	13.525	11.09	8.323		
<i>n</i> -Hexane	39.175	30.356	23.319	18.389	14.449	11.715
<i>n</i> -Heptane	90.897	66.559	50.618	38.246	29.328	23.399
2-Methyl-pentane	30.691	23.922	18.619	14.482	12.019	9.926
3-Methyl-pentane	34.607	27.125	21.358	16.77	13.487	11.41
Benzene	97.106	72.451	54.744	42.351	33.476	26.445
Toluene	235.44	169.84	123.941	91.414	69.741	53.632
Cyclohexane	74.389	57.106	44.007	34.218	26.791	21.699

Note: Stationary phase: MMM.

TABLE 9.B.3
Specific Retention Volume in mL/g

T (°C)	82	92	102	112	123	133
<i>n</i> -Pentane	15.803	12.58	10.341	8.067		
<i>n</i> -Hexane	37.093	28.536	22.103	17.575	14.291	11.052
<i>n</i> -Heptane	84.266	61.824	47.214	36.302	28.01	22.596
2-Methyl-pentane	28.69	22.432	17.473	13.829	11.433	9.33
3-Methyl-pentane	33.008	25.125	19.726	15.558	12.576	10.561
Benzene	105.237	77.315	59	46.098	34.87	27.754
Toluene	250.008	177.156	130.416	97.67	72.598	55.754
Cyclohexane	68.781	52.18	40.569	31.692	24.866	20.14

Note: Stationary phase: 8C8.

TABLE 9.B.4
Specific Retention Volume in mL/g

T (°C)	82	92	102	112	123	133
<i>n</i> -Pentane	15.772	12.92	10.023	8.432		
<i>n</i> -Hexane	38.571	29.43	22.959	18.083	14.644	11.976
<i>n</i> -Heptane	88.55	65.675	49.205	37.647	29.347	23.427
2-Methyl-pentane	29.374	22.84	18.173	14.563	11.875	9.806
3-Methyl-pentane	33.769	26.388	20.544	16.667	13.366	11.047
Benzene	93.42	69.591	53.302	41.705	32.528	25.958
Toluene	226.576	162.709	119.042	89.083	67.384	52.15
Cyclohexane	73.139	56.066	43.033	34.312	26.868	21.905

Note: Stationary phase: 0.4487 SSS, 0.5513 MMM.

TABLE 9.B.5
Specific Retention Volume in mL/g

T (°C)	82	92	102	112	123	133
<i>n</i> -Pentane	15.637	12.695	10.335	8.961		
<i>n</i> -Hexane	37.808	29.054	22.138	18.762	14.216	11.513
<i>n</i> -Heptane	87.566	64.7	48.113	38.308	28.667	22.664
2-Methyl-pentane	29.191	22.873	17.671	14.681	11.656	9.642
3-Methyl-pentane	33.639	26.154	20.204	16.969	13.17	10.806
Benzene	89.447	67.982	51.08	41.244	31.129	24.872
Toluene	216.024	157.377	114.093	88.601	65.358	50.193
Cyclohexane	71.81	55.042	42.012	34.242	26.328	21.026

Note: Stationary phase: 0.7116 SSS, 0.2884 MMM.

TABLE 9.B.6
Specific Retention Volume in mL/g

T (°C)	82	92	102	112	123	133
<i>n</i> -Pentane	16.106	12.78	10.684	7.576		
<i>n</i> -Hexane	38.33	29.045	23.253	18.239	15.18	11.53
<i>n</i> -Heptane	89.874	65.641	49.02	37.321	29.777	22.787
2-Methyl-pentane	29.958	22.945	18.225	14.872	12.261	9.598
3-Methyl-pentane	34.145	26.14	20.739	16.836	13.721	10.981
Benzene	103.725	76.097	58.447	44.336	35.324	27.454
Toluene	249.649	176.011	129.15	95.406	73.275	56.006
Cyclohexane	72.801	54.314	41.793	33.111	26.712	20.865

Note: Stationary phase: 0.1557 SSS, 0.8443 8C8.

TABLE 9.B.7
Specific Retention Volume in mL/g

T (°C)	82	92	102	112	123	133
<i>n</i> -Pentane	15.707	12.973	10.513	8.432		
<i>n</i> -Hexane	38.224	29.198	22.737	18.077	14.426	11.369
<i>n</i> -Heptane	88.634	63.696	48.437	37.146	28.879	22.157
2-Methyl-pentane	29.616	22.65	17.992	14.799	11.769	9.388
3-Methyl-pentane	33.493	25.654	20.25	16.368	12.962	10.658
Benzene	98.094	71.955	54.47	42.629	33.273	26.636
Toluene	235.818	166.864	121.852	91.705	68.986	52.84
Cyclohexane	72.015	53.896	41.858	32.677	26.331	21.08

Note: Stationary phase: 0.3593 SSS, 0.6407 8C8.

TABLE 9.B.8
Specific Retention Volume in mL/g

T (°C)	82	92	102	112	123	133
<i>n</i> -Pentane	16.053	12.907	10.38	8.446		
<i>n</i> -Hexane	38.167	28.82	23.03	18.049	14.425	11.9
<i>n</i> -Heptane	88.696	65.02	49.16	37.255	28.732	23.11
2-Methyl-pentane	29.275	23.16	18.376	14.462	11.607	9.706
3-Methyl-pentane	33.845	26.658	20.643	16.313	13.603	11.093
Benzene	93.481	70.449	53.696	41.189	32.5	26.462
Toluene	226.756	162.489	119.081	88.857	67.427	52.692
Cyclohexane	72.627	55.369	42.955	33.206	26.383	21.492

Note: Stationary phase: 0.6023 SSS, 0.3977 8C8.

APPENDIX 9.C: Purity of the TAGs Used in Section 9.7

TAG	Purity (%)	Main Impurities
SSS	99.6	—
PSP	99.3	—
MPM	>99.6	—
SEE	91.4	SES 8%
ESE	94.3	4.5% SSE, 1% SEO
PEE	91.1	8.6% PEP, PPE, EPE
EPE	89.8	9.1% PEP, PPE, PEE, 1.1% PEO
EEE	96.8	1.7% ESE, SEE
SOS	99.5	—
SSO	90.7	4% SOS, 3% SSE
POP	99.0	1% PEP
PPO	98.5	1.5% PPO

APPENDIX 9.D: BINARY PHASE DIAGRAMS OF TAGs: DATA

SSS–PSS			SSS–PSP			SSS–SPS		
X	Solidus	Liquidus	X	Solidus	Liquidus	X	Solidus	Liquidus
0.00	72.5	72.5	0.00	72.5	72.7	0.00	72.5	72.5
0.11	67.7	71.8	0.19	65.2	71.6	0.14	64.8	71.8
0.29	67.5	71.2	0.20		71.4	0.31	65.2	71.1
0.46	67.4	70.4	0.32	65.4	71.3	0.45	65.0	70.4
0.58		68.5	0.40		69.9	0.51	65.4	69.5
0.74		67.3	0.50		68.6	0.56	65.9	69.5
0.85		67.1	0.50	65.6	69.0	0.69		65.3
1.00	67.2	67.2	0.62	65.4	68.2	0.76		65.8
			0.70		66.0	0.90		66.4
			0.80	66.1	67.3	1.00	67.5	67.5
			0.88	65.7	67.8			
			1.00	68.4	68.4			
			1.00		68.7			
SSS–PPS			SSS–PPP			PSS–PSP		
X	Solidus	Liquidus	X	Solidus	Liquidus	X	Solidus	Liquidus
0.00		72.3	0.00	72.5	72.5	0.00	66.2	66.2
0.10	68.8	71.8	0.14	63.8	72.4	0.15		66.1
0.18	61.9	71.8	0.19	64.0	72.0	0.29		64.9
0.20	65.4	70.8	0.39	63.7	71.1	0.46		64.5
0.20		70.9	0.49	64.0	70.6	0.58	63.3	64.2
0.30	61.2	69.9	0.59	63.8	69.5	0.72	64.7	65.4
0.30	60.8	70.7	0.73	63.7	66.3	0.89	65.7	66.6
0.30		70.2	0.80	63.7	64.7	1.00	68.7	68.7
0.33	61.0	71.4	0.87	63.8	65.1			
0.40	61.1	69.6	0.94	63.8	65.2			
0.40	60.9		1.00	65.7	65.7			
0.50	61.0	68.9						
SSS–PPS			PSS–SPS			SSS–SPS		
X	Solidus	Liquidus	X	Solidus	Liquidus	X	Solidus	Liquidus
0.50	60.8	68.3	0.00	66.3	66.3	0.00	66.1	66.1
0.50	60.6	67.9	0.15		64.9	0.14		65.0
0.55	61.0	70.3	0.30		64.6	0.24		64.3
0.59	60.8	67.3	0.45		64.9	0.38		63.8
0.60	61.0	67.8	0.59		64.9	0.51		63.2
0.65	60.9	66.2	0.72		66.6	0.68		62.8
0.67	60.8	65.7	0.89	66.0	67.4	0.87		62.3
0.67	61.1		1.00	67.9	67.9	1.00	63.5	63.5
0.70	59.5	61.0						
0.70	60.2	61.2						

(continued)

(continued)

SSS-PPS			PSS-SPS			SSS-SPS		
X	Solidus	Liquidus	X	Solidus	Liquidus	X	Solidus	Liquidus
0.71	59.6	60.7						
0.73	62.3	69.3						
0.75	59.7	60.4						
0.75	59.7	60.8						
0.79	61.0	62.5	PSS-PPP			PSP-SPS		
0.80	59.8	60.4	X	Solidus	Liquidus	X	Solidus	Liquidus
0.80	59.6	60.8	0.00	66.1	66.1	0.00	68.5	68.5
0.85		60.7	0.17	63.0	65.3	0.20	65.2	68.1
0.85		60.0	0.25	62.4	64.9	0.26	65.2	67.4
0.85		60.4	0.42	62.9	64.2	0.37	65.3	66.1
0.91		60.8	0.53		62.7	0.48		65.6
0.91		60.5	0.68	62.8	65.0	0.53		65.2
0.91		60.2	0.90	62.8	66.0	0.66	64.6	66.1
0.94		61.6	1.00	66.0	66.0	0.79	64.6	66.7
0.95		60.6					0.91	64.4
0.95		61.1						67.5
0.99		60.2				1.00	67.6	67.6
0.99		61.7						
1.00	63.4	63.4						
PSP-PPS (De Bruijne)			PSP-PPP			SPS-PPS		
X	Solidus	Liquidus	X	Solidus	Liquidus	X	Solidus	Liquidus
0.00	68.6	68.6	0.00	68.6	68.6	0.00	67.6	67.6
0.10	60.6	67.1	0.20	61.7	67.4	0.20		66.3
0.21	60.4	66.2	0.46	61.5	65.1	0.34	61.1	65.7
0.30	60.8	65.7	0.66	61.7	63.2	0.40	60.8	65.3
0.40	60.8	64.8	0.80	61.7	63.3	0.54	61.1	64.9
0.50	61.1	63.5	1.00	65.8	65.8	0.60	61.3	64.2
0.60	60.7	62.7					0.75	62.7
0.71	61.2	61.2					0.86	60.6
0.9	61.3	62.4					0.92	60.3
1.0	63.4	63.4					1.00	63.3
PSP-PPS (Perron)			SPS-PPP			PPS-PPP		
X	Solidus	Liquidus	X	Solidus	Liquidus	X	Solidus	Liquidus
0.00		68.2	0.00	67.7	67.7	0.00	63.2	63.2
0.05	65.6	67.8	0.18	61.0	66.5	0.14		62.7
0.10	64.1	67.5	0.51	60.2	63.8	0.29		61.6
0.15	62.5	66.9	0.61		62.0	0.45		62.3
0.20	62.9	66.4	0.79	60.8	63.3	0.63		62.0
0.25	61.9	66.2	0.84	60.6	63.6	0.75	61.1	63.0
0.30	61.6	65.6	1.00	66.0	66.0	0.83	61.4	64.4

(continued)

PSP–PPS (Perron)			SPS–PPP			PPS–PPP		
X	Solidus	Liquidus	X	Solidus	Liquidus	X	Solidus	Liquidus
0.35	61.8	64.7				0.90	61.4	65.1
0.40	60.6	64.1				1.0	63.7	65.7
0.50	60.9	63.5						
0.60	60.9	61.9						
0.71	60.9	61.8	BBB–SSS			BBB–PPP		
0.75	60.4	61.3	X	Solidus	Liquidus	X	Solidus	Liquidus
0.80	60.6	61.5	0.00	81.7	81.7	0.00	81.1	81.1
0.85	60.9	61.6	0.12	71.0	81.5	0.13	67.0	80.9
0.90	60.4	61.5	0.23	71.0	80.7	0.25	65.4	80.0
0.95	60.7	61.8	0.33	71.0	80.0	0.31	65.4	79.0
1.00	62.2	62.2	0.44	71.0	79.5	0.47	65.4	78.5
		0.55	71.0	78.0	0.57	65.4	77.4	
		0.64	71.0	77.7	0.67	65.4	77.2	
		0.74	71.0	75.6	0.77	65.4	75.4	
		0.83	71.0	73.9	0.85	65.4	73.0	
		0.92	71.5	71.5	0.93	65.4	70.4	
		1.00	72.4	72.4	1.00	65.4		
SSS–LLL			SSS–888			PPP–MMM		
X	Solidus	Liquidus	X	Solidus	Liquidus	X	Solidus	Liquidus
0.00	72.6	72.6	0.00	72.5	72.5	0.00	64.3	64.3
0.15	45.7		0.23	50.2		0.11	64.0	64.0
0.25	66.7	71.0	0.52	8.4	67.0	0.22	64.0	64.0
0.39	59.9	70.1	0.78	8.4	65.9	0.32	61.8	61.8
0.48	45.7	69.2	0.94	8.4	60.6	0.43	61.4	61.4
0.59	45.7	68.0	0.96	7.0	59.1	0.53	60.1	60.1
0.68	45.7	66.9	0.97	8.4	57.7	0.63	59.8	59.8
0.79	45.7	65.1	0.99	8.4	54.1	0.72	57.2	57.2
0.85	45.7	63.6	1.00	8.4	8.4	0.82	52.9	52.9
0.937	45.7	60.0				0.91	53.2	53.2
0.955	45.7	58.4				1.00	54.5	54.5
0.975		56.4						
0.980	45.7	56.1						
0.983		54.6						
0.988	53.4	53.4						
0.993	51.6	51.6						
0.995	47.6	47.6						
1.000	46.4	46.4						

(continued)

(continued)

PPP–LLL			SSS–SES			SSS–SSE		
X	Solidus	Liquidus	X	Solidus	Liquidus	X	Solidus	Liquidus
0.00	65.1	65.1	0.00		72.2	0.00	72.2	72.2
0.12	63.9	64.9	0.10		71.7	0.10	69.8	71.9
0.17	59.7	64.2	0.20		71.2	0.20		71.2
0.25	56.0	63.8	0.30		70.6	0.2	68.0	71.5
0.31	55.6	63.5	0.40	69.9	0.3	67.3	71.2	
0.32	53.6		0.50		69.5	0.30		70.6
0.33	46.1		0.60		69.0	0.40		70.0
0.36		63.1	0.70		68.3	0.4	65.6	70.9
0.37	45.7	62.9	0.80		67.5	0.50		69.2
0.44		62.4	0.90		66.6	0.5	64.6	70.2
0.46		61.9	1.0		65.5	0.60		68.4
0.49	45.7	61.7				0.6	64.1	68.6
0.66	45.7	59.6				0.69	63.1	66.5
0.75	45.7				0.70			67.4
0.80		56.5			0.80	62.5		65.5
0.84		55.1	SSS–SEE		0.89	62.1		64.6
0.89		52.8	X Solidus	Liquidus	0.90			65.8
0.92	45.7		0.20	71.2	0.94	62.1		63.4
0.94		50.1	0.30	70.6	1.00	62.1		62.1
0.95		49.6	0.40	70.0				
0.967		47.1	0.50	69.2				
0.970		46.7	0.60	68.4				
0.973	45.7	45.7	0.70	67.4				
0.989		46.3	0.80	66.2				
0.995		46.4	0.90	65.8				
1.000	45.7	45.7	1.00	63.4				
	PPP–SSE			PPP–EEE			LLL–EEE	
X	Solidus	Liquidus	X	Solidus	Liquidus	X	Solidus	Liquidus
0.00	65.8	65.8	0.00	65.4	65.4	0.00	46.0	46.0
0.05	60.8	64.5	0.05	64.2	65.1	0.05	44.8	46.0
0.10	59.5	64.2	0.09	64.2	65.0	0.15	43.5	46.0
0.14		63.0	0.14	63.7	65.1	0.21	42.6	45.9
0.21	57.6	62.9	0.19	62.9	64.7	0.30	41.5	44.8
0.29	56.4	62.3	0.23	61.6	64.5	0.36	40.4	45.1
0.41	55.6	61.3	0.28	61.4	64.2	0.40	39.3	44.3
0.50		59.8	0.33	61.0	64.3	0.45	38.9	44.1
0.54	56.2	58.7	0.38	60.0	65.0	0.50	38.9	44.1
0.56		58.3	0.43	59.0	64.6	0.55	38.1	43.3
0.59	55.7	58.6	0.48	55.9	64.6	0.60	40.0	42.5
0.61		59.3	0.53	55.4	64.7	0.67	37.7	42.6
0.64	56.2	59.8	0.58	52.2	64.4	0.70	37.3	39.6
0.67	56.1	60.4	0.63	50.6	63.0	0.74	37.1	38.2

(continued)

PPP-SSE			PPP-EEE			LLL-EEE		
X	Solidus	Liquidus	X	Solidus	Liquidus	X	Solidus	Liquidus
0.70	56.0		0.68	46.9	62.5	0.80	37.8	39.1
0.76		61.3	0.73	43.9	61.3	0.84	37.8	39.7
0.81	56.0		0.78	40.3	61.2	0.89	38.4	40.2
0.87	57.1	61.6	0.84	40.0	60.0	0.95	38.9	40.0
0.92	59.3	61.9	0.89	39.8	58.0	1.00	39.5	40.3
1.00	61.9	61.9	0.95	39.3	55.0			
			1.00	40.3	40.3			
SSS-SOS			PPP-SOS			PPP-POP		
X	Solidus	Liquidus	X	Solidus	Liquidus	X	Solidus	Liquidus
0.00	72.8	72.8	0.00	65.8	65.8	0.00	65.9	65.9
0.06	65.5		0.09	61.6	65.5	0.06		65.4
0.17	53.6		0.19	54.5	64.7	0.10	58.4	65.0
0.23	44.3		0.26	50.0	64.2	0.13	49.6	64.6
0.27		70.9	0.35	44.0	63.7	0.25	44.8	63.6
0.51	44.3	69.3	0.47	40.6	62.6	0.35	35.2	62.7
0.61	44.3	68.3	0.57	41.0	61.1	0.45		61.6
0.75	44.3	66.1	0.69	41.2	59.0	0.56	35.2	60.5
0.83	44.3	64.5	0.79	41.0	56.1	0.63	35.2	59.5
0.91	44.3	61.3	0.88	41.6	49.5	0.80	34.5	56.4
0.95	44.3	57.8	0.93	41.0	44.0	0.85		53.6
0.97	44.3	52.0	0.94	41.6	41.3	0.88	34.7	50.7
0.99	44.3	44.8	0.97	41.8	41.8	0.95		43.0
1.00	44.3	44.3	1.00	42.3	42.3	0.97		39.5
						0.98		37.9
						0.99		37.1
						1.00	34.6	34.6
PPP-POO			SES-SSE			SOS-POS		
X	Solidus	Liquidus	X	Solidus	Liquidus	X	Solidus	Liquidus
0.00	65.7	65.7	0.00	65.4	65.4	0.00	36.5	36.5
0.06	65.3	65.3	0.10	65.3	65.3	0.10	34.2	36.5
0.08	64.5	64.5	0.20	65.2	65.2	0.20	34.2	37.0
0.15	13.6	64.7	0.30	65.0	65.0	0.30	34.5	38.5
0.32	14.7	63.3	0.40	64.9	64.9	0.40	35.0	39.0
0.49	17.1	61.3	0.50	64.7	64.7	0.50	35.5	40.5
0.68	17.7	58.1	0.60	64.5	64.5	0.60	35.5	41.8
0.83	17.9	54.5	0.70	64.2	64.2	0.70	36.5	42.5
0.92	18.5	50.0	0.80	64.0	64.0	0.80	38.0	43.0
1.00	18.6	18.6	0.90	63.6	63.6	0.90	40.5	43.5
			1.00	63.3	63.3	1.00	44.0	44.0

(continued)

(continued)

SOS-POP			POS-POP			POP-PEP		
X	Solidus	Liquidus	X	Solidus	Liquidus	X	Solidus	Liquidus
0.00	44.0	44.0	0.00	36.5	36.5	0.00	33.0	33.0
0.10	38.5	43.5	0.10	34.0	36.2	0.08	31.1	41.7
0.20	35.5	43.0	0.20	32.0	36.0	0.16	31.5	45.3
0.30	35.0	42.5	0.30	31.0	35.5	0.25	31.1	47.1
0.40	35.0	41.5	0.40	31.8	35.2	0.50	31.1	52.9
0.50	34.0	40.0	0.50	31.5	34.0	0.75	36.0	54.4
0.60	34.0	39.0	0.60	31.5	34.5	1.00	57.0	57.0
0.70	33.5	37.0	0.70	31.5	35.5			
0.80	33.5	36.0	0.80	31.5	35.5			
0.90	33.5	36.5	0.90	34.0	37.0			
1.00	37.2	37.2	1.00	37.2	37.2			
PPO-POO			PPO-OPO			POO-OPO		
X	Solidus	Liquidus	X	Solidus	Liquidus	X	Solidus	Liquidus
0.00	32.6	32.6	0.00	34.7	34.7	0.00	19.3	20.0
0.17	11.8	32.7	0.11	28.9	33.1	0.04	18.7	19.8
0.29	12.3	32.0	0.25	25.3	31.1	0.08	17.6	19.4
0.40	12.2	31.0	0.40	22.7	29.6	0.23	14.0	18.4
0.47	12.1	29.7	0.50	21.1	29.1	0.38	12.0	17.6
0.62	12.8	28.0	0.55	19.3	28.7	0.52	11.2	15.6
0.78	13.1	26.3	0.60	18.2	28.0	0.62	11.1	16.3
0.84	14.6	18.3	0.70	17.8	26.2	0.77	11.6	18.4
1.00	18.6	18.6	0.80	18.2	23.1	0.91	14.0	18.9
			0.85	17.8	20.2	1.00	19.8	19.8
			0.87	17.6	19.8			
			0.90	17.6	18.7			
			0.95	17.8	19.1			
			0.98	18.2	19.2			
			1.00	19.3	19.3			
SSS-OOO			PPP-OOO			SOS-OOO		
X	Solidus	Liquidus	X	Solidus	Liquidus	X	Solidus	Liquidus
0.00	73.9	73.9	0.00	64.5	64.5	0.00	42.8	42.8
0.01		72.5	0.10			0.12	42.4	42.4
0.11		71.9	0.20			0.33	41.3	41.3
0.29		70.3	0.30			0.52	40.3	40.3
0.33	5.4	68.9	0.40			0.81	35.3	35.3
0.51		68.4	0.50			0.90	32.1	32.1
0.54		64.5	0.60			0.96	30.0	30.0
0.58		64.2	0.70			0.98	28.2	28.2
0.62		65.4	0.80			1.00	5.4	5.4
0.71		64.9	0.83		54.3			
0.80		64.1	0.88		52.3			

(continued)

SSS-OOO			PPP-OOO			SOS-OOO		
X	Solidus	Liquidus	X	Solidus	Liquidus	X	Solidus	Liquidus
0.83	5.4	65.4	0.90					
0.84		62.7	0.91		50.3			
0.84		60.7	0.93		49.0			
0.85		66.1	0.942		47.3			
0.88		60.0	0.956		44.7			
0.89	4.9	62.4	0.971		42.7			
0.89		66.6	0.978		41.0			
0.899		61.9	0.989		38.0			
0.907		57.3	0.991		35.7			
0.920		56.0	0.993		34.3			
0.920		54.0	0.996		32.7			
0.947		54.7	1.000	6.7	6.7			
0.949		57.8						
0.960		52.0						
0.960		51.3						
0.974		47.3						
0.974		44.7						
0.975		55.0						
0.980		50.0						
0.987		41.3						
1.000	5.4	5.4						

Note: x in mole fraction, solidus and liquidus in °C.

REFERENCES

- Asselineau, L. and J. Jacq. 1989. Fifth Annual Conference on Fluid Properties and Phase Equilibria. Banff, Canada.
- Bailey, A.N. 1950. *Melting and Solidification of Fats*, New York: Interscience.
- Barbano, P. and J.W. Sherbon. 1977. *JAOCs*. 55: 478.
- Billmeyer, F.W. 1975. *J. Appl. Phys.* 28: 115.
- Birker, P.J.M.W.L., S. de Jong, E.C. Roijers, and T.C. van Soest. 1991. *JOACS* 68: 895.
- Bommel, M. 1986. Thesis. Rijksuniversiteit Utrecht.
- Broadhurst, M.G. 1962. *J. Res. NBS-A*. 66: 241.
- de Bruijne, P. and J. Eedenburg. 1983. Unilever Research Report PVD 83 3062.
- de Bruijne, O. and F. Reckweg. 1972. *Phase transition behaviour of mixtures of tri-behenate with tristearate and tripalmitate*. Unilever R&D internal report PVD 72 3275.
- de Bruijne, P. and F. Reckweg. *PVD*. 71: 3637.
- de Bruijne, P. and F. Reckweg. *PVD*. 72: 3275.
- de Bruijne, P., M. van den Tempel, and M. Knoester. 1972. *Chem. Phys. Lipids*. 9: 309.
- Brumbaugh, E.E., M.L. Johnson, and C. Huang. 1990. *Chem. Phys. Lipids*. 52: 69.
- Busfield, W.K. et al. 1990. *JAOCs*. 67: 171.
- Cebula, D.J., D.J. McClements, and M.J.W. Povey. 1990. *JAOCs*. 67: 76.
- Chanh, N.B. and Y. Haget. 1972. *Acta Cryst.* 28: 3400.

- Chanh, N.B. and Y. Haget. 1975. *J. Chem. Phys.* 72: 760.
- Chapman, D. 1962. *Chem. Rev.* 62: 433.
- Christophersen, M.J.N. 1986. Study of some fat blends with DCS. *Unilever Research Report.* 86: 3274.
- Clements, M.S. and J.B. Rossell. 1966. Internal Unilever Report P WN 660044.
- Crowe, C.M. and M. Nishio. 1975. *AIChE J.* 21: 528.
- De Smedt, A. and V. Gibon. 1990. Private communication.
- Desphande, D.D., D. Patterson, H.P. Schreiber, and C.S. Su. 1974. *Macromolecules* 7: 530.
- Desty, D.H. et al. 1962. *Gas Chromatography*, London: Buttersworth.
- Dijkstra, A.J., R.J. Hamilton, and W. Hamm. 2008. *Trans Fatty Acids*. Wiley-Blackwell.
- Dollhopf, W., H.P. Grossmann, and U. Leute. 1981. *Colloid and Polymer Sci.* 259: 267.
- Duffy, P. 1853. *J. Chem. Soc.* 5: 197.
- Fifth International Conference on Phase Equilibria for Chemical Process Design, 1989.
- Fischer, J. and D. Moeller. 1985. 1: 246.
- Fischer, J. and D. Möller. 1985. *Proc. of the 2nd CODATA symposium on critical evaluation and prediction of phase equilibria in multicomponent systems, Paris, France 11–13 september 1985*. Elsevier Amsterdam, Vol I, 246.
- Flory, P.J. and A. Vrij. 1963. *JAOCs.* 85: 3548.
- Fredenslund, A., A. Gmehling, and P. Rasmussen. 1977. *Vapor-Liquid Equilibria Using UNIFAC*, Amsterdam: Elsevier.
- Freeman, I.P. 1957. Internal Unilever Report, Port Sunlight Program. Spring 1957: 45.
- Gandasasmita, I. 1987. Thesis. Technische Universiteit Delft.
- Garti, N., J. Schlichter, and S. Sarig. 1988. *Fat Sci. Technol.* 90: 295.
- Gautam, R. and W.D. Seider. 1979. *AIChE J.* 25: 991, 999.
- Gibon, V. 1984. Thesis. Universite Notre Dame de la Paix, Namur.
- Gibon, V. 1986. Thesis. Universite de Namur.
- Gray, M.W. and N.V. Lovegren. 1978. *JAOCs.* 55: 310, 601.
- Grob, R.L. 1985. *Modern Practices of Gas Chromatography*, New York: J Wiley.
- Grootscholten, P.A.M. 1984. *Calculation of solid liquid equilibria in fats*. Unilever R&D internal report LPVD 84 3074.
- Grootscholten, P.A.M and S.J. Jančić. 1984. *Industrial Crystallization*. Springer.
- Grootscholten, P.A.M. 1986. Janeic: Industrial crystallization.
- Grootscholten, P.A.M. 1987. Unilever Research Vlaardingen, Private communication.
- Grootscholten, P.A.M. Calculation of solid liquid equilibria in fats. LPVD 3074; 84.
- Hagemann, H.W. 1975. *JAOCs.* 52: 204.
- Hagemann, H.W. 1975. *JAOCs.* 60: 1123.
- Hagemann, H.W. 1988. Crystallization and polymorphism of fats. In: *Surfactant Science*, Garti, N., K. Sato, Eds, New York: Marcel Dekker.
- Hagemann, J.W. and J.A. Rothfus. 1988. *JAOCs.* 65: 1493.
- Hagemann, J.W. and J.A. Rothfuss. 1983. *JAOCs.* 60: 1123.
- Haget, Y. et al. 1985. Second codata symposium on prediction of phase equilibria in multicomponent systems.
- Haget, Y. et al. 1985. *Proc. of the 2nd CODATA symposium on critical evaluation and prediction of phase equilibria in multicomponent systems, Paris, France 11–13 september 1985*. Elsevier Amsterdam, vol II, 636.
- Hannewijk, J., A.J. Haughton, and P.W. Hendrikse. 1964. *Analysis and Characterization of Oils, Fats, and Fat Products*, London: Interscience.
- Hansen, H.A. and A. Fredenslund. et al. 1987. A thermodynamic model for predicting wax formation in crude oils. Danmark: Tekniske Hojskole.
- Hendriske, P.W. Dilatation of fats. Unilever Research.
- Hernqvist, L. 1984. Thesis. University of Lund.
- Hernqvist, L. and K. Anjou. *Fette Seife Anstrichmittel.* 64: 85.

- Hernqvist, L. and K. Larsson. 1982. *Anstrichmittel*. 84: 349.
- Hernqvist, L. et al. 1981. *J. Sci. Food Agric.* 32: 1197.
- Human, H., J. Ende, and L. Alderliesten. 1989. Poster at AOCS meeting Maastricht, the Netherlands.
- Janelli, L. 1985. 1: 246.
- Janelli, L. 1985. *Proc. of the 2nd CODATA symposium on critical evaluation and prediction of phase equilibria in multicomponent systems, Paris, France 11–13 september 1985*. Elsevier Amsterdam, Vol II, 631.
- de Jong, S. 1980. Thesis. Rijksuniversiteit Utrecht.
- de Jong, S. and T.C. van Soest. 1978. *Acta Cryst.* B34: 1570.
- Juriaanse, A.C. 1985. Butterlike margarines. Unilever Research Report VD 85 6003.
- Kellens, M., W. Meeussen, C. Riekel, and H. Reynaers. 1990. *Chem. Phys. Lipids*. 52: 79.
- Kerridge, R. 1952. Unpublished work. Private communication to J.B. Rossel.
- Keulemans, K. 1986. Unilever Research Vlaardingen: Private communication.
- Kitaigorodskii, A.I. 1973. *Molecular Crystals and Molecules*, London: Academic Press.
- Kitaigorodskii, A.I. 1984. *Mixed Crystals: Solid State Sciences* 33, Berlin: Springer Verlag.
- Knoester, M., P. de Bruijne, and M. van den Tempel. 1968. *J. Crystal. Growth*. 3: 776.
- Knoester, M., P. de Bruijne, and M. van den Tempel. 1972. *Chem. Phys. Lipids*. 9: 309.
- Krautwurst, J. 1972. *Keiler Milchw. Forsch. Ber.* 22: 255.
- Kung, H.C. 1950. Internal Unilever Report LB 113.
- Larsson, K. 1964. *Arkiv. Kemi*. 23: 35.
- Larsson, K. 1986. In: *The Lipids Handbook*, Gunstone, F.D., J.L. Harwood, F.B. Padley, Eds, London: Chapman and Hall.
- Lovegren, N.V. 1976. *JAOCs*. 53: 519.
- Lutton, E.S. 1955. *JAOCs*. 32: 49.
- Luzatti, V., H. Mustacchi, A. Skoulios, and F. Husson. 1960. *Acta Cryst.* 13: 660.
- Malkin, T. and M.G.R. Carter. 1947. *J. Chem. Soc.* 1947: 554.
- Michelsen, M. 1982, 1982, 1989. *Fluid Phase Eq.* 9: 1, 9: 21, 1989: 16.
- Morancelli, M., H.L. Strauss, and R.G. Snyder. 1985. *J. Phys. Chem.* 89: 5260.
- Muller, A. 1932. *Proc. Roy Soc.* 138: 514.
- Murray, W., P.E. Gill, and M. Wright. 1981. *Practical Optimization*, London: Academic Press.
- Norton, I.T. 1984. Unilever Research Report PCW 84 1065.
- Norton, I.T. et al. 1985. *JAOCs*. 62: 1237.
- Norton, I.T., C.D. Lee-Tuffnell, S. Ablett, and S.M. Bociek. 1985a. *JAOCs*. 62: 1237, 1261.
- Norton, I.T., C.D. Lee-Tuffnell, and D.W. Rowlands. 1985b. *Unilever Research Colworth*. 85: 1175.
- Null, H.R. 1980. *Phase Equilibria in Process Design*, New York: Krieger.
- Nyvlt, J. 1967. *J. Chem. Prum.* 18: 260.
- Ollivon, M. and R. Perron. 1979. *Chem. Phys. Lipids*. 25: 395.
- Ollivon, M. and R. Perron. 1982. *Thermochimica Acta*. 53: 183.
- Pamplin, B.R. 1980. *Crystal Growth*, New York: Pergamon Press, pp. 526–530.
- Perron, R. 1984. *Rev. Fr. Corps. Gras*. 31: 171.
- Perron, R. 1986. *Rev. Fr. Corps. Gras*. 33: 195.
- Perron, R., J. Petit, and A. Matthieu. 1971. *Chem. Phys. Lipids*. 6: 58.
- Poot, C.G. and G. Biernorth. 1986. In: *The Lipids Handbook*, Gunstone, F.D., J.L. Harwood, F.B. Padley, Eds, London: Chapman and Hall.
- Prausnitz, J.M. 1986. *Molecular Thermodynamics of Fluid Phase Equilibria*, New York: Prentice Hall.
- van Putte, K. and B. Bakker. 1987. *JAOCs*. 64: 1138.
- Renon, H. (Editor). 1989. *Proceedings of the Fifth International Conference of Phase Equilibria for Chemical Process Design, Banff, Canada*. Elsevier Amsterdam.
- Rossell, J.B. 1967. *Adv. Lip. Res.* 5: 353.

- Sato, K. 1987. *Food Microstructure*. 6: 151.
- Sato, K. et al. 1989. *JAOCs*. 66: 664, 1614.
- Shah, V.B. 1980. Thesis. University of Toledo.
- Simpson, T.D. and J.W. Hagemann. 1982. *JAOCs*. 84: 349.
- Small, D. et al. 1984. *The Physical Chemistry of Lipids: Handbook of Lipid Research 4*, New York: Plenum Press.
- Smith, K. 1988. Unilever Research Colworth. Private communication.
- Smith, J.M. and H.C. van Ness. 1987. *Introduction to Chemical Engineering Thermodynamics*, 4th edn. New York: McGraw-Hill.
- Swank, D.H. and J.C. Mullins. 1986. *Fluid Phase Eq.* 30: 101.
- van den Tempel, M. 1979. Physicochimie des Composes Amphiphiles. *Colloques Nat* 938: 261.
- Timms, R.E. 1978. *Chem. Phys. Lipids*. 21: 113.
- Timms, R.E. 1984. *Prog. Lip. Res.* 23: 1.
- Vazquez Ladron, R. and R. Castro Ramos. 1971. *Gracas y Aceites*. 22: 401.
- Vetterling, W., S. Teukolsky, W. Press, and B. Flannery. 1990. *Numerical Recipes*, Cambridge: Cambridge University Press.
- Wesdorp, L.H. and J.A. van Meeteren. 1989. *The influence of TAG composition on crystallization rates, part II*. Unilever R&D internal report LP VD 89 3140.
- Wesdorp, L.H. and M. Struik. 1990. European Patent EP 0264149.
- Wesdorp, L.H. 1996. *Lipid Techn.* 8/6: 129.
- Wieske, T. 1970. Internal Unilever report BAH D7019.
- Wieske, T. and K. Brown. 1986. Private communication.
- Won, K.W. 1986. Fourth international conference on fluid properties and phase equilibria for chemical process design, Helsingør, Denmark.
- Won, K.W. 1989. Fifth international conference on fluid properties and phase equilibria for chemical process design, Banff, Canada.
- Wurflinger, A. 1972. Thesis. University of Bochum.
- Yap, P.H., J.M. de Man, and L. de Man. 1989. *JAOCs*. 66: 693.
- Zacharis, H.M. 1975. *Ad X-ray Anal.* 18: 535.
- Zacharis, H.M. 1977. *Chem. Phys. Lipids*. 18: 221.
- Zief, M. and W.R. Wilcox. 1967. *Fractional Solidification*, New York: Marcel Dekker.